GEOLOGICAL SURVEY OF DENMARK AND GREENLAND BULLETIN 20 • 2010

Review of Survey activities 2009

Edited by
Ole Bennike, Adam A. Garde and W. Stuart Watt

GEOLOGICAL SURVEY OF DENMARK AND GREENLAND
MINISTRY OF CLIMATE AND ENERGY

Geological Survey of Denmark and Greenland Bulletin 20

Keywords
Geological Survey of Denmark and Greenland, survey organisations, current research, Denmark, Greenland.

Cover photographs from left to right
1. The Swedish ice breaker *Oden* at the North Pole during the LOMROG II cruise on 22 August 2009. Photo: Adam Jeppesen.
2. Folded Permian volcanic rocks in Vietnam. Photo: Stig A. Schack Pedersen.
3. Field work in West Greenland. Photo: Denis Schlatter.
4. A seismometer is placed in a pit on the Greenland ice sheet. Photo: Hans Thybo.

Frontispiece: facing page
Tanzanian woman using mercury to extract gold. Photo: Peter W.U. Appel.

Printers: Rosendahls · Schultz Grafisk A/S, Albertslund, Denmark
Manuscripts submitted: 13 January – 16 April 2010
Final versions approved: February–May 2010
Printed: 7 July 2010

ISSN 1603-9769 (Review of Survey activities)
ISSN 1604-8156 (Geological Survey of Denmark and Greenland Bulletin)
ISBN 978-87-7871-282-0

Citation of the name of this series
It is recommended that the name of this series is cited in full, viz. *Geological Survey of Denmark and Greenland Bulletin*.
If abbreviation of this volume is necessary, the following form is suggested: *Geol. Surv. Den. Green. Bull.* 20, 106 pp.

Available from
Geological Survey of Denmark and Greenland (GEUS)
Øster Voldgade 10, DK-1350 Copenhagen K, Denmark
Phone: +45 38 14 20 00, fax: +45 38 14 20 50, e-mail: geus@geus.dk
And at *www.geus.dk/publications/bull*

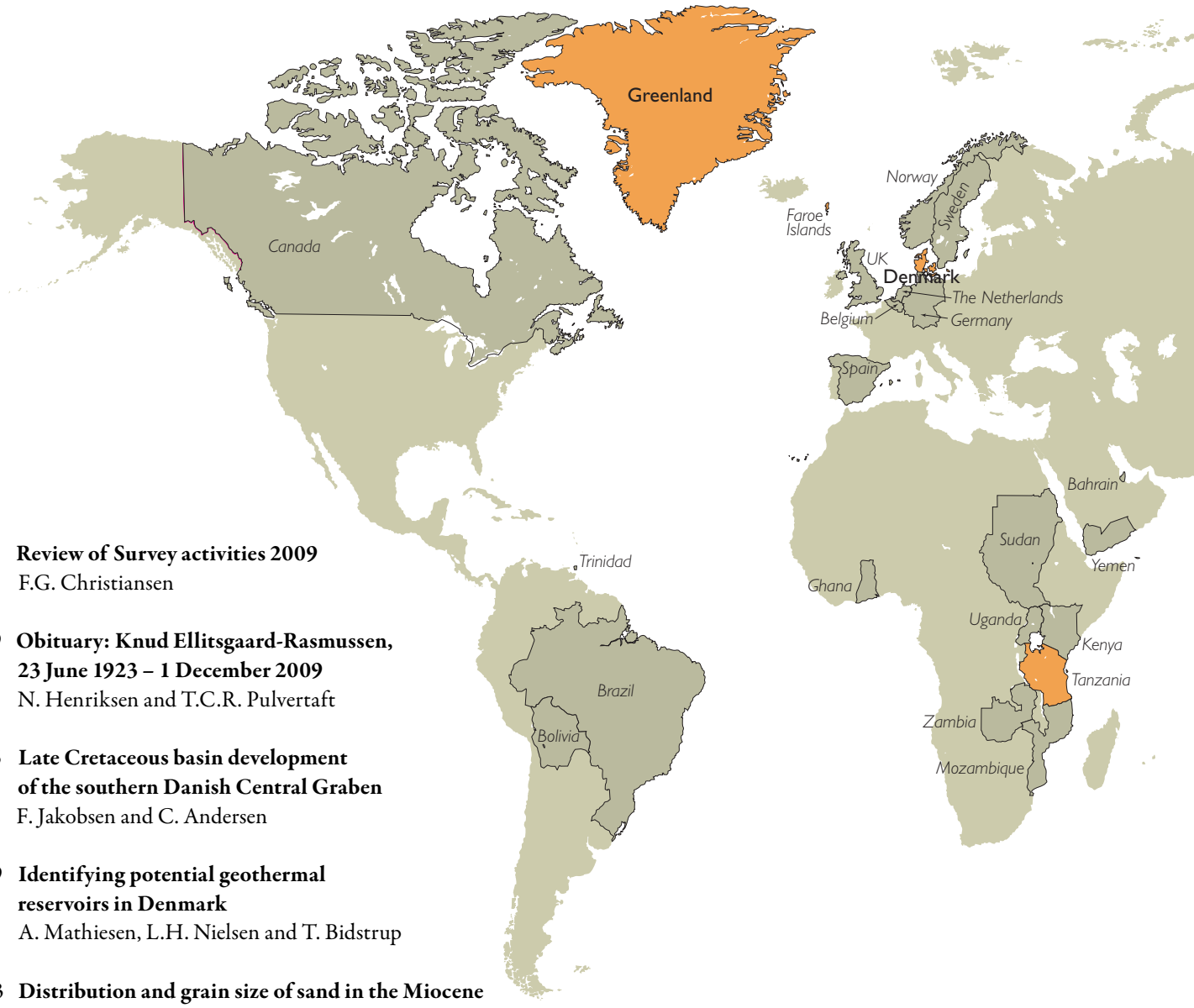

GEUS working areas 2009.
Orange areas are covered in this volume.

For further information on other working areas please refer to *www.geus.dk/international*

Review of Survey activities 2009

Flemming G. Christiansen

Deputy Director

2009 was a favourable year for the Geological Survey of Denmark and Greenland (GEUS) with focus on research, often in international collaboration. Many new projects have been initiated and many completed. In 2009, Copenhagen hosted COP15, and GEUS' involvement in the preparation for this event focussed on climate changes, reducing consumption of fossil fuels and CO_2 emissions.

This is also reflected in this seventh issue of Review of Survey activities that describes many projects that GEUS and its partners carry out in Denmark, Greenland and abroad. Together with the previous six issues, it provides a good overview of the Survey's range of research and advisory activities. The review contains a total of 23 four-page papers: nine on Scandinavia, primarily Denmark, one on the continental shelf project, eight on Greenland, four on international work and one on data management.

In addition, an obituary about Knud Ellitsgaard-Rasmussen, 1923–2009, is given. He was the first leader and subsequently formal director of the Geological Survey of Greenland (GGU) until he retired in 1983. The obituary gives an interesting overview of the post-war initiation and early history of GGU – merged in 1995 with the Geological Survey of Denmark (DGU) to form the present Geological Survey of Denmark and Greenland.

Energy policy is again high on the political agenda in Denmark. The financial crisis has emphasised the importance of revenues from the North Sea oil production, at a time when we also see strong national and international political demands for reduction of CO_2 emissions. GEUS gives high priority to research within both topics – but also to research on climate development, climate monitoring and adaptation to climate changes.

Two papers concentrate on petroleum geology in Denmark. One provides an overview of the Late Cretaceous basin development of the southern Danish Central Graben where most of the Danish oil and gas producing fields are found; the other discusses silica diagenesis and its effect on the porosity of impure Maastrichtian chalk.

Denmark has a large potential for subsurface geothermal energy. GEUS and the Danish Energy Agency have conducted a regional study to update the assessment of this potential; this work is summarised here, discussing future possibilities, including the geological risks and uncertainties. Wind power is another important energy source that contributes to CO_2 reduction. Most future wind power will probably come from large offshore wind farms. GEUS has been involved in the preparation of several projects, including evaluation of seabed features and subsurface characteristics of possible sites. One paper describes a case story from the Kattegat.

GEUS works on many other aspects of the geology of Denmark, in particular in relation to groundwater and the environment. One paper describes the distribution and grain size of sand in the Miocene Billund delta. Understanding these depositional systems is scientifically important and applicable for modelling of groundwater and petroleum resources. A second paper presents a detailed geological model of an area in eastern Jylland, demonstrating how SkyTEM, stratigraphic and lithological data have been integrated to provide better input to groundwater models. A third paper is on pre-Holocene sediments from the Baltic Sea, discussing amino acid analysis of foraminifera and their application to age determination of the deposits. A fourth paper presents new results on the radon content in till deposits that seems to be controlled by age and redox conditions. This is important when evaluating health risks in houses in Denmark. Finally, the timing and possible causes of past nutrient enrichment in a lake in Jylland have been investigated. Such studies are essential to understanding the environmental threat to the ecosystem of the lake.

2009 was a historic year for the Continental Shelf Project of the Kingdom of Denmark. The first partial claim (the area north of the Faroe Islands) was submitted to the Commission of the Limit of the Continental Shelf (CLCS) in the spring. Furthermore, a large number of data-acquisition surveys were completed, including LOMROG II with the Swedish icebreaker *Oden* that visited the North Pole area.

Data acquisition is now complete south of the Faroe Islands and south of Greenland. The technical work for the next submissions is well underway, but additional data from north-east and north of Greenland are still required. A status paper is given on the project, which started in 2003 and has progressed as planned. The project will continue until 2014, possibly requiring follow-up work and data management for several years until CLCS has submitted its recommendations to the United Nations.

In 2009, there was a high level of field activities on- and offshore Greenland. In addition to large campaigns in southern West, South-East, and East Greenland there were many other smaller activities. Results of ongoing work in southern West Greenland are described in two papers, one on the zircon record of the igneous and metamorphic history of the Fiskenæsset anorthosite complex, the other on the hydrothermal alteration and host rocks of a gold occurrence.

2009 was the first year in a mineral resource assessment project that is carried out together with the Greenland Bureau of Minerals and Petroleum in one of the least known regions of Greenland, namely the logistically challenging south-east coast. A paper describes the start of the reconnaissance work that focussed on collecting stream sediments for an assessment of the economic potential of the area.

Field work and shallow core drilling in North-East Greenland continued in 2009. Related ore geology studies are described in a paper on application of airborne hyperspectral data in mineral exploration. In another part of East Greenland, GEUS has been involved in 3-D photogeological studies of analogues to intrabasaltic reservoir sandstones elsewhere in the North Atlantic region; these studies are presented in a paper that gives a good 3-D understanding and also provides details on reservoir properties.

Over many years, studies of the ice sheet and glaciers in Greenland have attracted strong international interest due to the implications of global sea-level rise. GEUS is involved in many glaciological and meteorological projects and monitoring programmes. Three papers focus on ice and climate. The first describes the Greenland ice sheet monitoring network (GLISN) that records glacial earthquakes and provides important information on changes in glacier dynamics. The second presents results on bathymetry, shallow profiling and sediment coring in Sermilik near Helheimgletscher in South-East Greenland; work essential for studies of past ice fluctuations and their causes. The third is on glaciers in North-West Greenland with a case story on the advancing Berlingske Bræ glacier in a generally recessive ice regime.

GEUS works in many countries and with many projects types and has been active in Vietnam for several decades, in later years especially in the so-called ENRECA project that has completed two out of its three planned phases. A paper describes Vietnamese sedimentary basins, their geological evolution and petroleum potential. Another deals with offshore, thin-skinned thrust-fault tectonics.

Small-scale mining provides income for millions of people in Africa and Asia, but often with negative effects on the environment and health of miners, especially from the widespread use of mercury in gold extraction. GEUS has been involved in projects with the overall goal of reducing, or even stopping, the release of mercury into the environment. A case story from Tanzania with an alternative borax method is presented. The Survey has also been involved in many EU- and industry-financed projects of carbon-dioxide capture and storage in the past decade. The COACH project aims at applying this knowledge in China with its rapidly growing energy demand and where the use of coal-powered power stations is likely to continue for many years. A paper gives a first overview of CO_2 sources, proposed pipe lines and potential storage sites in eastern China.

The final paper describes the results of a project carried out in cooperation with DuPont Titanium Technologies featuring interactive web applications of scanning electron microscopy data. This project has been successful, and similar methods are likely to be used in mineral and petroleum exploration and for other projects with large databases.

Obituary: Knud Ellitsgaard-Rasmussen 23 June 1923 – 1 December 2009

Niels Henriksen and T. Christopher R. Pulvertaft

The former director of Grønlands Geologiske Undersøgelse (GGU; The Geological Survey of Greenland), Knud Ellitsgaard-Rasmussen, died on 1 December 2009, 86 years old. Ellitsgaard was for many years a driving force in the build-up of GGU and became, as a relatively young geologist, its leader in 1956. In 1966 he was formally appointed director and remained in this position until his retirement in 1983.

With Ellitsgaard as director for 27 years, GGU developed from a small institute with a small permanent staff, into an internationally oriented research institute with a staff of more than *c.* 120, almost half of which were geoscientists. The Survey's activities were based on an integrated cooperation between GGU personnel and a very large group of external geoscientists who came both from Danish universities and from international earth science institutes, mainly from Great Britain, Holland, Switzerland and Scandinavia, to take part in GGU's expeditions to Greenland. Every field season during the 1970s and 1980s, GGU sent between 100 and 150 participants to Greenland. These carried out geological investigations throughout the immense country with emphasis on basic research and geological mapping, but with a gradually increasing focus on economic geology. The financial support for these many activities was a combination of government grants and grants for specific projects provided by the Danish Natural Science Research Council and the Ministry for Trade (after 1979 the Ministry for Energy) as well as by private funds. During Ellitsgaard's directorship GGU's budget grew several fold from a few million Danish kroner a year to almost 50 million kroner in 1982.

On 1 January 1984 Ellitsgaard was succeeded as director by Martin Ghisler. On 1 June 1995 GGU was amalgamated with Danmarks Geologiske Undersøgelse (DGU; The Geological Survey of Denmark) to become the present Geological Survey of Denmark and Greenland (GEUS). Thus Ellitsgaard's achievements over the years were entirely related to Greenland and had no relation to the very wide range of activities now undertaken by GEUS.

Knud Ellitsgaard-Rasmussen originally trained as a joiner before he opted for a higher education and started studying geology, completing his studies in 1952 with a master's degree from the University of Copenhagen. While still a student he became involved in Greenland, and in his first field season in 1946 he partook as an assistant in the initial mapping of the Precambrian basement between Nuuk (then Godthaab) and Disko Bugt. In 1948 one of Ellitsgaard's tasks was to undertake a detailed study of a small group of islands with Archaean low-metamorphic supracrustal rocks *c.* 10 km north-east of Aasiaat (formerly Egedesminde). The results were published in 1954, having already formed the basis of his master's thesis for which he was awarded a gold medal from the University of Copenhagen.

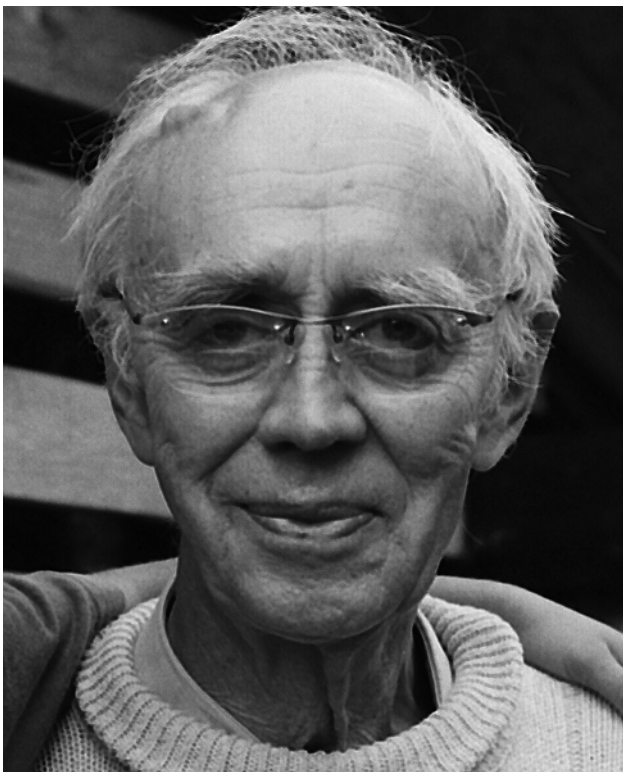

K. Ellitsgaard-Rasmussen, *c.* 2004.

In 1949–50 Ellitsgaard partook in the Danish Peary Land Expedition under the leadership of the archaeologist Eigil Knuth. This meant staying in Greenland for about a year and wintering in high-arctic conditions in the very desolate and isolated southern part of Peary Land in North Greenland. Taking advantage of winter conditions Ellitsgaard, accompanied by a Greenland sledge driver, travelled by dog sledge through the virtually unknown, northernmost part

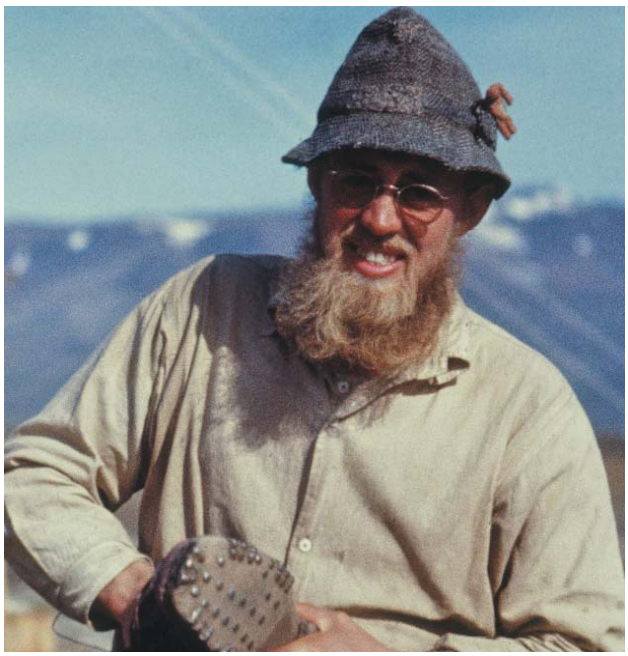

Ellitsgaard in Peary Land, 1950.

of Peary Land, mapping the deformed sedimentary rocks in the Palaeozoic Ellesmerian fold belt. The results of this reconnaissance survey were published in 1955.

After receiving his master's degree Ellitsgaard was employed as a scientific assistant at the Mineralogical-Geological Institute of the University of Copenhagen. Although at once involved in teaching, he continued to work in Greenland together with colleagues from the university.

Establishing GGU from 1946 to 1956

After the Second World War the government decided to initiate systematic geological investigations in Greenland by setting up GGU, and an advisory committee was established for the coming geological survey. The committee came to consist of three geologists (Professors Arne Noe-Nygaard and Alfred Rosenkrantz and the director of the Geological Survey of Denmark, Hilmar Ødum) together with the head of the Greenland Administration under the Prime Minister's office. The focus in the first phase should be on geological mapping and the provision of the necessary geological expertise by means of training and cooperation with Danish geologists at the university and Mineralogical Museum. The latter was achieved thanks to the efforts of Noe-Nygaard, who also, together with Hans Ramberg, initiated mapping of the Precambrian basement in southern West Greenland. Studies of the Cretaceous–Tertiary sediments and basalts in central West Greenland were led by Rosenkrantz. Several younger geologists and students were incorporated in the work, and Ellitsgaard took part in organising the work as well as participating in the field work. A section was established for providing expeditions with the necessary equipment for field work (tents, sleeping bags, provisions etc.). Two motor cutters transported field parties along the coast and into the fjords of Greenland. During this period 20–30 persons participated each summer in the field work in West Greenland, divided between Precambrian basement areas and the Cretaceous–Tertiary of the Disko–Nuussuaq area. Later more cutters were acquired as the number of parties in the field grew.

As the scope of activities in Greenland increased, the advisory committee wanted to be relieved of the day-to-day running of GGU and decided that Ellitsgaard should be appointed its leader, first for a trial period of three years. This arrangement was extended stepwise until 1966 when he was formally appointed director. He continued for a period to ply his research interests by working in the spectrometer laboratory, mainly analysing samples collected in the West Greenland basement areas, and he was lecturer in economic geology from 1962 to 1967.

GGU was from the start an integrated part of the geological milieu at the university and the Mineralogical Museum (later renamed the Geological Museum), and GGU was allocated rooms together with university and museum geologists in the complex at Øster Voldgade 5–7 in Copenhagen. At the same time the various institutes shared laboratories which were mainly used for analysis of Greenland material.

GGU's tasks from 1956 to 1964

In 1956 the only systematic geological mapping that had been carried out in West Greenland was the coastal reconnaissance of the area between 63°45′N and 69°N by Noe-Nyegaard and Ramberg. A very generalised map of southern West Greenland had been published in Ussing (1912), but otherwise the vast area of Precambrian basement from Kap Farvel to Thule was unmapped. Consequently the advisory committee decided that the first priority of future geological activities should be preparation of geological maps. This priority became the guiding line for formulating GGU's work programmes and was adhered to by Ellitsgaard until his retirement in 1983.

The new mapping campaign began in 1956 in the area around the cryolite mine at Ivituut in southern West Greenland, the choice of area being motivated by the hope of finding new deposits of cryolite, a mineral that had provided a substantial return to society since 1858. Mapping was carried out at scale 1:20 000 with a view to publishing maps at scale 1:100 000. Systematic mapping was extended to southern West Greenland

GGU's South Greenland team at Dyrnæs, 1959. Ellitsgaard is seated second from the left in the front row.

while at the same time detailed studies of the Ilímaussaq intrusion were initiated in cooperation with the Atomic Energy Commission and Copenhagen University. This intrusion hosts uranium-enriched rocks and therefore was seen as a possible source of uranium that could be used as fuel if a nuclear power station was to be built in Denmark.

The systematic mapping was carried out by geologists working in two-man teams from tents and supplied at regular intervals from two bases – one at Ivituut and the other at Dyrnæs near Narsaq. Ellitsgaard took part in the work in Greenland and spent the greater part of several summers organising the work from Dyrnæs. At first transport was provided entirely by GGU's own motor cutters, but boats could only service camps at the coast, making it difficult for geologists to map more remote inland areas. Ellitsgaard soon realised that the mapping could be carried out far more rationally with helicopter support, which at that time had seen limited use in Greenland. With great perseverance Ellitsgaard succeeded in obtaining funds for the purchase of two Bell 47-J helicopters that together had sufficient capacity to transport two geologists and their entire camp. The 1958 season was the first with these helicopters in operation, and the number of participants in GGU's campaign in southern West Greenland was *c.* 70.

This strategy, with two-man teams spread over a wide area and supported by helicopters and cutters operating from GGU's own base, was continued and refined in the coming years. As mapping progressed GGU moved its base progressively northwards, and by the beginning of the 1980s this mapping had made it possible to compile 1:100 000 geological maps of the greater part of West Greenland south of Nuuk.

In the 1960s systematic mapping was also carried out in West Greenland north of Nuussuaq where loose blocks of rich lead-zinc ore had been found in the 1930s. These blocks turned out to have fallen from a very rich lead-zinc deposit which was mined from 1973 to 1990 (Black Angel mine). Due to the severe alpine terrain, much of this area was inaccessible on foot, necessitating a change in tactics. However, Ellitsgaard realised that the solution in areas of this kind was to make intensive use of aerial photographs. Consequently GGU took on an experienced geologist who was accustomed to mapping combined with photogeological interpretation, and 1:100 000 maps were also compiled in this area. Later photogeological interpretation became an essential element in the mapping of North and North-East Greenland.

The preparation of 1:100 000 scale map sheets was accompanied by detailed studies of the material collected during the mapping, and by interpretation of the results. One of Ellitsgaard's great merits was to ensure from the start that there should be a scientific bonus from the mapping. To this end a large number of external, largely foreign, specialists were drawn into the work, cooperating closely with GGU's own geologists.

GGU's extended activities

By the middle of the 1960s it became evident that, with the speed at which mapping was progressing with the strategy then in use, it would be several decades before all Greenland was covered by 1:100 000 geological maps. A new goal for GGU was therefore formulated. By means of reconnaissance mapping, regional maps at scale 1:500 000 should be produced. Ellitsgaard's aim was that within five years the whole of West Greenland would be covered by 1:500 000 maps, given that areas already covered by 1:100 000 maps would not require remapping. In the end, however, it was many more years before all West Greenland was covered by four 1:500 000 geological maps. In later years the concept was extended to

One of GGU's Bell helicopters, 1958.

other parts of Greenland, and today the whole of Greenland is covered by 1:500 000 geological map sheets.

An important expansion of GGU's activities took place in 1967 when GGU took over the geological mapping of East and North Greenland. Previously geological investigations in these regions had been the preserve of the 'Danish Expeditions to North-East Greenland' under the leadership of Lauge Koch. Field work in these very remote and often extremely rugged areas required a much more intensive use of aeroplanes and helicopters than work in West Greenland. This new activity substantially increased the scope of GGU's tasks, as mapping in West Greenland was to continue with the same intensity as before. Ellitsgaard mobilised his persuasive talents and in 1968 secured funds enabling GGU to charter a polar vessel, not only to transport the expedition to and from East Greenland, but also to act as a floating base for operations throughout the season. Two helicopter landing platforms were mounted on the ship. This strategy was used for three seasons, after which operations were based entirely on tent base camps on land. The expedition with all its goods was transported to and from Greenland in a large aircraft, and small STOL aircraft and helicopters provided the daily transport of the mapping operation. As mapping progressed, base camps were moved according to logistic needs. By the early 1970s GGU's combined operations in West and East Greenland included 120–130 persons, five to six chartered helicopters and STOL aircraft, and five cutters. There was plenty for GGU's director to see to!

Ellitsgaard was always aware of the advantages to GGU of allowing geologists to partake in activities led by other organisations. Thus in North Greenland GGU personnel participated in the Geological Survey of Canada's Operation Grant Land in 1965–66 and in a reconnaissance in Peary Land in 1969 under the auspices of a British Joint Services Expedition. Thanks to these reconnaissance activities and its own pilot studies in the 1970s, GGU was well prepared when systematic mapping of North Greenland was started in 1978.

By 1970 GGU had made sufficient progress to compile the first ever geological map of the whole of Greenland at scale 1:2 500 000. This was not superseded until 1995 when a completely revised map at this scale was published. Unlike the 1970 map, this later map included offshore geology. Publication of the first geological map was followed up in 1971 by the publication of the first map of the Quaternary geology of Greenland, also at scale 1:2 500 000.

Although GGU's primary task was geological mapping, this was not its only activity. From the middle of the 1950s GGU was involved in economic geology, carrying out pilot studies for mining companies. In the 1960s the scope of GGU's glaciological studies was expanded to assessing possible sites for establishing hydroelectric power stations, with the result that the first hydropower station in Greenland could be inaugurated in 1993. In the late 1960s the oil industry began to show an interest in West Greenland, particularly offshore southern West Greenland. Ellitsgaard soon realised that GGU would need to react to this development, and a Department for Oil Geology was established with three functions: (1) acquiring oil-geologically relevant data from onshore sedimentary basins that could provide analogues

Ellitsgaard at Dyrnæs, *c.* 1960.

GGU's base camp at 'Mellembygd', near Paamiut (formerly Frederikshåb), 1964.

GGU's floating base in Scoresby Sund in 1968. The ship *Martin Karlsen* is the vessel formerly named *Kista Dan*.

to what can be expected to occur in offshore basins, (2) acquiring geophysical data offshore in relatively ice-free areas that were regarded as having a potential for hydrocarbon deposits and (3) advising the then Ministry for Greenland in assessing applications for petroleum exploration licences. The first licensing round covering blocks offshore southern West Greenland was opened in 1974. Five exploration wells were drilled in 1976–77, but all were declared dry and exploration in this region was not resumed until 1991.

GGU's offshore activities made a modest start in 1972 with a shallow seismic reconnaissance of the West Greenland shelf and fjords between 68° and 73°N. Following the energy crisis in 1973 the Natural Science Research Council and the Ministry for Trade (after 1979 the Ministry for Energy) made funds available for energy-related projects. GGU secured its share of these funds, and in 1978 GGU 'went offshore' in earnest. With support from the Danish Energy Authority under the Ministry for Trade, extended shallow marine surveys of the West Greenland shelf were carried out between 62° and 68°N. In 1979 GGU turned its attention to the East Greenland shelf which, prior to the opening of the North Atlantic, lay close to the major oil-producing areas of the North Sea and west Norwegian shelf. To start with, an aeromagnetic survey of the region was carried out in 1979 (Project Eastmar). With additional support from the EEC this was followed up by a reflection seismic survey (North Atlantic D) in 1980–82.

Other energy-related projects were a detailed mapping and evaluation of the coal deposits on Nuussuaq and an extensive uranium-prospecting project in South Greenland (Project Syduran), the latter inspired by reports of uranium occurrences in eastern Labrador in a geological setting similar to that in South Greenland.

From embryonic survey to formal state Survey

As soon as Ellitsgaard had been appointed leader of the institute now officially called Grønlands Geologiske Undersøgelse, the advisory committee wanted to hand over the full responsibility to Ellitsgaard, and GGU to be given a formal legal status. This suggestion was well received. However, the Ministry for Greenland also wanted a mining law for Greenland to be drafted and, as GGU would have a role to play in connection with mining activities, it was decided to hand these tasks over to a mining law commission. Two laws – the mining law and the law for GGU – were finally passed in the Danish parliament (Folketinget) in 1965 and GGU became a directorate under the Ministry for Greenland. Shortly afterwards Ellitsgaard was appointed GGU's first director after functioning as such for ten years with uncertain tenure. After this the committee for GGU dissolved itself (Noe-Nygaard 1986).

External cooperation

When work began in Greenland in 1946 there were no geologists in Denmark with expertise in basement geology. This situation was remedied, partly thanks to a determined effort by Professor Arne Noe-Nygaard at the University of Copenhagen, and partly by recruiting foreign geologists with experience in this field. With this policy the seed was sown for GGU later to become an internationally oriented institute, where geological mapping and research were carried out by Danish and foreign geologists employed at GGU in cooperation with a large number of research students and geologists based in foreign universities. The latter were attracted by the fantastic natural conditions for geological research offered by Greenland and by the very favourable working conditions offered by GGU. Thus an extensive

K. Ellitsgaard-Rasmussen receiving the honorary degree of Doctor of Science at the University of Exeter, U.K., in 1984.

international network of partners was built up, which raised the scientific standard in GGU to a level comparable to that of many leading international research institutes. GGU and Greenland geology also became more widely known in the western world when a review of all aspects of Greenland geology was published in 1976 (Escher & Watt 1976). In a review of this book John Sutton, then professor of geology at Imperial College, London, wrote: "The Survey collaborates with more than fifty Universities and Institutes, and moreover does so with a generosity and openness which has attracted able scientists from many countries. The heart of the undertaking lies, however, in Denmark. It is Danish resources and leadership that have brought the Geological Survey of Greenland to its present eminence." (Sutton 1976, p. 815).

A measure of GGU's high standard during this period is the fact that more than 25 of the then young geologists later became full professors at Danish and foreign universities.

Honours

Throughout his career Ellitsgaard partook in the work of several committees, commissions and scientific societies. Notably Ellitsgaard was a member of the Commission for Scientific Research in Greenland from 1965 to 1983, a member of the Danish Academy for Technical Sciences from 1967 to 1997, and in 1974 he was elected a member of the Royal Danish Academy of Sciences and Letters. He was also a member of the board of governors for Nordisk Mineselskab A/S and Arktisk Minekompagni A/S. From 1981 to 1986 he was a member of Greenland Home Rule's National Park Council.

In 1976 Ellitsgaard received the Egede Medal of the Royal Danish Geographical Society for his contribution to geological and geographical research in Greenland. The high esteem in which Ellitsgaard was held in foreign geological institutes was shown when he was awarded an honorary Doctorate of Science at the University of Exeter (UK) in 1984 and furthermore elected an Honorary Fellow of the Geological Society of London.

Final words

During the 27 years when he bore the main responsibility for the administration and development of GGU, Ellitsgaard succeeded in building up an organisation that became widely known in international geological circles and had a great influence on the coming development of economic geology in Greenland. Ellitsgaard had his principles and views and at times ran into political and administrative problems. However, he tackled these difficulties without GGU's personnel being affected by them. He has written his personal perception of the embryonic days of GGU in an internal survey report (Ellitsgaard-Rasmussen 1996).

Ellitsgaard had many good years as GGU's director, and his staff remember him as a friendly and approachable leader, although heavily involved in administrative duties. His philosophy for the daily leadership of the institute was that his staff would perform best if given a large degree of individual freedom and responsibility, a philosophy the success of which can be seen in GGU's substantial production of scientific papers and map sheets.

All honour to his name.

References

Ellitsgaard-Rasmussen, K. 1996: En stjerne fødes. Beretning om GGU's tilblivelse. Danmarks og Grønlands Geologiske Undersøgelse Rapport **1996/102**, 76 pp.

Escher, A. & Watt, W.S. (eds) 1976: Geology of Greenland, 603 pp. Copenhagen: Geological Survey of Greenland.

Noe-Nygaard, A. 1986: Til Knud Ellitsgaard-Rasmussen (in Danish, with English summary). Rapport Grønlands Geologiske Undersøgelse **128**, 5–11.

Sutton, J. 1976: Geological Survey of Greenland. Nature **264**, 815 only.

Ussing, N.V. 1912: Geology of the country around Julianehaab, Greenland. Meddelelser om Grønland **38**, 376 pp.

Authors' address

Geological Survey of Denmark and Greenland, Øster Voldgade 10, DK-1350 Copenhagen K, Denmark. E-mail: *nielshen@mail.dk*

Late Cretaceous basin development of the southern Danish Central Graben

Finn Jakobsen and Claus Andersen

The Danish oil and gas production mainly comes from fields with chalk reservoirs of Late Cretaceous (Maastrichtian) and early Paleocene (Danian) ages located in the southern part of the Danish Central Graben in the North Sea. The area is mature with respect to exploration with most chalk fields located in structural traps known since the 1970s. However, the discovery by Mærsk Oil and Gas A/S of the large non-structurally and dynamically trapped oil accumulation of the Halfdan Field in 1999 north-west of the Dan Field (e.g. Albrechtsen *et al*. 2001) triggered renewed exploration interest. This led to acquisition of new high quality 3-D seismic data that considerably enhanced imaging of different depositional features within the Chalk Group. Parallel to the endeavours by the operator to locate additional non-structural traps in porous chalk, the Geological Survey of Denmark and Greenland took advantage of the new data to unravel basin development by combining 3-D seismic interpretation of a large number of seismic markers, well log correlations and 2-D seismic inversion for prediction of the distribution of porous intervals in the Chalk Group. Part of this study is presented by Abramovitz *et al*. (in press). In the present paper we focus on aspects of the general structural development during the Late Cretaceous as illustrated by semi-regional time-isochore maps. The Chalk Group has been divided into two seismically mappable units (a Cenomanian–Campanian lower Chalk Unit and a Maastrichtian–Danian upper Chalk Unit) separated by a distinct basin-wide unconformity.

Study area and database

The mapped area comprises the Southern Salt Dome Province located in the southern part of the Danish Central Graben and adjacent parts of the Ringkøbing–Fyn High (Fig. 1). The seismic database used involves three separate 3-D data sets. The bulk of the area is covered by the 1150 km^2 *Kraka Extension survey*, which was acquired by Mærsk in 2000. To the south and east it is supplemented by data belonging to the Fugro multi-client *Entenschnabel 2002* survey and to the north-east by part of the Mærsk *Contiguous Area 3-D* from 1995. In addition, data from smaller surveys of different vintages were used in order to cover parts of the Coffee Soil Fault that separates the graben area from the platform.

Geological setting

Deposition of the Upper Cretaceous – Danian Chalk Group in the study area took place during a phase of regional post-rift subsidence following Late Jurassic rifting. This period was marked by high sea level, high seawater temperatures and a peak in production of organic matter. The Late Cretaceous regional subsidence was modified by movements of Zechstein salt and punctuated by widespread inversion in the form of compression along old extensional fault trends, resulting in flexuring and folding of basin infill (Vejbæk & Andersen 2002). This resulted in the development of areas with bathymetric elevations and formation of local depocentres in the intervening lows. The structural movements gave rise to a number of unconformities easily recognised as truncation and onlap surfaces on seismic profiles and to stratigraphic hiatuses in wells.

The chalk in the area is pelagic in origin and formed from settling of calcareous nannoplankton remains (coccoliths) and it consists generally of 95–99% calcite. After deposition the pelagic chalk was subjected to redistribution

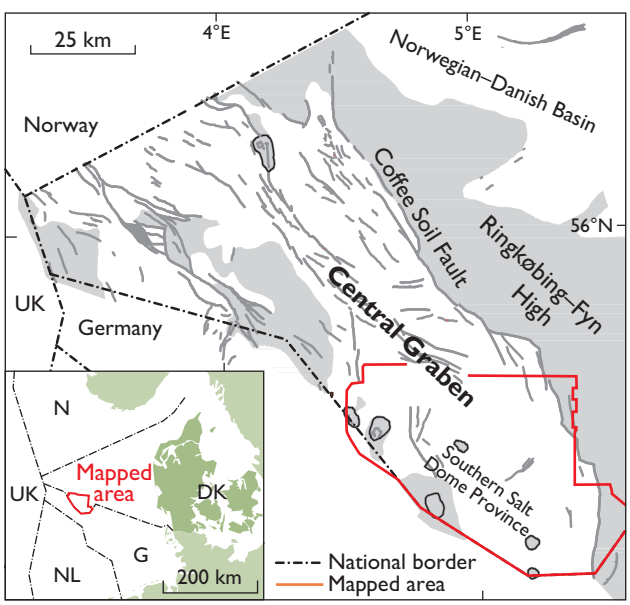

Fig. 1. Map of the Danish Central Graben region, showing the major structural elements and the location of the study area.

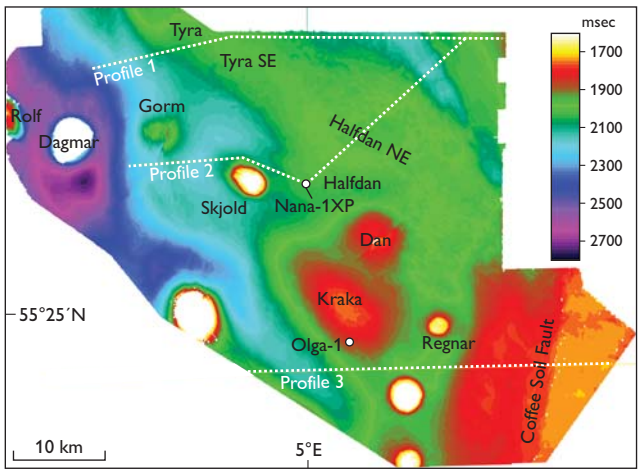

Fig. 2. Time-structure map of the Top Chalk Group with location of producing chalk fields, profiles and wells mentioned in the text. Contours on the shallow salt diapirs with thin chalk are not shown.

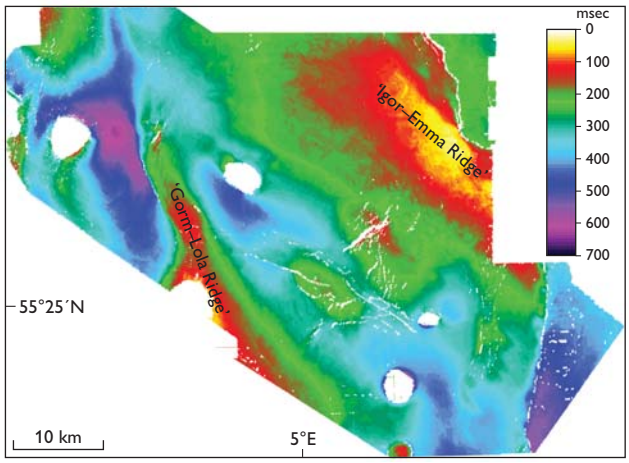

Fig. 3. Time-isochore map of the total Chalk Group with names of major inversion ridges indicated. Chalk Group isochores over the salt diapirs are not shown.

by various processes. These include downslope mass-flow movements arising from slope instability caused by syndepositional tectonic movements, or along-slope bottom currents that modified the seafloor forming channels, drifts, ridges and mounds. The interaction of downslope and along-slope processes has been demonstrated by Esmerode *et al.* (2008) in the lower part of the chalk section in the area immediately to the north of the study area.

The overall structural style is illustrated by a time-structure map of the Top Chalk Group (Fig. 2) and a time-isochore map of the total Chalk Group (Fig. 3). The latter shows very large thickness variations from less than 100 msec (< *c.* 200 m) on top of salt diapirs up to 650 msec (*c.* 1300 m) in the rim-syncline east of the Dagmar Field. Reduced thicknesses have been mapped over the Dan and Kraka structures, which are caused by growth of underlying salt pillows. On the NNW–SSE-trending 'Gorm–Lola Ridge' extending southwards from the Gorm Field, the thinning of the chalk is caused by a combination of halokinesis and structural inversion. The asymmetric, NW–SE-trending 'Igor–Emma Ridge' with less than 100 msec of chalk on its central part is located along the Coffee Soil Fault. The total chalk thickness is much larger on the stable Ringkøbing–Fyn High than on the adjacent inverted part of the graben.

The time-structure map of Fig. 2 shows the results of the Late Cretaceous tectonic movements combined with the effects of Cenozoic continued inversion/subsidence concentrated in the former graben area and halokinesis. Structural inversion affecting the Top Chalk Group surface is less pronounced and is restricted to the development of the centrally located, gentle, NW–SE-orientated 'Tyra–Igor Ridge' trapping the Tyra, Tyra SE and Halfdan NE gas accumulations. The large, dynamically trapped Halfdan oilfield is located on the south-western flank of this ridge.

Basin development

In modern 3-D seismic data, the Chalk Group is often characterised by discontinuous reflection patterns indicating spatial variations in lithology and depositional mode, and it is possible to identify and map a number of unconformities. The most prominent is here termed the Top Hod Unconformity (Fig. 4), which is generally expressed as a strong positive reflection. The unconformity divides the Chalk Group into a lower part comprising the Hod, Blodøks and Hidra Formations and an upper part comprising the Ekofisk and Tor Formations using the standard lithostratigraphic nomenclature for the Central North Sea (Surlyk *et al.* 2003). New palaeontological age determinations of the Olga-1x well, which is located on the flank of the Kraka structure, suggest that the unconformity here is of latest Campanian to early Maastrichtian age (Abramovitz *et al.* in press).

The seismic profiles in Fig. 4 are selected to illustrate reflection patterns and highlight aspects of the basin development. The northern profile in Fig. 4A crosses the gentle 'Tyra–Igor Ridge' that was mainly formed by inversion postdating chalk deposition. Several generations of channel-like features cut into the Top Hod Unconformity. Furthermore, the lower part of the chalk is extensively disturbed on the eastern flank. Esmerode *et al.* (2008) interpreted similar features as formed by interactions between downslope mass movements (slumps and slides) and along-slope currents. The uppermost part of the chalk is draped and rather uniform in thickness suggesting reduction in earlier bathymetric relief.

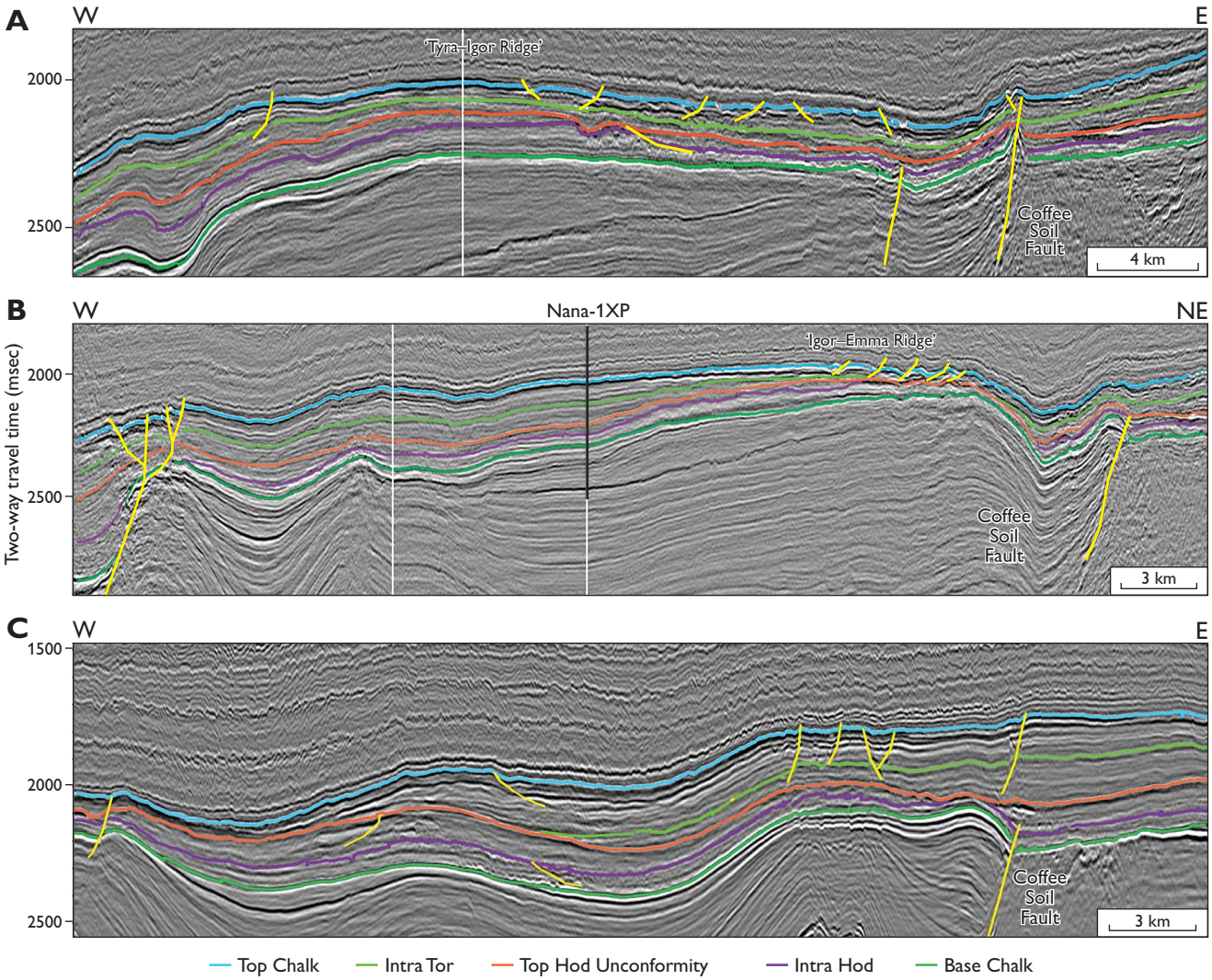

Fig. 4. **A:** Profile 1 crosses the gentle 'Tyra–Igor Ridge' mainly formed by inversion post-dating chalk deposition. Several generations of channel-like features cut into the Top Hod Unconformity. **B:** Profile 2 illustrates the asymmetric 'Igor–Emma Ridge' inversion anticline. The anticline is a result of both intra-chalk and post-chalk compression movements and developed with a steep north-eastern limb adjacent to the reversed Coffee Soil Fault. **C:** Profile 3 is located in the southern part of the study area that is characterised by an asymmetric basin development with an eastward shift in depocentres. Yellow lines show faults. For location of the profiles see Fig. 2.

The Top Chalk Group surface on the eastern flank is cut by low-angle listric faults, indicating early post-Danian slumping of poorly consolidated chalk caused by renewed inversion along the ridge.

Figure 4B illustrates the asymmetric 'Igor–Emma Ridge' inversion anticline trapping the Halfdan NE gasfield found in Danian chalk. The anticline is a result of both intra-chalk and post-chalk compression movements and developed with a steep north-eastern limb adjacent to the reversed Coffee Soil Fault. The lower part of the chalk is deeply eroded at the crest and the Top Hod Unconformity merges with older truncation surfaces. The Tor Formation above onlaps the western flank. The thinning and condensation of the Tor Formation is associated with deterioration of reservoir properties in the Upper Maastrichtian Tor Formation chalk arresting up-dip oil migration from the Halfdan Field, which was discovered from the Nana-1XP vertical well.

Figure 4C shows a W–E profile that crosses the Coffee Soil Fault. The profile is located in the southern part of the study area that is characterised by an asymmetric basin development with thick lower chalk below the Top Hod Unconformity in the Central Graben area to the west, and an eastward shift of depocentre above. The lower part of the Tor Formation is thick on the Ringkøbing–Fyn High. It gradually onlaps the unconformity indicating significant variations in time span of missing sections across this surface.

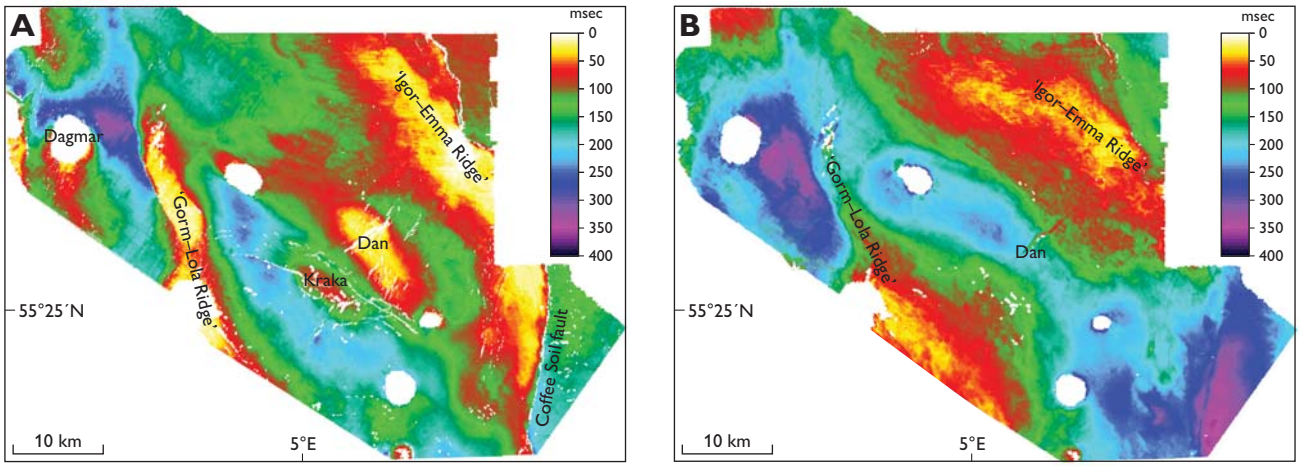

Fig. 5. Time-isochore maps. **A:** Lower Chalk Group interval. **B:** Upper Chalk Group interval. The isochores show shift of depocentres during the Late Cretaceous in a north-eastward direction.

The general basin development during the Late Cretaceous and Danian can further be visualised by comparing the semi-regional time-isochore maps of the lower and upper parts of the Chalk Group separated by the Top Hod Unconformity. The Lower Chalk Group interval shows large thickness variations with the main depocentre (up to 350 msec) found in the rim-syncline north and east of the Dagmar salt diapir (Fig. 5A). The 'Gorm–Lola Ridge' separates it from a NW–SE-orientated depocentre that covers the southern flank of the Kraka structure. The Lower Chalk Group interval is also thin over the Dan Field area, indicating structural growth caused by underlying halokinetic movements. A conspicuous feature is the asymmetric 'Igor–Emma Ridge' inversion anticline along the reversed Coffee Soil Fault where the lower chalk is thin and even seismically absent in the crestal part.

The time-isochore map of the Upper Chalk Group interval (Fig. 5B) shows more gradual thickness variations. The most notable difference between the two units is the north-eastward shift and widening of the NW–SE-orientated depocentre. At the Dan Field only an insignificant thinning of the interval is mapped, which shows that halokinetic movements waned here during the Maastrichtian and Danian. The expression of both the 'Gorm–Lola Ridge' and the 'Igor–Emma Ridge' is less distinct. The latter is confined to the northern part of the mapped area and orientated slightly obliquely to the NNW–SSE-trending segments of the Coffee Soil Fault Zone.

By using a simple two-fold subdivision of the Chalk Group, the present paper illustrates the dynamic basin development with spatial changes in subsidence patterns and structural growth caused by halokinesis and structural inversion. A more detailed analysis of the basin development with an additional subdivision of the Chalk Group is in progress in combination with mapping of sedimentary features. Based on the close relationship between erosion, re-deposition (deposition of reservoir chalk) and structural development, the basin development is used as a guide for prediction of hitherto unrecognised reservoir intervals.

References

Abramovitz, T., Andersen, C., Jakobsen, F.C., Kristensen, L. & Sheldon, E. (in press): 3-D seismic mapping and porosity variation of intra-chalk units in the southern Danish North Sea. In: Vining, B.A. (ed): Petroleum geology: from mature basins to new frontiers. Proceedings of the 7th Petroleum Geology Conference. London: Geological Society.

Albrechtsen, T., Andersen, S. J., Dons, T., Engstrøm, F., Jørgensen, O. & Sørensen, F.W. 2001: Halfdan: Developing non-structurally trapped oil in North Sea chalk. Paper SPE 71322. New Orleans, Louisiana: Society of Petroleum Engineers Annual Technical Conference and Exhibition.

Esmerode, E.V., Lykke-Andersen, H. & Surlyk, F. 2008: Interaction between bottom currents and slope failure in the Late Cretaceous of the southern Danish Central Graben, North Sea. Journal of the Geological Society (London) **165**, 55–72.

Surlyk, F., Dons, T., Clausen, C.K. & Higham, J. 2003: Upper Cretaceous. In: Evans, D. *et al.* (eds and co-ordinators): The millennium atlas: petroleum geology of central and northern North Sea, 213–233. London: Geological Society.

Vejbæk, O.V. & Andersen, C. 2002: Post mid-Cretaceous inversion tectonics in the Danish Central Graben – regionally synchronous tectonic events? Bulletin of the Geological Society of Denmark **49**, 129–144.

Authors' address

Geological Survey of Denmark and Greenland, Øster Voldgade 10, DK-1350 Copenhagen K, Denmark. E-mail: *fj@geus.dk*

Identifying potential geothermal reservoirs in Denmark

Anders Mathiesen, Lars Henrik Nielsen and Torben Bidstrup

Concerns about climate change have led to increased interest in geothermal energy as one way of reducing the consumption of fossil fuels and thus limit CO_2 emissions. Use of geothermal energy is based on well-established technologies, a high degree of security of supply, and little visual or noise inconvenience. More than one hundred plants have been established in Europe.

There is a large potential for using geothermal energy from the Danish subsurface, as first pointed out by Balling (1976). Geothermal energy is highly suitable for district heating systems and is expected to cover a large part of the demand for district heating in the future. Two Danish geothermal plants, the Thisted plant in northern Jylland and the Margretheholm demonstration plant near Copenhagen (Fig. 1), have shown that it is possible to produce large amounts of warm water for district heating. Only 5–10% of the total energy output from the plant is used to extract the heat from the subsurface by pumping warm formation water to the surface and returning it to the subsurface in a closed system. The plants use absorption warmth pumps, which need steam and hence give rise to consumption of (fossil) fuel. Both Danish plants have two wells, a production well and an injection well in which the cooled formation water is returned to the geological reservoir at about 1 km away from the production point, in order to avoid mixing of warm and cold water (Fig. 2). Geothermal energy can also be used for electricity production, but Danish subsurface temperatures are currently not believed to be sufficiently high to produce electricity directly.

Because geothermal energy is expected to play an increasingly important role in the energy strategy of Denmark, the

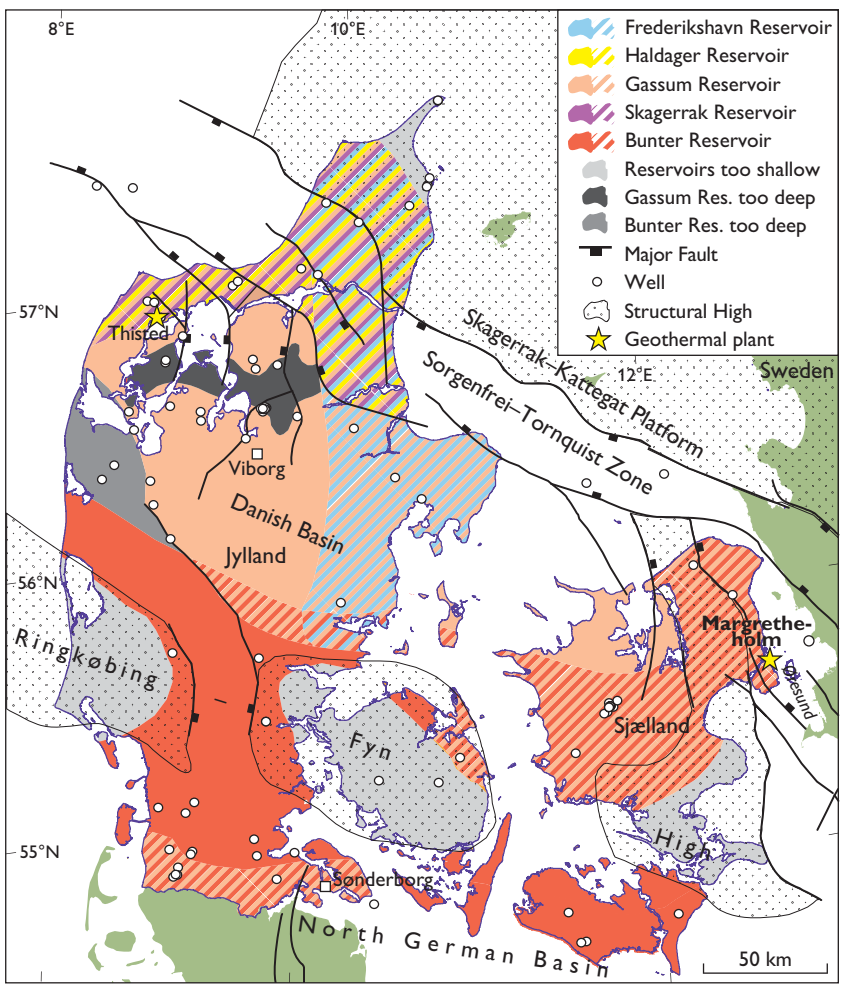

Fig. 1. The distribution of potential sandstone reservoirs in Denmark with depths in the 800–3000 m interval and thicknesses above 25 m. Dark grey and black areas indicate where the reservoirs are too deep (Gassum in northern Jylland; Bunter in western Jylland – both located in the central parts of the Danish Basin). Light grey areas indicate where reservoirs are absent (Ringkøbing–Fyn High) or too shallow (less than *c.* 800 m; northernmost Jylland). Hatched areas indicate two or more reservoirs with geothermal potential. Green areas: not mapped.

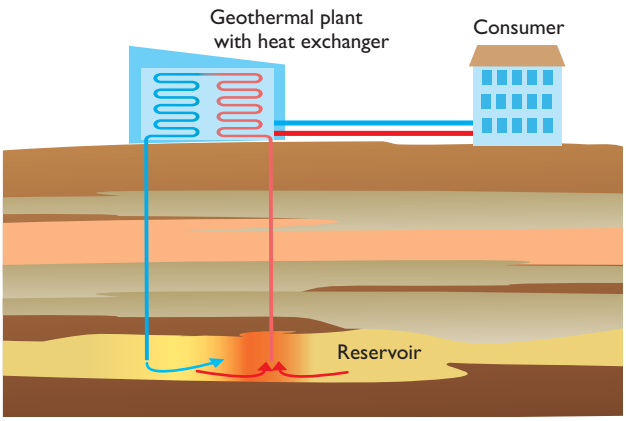

Fig. 2. Schematic diagram illustrating the geothermal concept used in Denmark. In the geothermal plant a production well pumps up warm water (red line) from the underground reservoir, and an injection well (blue line) returns the cooled water to the reservoir.

Geological Survey of Denmark and Greenland (GEUS) and the Danish Energy Agency have conducted a regional study to update the assessment of the geothermal potential in Denmark (Mathiesen *et al.* 2009). Based on existing well, seismic and temperature data and the detailed knowledge of the subsurface stratigraphy gathered by GEUS over many years, the assessment has documented a huge geothermal potential in many parts of Denmark. The focus of the study was to evaluate (1) the potential of geothermal energy in Denmark and (2) if it can contribute significantly to the Danish strategy for a safe, sustainable and reliable supply of energy. The specific potential in local areas was not evaluated in detail; however, a well-defined and stepwise procedure to develop local geothermal prospects by integrating existing and new data is suggested.

Potential reservoirs and areas of interest

The Danish subsurface can be divided into five major structural parts: the North German Basin, the Ringkøbing–Fyn High, the Danish Basin, the Sorgenfrei–Tornquist Zone and the Skagerrak–Kattegat Platform (Fig. 1). These structural divisions exert a decisive influence on the geothermal prospectivity of the Danish subsurface, as they essentially determine the distribution, thicknesses, facies types and burial depths of the potential reservoirs (Nielsen 2003; Nielsen *et al.* 2004). The 1–10 km thick Mesozoic succession has been the target for hydrocarbon exploration since 1935 and is thus relatively well known from about 60 deep wells and seismic data acquired over many years, although with a highly variable data coverage and quality. The data show that the most promising geothermal reservoirs occur within the Triassic – Lower Cretaceous succession in the Danish Basin and the North German Basin, separated by the Ringkøbing–Fyn High which shows a lower potential. Based on regional geological studies, four main stratigraphical units with a regional geothermal potential have been identified (Nielsen *et al.* 2004). Within these four main units, we have defined five geothermal reservoirs on the basis of their stratigraphical and spatial extent. Each reservoir comprises a large number of sandstone layers that are potential aquifers. The new assessment shows that large areas in both basins have a good geothermal potential, as they contain several porous, water-bearing sandstone reservoirs in the economic interval 800–3000 m below the surface with formation temperatures of 25–90°C (Mathiesen *et al.* 2009).

The principal challenge for successful geothermal exploration is to assess whether good reservoir properties are present in terms of sufficient layer thickness, porosity, permeability, temperature and formation water geochemistry. These geological factors are used to evaluate whether the thermal energy of the formation water can be exploited economically and used for heating purposes. By combining knowledge of the geographical distribution of the stratigraphical units with the potential reservoirs, their mapped burial depths and estimates of where the cumulative thickness of the reservoir sandstones exceeds *c.* 25 m at depths of 800–3000 m, a useful indication of the regional geothermal potential is provided.

Temperature and salinity of the formation water in the potential reservoirs increase with increasing depth. Based on data from a number of wells a general temperature–depth relation has been established, showing a gradient of 25–30°C/km. The salinity of the formation water shows a general increase of about 10%/km burial depth, but large variations are found. Porosity and permeability decrease with increasing depth due to mechanical compaction and formation of diagenetic minerals that reduce the pore volume (porosity) and the connections between the pores (permeability). Several of these properties are directly related to the petrography of the sediment source areas and the grain size distribution of the material supplied to the basins. Thus the various depositional processes during the formation of the reservoirs and their subsequent burial depths determine their qualities as geothermal reservoirs. However, the mutual dependency of the various factors and processes is not fully understood, which weakens the predictive strength and reliability of the geological models currently in use to identify areas of interest.

Figure 1 shows regions where sandstone-rich reservoirs are expected to have geothermal potential by combining geographical distribution and burial depth information of the five reservoirs. The map also indicates where further detailed research and investigations are required if geothermal ener-

gy production is to be further developed (Mathiesen *et al.* 2009). The central part of the Danish Basin is promising, whereas the potential of areas located around the 800 m and 3000 m cut-off limits is highly uncertain. Areas located along the Ringkøbing–Fyn High are considered less prospective.

The need for further development

Interest in the use of geothermal energy has increased over the past five years. So far, the Thisted and Margretheholm plants are the only working geothermal plants in Denmark. However, GEUS has carried out evaluations of the geothermal potential in several local areas in Denmark with positive conclusions. It is expected that new Danish geothermal plants will be established in Sønderborg and Viborg within the next few years. The existing Thisted plant has produced heat from the Gassum Formation (the Gassum reservoir) for almost 20 years without notable production or injection problems, and the newly established Margretheholm plant produces heat from the Bunter Sandstone Formation (the Bunter reservoir).

During planning of the Margretheholm plant new seismic data were acquired in 2001, and GEUS carried out a geological evaluation of the geothermal potential. The study used old and new seismic data to map the distribution, the tops and the lateral variations of the reservoirs, as well as faults. Faults may reduce the lateral continuity of a reservoir (Fig. 3). From this study it was concluded that the Bunter reservoir is found south of the Ringkøbing–Fyn High, on parts of the high and in the Danish Basin, and grades into the Skagerrak reservoir towards the north-eastern basin margin (Fig. 2; Mathiesen *et al.* 2009). The Bunter reservoir is dominated by fine-grained sandstones that were deposited in arid continental environments with fluvial channels, aeolian dunes and with some marine influence. In southern Sweden, analyses of existing cuttings from old wells and data from new wells documented the presence of a loose, medium- to coarse-grained, quartzitic sandstone composed of sub-rounded quartz and feldspar grains without overgrowth of minerals or other signs of corrosion and cementation. Data from the Swedish wells combined with log correlation to Danish wells indicated the presence of a *c.* 50 m thick, loose, conglomeratic sandstone unit in the basal part of the Bunter reservoir, and this unit was predicted to show high porosity and low degree of cementation at Margretheholm.

In 2002 and 2003 the Margretheholm-1 and -2 wells were drilled to about 2700 m depth and confirmed the presence of several sandstone-rich aquifers in both the Gassum and Bunter reservoirs. Studies of the new wells and results from log correlation with other wells in the Copenhagen region, Øresund and southern Sweden confirmed the previous geological model of the Bunter reservoir and strengthened the indications of a large geothermal potential in the Copenhagen area (Figs 3, 4). No cores were taken from the new wells, but both wells encountered a promising aquifer in the Bunter reservoir with satisfying test results, and in 2006 the Mar-

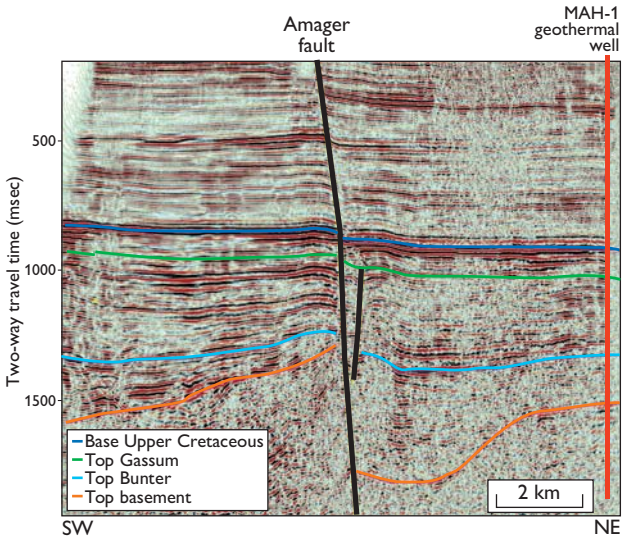

Fig. 3. SW–NE-trending seismic profile south-west from Margretheholm. The profile illustrates the importance of mapping faults, which can reduce the lateral reservoir continuity. For location see Fig. 4.

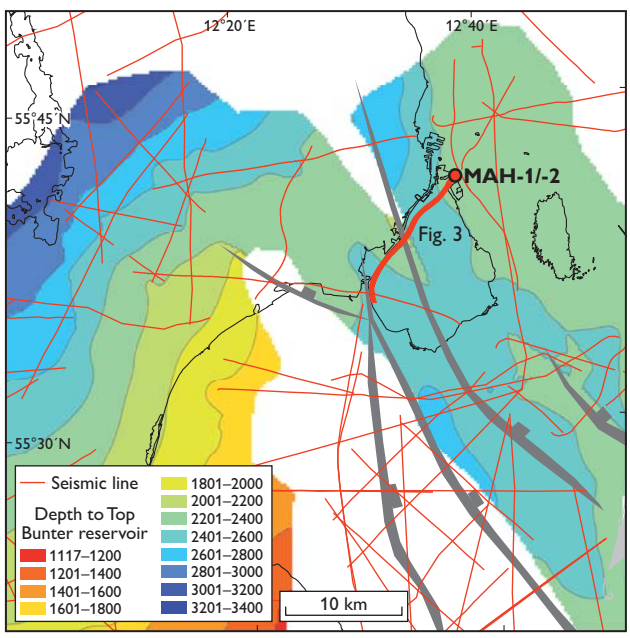

Fig. 4. Depth to the top of the Bunter reservoir, illustrating southwards shallowing of the reservoir top and its partition by faults (grey tone). Red dot: Margretheholm and the wells MAH-1 and MAH-2.

gretheholm geothermal plant was opened based on water with a temperature of 73°C.

Despite the encouraging results, a more detailed study of the new Margretheholm wells is required, including correlation with other wells in the Danish area and with the well-known Bunter Sandstein in the German part of the North German Basin to be able to estimate the potential of other sandstone-rich layers in the Bunter reservoir, both in the Copenhagen area and in other places in the southern part of Denmark. Further studies are needed because it has been decided that the Copenhagen area should be CO_2-neutral by 2025. To achieve this goal, the Margretheholm plant is expected to play a major role in the use of geothermal energy for district heating. This will require an expansion of the plant over the next five years. Therefore a more detailed evaluation is necessary, both to minimise the prospected risk and to enhance the optimal use of the subsurface below Copenhagen for geothermal energy.

Future potential – towards a new resource assessment

A more environmentally friendly Denmark has to include geothermal energy as a significant part of the energy supply. It is estimated that the geothermal resources in Denmark can last several hundred years with the present heat consumption, and only a small fraction of this potential is utilised by the two existing geothermal power plants (Mathiesen *et al*. 2009).

A major challenge within geothermal prospecting is to find suitable and sustainable reservoirs (small number of faults and lateral facies changes) and sufficient flow capacity (thickness, porosity and permeability) of warm water. Permeability is critical but difficult to predict since large variations occur depending on the depositional facies, provenance, mineralogical composition, burial history and position in the basin. One of the barriers for a significant increase in the exploitation of the large geothermal resources in Denmark is the geological uncertainty in the exploration phase. This uncertainty is related to the possibility of making accurate and reliable predictions about the presence of high-quality reservoirs with high lateral continuity below the urban areas, where infrastructure and consumers are located. Precise predictions depend not only on existing well and seismic data, which vary highly in density and quality, but also on our understanding of the geological processes that led to the formation of the geothermal reservoirs.

A large, newly funded, multi-disciplinary research project carried out jointly by GEUS, the University of Aarhus, the Geological Survey of Sweden, Deutsches GeoForschungs-Zentrum and DONG Energy aims to assess these challenges in detail in order to encourage the utilisation of geothermal energy by investigating the critical elements in the exploitation of the geothermal resources and integrating the results on a GIS platform. The project will use existing and new geological and geophysical data and methods. By conducting detailed studies of relevant, sandstone-rich reservoirs and the diagenetic processes that affected the reservoirs since deposition, the project will provide new data leading to improved understanding of the spatial variations in the physical characteristics and quality of the reservoirs. New seismic data will be acquired, and interpretations of these data and old data will increase our knowledge about lateral reservoir variations and will form the basis of a new consistent 3-D subsurface temperature model.

Thermal and fluid flow modelling using various schemes of combined production and re-injection wells can provide more detailed information on the thermal resources that can be extracted from the reservoirs and their thermal life-time, and it will be possible to quantify the additional amount of heat that can be extracted from less prospective layers both within and adjacent to the geothermal reservoirs. Traditionally this is not included in estimates of resources, but it will provide higher and more realistic values.

References

Balling, N. 1976: Geothermal models of the crust and uppermost mantle of the Fennoscandian Shield in South Norway and the Danish Embayment. Journal of Geophysics **42**, 237–256.

Mathiesen, A., Kristensen, K., Bidstrup, T. & Nielsen, L.H. 2009: Vurdering af det geotermiske potentiale i Danmark. Danmarks og Grønlands Geologiske Undersøgelse Rapport **2009/59**, 30 pp.

Nielsen, L.H. 2003: Late Triassic – Jurassic development of the Danish Basin and the Fennoscandian Border Zone, southern Scandinavia. In: Ineson, J.R. & Surlyk, F. (eds): The Jurassic of Denmark and Greenland. Geological Survey of Denmark and Greenland Bulletin **1**, 459–526.

Nielsen, L.H., Mathiesen, A. & Bidstrup, T. 2004: Geothermal energy in Denmark. Geological Survey of Denmark and Greenland Bulletin **4**, 17–20.

Authors' address

Geological Survey of Denmark and Greenland, Øster Voldgade 10, DK-1350 Copenhagen K, Denmark. E-mail: *anm@geus.dk*

Distribution and grain size of sand in the Miocene wave-dominated Billund delta, Denmark

Erik S. Rasmussen and Jens Bruun-Petersen

The distribution of sand in deltas depends on the delta regime: wave, fluvial or tidal-dominated delta (Orton & Reading 1993; Bhattacharya & Giosan 2003). During the Early Miocene, three delta complexes built out from the Fennoscandian Shield into the eastern North Sea Basin (Rasmussen 2004). The oldest delta complex, which is informally named the Billund delta, is located in Jylland (Fig. 1). This delta complex was mainly wave-dominated (Rasmussen & Dybkjær 2005; Hansen & Rasmussen 2008; Rasmussen 2009a). Recently, it has been demonstrated that in modern wave-dominated delta environments sand mostly accumulates on the updrift portion of the delta (Fig. 2) whereas alternating mud and sand, e.g. barrier-lagoon complexes, occupy the downdrift portion of the delta system (Bhattacharya & Giosan 2003). The current study shows that most of the sand in the submarine part of the Miocene wave-dominated Billund delta (mainly lower shoreface and delta slope sand) was deposited downdrift to the delta front and thus differs from the foreshore and uppermost shoreface accumulation found in recent delta complexes.

The aim of this study is to map the distribution of submarine delta sand in the Billund delta complex. A detailed understanding of the distribution of delta sand, such as found in this delta complex, is crucial for developing predictive tools in sequence stratigraphy and for seismic interpretation, especially in the application of seismic attribute analysis of the subsurface.

Geological setting

The eastern North Sea Basin was subject to inversion in the Early Miocene (Rasmussen 2009b). The inversion tectonism resulted in high sediment input into the Norwegian–Danish Basin and progradation of delta complexes. During the Early Miocene, the deltas built far out into the basin (Rasmussen 2004) and were predominantly wave-dominated (Rasmussen & Dybkjær 2005; Fig. 1). The Middle – Late Miocene was characterised by deposition of marine, clayey sediments at water depths of more than 100 m (Rasmussen 2009a). At the end of the Late Miocene and during the Pliocene the shoreline prograded several times across Denmark (Rasmussen *et al.* 2008) and reached the central part of the North Sea both during the latest Late Miocene and Late Pliocene.

In the Early Miocene, a warm temperate to subtropical, humid climate prevailed (Larsson-Lindgreen 2009). The subtropical climate continued into the early Middle Miocene, but was succeeded by a marked climatic cooling in the middle Middle Miocene. Apart from an interval in the Early Pliocene the climate was relatively cool during the remaining part of the Neogene. During the Miocene and Pliocene, the region was located in the northern part of the zone of prevailing westerly winds, which led to a high wave energy regime in the eastern part of the North Sea Basin due to the long fetch across the North Sea (Galloway 2002; Rasmussen *et al.* 2008).

Fig. 1. Palaeogeographical reconstruction of the Billund delta. The Billund delta is located in the central part of Jylland.

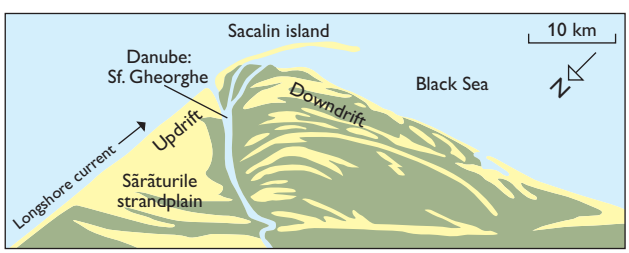

Fig. 2. Example of a modern wave-dominated delta. Note the amalgamation of beach ridges on the updrift portion of the delta, and spits and barriers that enclose lagoons on the downdrift flank. Yellow: sand. Green-grey: mud. Modified from Bhattacharya & Giosan (2003).

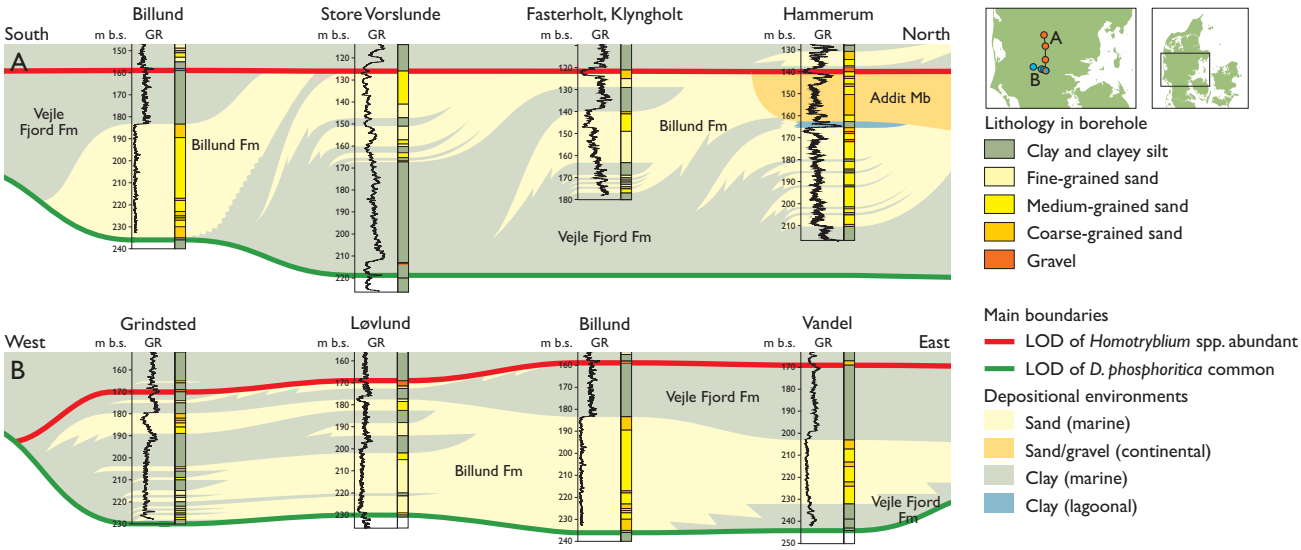

Fig. 3. Two correlation panels of the Billund Formation. **A**: N–S correlation panel showing a strike section of the Billund Formation. The length of the profile is *c.* 45 km. **B**: E–W correlation panel showing a cross section of the Billund Formation. The length of the profile is *c.* 20 km. **GR**: gamma-ray log. **LOD**: last occurrence datum. **m b.s.**: m below surface.

Sand distribution in the Billund delta

The development of the Billund delta complex was studied from high-resolution seismic data and borehole data. The delta complex was deposited during a period of a high rate of sediment supply (Rasmussen 2009a). Based on a number of boreholes drilled in central Jylland it is possible to reconstruct the Billund delta system in the area. The N–S-orientated correlation panel shows a series of sand-rich lobes prograding across clay-rich successions (Fig. 3A). The gamma-ray log of the sand-rich units shows a serrated pattern, with generally decreasing values upwards. The grain size is dominated by fine- to medium-grained sand with the latter dominating in the upper part of the succession. Coarse-grained sand and gravel occur in the uppermost part (Fig. 3A). At the northernmost borehole, the upper part is characterised by coarse-grained sand overlain by a succession of alternating fine- and medium-grained sand. The log pattern at this site is characterised by generally upward increasing gamma-ray values (Fig. 3A). The sand was deposited in clinoforms, with a dip of 7–10° according to seismic data (Hansen & Rasmussen 2008; Rasmussen 2009a). Locally, at the top of the clinoformal package, erosive features are seen with concave-upward structures that are filled with a succession showing transparent or subparallel reflection patterns (e.g. Rasmussen 2009a).

The updrift part of the delta complex is represented by the Løvlund and Grindsted boreholes (Fig. 3B). At these sites alternating sand- and mud-rich successions dominate. The 10–20 m thick sand-rich part is dominated by grey, fine-grained sand. Medium- to coarse-grained sand occurs in the upper part. In the westernmost borehole, at Grindsted, the lower part is dominated by 1–2 m thick sand-rich deposits intercalated in a mud-dominated succession. Large cuttings show that a substantial part of the succession at this site consists of alternating thin sand beds and clay layers. The sand beds are normally graded.

The downdrift flank of the delta complex is characterised by grey, medium- to coarse-grained sand. Pebbles are common and clasts with diameters up to 2 cm have been found. The sand-rich succession is 20–50 m thick (Fig. 3B), but seismic data indicate a thickness up to 75 m immediately north of the Billund well (Hansen & Rasmussen 2008). Thin mud layers have been found in a few samples, but mud is not a common lithology.

Depositional environment

A prograding depositional system is indicated by the sedimentary succession characterised by S–SW- dipping clinoforms and the general coarsening-upward trend seen in the boreholes (Fig. 3). The mud-dominated part of this prograding system is dominated by marine palynomorphs (Dybkjær 2004). Their concentration decreases upward, indicating a shallowing-upward succession with increasing terrestrial influence. The fining-upward succession found in the upper part of the Hammerum well is interpreted as fluvial channel deposits (Rasmussen *et al.* 2006; Rasmussen 2009a).

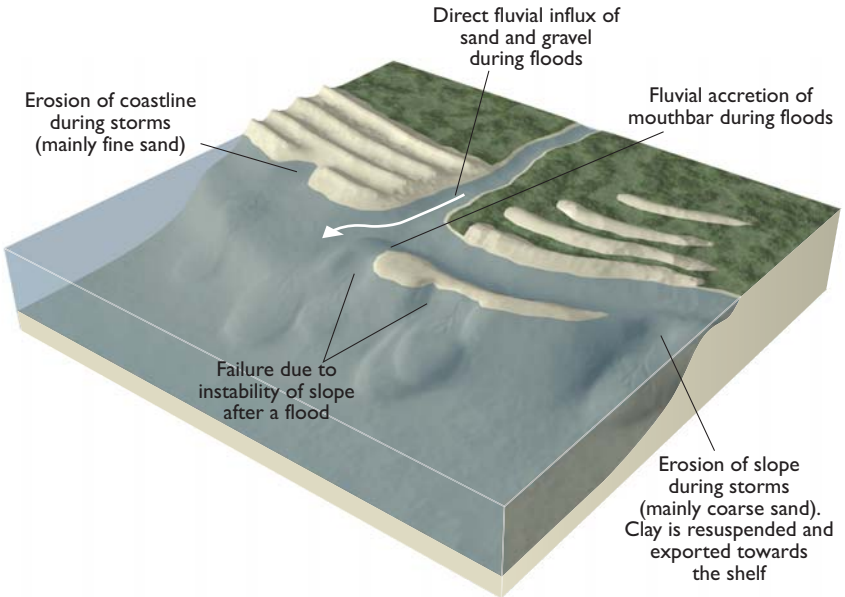

Fig. 4. Depositional model for a wave-dominated delta showing typical areas with erosion and deposition. At the river mouth fluvial sand accretes to the mouth bar, with high potential for slope failure. Direct influx of sediment onto the delta slope may occur during floods. In the downdrift portion of the delta front wave-reworked sand (relatively coarse-grained) forms spits and barriers that may be eroded during storms. On the updrift flank fine- to medium-grained sand is deposited as beach ridges which are a source of sediment supply to the delta slope. Consequently, finer-grained sand is deposited in this area.

A prograding system overlain by fluvial channels (Hansen & Rasmussen 2008; Rasmussen 2009a) indicates a deltaic depositional environment. The development of spits and barrier complexes south-east of the main area of progradation implies a depositional system characterised by longshore transport of sediment (Rasmussen & Dybkjær 2005). The predominance of storm deposits with hummocky and swaley cross-stratification and other types of tempestites (Rasmussen & Dybkjær 2005) indicates a wave-dominated delta front.

In the modern wave-dominated Rhône Delta, sediment (sand) transport to the delta platform and prodelta slope occurs in two ways (Maillet *et al.* 2006). (1) During storms, erosion of the foreshore and upper shoreface leads to transport of sand partly to the outer delta platform and partly to the delta slope and (2) during floods, sand is transported in migrating dunes from the fluvial system towards the mouth bar. Sand accumulations at the slope break of the delta platform may destabilise the area by increasing the angle of the delta slope (the equilibrium profile). Slope failure may result from the steepened slope or from changes in pore-water pressure due to wave action, resulting in deposits being shed directly down the delta front as mass-flow deposits. High sediment supply to the Billund delta occurred from the rivers (Rasmussen 2009a). The supply was probably dominated by bedload transport as indicated by the braided channels that dominated the fluvial system feeding the delta (Rasmussen *et al.* 2006). Therefore, migration of dunes towards the delta platform was more effective than in the modern Rhône Delta, where man-made constructions have significantly reduced the sediment influx to the delta. Direct sediment supply from the fluvial system to the Billund delta complex is indicated by the occurrence of large clasts, up 2 cm, in the lower part of the delta slope. Such large clasts have never been reported from Miocene shoreface deposits (e.g. Rasmussen & Dybkjær 2005) indicating that the hydro-dynamic conditions in the shoreface zone was unfavourable for transport of clasts of that size. The central and the downdrift parts of the Billund delta slope were thus dominated by sedimentation of medium- to coarse-grained sand with its source in the main river system. Failure at the mouth bar, spit and downdrift beach thus sourced sediments for deposition on the delta slope (Fig. 4). The deposition of graded, predominantly fine-grained, sand beds in the updrift part of the delta complex indicates sedimentation from suspended sand clouds generated by storms or from diluted turbidity currents (Fig. 4). The finer-grained character here reflects that the source was the stacked beach ridges from the updrift flank of the delta. The sand in this part of the delta has been effectively sorted during transport along the shoreline before deposition and is therefore finer grained. For example, the barrier and spit systems of the Billund delta found 25 km south-east of the main delta consists of fine- to medium-grained sand with few intercalations of gravel (Rasmsussen & Dybkjær 2005). The clasts of the intercalated gravel layers do not exceed 5 mm.

Discussion

The distribution of sand in recent wave-dominated deltas is characterised by coherent sand accumulation, e.g. amalgamated beach ridges in the updrift portion of the delta complex (Fig. 2; Bhattacharya & Giosan 2003). The downdrift

flank is commonly dominated by river-borne clay and sand deposited in lagoons protected by spits and barriers. A different pattern of sand distribution is seen in the Billund delta where most of the sand was deposited in a downdrift position of the main delta (Fig. 4). This different depositional pattern can be explained by both the depositional environment and the geological setting. The Billund delta prograded into a basin with relatively deep water (*c.* 100 m) and the delta front was relatively steep (*c.* 7–10°; Hansen & Rasmussen 2008). Fluvially transported, coarse-grained sediments were at times shed directly down the delta slope as mass-flow deposits (Fig. 4). The high-wave energy regime in the region and the high frequency of storms also enhanced sand transport downdrift of the main delta lobe and some of this was directed offshore beyond the delta slope break and deposited in deeper water (Fig. 4). The distribution of submarine sand in the downdrift setting is important, because foreshore and uppermost shoreface sediments are rarely preserved in the geological record. Therefore, in deltaic systems of the same character as the Billund sand, with steeply dipping, 50–100 m high and asymmetric clinoforms, the reservoir sand is most likely found in the downdrift portion of the wave-dominated delta. This type of delta is best developed in a ramp setting that has undergone a tectonic phase, which resulted in a sudden increase in accommodation space, and is characterised by a high sediment supply due to the formation of a high relief in the hinterland. In such a setting, the fluvial system is dominated by bed-load transport and migration of dunes to the delta front is a common phenomenon. The proportion of river-borne sediment is also important. Longshore currents and wave processes can move the fine-grained fraction downdrift and offshore and thereby lead to concentration of sand on the main delta platform.

Acknowledgements

Environment Centres Ribe, Ringkøbing and Århus are thanked for financial support.

References

Bhattacharya, J. P. & Giosan, L. 2003: Wave-influenced deltas: geomorphological implications for facies reconstruction. Sedimentology **50**, 187–210.

Dybkjær, K. 2004: Dinocyst stratigraphy and palynofacies studies used for refining a sequence stratigraphic model – uppermost Oligocene to lower Miocene, Jylland, Denmark. Review of Palaeobotany and Palynology **131**, 201–249.

Galloway, W.E. 2002: Paleogeographic setting and depositional architecture of a sand-dominated shelf depositional system, Miocene Utsira Formation, North Sea. Journal of Sedimentary Research **72**, 447–490.

Hansen, J.P.V. & Rasmussen, E.S. 2008: Structural, sedimentologic, and sea-level controls on sand distribution in a steep-clinoform asymmetric wave-influenced delta: Miocene Billund Sand, eastern Danish North Sea and Jylland. Journal of Sedimentary Research **78**, 130–146.

Larsson-Lindgren, L. 2009: Climate and vegetation during the Miocene – evidence from Danish palynological assemblages. Litholund theses 19, 20 pp. + 3 appendices.

Maillet, G.M., Vella, C., Berné, S., Friend, P.L., Amos, C.L., Fleury, T.J. & Normand, A. 2006: Morphological changes and sedimentary processes induced by the December 2003 flood event at the present mouth of the Grand Rhône River (southern France). Marine Geology **234**, 159–177.

Orton, G.J. & Reading, H.G. 1993: Variability of deltaic processes in terms of sediment supply, with particular emphasis on grain size. Sedimentology, **40**, 475–512

Rasmussen, E.S. 2004: Stratigraphy and depositional evolution of the uppermost Oligocene – Miocene succession in western Denmark. Bulletin of the Geological Society of Denmark **51**, 89–109.

Rasmussen, E.S., 2009a: Detailed mapping of marine erosional surfaces and the geometry of clinoforms on seismic data: a tool to identify the thickest reservoir sand. Basin Research **21**, 721–737.

Rasmussen, E.S. 2009b: Neogene inversion of the Central Graben and Ringkøbing–Fyn High, Denmark. Tectonophysics **465**, 84–97.

Rasmussen, E.S. & Dybkjær, K. 2005: Sequence stratigraphy of the Upper Oligocene – Lower Miocene of eastern Jylland, Denmark: role of structural relief and variable sediment supply in controlling sequence development. Sedimentology **52**, 25–63.

Rasmussen, E.S., Dybkjær, K. & Piasecki, S. 2006: Neogene fluvial and nearshore marine deposits of the Salten section, central Jylland, Denmark. Bulletin of the Geological Society of Denmark **53**, 23–37.

Rasmussen, E.S., Heilmann-Clausen, C., Waagstein, R. & Eidvin, T. 2008: The Tertiary of Norden. Episodes **31**, 66–72.

Authors' addresses

E.S.R., *Geological Survey of Denmark and Greenland, Øster Voldgade 10, DK-1350 Copenhagen K, Denmark*. E-mail: *esr@geus.dk*

J.B.-P., *Environment Centre Ribe, Sorsigvej 35, DK-6760 Ribe, Denmark.*

3-D geological modelling of the Egebjerg area, Denmark, based on hydrogeophysical data

Flemming Jørgensen, Rasmus Rønde Møller, Peter B.E. Sandersen and Lars Nebel

Contamination of groundwater with pesticides and nitrate has compelled the Danish Government to launch a major hydrogeological mapping programme covering about 40% of the land area of Denmark. Numerous geophysical surveys are currently being carried out in order to acquire the necessary data. These new data are crucial for the 3-D geological models that are used in the planning of future water supply and landuse. Normally, site-specific groundwater protection zones (Thomsen *et al.* 2004) are based on groundwater-modelled catchment areas for each well, but proper 3-D geological models are needed in order to create a valid basis for the groundwater models. Since most of the Danish near-surface geology is complex, a full geological understanding is required combined with in-depth interpretation of geological and geophysical data.

Much research has dealt with geophysical mapping and numerical groundwater modelling, but only limited research has combined these topics for geological modelling. Prior to geophysical mapping, groundwater models were based on simple data extraction from well databases without inclusion of geophysical data. In the following, a concept for detailed 3-D geological modelling with hydrogeophysical data is presented for a specific area.

Data and study area

The 150 km^2 area for modelling is located in Jylland (Fig. 1). The surface is dominated by clayey tills and reaches an elevation of more than 160 m above sea level.

Prior to the geophysical survey, the only useful data for a geological model in this area came from boreholes. Lithological descriptions were only available for 50–75% of the boreholes, and the boreholes were too widely spaced to provide an overview of the subsurface geology. Hence a detailed geological model could not be constructed.

Two geophysical methods were employed in the model area, the airborne transient electromagnetic method (SkyTEM; Sørensen & Auken 2004) and the pulled array continuous electrical sounding method (PACES; Sørensen 1996). The SkyTEM survey was to map the deeper sections of the subsurface down to depths of 200 m, while the PACES survey focused on the uppermost 25 m. Both surveys were conducted along lines with a spacing of 250 m. The heterogeneity in the shallowest parts of the subsurface is commonly too great to obtain a proper correlation between the PACES survey lines, but at larger depths a better correlation is achieved by the SkyTEM data. By combining SkyTEM and borehole data a solid basis for geological modelling was obtained in the study area.

Model concept

A three-step approach for 3-D geological modelling used for hydrogeological purposes has recently been developed in Denmark (Jørgensen *et al.* 2008). With this approach the modelling both ensures a thorough data interpretation and utilises the potential that lies in establishing an understanding of the geological history. The approach divides the geological model into three submodels:

1. A general, conceptual geological model which is primarily descriptive and imaged in conceptual cross-sections. The conceptual geological model is based on a review of former work and existing literature.

Fig. 1. Map of Denmark showing the location of the study area, Egebjerg, north of the city of Horsens.

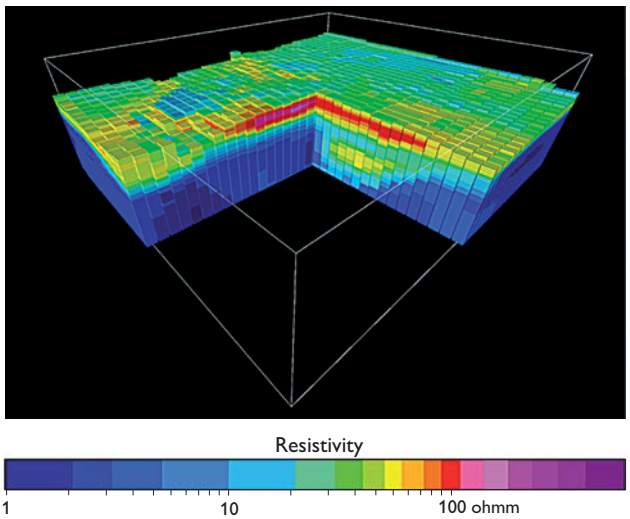

Fig. 2. Selected section of the SkyTEM resistivity voxel grid. Cell size: 100 × 100 × 5 m.

2. A 3-D geological model, which is intended to serve as a geological database for a given model area and may contain all kinds of geological information, both lithological and stratigraphical. The 3-D model is not necessarily established in areas with poor data coverage.
3. A 3-D hydrostratigraphic model, which is intended to serve as the input for numerical groundwater models. This model is based on the 3-D geological model but focuses on lithological and hydraulic parameters. Normally it will cover the entire model space, incorporating a 'best guess' in areas with poor data coverage.

Traditional 3-D geological models for hydrogeological purposes are constructed as layer-cake models, where the layers are defined as the volume between two surfaces. Elements in such models are thus defined by bounding surfaces. The surfaces are defined by digitised points and/or interpolated grids from the digitised points. Such models do not require advanced modelling software, but critical restrictions may arise in areas of complex geology where layer variations may be difficult or impossible to model (Turner 2006).

As the geology in Denmark is rarely organised as well-defined layers and hence cannot be properly described in a layer-based model, a different approach is needed. The challenge is to resolve heterogeneity to a degree that meets the demands of the user, e.g. numerical groundwater modelling. One way to do this is by 'voxel' (voxel = volumetric pixel) modelling (e.g. Turner 2006).

Due to the high complexity in the Egebjerg area voxel modelling has therefore been implemented and tested here. The voxel discretisation is 100 × 100 m in the X–Y direction and 5 m in the Z direction resulting in a 3-D voxel grid

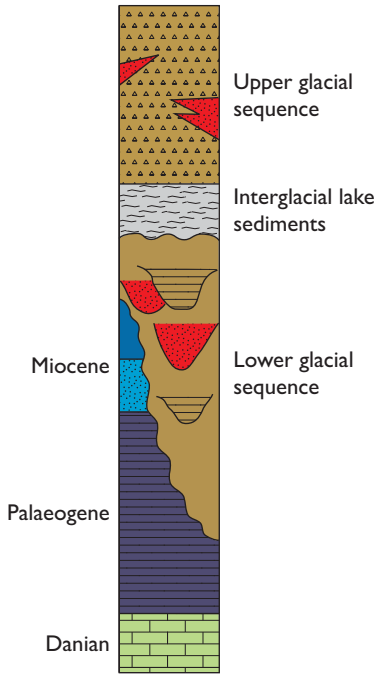

Fig. 3. Stratigraphical log for the model area. The thickness of the entire section corresponds to about 200 m. For explanation see the text.

composed of 1.5 million voxels organised in 74 voxel layers. As the SkyTEM data cover large parts of the area, a resistivity grid with discretisation and dimensions identical to the voxels is generated, basically supplying the voxel grid with a resistivity value (Fig. 2). The voxel model is supplemented by a number of layer boundaries modelled as surfaces. These layer boundaries are based on digitised point swarms and interpolated to contoured 2-D grids. The software package GeoScene 3D (I-GIS 2010) is used for the modelling.

The Egebjerg model follows the three-step approach for geological modelling as described above, but minor adjustments were required in order to make use of the voxel model approach. The chosen model concept is as follows:

1. A general, conceptual geological model identical to the one described in the three-step approach above.
2. A 3-D stratigraphical model, in which the geological history of the model area is in focus. Geological elements, structures and stratigraphical boundaries are modelled and subdivided according to their origin. The geological elements comprise boundaries such as Top Chalk, Top Palaeogene, erosional unconformities, stratigraphical units such as Palaeogene and Miocene, buried tunnel valleys, glaciotectonic complexes and interglacial units. This model is a combined layer-based and voxel model and is generally comparable to the 3-D geological model within the three-step approach.

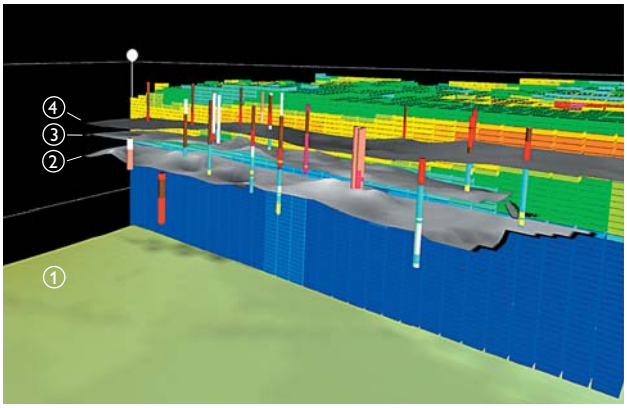

Fig. 4. 3-D stratigraphical model section showing from below the boundaries of Top Chalk (**1**: green surface), Top Palaeogene (**2**: lower grey surface), an internal Miocene boundary (**3**: middle grey surface) and the pre-Quaternary surface (**4**: upper grey surface). Boreholes and the SkyTEM resistivity grid are also shown. Vertical exaggeration: 5 times.

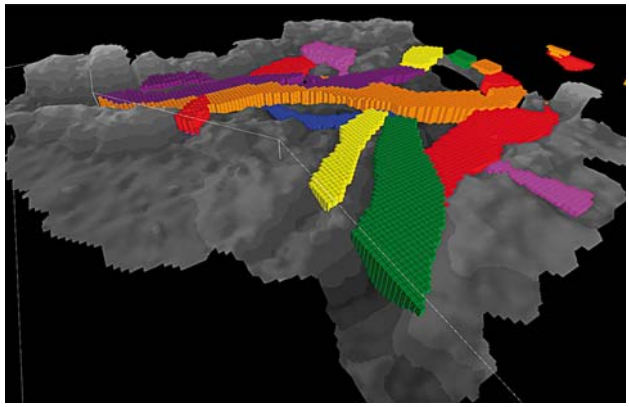

Fig. 5. A series of buried tunnel valleys modelled by voxels in the 3-D stratigraphical model: Each colour represents one buried tunnel valley. The Palaeogene surface is shaded in grey. Vertical exaggeration: 5 times.

3. A 3-D lithofacies model that is entirely voxel based, and in which all voxels are allocated an attribute for lithofacies. The model is based on the 3-D stratigraphical model. A challenge here is to estimate the lithofacies in heterogeneous areas or areas with poor data coverage. A qualitative approach for uncertainty assessment of the interpretations is used and attributed to each voxel in order to visualise the overall model uncertainties (Sandersen 2008). This is important in connection with the subsequent implementation in a numerical groundwater model. The uncertainty approach is also applied to the 3-D stratigraphical model.

Model results

The geological modelling resulted in the stratigraphical log shown in Fig. 3. It comprises a Tertiary sequence followed by glacial and interglacial sediments above the pre-Quaternary surface. This surface unconformably cuts layers of Miocene clay, silt and sand, and Palaeogene clay, which in turn overlie Danian limestone at depths of about 200 m. Only one borehole in the area reaches the limestone, but in some areas, where the SkyTEM soundings penetrate the Palaeogene clay, the limestone is seen as a layer with slightly elevated resistivity values. The Palaeogene clay shows high electrical conductivity and responds as a distinct and well-defined surface in the SkyTEM data. Erosional remnants of Miocene deposits are only found in minor parts of the study area. A model section showing parts of the pre-Quaternary sequence is shown in Fig. 4.

The Quaternary sequence is divided into an upper glacial/interglacial sequence and a lower glacial sequence. Several buried valleys are present within the lower glacial sequence, and at least four generations occur here. The valleys are interpreted as tunnel valleys (*sensu* Jørgensen & Sandersen 2006), and the sequence comprises a complex setting of cross-cutting valleys that have repeatedly been incised and filled. The valleys are primarily filled with till and glaciolacustrine clay but coarse meltwater deposits also occur. The valleys are modelled by voxels due to their high spatial complexity (Fig. 5).

In the SkyTEM data, the lower glacial and upper glacial/interglacial sequences are divided by an apparently widespread, gently undulating resistivity boundary that is considered to be an erosional unconformity. This unconformity appears as a widespread and more or less horizontal contrast in the resistivity data; with alternating high and low resistivity values on each side of the boundary. Above the unconformity a unit of interglacial diatomaceous lake sediments is found in boreholes. Pollen analyses show that these sediments were deposited during the Holsteinian interglacial (Odgaard 2010), and the erosional unconformity and the glacial sequence below, including most of the tunnel valleys, are therefore of Elsterian age or older.

Some subareas in the study area are glaciotectonically deformed. This is seen where Tertiary clay is found above glacial sediments in the boreholes. These large rafts of Palaeogene clay, only indicated by a few boreholes, are well resolved in the SkyTEM data. The deformed layers are in some places found inside the buried tunnel valleys showing that the deformation took place after the valley formation.

The 3-D stratigraphical model as described above is used as the basis for the construction of the 3-D lithofacies model. Some units in the 3-D stratigraphical model are more or less directly converted to lithofacies, but other units are subdivided, merged or reordered prior to incorporation into the

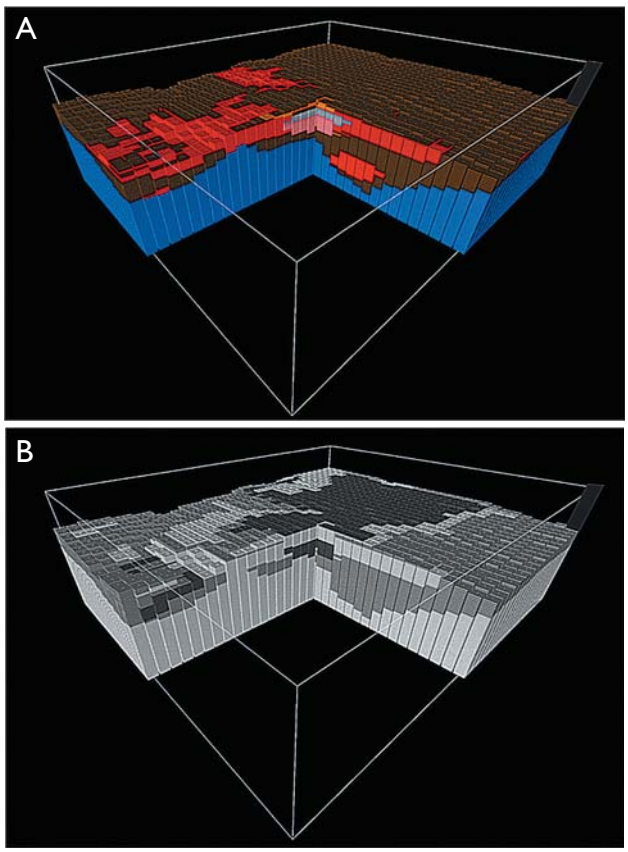

Fig. 6. Selected section of the 3-D lithofacies model (identical to Fig. 2). **A**: The lithofacies voxel model. Blue: Palaeogene clay. Dark brown: clay till. Light brown: sand till. Red: meltwater sand/gravel. Light red: sand. Grey: diatomite. **B**: Uncertainty of the lithofacies model. Light grey: low uncertainty. Grey: medium uncertainty. Dark grey: high uncertainty. Vertical exaggeration: 3 times.

3-D lithofacies model. A selected part of the model and its corresponding uncertainty is shown in Fig. 6.

Concluding remarks

In the Egebjerg study area detailed stratigraphical and lithological information has been obtained by studying 3-D resistivity grids based on the SkyTEM data and evaluating these against borehole data. In order to make full use of the new information for numerical groundwater modelling or for other purposes, the data have been incorporated in a 3-D geological model. The 3-D modelling was carried out in two steps, where two differently focused 3-D models were constructed. First a 3-D model focusing on stratigraphy was constructed and subsequently, based on this, a 3-D lithofacies model was constructed. This approach enables in-depth geological interpretation and secures maximum utilisation of the large data sets. The heterogeneous geology revealed by the SkyTEM data cannot be sufficiently incorporated into a simple layer-based model, and a combination of a voxel and a layer model has therefore proven successful for the Egebjerg study area.

Acknowledgements

The project is supported by Environment Centre Aarhus. We thank Klaus Petersen and Stine Rasmussen for helpful discussions.

References

I-GIS 2010: GeoScene 3D. http://www.i-gis.dk/Default.aspx?tabid=132.

Jørgensen, F. & Sandersen, P.B.E. 2006: Buried and open tunnel valleys in Denmark – erosion beneath multiple ice sheets. Quaternary Science Reviews **25**, 1339–1363.

Jørgensen, F., Kristensen, M., Højberg A.L., Klint, K.E.S., Hansen, C., Jordt, B.E. Richardt, N. & Sandersen, P. 2008: Opstilling af geologiske modeller til grundvandsmodellering. Geo-Vejledning **3**, 176 pp. Copenhagen: Geological Survey of Denmark and Greenland.

Odgaard, B. 2010: Pollenanalytisk datering af ferskvandsaflejring i DGU nr. 107.733, Horsens Vandværk, 2 pp. Unpublished report, Aarhus Universitet, Danmark.

Sandersen, P.B.E. 2008: Uncertainty assessment of geological models – a qualitative approach. In: Refsgaard, J.C. *et al*. (eds): Calibration and reliability in groundwater modelling: credibility of modelling. International Association of Hydrological Sciences Publication **320**, 345–349.

Sørensen, K. 1996: Pulled array continuous electrical profiling. First Break **14**, 85–90.

Sørensen, K.I. & Auken, E. 2004: SkyTEM – a new high-resolution helicopter transient electromagnetic system. Exploration Geophysics **35**, 191–199.

Thomsen, R., Søndergaard, V.H. & Sørensen, K.I. 2004: Hydrogeological mapping as a basis for establishing site-specific groundwater protection zones in Denmark. Hydrogeology Journal **12**, 550–562.

Turner, A.K. 2006: Challenges and trends for geological modelling and visualisation. Bulletin of Engineering Geology and the Environment **65**, 109–127.

Authors' addresses

F.J. & R.R.M., *Geological Survey of Denmark and Greenland, Øster Voldgade 10, DK-1350 Copenhagen K, Denmark*. E-mail: *flj@geus.dk*

P.B.E.S., *Grontmij | Carl Bro A/S, Dusager 12, DK-8200 Århus N, Denmark*.

L.N., *I-GIS, Voldbjergvej 14, 2., DK-8240 Risskov, Denmark*.

Late Quaternary geology of a potential wind-farm area in the Kattegat, southern Scandinavia

Jørgen O. Leth and Bernhard Novak

Following the proposal of the offshore Anholt wind-farm project with an energy capacity of 400 megawatt in the Kattegat, southern Scandinavia, an evaluation of the geotechnical properties of the subsurface of the area is required. As a first step to map the seabed geology the Geological Survey of Denmark and Greenland (GEUS) conducted a geophysical survey (Leth *et al.* 2009) which, together with cone penetration tests and data from boreholes, lead to a greater understanding of the geological architecture and development of the 144 km^2 survey area (Figs 1, 2).

Methods

We used a multibeam echo-sounder for detailed mapping of the bathymetry, and shallow seismic equipment and coring to map the shallow seabed geology including the distribution and thickness of the main geological units. A combination of two seismic devices (chirp and sparker systems) was chosen to ensure good penetration and high resolution. The sparker system provides data from the sea floor down to about 45 m into the seabed with a vertical seismic resolution in the order of 50 cm, while the chirp system provides high-resolution seismic data from the upper 5–10 m of the seabed with a vertical seismic resolution at decimetre scale. A side-scan sonar was used for mapping of surface sediments. At seven sites, boreholes were made to a depth of 40 m and selected intervals sampled. Cone penetration tests were carried out at the same sites (Fig. 2) and surface sediment samples collected for biological studies.

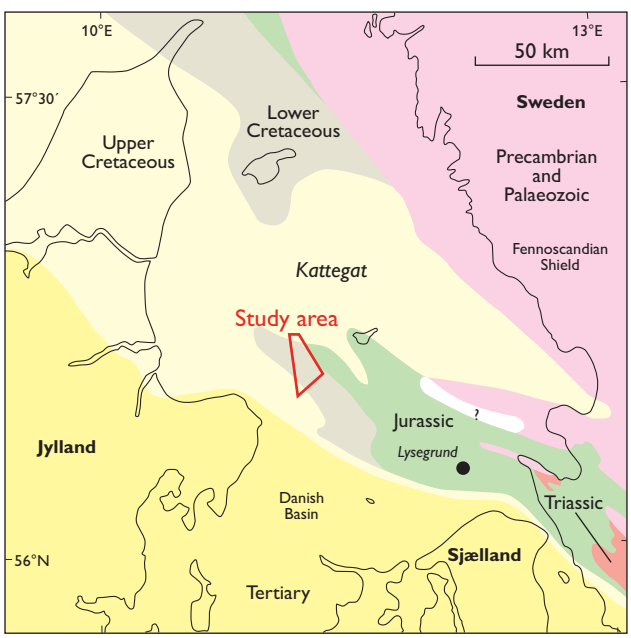

Fig. 1. Pre-Quaternary geology of the Kattegat. Redrawn and simplified from Lykke-Andersen *et al.* (1993).

Geological setting and seabed

The Kattegat region is located in the transition zone between the Fennoscandian Shield and the Danish Basin (Fig. 1), and studies of the pre-Quaternary surface morphology show that the NW–SE-trending anticlinorium follows the trend of

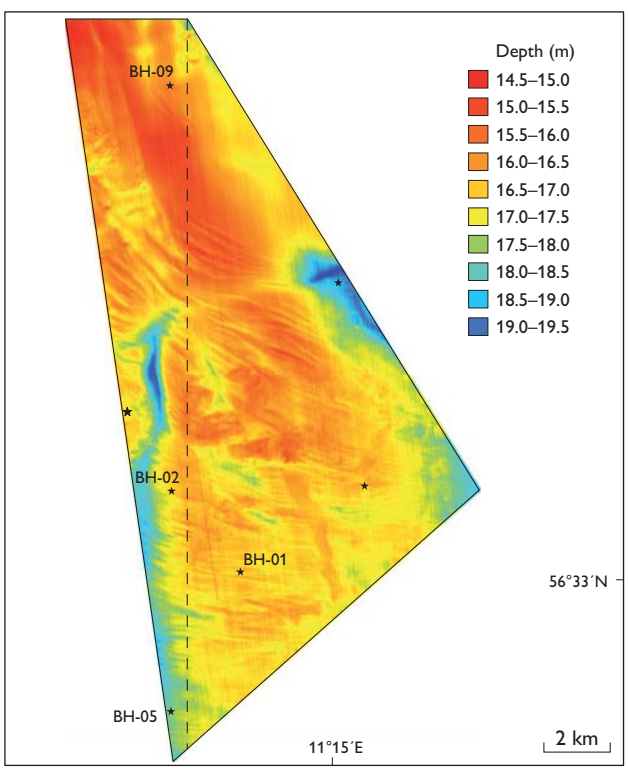

Fig. 2. Bathymetry of the survey area. The stars show sites with combined coring and cone penetration tests. The dashed line shows the position of the profile in Fig. 3.

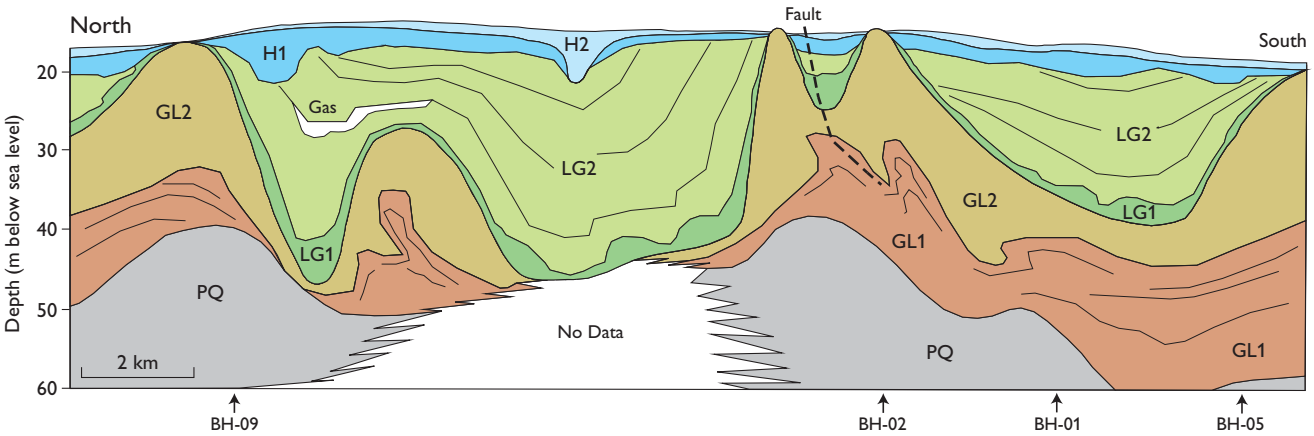

Fig. 3. Schematic model of the seismic units based on a N–S-trending section along UTM 634000 mE (WGS84). The unit names refer to descriptions in the text. The boreholes (BH-01, BH-02, BH-05 and BH-09) are located at distances from 400 m to 1.5 km from the profile (Fig. 2).

dextral wrench faults that have repeatedly affected the Fennoscandian Border Zone (Lykke-Andersen *et al.* 1993). The latest major tectonic event was an inversion episode which started in the Late Cretaceous. After that inversion the Kattegat became an area of non-deposition and net-erosion until net-sedimentation was resumed in the Saalian. At that time the basin floor of the Kattegat was characterised by strongly undulating relief controlled by large- and small-scale structures in the pre-Quaternary basement.

The survey area can be divided into several subareas, based on bathymetry and seabed sediment types (Fig. 2). The northern part of the survey area is smooth, with sand and silt. The central and southern parts show ridges with a relief of more than 1 m. It is suggested that the ridges were formed by waves at a time of lower than present sea level (Leth *et al.* 2009). The area with the highest density of gravel and boulders corresponds to the shallowest part of the central survey area. The boulders are generally located in arc-like, NW–SE-striking, narrow structures found mainly in the southern and western parts of the survey area (Figs 1, 2). Depths over 18 m characterised by sand and silt with pebbles occur near the western and eastern margins of the survey area.

Pre-Quaternary strata – Unit PQ

The pre-Quaternary surface is a regional erosional unconformity with high amplitude seismic reflection. The reflector has been mapped throughout the area down to the limit of the penetration of the sparker system at *c.* 60 m below sea level (b.s.l.; Figs 3, 4D). The pre-Quaternary surface lies deeper than 60 m b.s.l. in the eastern part of the area.

Two boreholes penetrated several metres of pre-Quaternary silty, fine sand. Analysis of palynomorphs in two samples yielded an Upper Cretaceous age (K. Dybkær and E. Sheldon, personal communication 2009).

Glacial deposits – Unit GL

The glacial deposits have been divided into two subunits, GL1 and GL2. The lower subunit GL1 is found in the central and southern parts of the survey area. It shows a characteristic medium- to low-amplitude, parallel, wavy and chaotic seismic pattern. The parallel or wavy pattern is interpreted as representing undisturbed sorted and layered sediments, whereas the wavy or chaotic pattern is interpreted as representing glacially dislocated sediments. A unit with a similar seismic character as GL1 has been found in various parts of the Kattegat, and has been referred to the Late Saalian, Eemian and Middle Weichselian (Vangkilde-Pedersen *et al.* 1993). Marine and glaciogene sediments of these ages have been recorded in sediment cores from other parts of the Kattegat region (Larsen *et al.* 2009).

The transition to seismic subunit GL2 is sharp in the southern part of the survey area, whereas it is more gradual in the central part. Internally GL2 shows a medium- to high-amplitude, seismic facies pattern that is chaotic, mounded and channelled. Low-angle oblique reflectors cutting through the whole subunit are interpreted as large-scale, glaciotectonic deformation structures. Data from sediment samples show that the subunit mainly consists of sand with poorly and well-sorted layers of clay, silt and gravel. A high density of cobbles and boulders is seen where GL2 crops out on the sea floor, as confirmed by surface samples (Fig. 4A). A unit showing a similar seismic pattern and with similar deposits from the Lysegrund area (Fig. 1) has been interpreted as subglacial and glaciofluvial deposits. The GL2 subunit probably corresponds to the M3 unit at Lysegrund, which consists of ice-margin sediments deposited during the retreat stage of the Main Advance (Novak 1996). The seismic pattern, facies association, unit morphology, sea-floor character and lithology all suggest that GL2 represents similar ice marginal deposits.

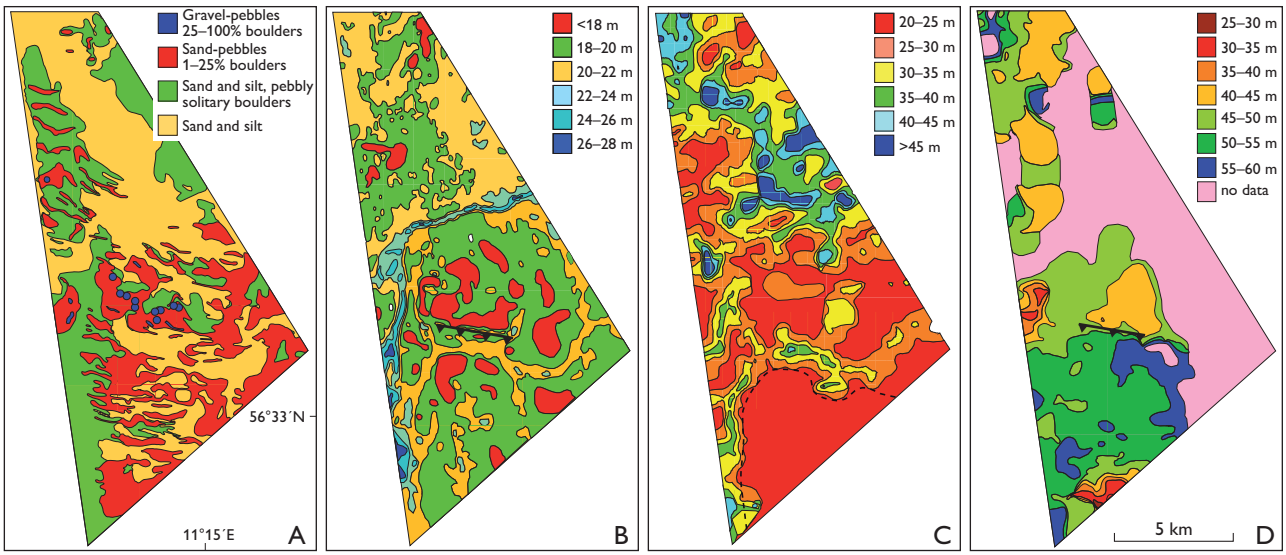

Fig. 4. Maps showing seabed sediments and three seismic stratigraphic levels. **A**: Seabed sediment types. **B**: Depth of base Holocene. Black line indicates fault. **C**: Depth to the top of the glacial deposits. The dashed line shows the disturbed–undisturbed GL1 interface (see text). **D**: Pre-Quaternary surface morphology. Black line indicates fault.

Late glacial deposits – Unit LG

The distribution of the late glacial seismic unit LG is governed by the morphology of the underlying glacial surface (Fig. 4C). Its maximum thickness is 45 m. Towards the south the depressions in the glacial surface are characterised by shallow channels and small basins, and it is possible to correlate these depressions to a system of elongated fault-related basins in the pre-Quaternary surface SW of Anholt (Binzer & Stockmarr 1994).

The seismic unit LG is subdivided into two subunits, LG1 and LG2, with a gradational boundary. LG1 shows an external apron or mound morphology with internal composite mounds as well as a hummocky, shingled, parallel reflection pattern. At its base, LG2 shows an onlap-downlap, draping style. Upwards it shows a gradually decreasing amplitude and a more pronounced semi-transparent, parallel seismic facies. In general, LG2 terminates upwards into an erosional unconformity. A seismic 'blacking out' area internally in LG2 indicates gas content in a discrete level associated with a pronounced reflector that probably represents a sealing clay layer.

Data from boreholes show that unit LG consists of a fining-upward sequence with sand and gravel at its base and layers of clay with sand and silt laminae towards its top. The characteristic seismic expressions of unit LG have also been recorded from other parts of southern Kattegat. For instance, Jensen *et al.* (2002) reported two stages in a Late Glacial unit located in elongated fault-related basins and suggested that the two stages are related to re-activation of normal fault activity in the elongated depressions in the period from 15 to 13.5 calendar ka BP.

Holocene deposits – Unit H

The transition from the late glacial to the Holocene unit H is seen as a shift to high-amplitude reflectors. Truncation of the rhythmic parallel facies of LG2 is succeeded by mounds, hummocky oblique and sub-parallel reflector patterns in the Holocene subunit H1. This subunit was previously referred to the Late Glacial (Leth *et al.* 2009), but after reassessment of the abrupt changes in the seismic signature and its distribution we conclude that the subunit is of early Holocene age. In the southern part of the survey area, 400–600 m wide channels orientated WSW–ENE and SSW–NNE are filled with Late Glacial and early Holocene (H1) deposits. The base level of H1 in these channels is around 22 m b.s.l. H1 is deposited above the truncated LG2 unit and its distribution is confined by the older LG basins. The same base level is found in wider areas in the north and is likewise unconformable to the underlying LG unit. A significantly deeper channel crosses the central survey area with internal seismic structures that indicate a unidirectional flow from west to east (H2; Fig 3). The base of this channel is generally at 26–28 m b.s.l. Locally the channel widens to 1000 m.

Organic-rich sediments of Holocene age representing a lowstand at 35 m b.s.l. are well-known from the Kattegat area. After a fluvial event west of Lysegrund the water level stabilised at 34 m b.s.l. (Novak & Björk 1998). Lagoonal deposits overlying truncated, rhythmic, Late Glacial clay-sand layers are found south-east of the survey area (Bennike *et al.* 2000; Novak & Pedersen 2000). In a major area these sediments are mostly found between 35 and 24 m b.s.l. and have been dated to the early Holocene (Bennike *et al.* 2000).

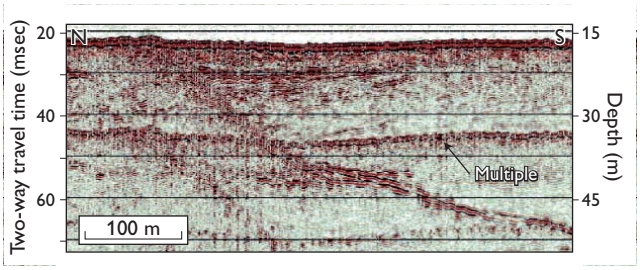

Fig. 5. Part of the N–S-orientated seismic profile AW039 showing a fault that dips to the south. A ridge is seen along the top of the fault. Note the subsidence of the seabed above the fault.

Lagoonal sediments at 18 m b.s.l., found 30 km east of the study area, were also dated to the early Holocene (Novak & Pedersen 2000).

At most sites H2 only represents a veneer of fine- to coarse-grained sand with gravel, occasionally with silt and clay laminae as well as shell fragments of marine molluscs. However, in one of the samples marine shells and organic material are found at 9 m below the sea floor. It is suggested that the Early Holocene transgression reached a level high enough to submerge the survey area prior to 9.9 calendar ka BP. A channel in the central part of the survey area drained towards the east.

Structural features

In the central survey area, reflectors in the sparker profiles indicate listric normal faults dipping south-wards (Fig. 5). A 2.9 km long, E–W-striking sea-floor lineament (Fig. 4B, C) represents the top of the headwall scar, and the fault has a significant signature through the whole Quaternary package. The location and strike of the faults follow the structures in the pre-Quaternary basement (Binzer & Stockmarr 1994), which indicates that they represent re-activations of old faults.

Final remarks

Based on geophysical data, boreholes and cone penetration tests we have documented that the geological architecture of the study area is very complex. The pre-Quaternary (Late Cretaceous) basement is overlain by two glacial, two Late Glacial and two Holocene subunits. The widespread Late Glacial deposits that are up to 45 m thick are dominated by fine-grained sediments, in some areas with gas. The distribution of the Holocene deposits indicates the presence of channels that drained into the deeper part of the Kattegat during the early Holocene. The data described here are of great importance to the geotechnical evaluation prior to the planned foundation of windmills.

Acknowledgements

We thank Energinet.dk for permission to use the above data and to publish the geological results from the Anholt wind-farm project.

References

Bennike, O., Jensen, J.B., Konradi, P.B., Lemke, W. & Heinemeier 2000: Early Holocene drowned lagoonal deposits from the Kattegat, southern Scandinavia. Boreas **29**, 272–286.

Binzer, K. & Stockmarr, J. 1994: Geological map of Denmark, 1:500 000. Pre-Quaternary surface topography of Denmark. Danmarks Geologiske Undersøgelse Kortserie **44**, 10 pp., 2 maps.

Jensen, J.B., Petersen, K.S., Konradi, P., Kuijpers, A., Bennike, O., Lemke, W. & Endler, R. 2002: Neotectonics, sea-level changes and biological evolution in the Fennoscandian Border Zone of the southern Kattegat Sea. Boreas **31**, 133–150.

Larsen, N.K., Knudsen, K.L., Krohn, C.F., Kronborg, C., Murray, A.S. & Nielsen, O.B. 2009: Late Quaternary ice sheet, lake and sea history of southwest Scandinavia – a synthesis. Boreas **38**, 732–761.

Leth, J.O., Alhamdani, Z., Novak, B., Barzani, S.M. & Hindrichsen, C. 2009: Anholt offshore wind farm. Marine geophysical investigations. Danmarks og Grønlands Geologiske Undersøgelse Rapport **2009/45**, 411 pp.

Lykke-Andersen, H., Knudsen, K.L. & Christiansen, C. 1993: The Quaternary of the Kattegat area, Scandinavia: a review. Boreas **22**, 269–281.

Novak, B. 1996: En maringeologisk undersøgelse af kvartære lag på Lysegrund, sydlige Kattegat, Danmark. Geologisk Tidsskrift **2**, 21–25.

Novak, B & Björck, S. 1998: Marine seismic studies in southern Kattegat, with special emphasis on longitudinal bars and their possible relationship to the drainage of the Ancylus Lake. GFF **120**, 297–306. Stockholm: Geological Society of Sweden.

Novak, B. & Pedersen, G.K. 2000: Sedimentology, seismic facies and stratigraphy of a Holocene spit-platform complex interpreted from high-resolution shallow seismics, Lysegrund, southern Kattegat, Denmark. Marine Geology **162**, 317–335.

Vangkilde-Pedersen, T., Lykke-Andersen, H. & Lind, G. 1993: Dislocated Quaternary deposits in southeastern Kattegat – a glacial or gravitational phenomenon? Boreas **22**, 329–336.

Authors' address

Geological Survey of Denmark and Greenland, Øster Voldgade 10, DK-1350 Copenhagen K, Denmark. E-mail: *jol@geus.dk*

Amino acid analysis of pre-Holocene foraminifera from Kriegers Flak in the Baltic Sea

Ole Bennike and Bernd Wagner

The Geological Survey of Denmark and Greenland (GEUS) and the Institute of Baltic Sea Research in Warnemünde (formerly the Institut für Meereskunde of the DDR) have co-operated for more than two decades on unravelling the history of the south-western part of the Baltic Sea, mainly based on shallow seismic profiling, sampling of sediment cores and analyses of core samples (Jensen *et al.* 2002). Here we report on some results from one of the latest joint cruises with the German research vessel *Maria S. Merian*.

The Baltic Sea is one of the largest brackish-water seas in the world. However, during wide periods of the Quaternary, the Baltic Sea area was either covered by the Scandinavian ice sheet, or was a lake or a land area. Well-dated marine deposits are only known from the last interglacial stage (the Eemian) and from the Holocene. During the Eemian, connections to the Baltic Sea were found via Karelia to the White Sea, and via Denmark and northern Germany to the North Sea (Funder *et al.* 2002). During the Holocene, a connection to the North Sea was first established during the Yoldia Sea stage via south-central Sweden, and later during the Littorina Sea stage via the Danish/German/Swedish straits (Björck 1995).

In addition to Holocene and Eemian deposits, pre-Holocene marine sequences from Germany, Poland, Estonia and Latvia have been referred to the Holsteinian, the Saalian and the Weichselian (e.g. Kalnina 2001). In Poland seven marine sequences of Weichselian ages were reported by Gałązka & Marks (2009). However, the chronology and correlation of these deposits are uncertain.

During regional mapping in the early 1990s, the Geological Survey of Sweden discovered pre-Holocene marine sediments to the north-east of Kriegers Flak in the western part of the Arkona Basin (Fig. 1A). This find has major palaeogeographical implications because it is the only interstadial marine deposit reported from the area. The occurrence was described by Klingberg (1998). However, the age of the deposit was uncertain, with the only hint coming from a non-finite radiocarbon age determination which showed that the deposit is older than 40 000 ^{14}C years (lab. no. Ua-4116). Recently, five samples from non-marine sediments deposited above the brackish unit at Kriegers Flak, but in connection with it, have been radiocarbon dated – and gave finite ages

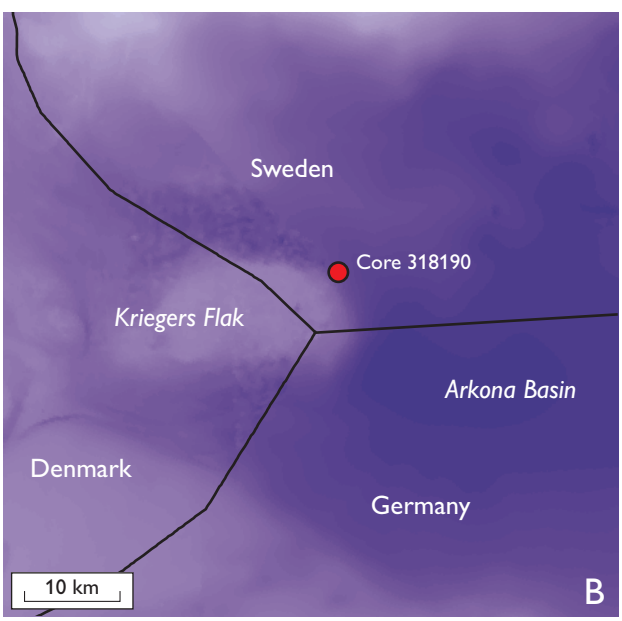

Fig. 1. **A**: Map of north-western Europe showing the location of Kriegers Flak and the location of place names mentioned in this paper. **B**: Bathymetrical map of the Kriegers Flak area, showing the location of the studied core. The water depth varies from *c.* 15 m (the lightest areas) to *c.* 45 m (the darkest areas).

of *c.* 36 000 – 41 000 calendar years BP, indicating a Middle Weichselian age (Anjar *et al.* 2010).

Klingberg (1998) noted that the sequence consists of stiff clay underlain and overlain by till. Part of the marine clay contains species-poor foraminiferal faunas dominated by *Elphidium excavatum* and *Elphidium albiumbilicatum*. The fauna implies brackish-water conditions, which was confirmed by extremely low $\delta^{18}O$ values of carbonate from the foraminifera tests at between –11.2 and –11.9‰ (Klingberg 1998). Ordinary sea water and carbonates precipitated from it have values close to zero, whereas the Greenland ice sheet ranges between –32 and –44‰ (North Greenland Ice Core Project members 2004). A reasonable way to explain the low values from Kriegers Flak is by assuming a mixture of sea water and meltwater from the Scandinavian ice sheet. Five samples from the clay were analysed for pollen, but the interpretation of the pollen spectra was hampered by the presence of reworked pollen grains (Klingberg 1998).

In order better to constrain the age of the deposit, new material was collected and a sample of foraminifera tests analysed for the ratio between L-isoleucine and D-alloisoleucine. Since its development in the late 1960s, amino acid geochronology has been increasingly used for dating and correlating late Cenozoic deposits that are beyond the range of radiocarbon dating (Miller & Brigham-Grette 1989). Most studies are performed on mollusc shells and tests of foraminifera. Protein in live organisms consists of amino acid molecules in the L-isomer form. After the death of the organism, some of the amino acid molecules change to the D-form until an equilibrium is reached. The D/L ratio depends on the time elapsed since the death of the organism, the diagenetic temperature history and the species analysed. If the temperature history of a fossil sample is known, it is possible to calculate its age. This, however, is very difficult for the Late Quaternary which is known for its large and rapid temperature shifts. Yet, sites with similar diagenetic temperature histories may be correlated even if that history is unknown. We suggest that deposits in the southern Baltic have experienced approximately similar temperature histories as those in the North Sea and will compare with sites of known age there. We do not consider onshore deposits because these may have experienced different diagenetic temperature histories.

The pioneering study on amino acid geochronology in North-West Europe by Miller & Mangerud (1985) used mollusc shells from onshore marine interglacial deposits. Following a pilot study by Sejrup *et al.* (1984), amino acid stratigraphy using foraminiferal tests has been widely used for dating and correlating interglacial marine sequences in the North Sea region (e.g. Knudsen & Sejrup 1988; Sejrup & Knudsen 1993, 1999).

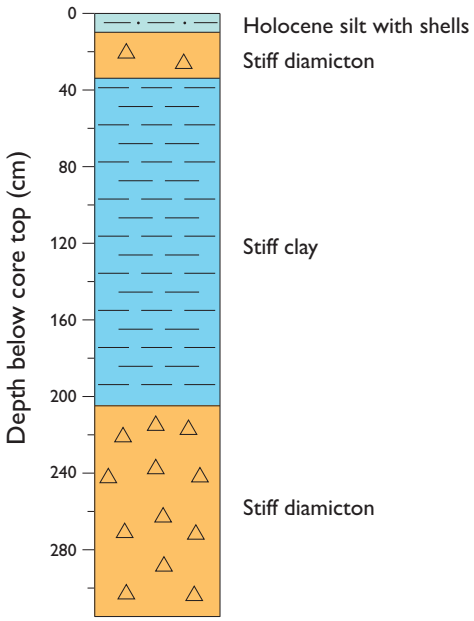

Fig. 2. Lithological log of the sediment core.

In the present study, amino acid analysis was carried out to obtain more information about the age of the deposits from Kriegers Flak. For this purpose, we used tests of the foraminifera *Elphidium excavatum* as this species has already been widely used in other studies of amino acid ratios in the region. Assuming that Kriegers Flak has experienced a similar temperature history as Denmark and the North Sea, we only compare the D/L ratio of *Elphidium excavatum* with D/L ratios from the same species, in order to avoid taxonomical effects which can be significant (e.g. Miller & Mangerud 1985).

Material and methods

Vibro-coring was carried out in the north-eastern Swedish part of Kriegers Flak, at the position 55°04.08′N, 13°11.63′W, at a water depth of 39.7 m (Fig. 1B). A 6 m long corer was used, but it only penetrated 315 cm. The core (no. 318190, Institute of Baltic Sea Research) consisted of diamicton (315–205 cm), light, olive-grey, stiff clay (205–34 cm), diamicton (34–10 cm) and silt with shells of marine molluscs (10–0 cm; Fig. 2). A series of samples from the clay unit was dried and wet sieved on 0.4, 0.2 and 0.1 mm sieves. Most of the samples were barren or only contained rare foraminifera, but one of the samples (from 198–193 cm core depth) contained abundant tests of the benthic foraminifera *Elphidium excavatum*. The foraminifera tests were picked out and split into two subsamples, each weighing around 6 mg. Both subsamples were analysed in the Amino Acid Geochronology Laboratory at the Institute of Arctic and Alpine Research,

Boulder, Colorado. Three measurements were carried out on each subsample. Peptide-bound amino acids were decomposed in the laboratory by hydrolysis, and the analyses were made with a chromatograph. The ratio of D-alloisoleucine to L-isoleucine (D/L) is based on the peak height in the total population, i.e. both free and peptide-bound amino acids.

Results

Subsamples AAL-11579A and B gave D/L ratios of 0.106 ± 0.000 and 0.106 ± 0.002, respectively. Although most analyses of foraminifers in North-West Europe have been carried out at the amino acid chronological laboratory at the Geological Institute, Bergen University, we regard the amino acid analyses from the Institute of Arctic and Alpine Research as nearly identical to those from Bergen, since samples processed at both places have yielded similar results (Miller & Mangerud 1985).

Discussion of age

Amino acid analyses of numerous samples of *Elphidium excavatum* tests from various interglacial and interstadial deposits from the North Sea region have been summarised by Sejrup & Knudsen (1993, 1999). In the latter work, the authors divided the North Sea sequence into four amino zones. Zone 1 corresponds to the Holocene and the Late Weichselian, zone 2 includes samples of Eemian age, as well as samples of Late Saalian and Early Weichselian age, zone 3 includes samples of Holsteinian age and zone 4 is correlated with marine isotope stage 11 (420–360 ka). The D/L ratios in amino zone 2 range from 0.08 to 0.12, and those in amino zone 3 show ratios between 0.14 and 0.16. Subsamples AAL-11579A and B from Kriegers Flak have ratios similar to those of amino zone 2, and thus imply an Eemian, Late Saalian or Early Weichselian age.

Eemian age? An Eemian age for the clay sequence from Kriegers Flak is unlikely, since the foraminiferal faunas consist almost entirely of the two benthic species *Elphidium excavatum* and *Elphidium albiumbilicatum*, an assemblage indicating brackish waters in an Arctic/subarctic environment (Klingberg 1998). The fauna is clearly different from Eemian foraminiferal faunas from the region, as they are dominated by species-rich assemblages implying warmer conditions. *Elphidium excavatum* is common in Late Eemian deposits at Mommark on Als, southern Denmark (e.g. Kristensen & Knudsen 2006). However, the Eemian deposits at this site show normal marine oxygen isotope ratios, whereas the ratios at Kriegers Flak seem to suggest deposition during a time with extensive melting of glacial ice as noted above.

Early Weichselian age? An Early Weichselian age is also considered unlikely. During the Early Weichselian, the global sea level was lower than at present (e.g. Siddall *et al.* 2003) and the North Sea as well as the Danish/German/Swedish straits are generally believed to have been dry land (Houmark-Nielsen 1989). According to the glaciation curves of e.g. Lundquist (1986), Houmark-Nielsen (1989) and Mangerud (2004), the Scandinavian ice sheet did not advance to the south-western Baltic during the Early Weichselian. Hence, Arctic/subarctic brackish-water conditions with marked meltwater influence would not be expected in the Kriegers Flak region during this time interval.

Late Saalian age? During the Late Saalian, the sea transgressed large parts of the North Sea and reached as far south as the Roar, where boreo-Arctic and Arctic conditions were found (Fig. 1A; Knudsen 1986). In northern Denmark, the Børglum chronozone of Lykke-Andersen & Knudsen (1991) reflects interstadial conditions of Late Saalian age. Deposits from an Arctic sea have also been recorded in southern Sweden (Påsse *et al.* 1988). According to the reconstruction by Houmark-Nielsen (1989), the margin of the Scandinavian ice sheet retreated from the south-western Baltic Sea. We consider it possible that the Øresund region was isostatically depressed following the extensive Late Saalian glaciation and transgressed by the sea for a short time interval after recession of the ice. Brackish waters may have extended to the south-western part of the Baltic Sea, including Kriegers Flak.

Middle Weichselian age? A Late Saalian age is obviously not in accordance with the radiocarbon dates reported by Anjar *et al.* (2010). The radiocarbon dates are close to the limit of radiocarbon dating and it could be argued that they are unreliable, in particular because four of them were made on bulk sediment samples. Dating of bulk sediment samples commonly yields erroneous results, but usually dates of bulk samples are too old – not too young. Also, all five age determinations gave finite dates, which is a good indication that they are reliable.

We find it difficult to reconcile a Middle Weichselian age with the amino acid data, which suggest an older age. However, in the past decade it has become more and more obvious that amino acid ratios should be used with caution due to their strong dependency on the temperature histories of the deposits. Hence, a Middle Weichselian age cannot be excluded from the amino acid data.

Figure 3 shows a possible palaeogeographical reconstruction. We suggest that the Øresund region was isostatically depressed and transgressed by the sea for a short time interval after recession of the Scandinavian ice sheet.

Fig. 3. Palaeogeographical model of southern Scandinavia during deposition of the Kriegers Flak sequence.

Conclusions

The amino acid ratios from brackish-water deposits on Kriegers Flak suggest a Late Quaternary age, either Late Saalian, Eemian or Early Weichselian. A strong $\delta^{18}O$ meltwater signal and the foraminiferal assemblage are not compatible with an Eemian age. An Early Weichselian age is also considered unlikely because the sea level was probably too low at this time to allow the sea to transgress the Baltic Sea, and because the margin of the Scandinavian ice sheet was too far away to give a strong meltwater signal. The last option, a Late Saalian age, does not agree with a Middle Weichselian age of the fresh-water deposits that are connected to the brackish-water deposits. Hopefully, other dating methods can be applied at Kriegers Flak in the future to better constrain the age of the sequence.

References

Anjar, J., Larsen, N.K., Björck, S., Adrielsson, L. & Filipsson, H.L. 2010: MIS 3 marine and lacustrine sediments at Kriegers Flak, southwestern Baltic Sea. Boreas **39**, 360–366.

Björck, S. 1995: A review of the history of the Baltic Sea, 13-8 ka BP. Quaternary International **27**, 19–40.

Funder, S., Demidov, I. & Yelovicheva, Y. 2002: Hydrography and mollusc faunas of the Baltic and the White Sea – North Sea seaway in the Eemian. Palaeogeography, Palaeoclimatology, Palaeoecology **184**, 275–304.

Gałązka, D. & Marks, L. 2009: Geology of the Lower Vistula region, northern Poland. Polish Geological Institute, Special Papers **25**, 13–20.

Houmark-Nielsen, M. 1989: The last interglacial–glacial cycle in Denmark. Quaternary International **3/4**, 31–39.

Jensen, J.B., Kuijpers, A., Bennike, O. & Lemke, W. 2002: BALKAT. The Baltic without frontiers. Geologi – Nyt fra GEUS **4**, 19 pp. Copenhagen: Geological Survey of Denmark and Greenland.

Kalnina, L. 2001: Middle and Late Pleistocene environmental changes recorded in the Latvian part of the Baltic Sea basin. Quaternaria **A9**, 173 pp.

Klingberg, F. 1998: A Late Pleistocene marine clay succession at Kriegers Flak, westernmost Baltic, southern Scandinavia. Journal of Quaternary Science **13**, 245–253.

Knudsen, K.L. 1986: Middle and Late Quaternary foraminiferal stratigraphy in the southern and central North Sea area. Striae **24**, 201–205.

Knudsen, K.L. & Sejrup, H.P. 1988: Amino acid geochronology of selected interglacial sites in the North Sea area. Boreas **17**, 347–354.

Kristensen, P.H. & Knudsen, K.L. 2006: Palaeoenvironments of a complete Eemian sequence at Mommark, south Denmark: foraminifera, ostracods and stable isotopes. Boreas **35**, 349–366.

Lundquist, J. 1986: Stratigraphy of the central area of the Scandinavian glaciation. Quaternary Science Reviews **5**, 251–268.

Lykke-Andersen, A.L. & Knudsen, K.L. 1991: Saalian, Eemian and Weichselian in the Vendsyssel–Kattegat region, Denmark. Striae **34**, 135–140.

Mangerud, J. 2004: Ice sheet limits on Norway and the Norwegian continental shelf. In: Ehlers, J. & Gibbard, P. (eds): Quaternary glaciations – extent and chronology **1**, 271–294. Amsterdam: Elsevier.

Miller, G.H. & Brigham-Grette, J. 1989: Amino acid geochronology: resolution and precision in carbonate fossils. Quaternary International **1**, 111–128.

Miller, G.H. & Mangerud, J. 1985: Aminostratigraphy of European marine interglacial deposits. Quaternary Science Reviews **4**, 215–278.

North Greenland Ice Core Project members 2004: High-resolution record of northern hemisphere climate extending into the last interglacial period. Nature **431**, 147–151.

Påsse, P., Robertsson, A.-M., Miller, U. & Klingberg, F. 1988: A Late Pleistocene sequence at Margreteberg, southwestern Sweden. Boreas **17**, 141–163.

Sejrup, H.P. & Knudsen, K.L. 1993: Paleoenvironments and correlations of interglacial sediments in the North Sea. Boreas **22**, 223–235.

Sejrup, H.P. & Knudsen, K.L. 1999: Geochronology and palaeoenvironment of marine Quaternary deposits in Denmark: new evidence from northern Jutland. Geological Magazine **136**, 561–578.

Sejrup, H.P., Rokoengen, K. & Miller, G.H. 1984: Isoleucine epimerization in Quaternary benthonic foraminifera from the Norwegian continental shelf: a pilot study. Marine Geology **56**, 227–239.

Siddall, M., Rohling, E.J., Almogi-Laban, A., Hemleben, C., Meiscner, D., Schmelzer, I. & Smeed, D.A. 2003: Sea-level fluctuations during the last glacial cycle. Nature **423**, 853–858.

Authors' addresses

O.B., *Geological Survey of Denmark and Greenland, Øster Voldgade 10, DK-1350 Copenhagen K, Denmark*. E-mail: *obe@geus.dk*

B.W., *Baltic Sea Research Institute, Seestrasse 15, D-18119 Rostock-Warnemünde, Germany*. Present address: *Institute for Geology and Mineralogy, University of Cologne, Zülpicher Str. 49a, D-50674 Cologne, Germany.*

Radon content in Danish till deposits: relationship with redox conditions and age

Peter Gravesen and Peter Roll Jakobsen

Radon (^{222}Rn) is a radioactive, noble insoluble gas with a half-life of 3.8 days. It belongs to the uranium (^{238}U) decay chain where radon is formed from radium (^{226}Ra). Uranium and radium are built into mineral structures or are, for example, adsorbed on the surface of clay minerals, limonite or organic material. When radon is formed by radioactive decay from radium, parts of it enter the pores of rocks and soils and are transported by diffusive or advective forces in the pores. The transport rate depends on the permeability and water content in the pores (Nazaroff 1992).

Radon may enter into buildings through fractures in the walls driven by forces such as pressure gradients between the outside and the inside. Radon and its radioactive decay products are inhaled by living beings and are the main source of radiation to which humans are exposed. The radiation presents an increased risk of lung cancer and may cause leukaemia, which mainly occurs in children. On the basis of risk analyses it has been estimated that 10% of all cases of lung cancer in Denmark are caused by radon inhalation (Sundhedsstyrelsen 1987). It has been demonstrated that rocks and soils around and below houses are the main sources of radon emanation.

Several studies have analysed and described the radon content in Danish sediments and rocks (e.g. Damkjær & Korsbech 1985; Gravesen *et al.* 1996) and have demonstrated its relationship to radon levels in Danish buildings (Andersen *et al.* 2006; Raaschou-Nielsen *et al.* 2008). A nation-wide mapping of radon levels in Danish dwelling houses based on, e.g. mapping of Quaternary surface deposits and information about radon in sediments and rocks was performed by Andersen *et al.* (2001).

This paper presents some results concerning the radon content and emanation rates in different Danish till deposits of Saalian and Weichselian age from a study carried out by the Geological Survey of Denmark and Greenland (GEUS).

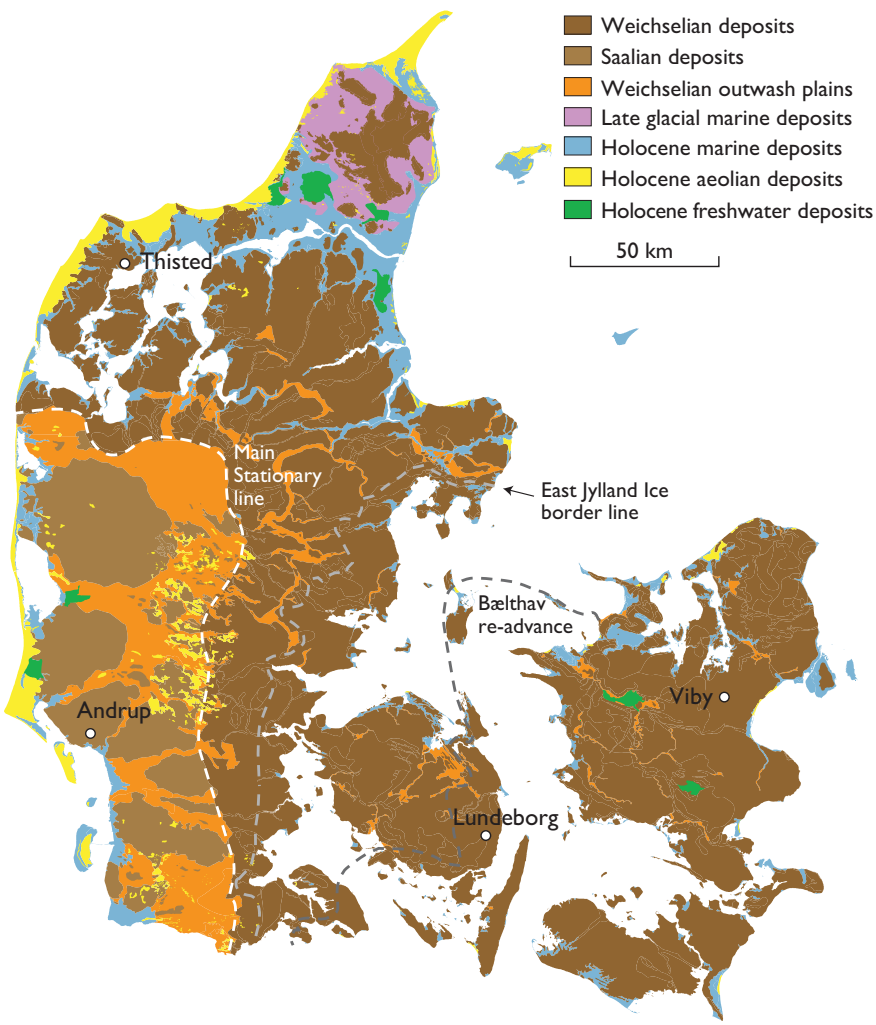

Fig. 1. Simplified geological map of Denmark, showing the general distribution of surface lithologies, the most important ice-margin lines from the Weichselian and the four investigated localities.

Geological setting

Clayey and sandy tills have been analysed for uranium, radium and radon content at the four localities Viby, Lundeborg, Thisted and Andrup (Fig. 1). The Andrup locality is situated outside the limit of the Weichselian glaciation and the till is considered to be of Saalian age deposited by a Warthe ice advance about 180 000–160 000 years ago (Houmark-Nielsen 2007). The Thisted, Lundeborg and Viby localities are located inside the maximum extent of Weichselian glaciacion and the tills are referred to the Weichselian. A relatively thin layer of till covers limestone and chalk deposits at Thisted. The till is regarded as deposited during the late Weichselian by the Norwegian advance or from the main glacial advance from the north-east about 25 000–20 000 years ago (Gry 1979). At Lundeborg and Viby the latest glacial advances are the East Jylland advance and the Bælthav re-advance about 19 000 years ago. In sections close to the Lundeborg locality the slightly older Mid Danish Till, deposited during the North-East advance, is seen below the till from the Young Baltic advance. Some of the borehole samples may represent the Mid Danish Till (Houmark-Nielsen & Kjær 2003).

Materials and methods

Trenches were excavated at the four localities down to a depth of *c*. 2 m into till deposits (Fig. 2). The sections were described with respect to lithology, structures and macropores, and samples of the clayey and sandy till units were collected at each locality. Five 5–6 m deep boreholes were drilled with an 8 inch twist auger close to the excavations. The nearly undisturbed till samples were described, and samples were collected at 30 cm intervals. The samples from the excavations had a weight of at least 500–1000 g, and those from the boreholes 300–500 g.

Fig. 2. Field investigations at the Lundeborg locality. Drilling close to the excavated trench.

A total of 155 samples were collected, with each sample consisting of two subsamples. One subsample was collected in a sealed plastic bin for radon analysis, and the other was analysed for chemical compounds including uranium and radium. Uranium was measured by instrumental neutron activation analysis at Activation Laboratories LTD and radium by a germanium detector at the National Institute of Radiation Protection. The radon emanation rate was measured by the closed-chamber method using ZnS(Ag) scintillation cells at Risø National Laboratory, Danish Technical University. Prior to the radon analyses the samples were fragmented. The purpose was to increase the surface area of the sediment to promote the release of radon produced by radium decay. In addition to the chemical analyses, grain-size distribution, clast composition, organic content and water content were analysed at GEUS immediately after sampling.

Results and discussion

This paper focuses on the measured radon emanation rates related to the weathering and redox (reduction–oxidation) conditions in the tills and the age difference between the tills at the four localities.

Till composition. The investigated tills are heterogeneous sediments with a matrix consisting of up to 20% clay, *c*. 70% silt and sand, and 4–10% gravel and stones. The clasts normally consist of Norwegian and Swedish basement rocks, quartz, Danish chert and limestone fragments. The matrix is a mixture of crushed basement rocks and local sediments dominated by quartz, feldspar, mica, smectite, kaolinite and illite. As a consequence of the heterogeneous sediment types uranium and radium are related to the source material and not uniformly distributed.

Weathering and redox conditions. The upper 0–3 m of the till profiles have been subject to weathering after the last deglaciation (Weichselian: Thisted, Lundeborg and Viby; Saalian: Andrup). Rainwater has percolated through pores in the till and caused decomposition and leaching of clay minerals, limonite and $CaCO_3$. Measurements of the $CaCO_3$ content show deep weathering at Andrup and nearly none at Viby.

Most till profiles in Denmark have an upper, yellow-brown coloured, oxidised zone and a lower, olive-grey-reduced zone separated by a redox interface. At Andrup the redox interface coincides with the $CaCO_3$ leaching boundary, while at Lundeborg it is situated in the oxidised zone. At Viby only slight $CaCO_3$ leaching has occurred in the top of the profile.

The redox zones are seen in the sections at Andrup, Lunderborg and Viby. In Table 1 the measured uranium and radium content and radon emanation rates are shown in relation to their occurrence in the two redox zones. The development

Table 1. Uranium and radium contents and radon emanation rates at the four localities

Locality	Lithology	Age	Uranium (ppm)	Radium (oxidised) Bq/kg	Radium (reduced) Bq/kg	Radon (oxidised) Atom/kg/s	Radon (reduced) Atom/kg/s
Viby	Sandy till	Weichselian	1.4–2.6	22.4–24.5	-	7.9–11.3	-
	Clayey till	~18 ka		17.6–26.1	22.1–35.9	5.2–13.9	4.5–6.7
Lundeborg	Sandy till	Weichselian	1.1–1.9	18.5	-	7.3	-
	Clayey till	~18 ka		13.8–24.9	14.8–15.5	7.3–15.6	3.2–6.8
Thisted	Sandy till	Weichselian	0.5–1.6	18.7–24.7	-	7.5–10.4	-
	Clayey till	~23 ka		14.1	-	13.6	-
	Limey till			1.2–6.6	-	0.9–1.5	-
Andrup	Clayey till	Saalian ~170 ka	1.2–1.9	14.1–20.6	12.6–19.1	6.2–10.6	2.6–3.7

75 samples were analysed in total

of the redox zones depends on chemical and physical processes and therefore the behaviour of U and Ra in the zones is related to these processes. In the oxidised zone oxygen and for example nitrate influence the compositions of the minerals. The original uranium contained in the minerals is oxidised and mobilised, whereas the decay product radium is less mobile. Radium is not uniformly distributed and often precipitated as films or crusts at the rim of the sediment pores between grains of clay minerals, limonite and $CaCO_3$ where it produces radon. In the reduced zone the U-bearing minerals are more stable and emit less radon (Ball *et al.* 1991).

The investigation demonstrates larger rates of radon emanation in the oxidised zone than in the reduced zone (Table 1). The radium and radon levels seem to be comparable with the measurements reported by Damkjær & Korsbech (1985). The radium concentration is fairly constant in the two redox zones (Table 1). The higher radon content in the oxidised zone may be caused by enhanced emanation conditions. It may be due to opening of mineral pores in the oxidised zone as a result of an increase in number and size of macro-pores and higher permeability than in the reduced zone where radon is often trapped in smaller pores.

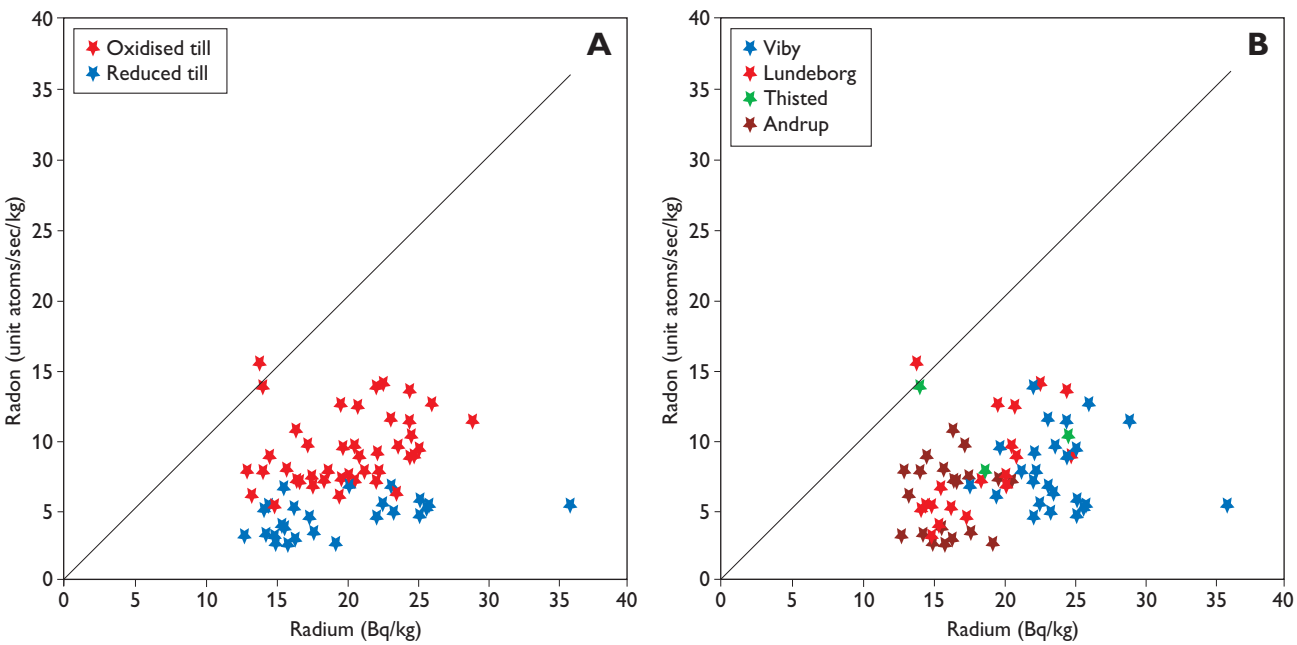

Fig. 3. Comparison between radium content and radon emanation rates in Danish tills. A radium content of 1 Bq kg^{-1} yields a total radon production rate of 1 atom kg^{-1} sec^{-1}. This relationship is represented by the diagonal line in the diagrams. **A**: Plot of radium versus radon based on values for oxidised and reduced zones at the four studied localities. **B**: Plot of radium versus radon in the oxidised and reduced zones at the four localities. One sample seems to produce more radon than the radium content can explain. The value is 15 616 ± 1710 atoms kg^{-1} sec^{-1}.

Water content is also a factor to consider because it influences the distance the radon atoms have to travel to enter the pores. According to Damkjær & Korsbech (1985) up to 17% of water in the pores will increase the emanation rate. The water content in the tills is mostly below 17% but above the ideal content of 3–7%, and the content is slightly higher in the oxidised than in the reduced zone.

Radon emanation rates in the two redox zones appear to be independent of the geographical distribution of the till. In Fig. 3 the distribution of radon and radium is seen in relation to redox zones. The radon emanation rates in both zones are lower than the corresponding radium content, which indicates that only some of the radon leaves the mineral grains and enters the pores of the till. The reduced zone has lower radon emanation rates than the oxidised zone in nearly all cases.

Transport conditions. After the radon atoms have moved into the pores the transport is controlled by the porosity and permeability of the till. Till has a relatively high matrix porosity but the occurrence of macro-pores in the form of roots, fractures and faults is of considerable importance. Macropores are most frequent in the oxidised zone. They were found in all sections, and their distribution explains the large difference in hydraulic conductivity between the two zones. The oxidised zone shows systematically decreasing values of hydraulic conductivity from the surface to a depth of 2–4 m (the redox interface) from 10^{-3} m/s to 10^{-11} m/s. Below the redox interface the hydraulic conductivity varies unsystematically from 10^{-10}m/s to 10^{-5} m/s (Nilsson & Klint 2009).

Age relationship. A comparison between radon and radium values from the Saalian locality (Andrup) and the Weichselian localities (Thisted, Lundeborg and Viby) show differences that appear to be related to the age of the till. Figure 3 shows that average radon emanation rates generally increase from the Saalian till to the younger Weichselian till and it is seen that there is a clear difference between the Andrup and Viby localities. This is probably because the till at Andrup has been exposed to weathering and precipitation for a longer time than that at Viby. These processes have led to removal of uranium and fixed radium at a lower level than seen for the Weichselian till. The *in-situ* radon producing radioactive decay in the Saalian till lasted more than 150 000 years longer than in the Weichselian till. Another explanation could be different bulk mineralogy in the tills deposited by ice advances of different ages.

Final remarks

Our investigation indicates that radon emanation rates in till are higher in the oxidised zone than in the reduced zone at all four localities and that they are higher in Weichselian till than in Saalian till. However, only limited data are available for this conclusion. Many Danish dwelling houses are built on clayey tills, and the new information concerning the redox conditions is important when evaluating transport and impact of radon into dwelling houses and the risk of exposure to inhalation of radon in Denmark.

Acknowledgement

The Ministry of Health and Prevention is thanked for financial support.

References

Andersen, C.E., Ulbak, K., Damkjær, A. & Gravesen, P. 2001: Radon i danske boliger. Kortlægning af lands-, amts- og kommuneværdier, 132 pp. Copenhagen: Sundhedstyrelsen, Statens Institut for Strålehygiejne.

Andersen, C.E., Raaschou-Nielsen, O., Andersen, H.P., Lind, M., Gravesen, P., Thomsen, B. & Ulbak K. 2006: Prediction of ^{222}Rn in Danish dwellings using geology and house construction information from central databases. Radiation Protection Dosimetry **27**, 10–21.

Ball, T.K., Cameron, D.G., Colman, T.B. & Roberts, P.D. 1991: Behaviour of radon in the geological environment: a review. Quarterly Journal of Engineering Geology and Hydrogeology **24**, 169–182.

Damkjær, A. & Korsbech, U. 1985: Measurement of the emanation of radon-222 from Danish soils. The Science of the Total Environment **45**, 343–350.

Gravesen, P., Jakobsen, P.R. & Kelstrup, N. 1996: Radon i danske jordarter II. Undersøgelser og konklusioner. Danmarks og Grønlands Geologiske Undersøgelse Rapport **1996/78**, 113 pp.

Gry, H. 1979: Beskrivelse til geologisk kort over Danmark. Kortbladet Løgstør. Kvartære aflejringer 1:100 000/1:50 000. Danmarks Gelogiske Undersøgelse I. Række **26**, 58 pp.

Houmark-Nielsen, M. 2007: Extent and age of Middle and Late Pleistocene glaciations and periglacial episodes in southern Jylland, Denmark. Bulletin of the Geological Society of Denmark **55**, 9–35.

Houmark-Nielsen, M. & Kjær, K. 2003: Southwest Scandinavia, 40–15 kyr BP: palaeogeography and environmental change. Journal of Quaternary Science **18**, 769–786.

Nazaroff, W.W. 1992: Radon transport from soil to air. Reviews of Geophysics **30**, 137–160.

Nilsson, B. & Klint, K.E. 2009: Bilag 7. Sammenstilling af data fra hydrauliske undersøgelser i moræneler – videnstatus. In: Gravesen, P. & Rosenberg, P. (eds): Særligt pesticidfølsomme leromåder: datagrundlag og mulige veje mod zonering, KUPA, 70 pp. + appendices (report). Copenhagen: Geological Survey of Denmark and Greenland.

Raaschou-Nielsen, O., Andersen, C.E., Andersen, H.P., Gravesen, P., Lind, M., Schüz, J. & Ulbak, K. 2008: Domestic radon and childhood cancer in Denmark. Epidemiology **19**, 536–543.

Sundhedsstyrelsen 1987: Radon-Boliger-Strålingsdosis-Lungekræftrisiko, 14 pp. Copenhagen: Statens Institut for Strålehygiejne.

Authors' address

Geological Survey of Denmark and Greenland, Øster Voldgade 10, DK-1350 Copenhagen K, Denmark. E-mail: *pg@geus.dk*

Recent changes in the nutrient status of a soft-water *Lobelia* lake, Hampen Sø, Denmark

Kaarina Weckström, Peter Rasmussen, Bent Vad Odgaard, Thorbjørn Joest Andersen, Tarmo Virtanen and Jesper Olsen

Nutrient-poor, low-productive (oligotrophic) soft-water lakes in the Atlantic areas of West and North-West Europe – the so-called *Lobelia* lakes – are of high conservation value as their low nutrient status favours a particular submerged macrophyte flora with isoetids, which are becoming increasingly rare or threatened due to nutrient enrichment (eutrophication) associated with landuse changes and urbanisation. European Union member states have a duty of care, under the Habitats Directive, to protect the biodiversity of oligotrophic to mesotrophic (moderately productive) standing waters.

In Denmark the majority of *Lobelia* lakes are located on sandy soils in central and western Jylland. These lakes are clear-water ecosystems poor in nutrients and organic carbon and with a unique macrophyte vegetation of predominantly *Lobelia dortmanna* (Water Lobelia), *Littorella uniflora* (Shore-weed) and *Isoëtes lacustris* (Quill-wort). Severe deterioration of isoetid plant communities is reported from Denmark and many other European countries (e.g. Arts 2002; Pedersen *et al.* 2006). The isoetids are low and slow growing with relatively poor competitive capabilities. These characteristics make them more sensitive to decreased light levels than other macrophyte groups (Middelboe & Markager 1997) and consequently also particularly vulnerable to eutrophied and turbid waters.

In an ongoing project we are investigating the limnological development of two *Lobelia* lakes in mid-Jylland during the last 1000 years (Hampen Sø and Rævsø, situated 2.5 km apart). The Hampen Sø investigation is part of a Geocenter Denmark funded project with the title: *Lake response to climate change during the last 1000 years*. In this paper we present the first results from Hampen Sø with emphasis on changes in the nutrient status of the lake through the last *c.* 300 years as inferred from diatom and macrofossil analyses. Today Hampen Sø is influenced by nutrient enrichment and has a mixture of two vegetation types that normally belong to two different lake types, namely the lake's original isoetid vegetation plus species of fast-growing and tall elodeids, the latter being favoured by increased nutrient levels (Moeslund 2000). Palaeolimnological methods are used to explore the timing and possible causes of the nutrient enrichment. These are of significance for understanding the environmental threat to the lake ecosystem, and for determining its baseline, or reference conditions, defined by the European Water Framework Directive (WFD) as conditions under minimal anthropogenic disturbance.

Material and methods

Hampen Sø is located in mid-Jylland on sandy soils just west of the Main Stationary Line (Fig. 1). The lake has a surface area of 76 ha, a mean water depth of 4.3 m, a maximum depth of 13.1 m, and a topographic catchment area of 916 ha (Moeslund 2000). The lake is a seepage lake, i.e., a closed lake without natural inlets or outlets. In 2009 a *c.* 2 m long sediment core with humic, slightly silty and sandy gyttja was retrieved from the lake at a water depth of 9.66 m. The uppermost 1 m of the sediment sequence, which spans approximately the last 1000 years, has been dated by accelerator mass spectrometry (AMS) ^{14}C-age determination (one sample) and the ^{210}Pb dating method (Appleby 2001); here we focus on the period between *c.* AD 1750 and today. The nutrient status of the lake during this time period is inferred from diatom and macrofossil analyses, and changes in the catch-

Fig. 1. Map of Denmark with the location of the study site, Hampen Sø. Sandy soils dominate west of the Main Stationary Line.

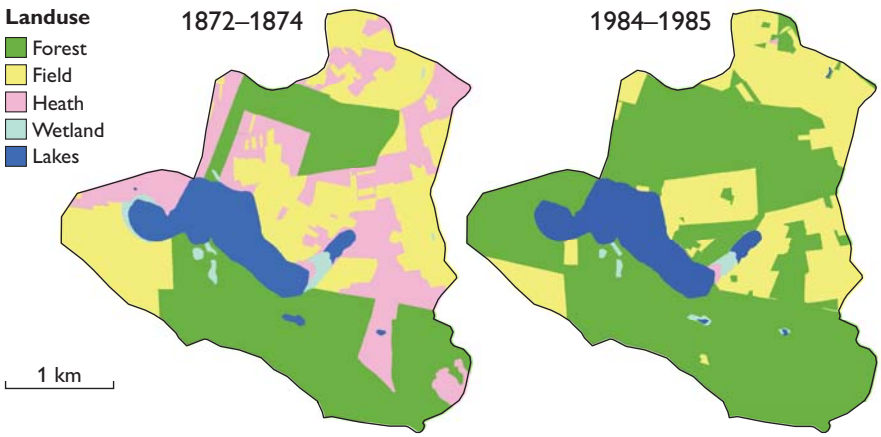

Fig. 2. Landuse in the topographic catchment of Hampen Sø in 1872–1874 (left) and 1984–1985 (right).

ment landuse are estimated from land classification on two cadastral maps from 1872–74 and 1984–85. Diatom data are presented as percentages and 300–400 valves (halves of their siliceous cell walls) were counted per sample. Macrofossils are presented as concentrations.

Chronology

The uppermost 28 cm of the lake sediments were dated by ^{210}Pb and ^{137}Cs assay, estimated from 15 samples spanning the time period 1900–2009. A sample of deciduous leaf fragments found at 117 cm depth was AMS ^{14}C-dated with the result cal. AD 910–1020 (range 2 σ). An age–depth curve was constructed for the depth interval 0–117 cm by linear interpolation between the ^{210}Pb- and ^{137}Cs-dated sediments and the ^{14}C date at 117 cm.

Landuse change in the catchment area

According to the cadastral maps the most significant landuse change in the Hampen Sø catchment area since the end of the 19th century is the virtual disappearance of heathland (Fig. 2). Between *c.* 1870 and 1980 its area has decreased from *c.* 24% to less than 1%, while the forested area has increased from *c.* 36% to 64%. The area of arable land has stayed approximately the same during this time period. The former heathland has been planted with predominantly coniferous trees (pine and spruce) for timber.

Development of the nutrient status over the last *c.* 300 years

There are two distinct changes in the Hampen Sø diatom assemblages: in the mid-18th century and around the 1940s (Fig. 3). The first change is defined by a clear decrease in planktonic taxa from *c.* 28% to 8%. Variations in the abundance of planktonic species in temperate lakes are often associated with either changing water levels (Heinsalu *et al.* 2008; Laird & Cumming 2009) or eutrophication (Sayer *et al.* 1999; Bennion *et al.* 2004). *Cyclotella comensis*, an oligotrophic species, dominates the planktonic assemblages prior to the decrease, after which benthic taxa belonging particularly to the genus *Fragilaria* (including *Staurosira*, *Staurosirella* and *Pseudostaurosira*) increase. Such a change most likely signifies lowering of the water level. The macrophyte vegetation on the other hand does not show distinct changes, although an increase in carophytes (*Nitella* sp. and *Chara* sp.) can be observed and might suggest that they have been favoured by better light conditions due to shallower water. As the core was collected in the deepest part of the lake, the concentrations of littoral species such as *Lobelia* and *Isoëtes* should be considered with some caution, due to their limited seed and spore dispersal.

The first forest plantations in the Hampen Sø catchment area date back to 1805. At first success was limited until the planting methods were changed in the 1830s. An increase in forest cover will increase evapotranspiration from the catchment area and hence could affect the water level in the lake due to a decrease in the ground water table. We initially assumed that the plantations may have affected the lake levels of Hampen Sø, however, the water-level decrease indicated by the diatom assemblages clearly occurs before the planting of trees. On the other hand, there is evidence from several studies based on a number of proxies that precipitation decreased in Scandinavia during the latter part of the Little Ice Age (e.g. Linderholm & Chen 2005; De Jong *et al.* 2009). Hence the diatom-inferred decrease in Hampen Sø water levels in the mid-18th century could reflect this suggested change in precipitation.

The second clear change in the diatom assemblages occurs around the 1940s, marked by a pronounced increase in the mesotrophic species *Cyclotella pseudostelligera* and *Fragilaria*

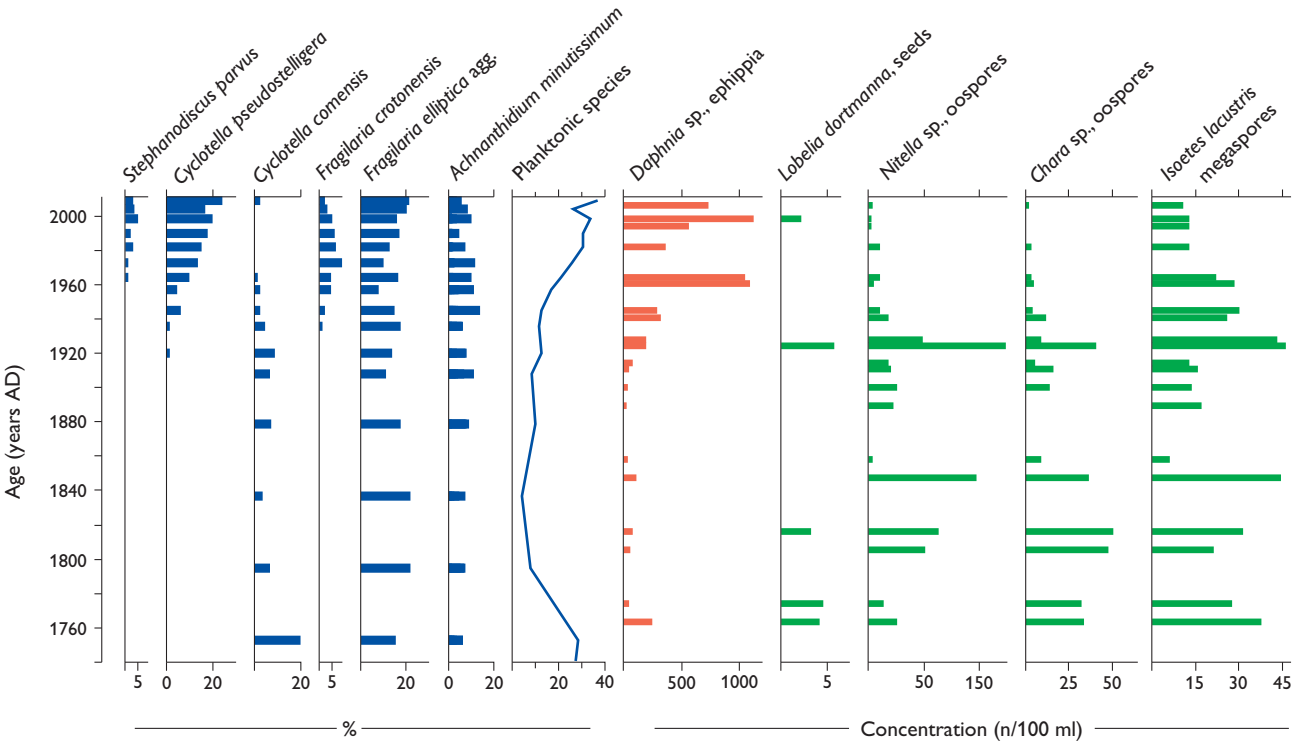

Fig. 3. Diatom and macrofossil diagram showing selected abundant species. Diatoms (blue) are given as percentages. Macrofossils (*Daphnia* ephippia (red) and submerged macrophyte remains (green)) are shown as concentrations (remains per 100 ml fresh sediment). Ages based on the constructed age–depth curve are given on the left of the diagram.

crotonensis (up to 23% and 9%, respectively). Their increase is followed by the appearance of the eutrophic *Stephanodiscus parvus* in the early 1960s. These taxa indicate increased nutrient concentrations and, with higher phytoplankton productivity, also decreased transparency of the lake water. The charophytes *Nitella* sp. and *Chara* sp., which can occur at water depths of over 10 m, exhibit a decreasing trend from the 1920s (Fig. 3), whereas according to recent surveys (Moeslund 2000), tall elodeids, which occur in shallower water (such as *Potamogeton* and *Myriophyllum* species), have become more abundant. Many elodeids are scarce in sediment records (such as in Hampen Sø) due to lower seed production and limited dispersal compared to other macrophytes. The reasons for these changes are likely to be the increased nutrient load from the catchment area (intensified field fertilisation and particularly waste waters from a farm and summer houses near the lake, Moeslund 2000) which, with increasing phytoplankton productivity, also affect water transparency.

Concentrations of ephippia (resting eggs) of the water flea genus *Daphnia* began to increase around the same time as the change in macrophyte vegetation is observed with the highest concentrations from the 1960s onwards (Fig. 3). *Daphnia* resting eggs are generally produced when conditions deteriorate due to e.g. overcrowding, limited food availability, extreme changes in the environment or increased predation (Korhola & Rautio 2001). In Hampen Sø, we interpret the increased numbers of resting eggs as simply an indication of larger *Daphnia* populations due to a general increase in biological production. In addition, more suitable habitats could be represented by the tall elodeids, which function as refuge from fish predation (Jeppesen *et al*. 1997).

According to surveys made in Hampen Sø from 1971 to 1999, nutrient concentrations were high from the beginning of the survey until the mid-1980s (summer-time total phosphorus value *c*. 70–80 µg l^{-1} and total nitrogen *c*. 800–1000 µg l^{-1}), after which concentrations decreased to present-day levels of <30µg l^{-1} total phosphorous and <600 µg l^{-1} total nitrogen (Moeslund 2000). This decrease in concentrations is attributed to the cessation of waste water effluents (in particular animal manure) from the nearby farm. The decreased nutrient concentrations from the mid-1980s onwards are not reflected in the biota. This could be explained by the sediment nutrient pool which, due to its limited binding capacity (low iron:phosphorus ratio), releases particularly phosphorus back into the water. This is then taken up by phytoplankton and macrophytes (Moeslund 2000).

It is noteworthy that the abundance of planktonic diatoms slowly begins to increase before the appearance of the meso- and eutrophic diatom taxa (Fig. 3). This could suggest slightly increasing water levels from the late 19th century onwards, which may partly have been masked by the marked increase in the planktonic diatom taxa indicating eutrophication.

Conclusions and future work

Distinct signs of anthropogenic disturbance in Hampen Sø can be seen in the 1920s (reflected in macrophyte vegetation and *Daphnia* abundance) indicating the onset of nutrient enrichment. Clear indications of eutrophication are evident from the 1960s onwards in all proxies. Although water-column nutrient concentrations have decreased since the mid-1980s, no change is observed in the biota. This could be attributed to increased internal loading of nutrients from the sediments. Compared to the majority of Danish lakes, which have been impacted by anthropogenic activities for centuries (Bradshaw *et al.* 2005, 2006), the timing of these changes is surprisingly late. It appears that sandy soils of central and western Jylland have been less intensively used for crop cultivation in the past and hence lakes located in such settings are less affected. According to our results, baseline or reference conditions at Hampen Sø, as defined by the European Water Framework Directive, could be set at the early 1900s. These reference conditions only define the state of the lake before intensified human impact. Our data show that climate exerts a notable influence on the groundwater-fed lake and its biota implying that the physical, chemical and biological status of the lake has changed naturally in the past. In the ongoing work the lake's response to climate change will be explored further.

References

Appleby, P.G. 2001: Chronostratigraphic techniques in recent sediments. In: Last, W.M. & Smol, J.P. (eds): Tracking environmental change using lake sediments. **1**. Basin analysis, coring, and chronological techniques, 171–203. Dordrecht: Kluwer Academic Publishers.

Arts, G.H.P. 2002: Deterioration of Atlantic soft water macrophyte communities by acidification, eutrophication and alkalinisation. Aquatic Botany **73**, 373–393.

Bennion, H., Fluin, J. & Simpson, G.L. 2004: Assessing eutrophication and reference conditions for Scottish freshwater lochs using subfossil diatoms. Journal of Applied Ecology **41**, 124–138.

Bradshaw, E.G., Rasmussen, P., Nielsen, H. & Anderson, N. J. 2005: Mid- to late-Holocene land-use change and lake development at Dallund Sø, Denmark: trends in lake primary production as reflected by algal and macrophyte remains. The Holocene **15**, 1130–1142.

Bradshaw, E.G., Nielsen, A.B. & Anderson, N.J. 2006: Using diatoms to assess the impacts of prehistoric, pre-industrial and modern land-use on Danish lakes. Regional Environmental Change **6**, 17–24.

De Jong, R., Hammarlund, D. & Nesje, A. 2009: Late Holocene effective precipitation variations in the maritime regions of south-west Scandinavia. Quaternary Science Reviews **28**, 54–64.

Heinsalu, A., Luup, H., Alliksaar, T., Nõges, P. & Nõges, T. 2008: Waterlevel changes in a large shallow lake as reflected by the plankton:periphyton ratio of sedimentary diatoms. Hydrobiologia **599**, 23–30.

Jeppesen, E., Lauridsen, T.L., Kairesalo, T. & Perrow, M.R. 1997: Impact of submerged macrophytes on fish-zooplankton interactions in lakes. In: Jeppesen, E. *et al.* (eds): The structuring role of submerged macrophytes in lakes. Ecological Studies **131**, 91–114.

Korhola, A. & Rautio, M. 2001: Cladocera and other branchiopod crustaceans. In: Smol, J.P., Birks, H.J.B. & Last, W.M. (eds): Tracking environmental change using lake sediments. **4**. Zoological indicators, 5–41. Dordrecht: Kluwer Academic Publishers.

Laird, K.R. & Cumming B.F. 2009: Diatom-inferred lake level from nearshore cores in a drainage lake from the experimental lakes area, northwestern Ontario, Canada. Journal of Paleolimnology **42**, 65–80.

Linderholm, H.W. & Chen, D. 2005: Central Scandinavian winter precipitation variability during the past five centuries reconstructed from *Pinus sylvestris* tree rings. Boreas **34**, 43–52.

Middelboe, A.L. & Markager, S. 1997: Depth limits and minimum light requirements of freshwater macrophytes. Freshwater Biology **37**, 553–568.

Moeslund, B. 2000: Hampen Sø. Miljøtilstanden 1971–1999, 103 pp. Vejle Amt.

Pedersen, O., Andersen, T., Ikejima, K., Zakir Hossain, M.D. & Andersen, F.Ø. 2006: A multidisciplinary approach to understanding the recent and historical occurrence of the freshwater plant, *Littorella uniflora*. Freshwater Biology **51**, 865–877.

Sayer, C., Roberts, N., Sadler, J., David, C. & Wade, P.M. 1999: Biodiversity changes in a shallow lake ecosystem: a multi-proxy palaeolimnological analysis. Journal of Biogeography **26**, 97–114.

Authors' addresses

K.W. & P.R., *Geological Survey of Denmark and Greenland, Øster Voldgade 10, DK-1350 Copenhagen K, Denmark*. E-mail: *kaaw@geus.dk*

B.V.O., *Department of Earth Sciences, University of Aarhus, C.F. Møllers Allé 120, DK-8000 Århus C, Denmark.*

T.J.A., *Department of Geography & Geology, University of Copenhagen, Øster Voldgade 10, DK-1350 Copenhagen K, Denmark.*

T.V., *Department of Environmental Sciences, P.O. Box 65, 00014 University of Helsinki, Finland.*

J.O., *Centre for Climate, the Environment & Chronology, Archaeology & Palaeoecology Building, Queen's University Belfast, 42 Fitzwilliam Street, Belfast BT9 6AX, UK.*

Silica diagenesis and its effect on porosity of upper Maastrichtian chalk – an example from the Eldfisk Field, the North Sea

Heine Buus Madsen

Diagenetic precipitation of silicate minerals such as quartz and clay minerals can reduce the permeability and porosity of chalk as they precipitate as cement in pores (e.g. Taylor & Lapré 1987; Maliva & Dickson 1992). However, the precipitation can also result in early lithification and help to preserve porosity during burial.

Several studies of diagenesis have been carried out on chalk samples from the North Sea oil fields (e.g. Scholle 1977; Maliva & Dickson 1992; Hancock 1993) but only a few have focused on silica diagenesis (Fabricius & Borre 2007; Fabricius *et al.* 2007). Silica is not a major constituent of chalk but is abundant in some intervals where it influences the reservoir properties, as seen for example in the Ekofisk Formation and in a few intervals in the underlying Tor Formation in the Eldfisk and Ekofisk fields. This distribution may indicate that the variations are linked to facies and palaeo-oceanography; the silica either representing diagenetically reprecipitated biogenic silica, volcanic ash falls or a high input of detrital minerals (Scholle 1977; Kennedy 1987; Fabricius & Borre 2007).

This paper discusses diagenesis of quartz- and kaolinite-rich intervals in the deeply buried upper Maastrichtian chalk of the upper Tor Formation (TA layer) in core 2/7-B-12 A from the Eldfisk Field in the Norwegian sector of the North Sea (Fig. 1). The study was carried out as part of a PhD project at the Geological Survey of Denmark and Greenland and the Department of Geography and Geology, University of Copenhagen (Madsen 2009). The objective of the study was to understand the processes leading to formation and enrichment of quartz and kaolinite and the resulting influence on porosity.

Lithology and mineralogy

The upper Tor Formation consists of grey bioturbated chalk with stylolites, argillaceous solution seams and a few marly layers in the studied core (Fig. 2). A single firmground is present at 10 480 ft. The chalk is usually almost pure carbonate with 96–97% calcite. The insoluble residue mainly consists of quartz and kaolinite, with small amounts of illite-smectite, feldspar, fluor-apatite, crandelite ($CaAl_3(PO_4)_{1.5}(OH)\cdot 5H_2O$), dolomite, pyrite and fluorite. However, up to 12% insoluble residue is present in two intervals at 10 420–10 431 and 10 470–10 480 ft. The 10 420–10 431 ft interval contains abundant stylolites, and overall the insoluble residue consists of the same minerals as in the pure chalk. The 10 470–10 480 ft interval only contains few marly layers and stylolites, and the insoluble residue in this interval is dominated by kaolinite and quartz.

Quartz occurs as euhedral crystals, aggregates and subhedral crystals. The euhedral crystals are six-sided and double-terminated by six-faced pyramids up to 10 µm long (Fig. 3A). Both crystals and aggregates are commonly associated with kaolinite. The quartz crystals commonly sit on kaolinite crystals but may also enclose the kaolinite (Fig. 3C). In the 10 420–10 431 ft interval the subhedral quartz crystals, up to 25 µm in size, enclose recrystallised coccolith fragments and older quartz crystals. The subhedral quartz crystals only show few well-developed crystal faces, commonly with imprints from recrystallised coccolith fragments.

Kaolinite occurs as hexagonal crystals arranged in booklets, commonly around 5 µm in diameter (Fig. 3A–C). The kaolinite is found both in voids and as part of the matrix. It is often associated with quartz aggregates and single quartz crystals (Fig. 3A, B). Energy-dispersive X-ray spectroscopy

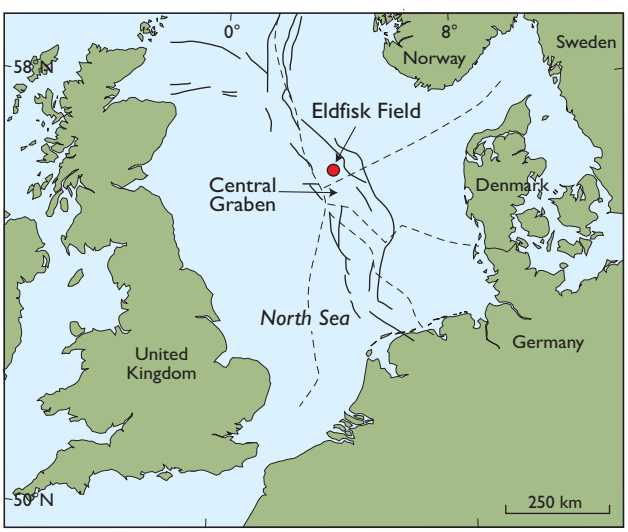

Fig. 1. Map of the North Sea region showing structural elements and the location of the Eldfisk Field. Dashed lines: national borders.

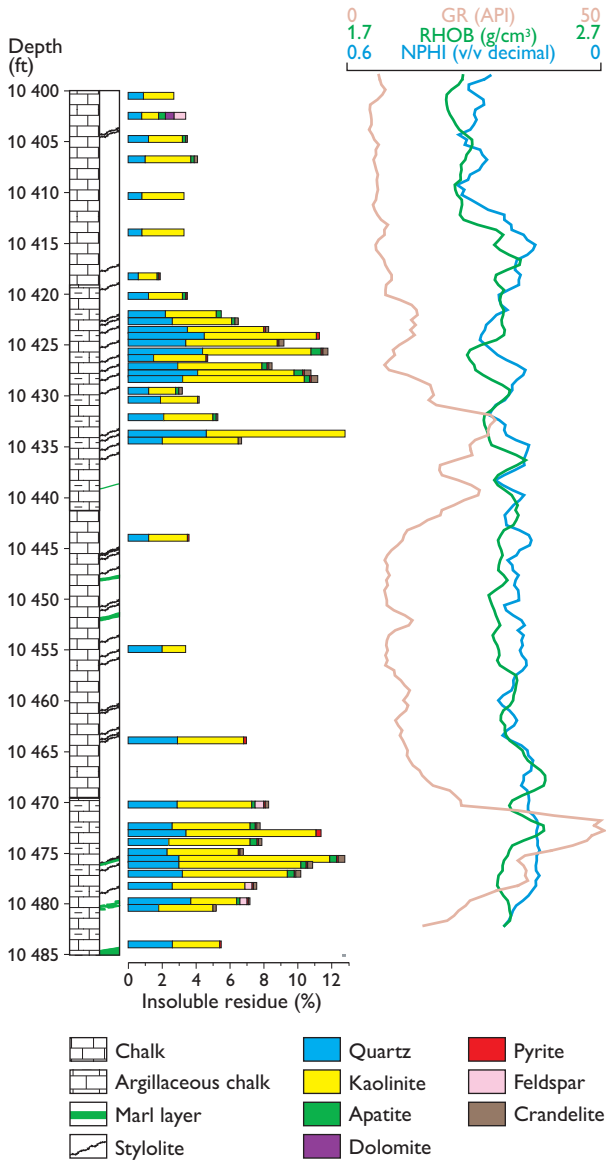

Fig. 2. Lithological and petrophysical logs of the upper part of the Tor Formation, showing the 10 400–10 495 ft interval in the 2/7-B-12 A core.

analyses show that the kaolinite primarily consists of Si, Al and O. Illite-smectite is present in trace amounts in all samples analysed by X-ray diffraction. It has a delicate, flaky morphology (Fig. 3D) and contains small amounts of K and Mg in addition to Si, Al and O.

Petrophysical characteristics of intervals rich in insoluble residue

In order to determine the petrophysical properties of the intervals high in insoluble residue, petrophysical logs, lithological variations and mineralogy were compared with each other. The interval 10 420–10 431 ft contains much more quartz and kaolinite than the surrounding chalk. The lower part of the interval shows high gamma-ray values (GR; Fig. 2). The neutron log (NPHI) and density log (RHOB) responses are similar to the surrounding chalk. High GR values are also seen below the 10 420–10 431 ft interval, indicating that the interval rich in insoluble residues extends down to 10 440 ft. In the 10 470–10 480 ft interval high GR values correlate with high contents of kaolinite and quartz, whereas no obvious peaks in NPHI and RHOB can be related to changes in the mineralogy (Fig. 2).

A neutron log versus density log plot of the studied succession shows that the chalk mainly plots between the sandstone and limestone trends (Fig. 4). This is due to the presence of hydrocarbons which are lighter than saline pore water. Both intervals rich in insoluble residue and the chalk between 10 415–10 485 ft have higher density and lower porosity than the upper interval at 10 400–10 415 ft. The estimated porosity of the chalk in the 10 400–10 415 ft interval is around 35% whereas the quartz- and kaolinite-rich intervals have porosities around 25% (Fig. 4). The high gamma-ray values (dark-brown plus signs) represent clay-rich parts and have estimated porosities of 20–25%.

Silicate diagenesis

The quartz and kaolinite may either have derived from detrital grains or from devitrification of volcanic ash. However, the latter produces bentonite which is dominated by illite and montmorillonite. Hence, volcanic ash cannot be the source. Weathering products such as smectite, kaolinite, quartz and feldspar from the nearby Baltic Shield are a more likely source for the quartz and kaolinite as also suggested by Kennedy (1987). The distribution of quartz and kaolinite in the two insoluble-rich intervals also indicates an event of longer duration than a volcanic eruption. However, some of the authigenic quartz probably originated from phase transformations of biogenic opal-A to opal-CT and finally to quartz.

The occurrence of long booklets of kaolinite indicates that some of it precipitated from solution (Fig. 3B). But the close association between quartz and kaolinite seen in the scanning electron microscope images indicates that they originated from mineral reactions (Fig. 3A, C). The disappearance of smectite and the formation of illite with depth are well known in the Central Graben in the North Sea and in other sedimentary basins (Compton 1991; Abercrombie *et al.* 1994; Drits *et al.* 1997). However, since kaolinite is the most abundant clay mineral in the studied interval, a slight-

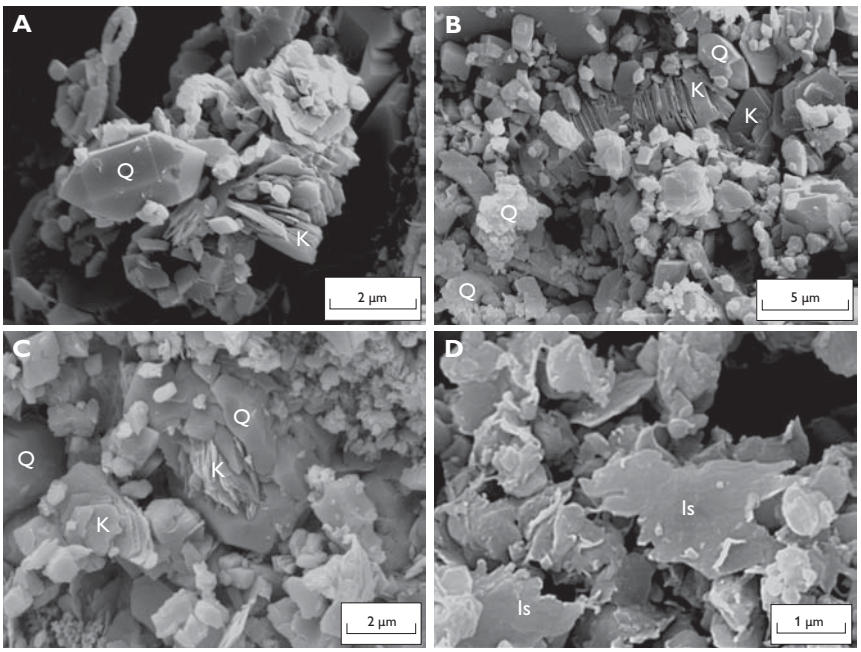

Fig. 3. Scanning electron microphotographs of chalk samples illustrating components of the insoluble residue. **A**: Double-terminated quarts crystal (**Q**) sitting on kaolinite (**K**). **B**: Quartz aggregates (lower left corner (**Q**), consisting of sub-micron sized quartz crystals) and booklets of kaolinite (**K**). **C**: Kaolinite (**K**) embedded in quartz (**Q**). **D**: Flaky illite-smectite (**Is**).

ly different mineral reaction is suggested where smectite is mainly transformed to kaolinite, following the equation:

smectite + K-feldspar → kaolinite + quartz + illite-smectite

The formation of kaolinite and illite-smectite is probably the result of release of Mg and Fe from the octahedral layer and Si from the tetrahedral layer in the smectite (Hower *et al.* 1976), which enables precipitation of quartz near the kaolinite as seen in Fig. 3. During this transformation aluminium is preserved in the structure (Compton 1991). The released Mg and Fe must have diffused away because only small amounts of dolomite or other Mg- and Fe-rich minerals are observed in the chalk (Fig. 2). Alternatively the smectite was originally poor in Mg and Fe.

Additional potassium, from K-feldspar or other sources is needed to form smectite-illite (Hoffman & Hower 1979; Compton 1991). The fact that kaolinite is the most common authigenic clay mineral indicates that detrital potassium-rich minerals were rare. However, dissolution of potassium-rich minerals has probably contributed with Al, Si and some K to the formation of kaolinite and smectite-illite, with excess Si precipitating as quartz. The mineral assemblage with kaolinite and quartz indicates a potassium-poor system, but the high gamma-ray values recorded in the two insoluble-rich intervals imply that minerals containing potassium or other radiogenic elements are indeed present (Fig. 2).

Porosity reduction

Due to a high primary content of detrital smectite and illite-smectite in the 10 420–10 431 and 10 470–10 480 ft intervals, the primary sorting and hence the initial porosities were lower than in the surrounding chalk. The neutron log versus density log plot (Fig. 4) shows an estimated porosity of *c.* 35% for samples of pure chalk (the 10 400–10 415 ft interval), and porosities of *c.* 27% and 22% for the 10 420–10 431 and 10 470–10 480 ft intervals that are rich in insoluble residue. This confirms that the content of detrital minerals had a great effect on the initial porosities. However, precipitation of quartz and kaolinite in pores reduced the porosity further.

Conclusions

Two intervals with high contents of insoluble residue, up to 12%, were found in the upper Tor Formation in the 2/7-B-12 A core from the Eldfisk Field. The insoluble residue primarily consists of authigenic quartz and kaolinite with subordinate illite-smectite. The kaolinite, illite-smectite and quartz formed both by precipitation from solution and by mineral reactions during burial. The release of Mg, Fe and Si and the addition of Al in the crystal latice of detrital smectite resulted in a mineral reaction that formed most of the kaolinite. Dissolution of feldspar contributed Al, and the released Si precipitated as quartz at or near the kaolinite. The intervals represent potassium-poor systems where kaolinite precipitat-

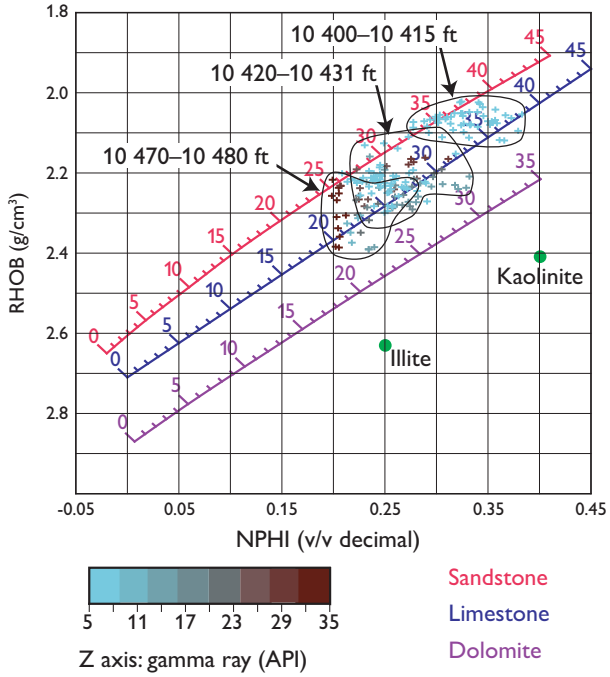

Fig. 4. NPHI versus RHOB plot of the 10 400–10 495 ft interval in core 2/7-B-12 A from the Eldfisk Field. Trends for sandstone, limestone and dolomite porosities are shown for comparison. The pure chalk at 10 400–10 420 ft mostly shows high estimated porosities (*c.* 35%), whereas the lower section and the intervals rich in insoluble residue show lower porosities. The dark brown coloured data points reflect high gamma-ray value samples, which also have the lowest estimated porosities (the 10 470–10 480 ft interval).

ed rather than illite-smectite. The high content of insoluble residue in the 10 420–10 431 ft and 10 470–10 480 ft intervals was probably caused by a high content of detrital minerals, causing poor sorting and lower porosities compared to the more pure chalk. Precipitation of kaolinite and quartz caused a minor additional reduction of the porosity in the insoluble residue-rich intervals.

Acknowledgements

ConocoPhillips Norway is thanked for financial support and for providing core material and geophysical logs.

References

Abercrombie, H.J., Hutcheon, I.E.. Bloch, J.D. & Decaritat, P. 1994: Silica activity and the smectite-illite reaction. Geology **22,** 539–542.

Compton, J.S. 1991: Origin and diagenesis of clay minerals in the Monterey Formation, Santa Maria Basin area, California. Clays and Clay Minerals **39**, 449–466.

Drits, V.A., Sakharov B.A., Lindgreen, H. & Salyn, A. 1997: Sequential structure transformation of illite-smectite-vermiculite during diagenesis of Upper Jurassic shales from the North Sea and Denmark. Clay Minerals **32**, 351–371.

Fabricius, I.L. & Borre, M.K. 2007: Stylolites, porosity, depositional texture, and silicates in chalk facies sediments. Ontong Java Plateau – Gorm and Tyra fields, North Sea. Sedimentology **54**, 183–205.

Fabricius, I.L., Røgen, B. & Gommesen, L. 2007: How depositional texture and diagenesis control petrophysical and elastic properties of samples from five North Sea chalk fields. Petroleum Geoscience **13**, 81–95.

Hancock, J.M. 1993: The formation and diagenesis of chalk. In: Downing, R.A., Price, M. & Jones, G.P. (eds): The hydrogeology of the chalk of North-West Europe, 14–34. New York: Oxford University Press.

Hoffman, J. & Hower, J. 1979: Clay mineral assemblages as low grade metamorphic geothermometers: application to the thrust faulted disturbed belt of Montana, U.S.A. In: Scholle, P.A. & Schluger, P.R. (eds): Aspects of diagenesis. Society of Economic Paleontologists and Mineralogists (SEPM) Special Publications **26**, 55–79.

Hower, J., Eslinger, E.V., Hower, M. & Perry, E.A. 1976: The mechanism of burial metamorphism of argillaceous sediments: **1**. Mineralogical and chemical evidence. Geological Society of America Bulletin **87**, 725–737.

Kennedy, W.J. 1987: Sedimentology of Late Cretaceous–Paleocene chalk reservoirs, North Sea Central Graben. In: Brooks, J. & Glennie, K.W. (eds): Petroleum geology of North West Europe, 469–481. Proceedings of the 3rd conference on petroleum geology of North West Europe. London: Graham & Trotman.

Madsen, H.B. 2009: Microbial and burial induced silica diagenesis in Upper Cretaceous – Paleogene chalk in Denmark and the North Sea. PhD thesis, University of Copenhagen, Denmark. Danmarks og Grønlands Geologiske Undersøgelse Rapport **2009/41**, 33 pp.

Maliva, R.G. & Dickson, J.A.D. 1992: Microfacies and diagenetic controls of porosity in Cretaceous/Tertiary chalks, Eldfisk, Norwegian North Sea. AAPG Bulletin **76**, 1825–1838. Tulsa, Oklahoma: American Association of Petroleum Geologists.

Scholle, P.A. 1977: Chalk diagenesis and its relation to petroleum exploration. AAPG Bulletin **61**, 982–1009. Tulsa, Oklahoma: American Association of Petroleum Geologists.

Taylor, S.R. & Lapré, J.F. 1987: North Sea chalk diagenesis: its effect on reservoir location and properties. In: Brooks, J. & Glennie K.W. (eds): Petroleum geology of North West Europe, 483–495. Proceedings of the 3rd conference on petroleum geology of North West Europe. London: Graham & Trotman.

Author's address

Geological Survey of Denmark and Greenland, Øster Voldgade 10, DK-1350 Copenhagen K, Denmark. E-mail: *heinebuus@yahoo.com*

The Continental Shelf Project of the Kingdom of Denmark – status at the beginning of 2010

Christian Marcussen and Martin V. Heinesen

The Kingdom of Denmark (Denmark, Faroe Islands and Greenland) ratified the United Nations Convention on the Law of the Sea (UNCLOS) on 16 November, 2004 and this allows for a period of ten years to submit extended continental shelf claims beyond 200 nautical miles (NM) to the Commission on the Limits of the Continental Shelf. To acquire the necessary data for delineating the extended continental shelf, the Continental Shelf Project of the Kingdom of Denmark was launched by the Ministry of Science, Technology and Innovation in cooperation with the Faroese and Greenland governments. Several institutions participate in the project. The technical work for the Greenland part is coordinated by the Geological Survey of Denmark and Greenland (GEUS) and the coordination of the Faroese part is shared between the Faroese Earth and Energy Directorate (Jarðfeingi) and GEUS. Further information can be found on the project website www.a76.dk.

Background

Article 76 of UNCLOS is the key to future jurisdiction over resources on and below the seabed beyond the 200 NM limit. The right to explore and exploit these resources, which include both non-living resources (hydrocarbons and minerals) and bottom-dwelling living resources, may have significant economic implications. According to Article 76, a variety of scientific and technical data are required to be submitted to the Commission on the Limits of the Continental Shelf. These include geodetic, bathymetric, geophysical and geological data regarding e.g. the 200 NM and 350 NM limits from the territorial baselines, the location of the foot of the continental slope, the 2500 m isobath and the sediment thickness beyond the foot of the slope. The latter is defined as the point of maximum change in the gradient at the base of the continental slope.

Areas of interest – the Faroe Islands

The continental shelf of the Faroe Islands extends beyond 200 NM in two geographical regions, here referred to as the Northern and the Southern Area (Figs 1, 2). The geomorphological and geological settings are fundamentally different in the two areas. Already in the early phase of the project, informal arrangements were made with the neighbouring states for exchange of data, and these data form a significant part of the overall data base in both areas.

Field work has been carried out in 2003, 2004, 2005, 2007 and 2008. A wide range of data and samples has been collected including seismic reflection and refraction data, single- and multibeam echo sounder bathymetric data, sediment cores, marine gravity data and airborne magnetic data.

Northern Area. North of the Faroe Islands (Fig. 1), the continental margin is characterised by a number of ridges and elevated sea-floor highs that extend from the shelf and slope region into the Northern Deep. The most pronounced of these sea-floor highs is the Ægir Ridge, which is an extinct part of the spreading system that created the oceanic sea floor of the Northern Deep. The Northern Deep is a large sedimentary

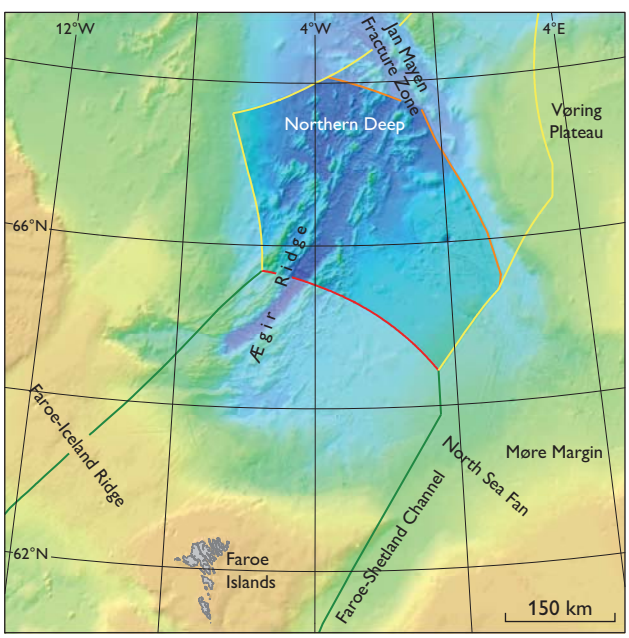

Fig. 1. The Northern Continental Shelf of the Faroe Islands. The continental shelf beyond 200 NM in the area north of the Faroe Islands, as delineated in the submission, amounts to 87 792 km^2 and is highlighted. Green: agreed borders within 200 NM. Red: Faroese 200 NM limit. Yellow: Iceland's and Norway's EEZ (exclusive economic zone; 200 NM). Orange: outer limit of the continental shelf.

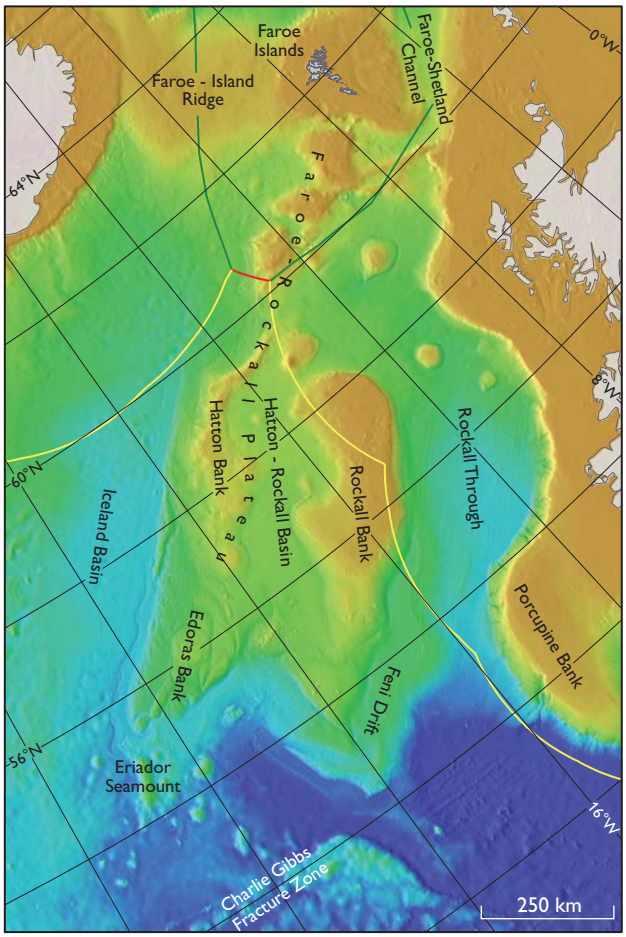

Fig. 2. The Southern Continental Shelf of the Faroe Islands. Green: agreed borders within 200 NM. Red: Faroese 200 NM limit. Yellow: Iceland's, Ireland's and UK's EEZ (200 NM). The outer continental shelf in this area amounts to *c*. 500 000 km^2.

basin with sediment thicknesses locally reaching 3 km. The continental margin is strongly affected by slope-related processes (mass wasting, turbidity currents, etc.) and complex erosional and depositional actions of strong ocean currents.

After a period of processing, interpreting and analysing the data in accordance with Article 76 of UNCLOS and the Technical and Scientific Guidelines of the Commission on the Limits of the Continental Shelf (1999), a special task force was established with the responsibility of producing the formal documentation for the Northern Area to be submitted to the Commission. Nine task force members were selected for their expertise in a wide range of geoscientific and legal disciplines and they represent a number of governmental institutions and ministries in Denmark and the Faroe Islands.

The task force initiated its preparation of the submission in April 2008, and by April 2009 the documentation was delivered to the Danish Ministry of Foreign Affairs who formally submitted it to the Commission on the Limits of the Continental Shelf on 29 April, 2009 on behalf of the Kingdom of Denmark. On 27 August, 2009 the submission was presented to the Commission by a Danish–Faroese delegation during its 24th formal session.

The continental shelf beyond 200 NM in the area north of the Faroe Islands, as delineated in the submission, amounts to 87 792 km^2 (Fig. 1). The area overlaps with regions that are also covered by submissions of the two neighbouring states, Norway and Iceland. The three nations have made a mutual agreement on how to divide the continental shelf area between themselves that is without prejudice to the work of the Commission on the Limits of the Continental Shelf.

Southern Area. The Southern Area (Fig. 2) is dominated by the continental Faroe-Rockall Plateau that extends several hundred nautical miles toward the south-west. Three additional states, the United Kingdom, Ireland and Iceland, include the area as part of their outer continental shelf. Geologically and geomorphologically the plateau is characterised by a number of banks and basins where continental crust and older sediments are covered by Palaeogene syn- and post-breakup volcanic strata that are similar to those found on the Faroe Islands. The marginal parts of the plateau are characterised by extensive sediment accumulations, mainly contourites that were deposited by bottom currents along the lower part of the continental slope. The task force is presently preparing the submission documents for the Southern Area and expects to deliver the final documentation to the Ministry of Foreign Affairs by the end of 2010.

Areas of interest – Greenland

Three areas around Greenland have been defined as areas of interest regarding an extension of the continental shelf beyond 200 NM: an area south of Greenland (including the Eirik Ridge), an area off North-East Greenland near the East Greenland Ridge and an area north of Greenland along the Lomonosov Ridge and in the Amundsen Basin (Figs 3–5). The three areas are briefly described in Marcussen *et al.* (2004). As with the Faroe Islands work commercial contractors were used to acquire seismic reflection and bathymetric data. However, because of the sea-ice conditions off North-East and North Greenland data from these regions have been acquired in cooperation with Canada and Sweden.

Area south of Greenland. The region south of Greenland (Fig. 3) is characterised by a fairly narrow shelf and by thick sedimentary successions between Greenland and Canada, especially within the extinct spreading zone. The main tasks

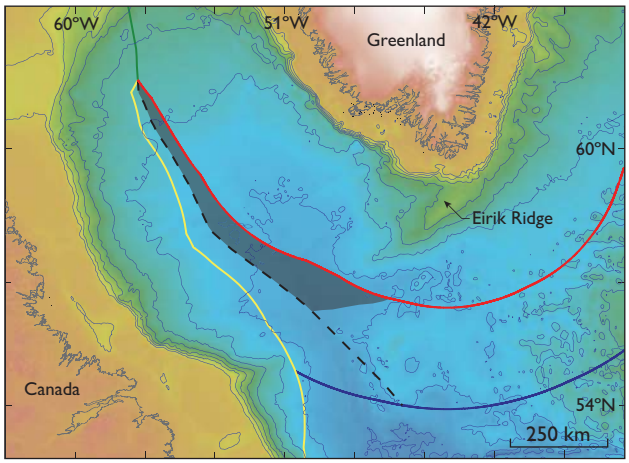

Fig. 3. The potential claim area off southern Greenland (grey tone) has a size of approximately 45 000 km^2. Green: agreed border within 200 NM. Red: Greenland's EEZ. Yellow: Canada's EEZ. Blue: 350 NM limit. Dashed line: unofficial median line between Greenland and Canada.

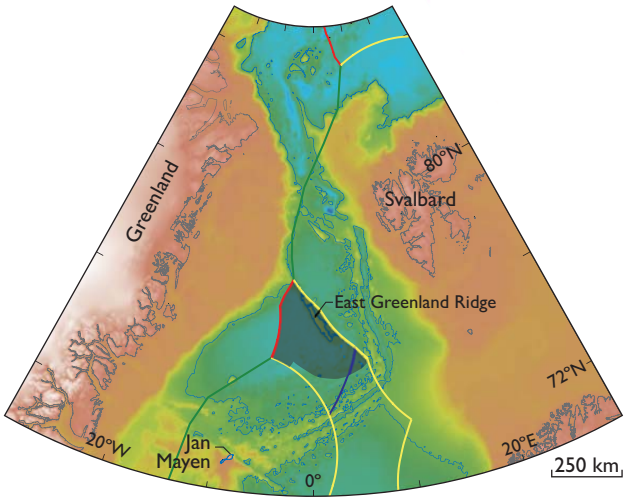

Fig. 4. The potential claim area off North-East Greenland (grey tone) with an approximate size of 63 000 km^2. Green: agreed boundaries within the 200 NM limit between Greenland–Svalbard and Greenland–Jan Mayen. Red: Greenland's EEZ. Yellow: Norway's EEZ from Svalbard and Jan Mayen. Blue: 350 NM limit.

in this region are threefold: to map the bathymetry of the continental slope especially along the Eirik Ridge in order to outline the foot of the continental slope, to map the sediment thickness and to investigate the nature of the Eirik Ridge.

Two seismic surveys were carried out in 2003 and 2006 to map the sediment thickness. A total of *c.* 4000 km of data were acquired. Other already existing commercial and scientific data supplement these acquired data. In 2008 the bathymetry of the continental slope and parts of Eirik Ridge was mapped by multibeam echo sounding. This data set was supplemented in 2009 with data acquired during a German research cruise (Uenzelmann-Neben 2009). Also in 2009, a joint Canadian-Danish cruise mapped the deeper structure of the Eirik Ridge using refraction seismic profiling (Funck *et al.* 2009). Data acquisition in the area south of Greenland within the Continental Shelf project is now completed and a task force will prepare the submission documents for this area in 2011.

Area north-east of Greenland. This region (Fig. 4) is characterised by a wide continental shelf. The East Greenland Ridge is assumed to be a natural prolongation of north-eastern Greenland.

In the summer of 2002, GEUS and the University of Bergen carried out a joint seismic refraction and reflection survey of the East Greenland Ridge. Interpretations of the refraction data show that the velocity structure of the East Greenland Ridge is consistent with continental crust (Døssing *et al.* 2008). During the LOMROG I cruise with the Swedish icebreaker *Oden* bathymetric mapping of the East Greenland Ridge and the continental slope of the East Greenland shelf south-west of the ridge was initiated. The plan is to complete this mapping over the next few years and to supplement it with seismic data and geological sampling.

Area north of Greenland. The Lomonosov Ridge and the Morris Jesup Rise are assumed to be natural prolongations of northern Greenland (Fig. 5). Older seismic data from the Amundsen Basin have shown sediments with sufficient thickness to be used in extending the continental shelf (Weigelt & Jokat 2001).

Due to the difficult year-round sea-ice conditions in this region and the lack of appropriate Danish logistical possibilities and research platforms, data collection in this area requires cooperation with other countries (MacDougall *et al.* 2008). Therefore, in 2005 a Memorandum of Understanding was signed with Canada that forms the basis for six major data acquisition programmes mainly in the area north of Greenland.

In the spring of 2006, seismic refraction data were collected from the sea ice during the LORITA expedition (Jackson & Dahl-Jensen 2007). Field work in the spring of 2009 concentrated on bathymetric and gravimetric data acquisition supplemented by aerogeophysical measurements. In order to acquire seismic data under difficult ice conditions, a seismic reflection acquisition system has been developed in cooperation with the Department of Earth Sciences, Aarhus University, based on experience gained from other surveys in the Arctic by Canadian, German, Norwegian and US institutions. By cooperating with the Swedish Polar Research Secretariat it was possible to use *Oden* during two cruises (Jakobsson *et*

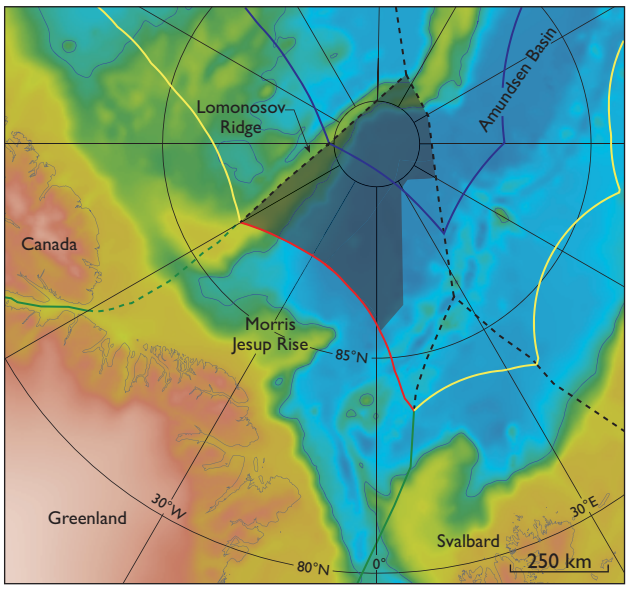

Fig. 5. The potential claim area off North Greenland (grey tone) can have a size up to 150 000 km^2. Red: Greenland's EEZ. Yellow: Canada's, Norway's and the Russian Federation's EEZ. Blue: the 350 NM limit. Green: the agreed boundaries within 200 NM between Greenland–Svalbard and Greenland–Canada. Stippled green line: Greenland's EEZ north of the agreed boundary with Canada (1973, but within 200 NM). Black stippled lines: unofficial median lines.

al. 2008, Marcussen *et al.* 2010). Further work is planned for either 2011 or 2012. Since 2007 the Canadian, Russian and Danish continental shelf projects have discussed scientific issues regarding the Lomonosov Ridge on a regular basis.

Conclusions

Since the start of the project the work has progressed according to plan and submissions for the two Faroese areas will be completed in 2010. Data acquisition is complete for the area south of Greenland. Due to difficult ice conditions, work in the areas north-east and north of Greenland will not be completed until the end of 2014.

Due to the high number of submissions received by the Commission on the Limits of the Continental Shelf, final processing of the two partial submissions for the Faroe Islands may not start until several years after the submissions. The Commission on the Limits of the Continental Shelf could spend 1–2 years considering the documents before reaching a conclusion and submitting a recommendation for the final outer limits of the continental shelf.

References

Commission on the Limits of the Continental Shelf 1999: Scientific and Technical Guidelines of the Commission, CLCS/11 (http://www.un.org/Depts/los/clcs_new/commission_documents.htm#Guidelines).

Døssing, A., Dahl-Jensen, T., Thybo, H., Mjelde, R. & Nishimura, Y. 2008: East Greenland Ridge in the North Atlantic Ocean: an integrated geophysical study of a continental sliver in a boundary transform fault setting. Journal of Geophysical Research **113**, B10107, 33 pp.

Funck, T., Dehler, S.A., Chapman, C.B., Delescluse, M., Iuliucci, J., Iuliucci, R., Judge, W., Meslin, P. & Ruhnau, M. 2009: Cruise report of the SIGNAL 2009 refraction seismic cruise (Hudson 2009-019). Danmarks og Grønlands Geologiske Undersøgelse Rapport **2009/74**, 60 pp., 2 appendices + 1 CD.

Jackson, H.R. & Dahl-Jensen, T. (eds) 2007: Field report for LORITA 2006 – Lomonosov Ridge test of appurtenance. Danmarks og Grønlands Geologiske Undersøgelse Rapport **2007/5**, 184 pp.

Jakobsson, M., Marcussen, C. & LOMROG Scientific Party 2008: Lomonosov Ridge off Greenland 2007 (LOMROG) cruise report, 122 pp. Copenhagen: Geological Survey of Denmark and Greenland.

MacDougall, J.R., Verhoef, J., Sanford, W. & Marcussen, C. 2008: Challenges of collecting data for Article 76 in ice covered waters of the Arctic. 5th ABLOS Conference Difficulties in Implementing the Provisions of UNCLOS 15–17 October 2008, 21 pp. (http://www.gmat.unsw.edu.au/ablos/ABLOS08Folder/Session4-Paper1-Macdougall.pdf).

Marcussen, C., Christiansen, F.G., Dahl-Jensen, T., Heinesen, M., Lomholt, S., Møller, J.J. & Sørensen, K. 2004: Exploring for extended continental shelf claims off Greenland and the Faroe Islands – geological perspectives. Geological Survey of Denmark and Greenland Bulletin **4**, 61–64.

Marcussen, C. & LOMROG II Scientific Party 2010: LOMROG II – continued data acquisition in the area north of Greenland. 2009 yearbook of the Swedish Polar Research Secretariat, Stockholm, 43–51. (http://www.polar.se/organisation/pdf/yearbook2009.pdf).

Memorandum of Understanding between the Earth Sciences Sector of the Department of Natural Resources of Canada and the Geological Survey of Denmark and Greenland of the Ministry of the Environment of Denmark concerning cooperation relating to the delineation of their continental shelves, signed 21 June 2005.

The Government of the Kingdom of Denmark together with the Government of the Faroes 2009: The continental shelf north of the Faroe Islands. Partial submission. Executive Summary, 20 pp. (http://a76.dk/xpdf/dnk2009executivesummary_s.pdf).

Uenzelmann-Neben, G. (ed.) 2009: The expedition of the research vessel 'Maria S. Merian' to the Labrador Sea in 2009 (MSM 12/2) Reykjavik – Reykjavik 17 June – 13 July 2009. Berichte zur Polar- und Meeresforschung **599**, 91 pp. (http://hdl.handle.net/10013/epic.33539).

Weigelt, E. & Jokat, W. 2001: Peculiarities of roughness and thickness of oceanic crust in the Eurasian Basin, Arctic Ocean. Geophysical Journal International **145**, 505–516.

Authors' addresses

C.M., *Geological Survey of Denmark and Greenland, Øster Voldgade 10, DK-1350 Copenhagen K, Denmark*. E-mail: *cma@geus.dk*

M.V.H., *Faroese Earth and Energy Directorate (Jarðfeingi), Brekkutún 1, 188 Hoyvík, Faroe Islands*.

Greenland ice sheet monitoring network (GLISN): a seismological approach

Trine Dahl-Jensen, Tine B. Larsen, Peter H. Voss and the GLISN group

The dynamics of the large outlet glaciers in Greenland is attracting both scientific and political attention due to the possible implications of a rising global sea level. Extensive glaciological and meteorological monitoring programmes have been implemented to quantify and track changes in the ice sheet and local glaciers (Ahlstrøm *et al.* 2008). The dynamic processes controlling the flow of the outlet glaciers are complex and poorly understood, involving a wealth of parameters such as bed conditions, hydrology and meteorological conditions. It is desirable to obtain as many fundamentally independent data sets as possible to understand and eventually predict the behaviour of the outlet glaciers.

Some processes related to ice dynamics can be detected seismologically and thus completely independently from classical ice-monitoring techniques, such as satellite remote sensing, global positioning system (GPS) geodesy and automatic weather stations. Detectable cryo-seismological events include high-frequency ice quakes (Anandakrishnan & Bentley 1993; Harrison *et al.* 1993), calving events (O'Neel *et al.* 2006; Nettles *et al.* 2008) and less well understood processes such as low-frequency glacial earthquakes (Ekstrom *et al.* 2003; Nettles *et al.* 2008)) and glacial rumblings (Rial *et al.* 2009). Changes in ice load along the margin of the ice sheet can lead to earthquakes from glacial rebound, and earthquakes can provide an independent constraint on ice mass redistribution (Johnston 1987; Stewart *et al.* 2000; Lund & Näslund 2009).

The Greenland ice sheet monitoring network (GLISN) project will monitor changes in glacier dynamics using a large broadband seismological network. The network will also improve the detection of tectonic earthquakes in Greenland, thereby establishing a better baseline for local seismicity. The baseline will allow detection of future changes in seismicity caused by changes in ice load. It is the objective of the project to contribute significantly to understanding the dynamics of the Greenland ice sheet and glaciers by studying cryo-seismological processes.

Installing and operating a large real-time seismological network in Greenland is logistically complicated and expensive. An international team consisting of researchers from 10 institutions in 8 countries in Europe, North America and Asia are working together to meet this challenge (Fig. 1).

Glacial earthquakes and rumblings

Cryo-seismological events such as glacial earthquakes and rumblings can be linked to large-scale glacier dynamics. Glacial earthquakes are produced at large outlet glaciers and appear to be associated with large calving events (Amundson *et al.* 2008; Nettles *et al.* 2008). However, the processes leading

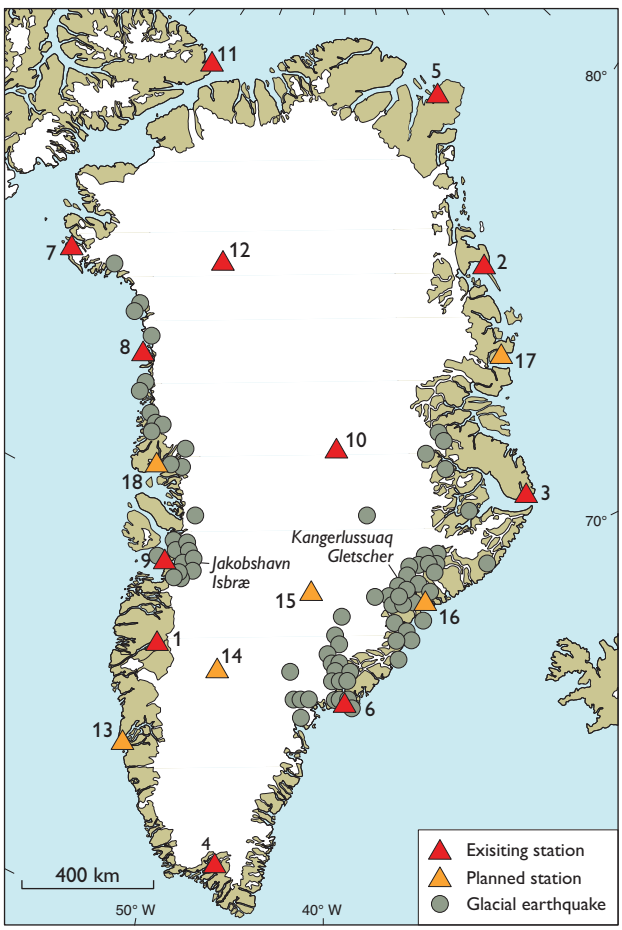

Fig. 1. Map of broadband seismographs in Greenland. 1–4: permanent stations operated by GEUS in cooperation with other institutions. 5–7: long-term stations maintained by GEUS. 8–9: new GLISN long-term stations run by ETH (Switzerland). 10: a long-term station run by GEOFON (Germany). 11: a permanent station at Alert in Canada run by IRIS (USA). 12: a temporary station run by GEUS. 13–18: planned and funded new GLISN stations to be installed by IRIS and ETH.

to a glacial earthquake are still poorly understood, as are the changes in dynamics following an earthquake.

Glacial earthquakes are slow, low-frequency events that can be detected on seismographs worldwide. The vast majority of glacial earthquakes in Greenland occur at the large outlet glaciers in western and eastern Greenland (Fig. 1; Ekstrom *et al.* 2003). During a period with warmer than average temperatures in Greenland, a sharp increase in the number of glacial earthquakes has been observed (Ekstrom *et al.* 2006); during the same period there was no change in the number of observed tectonic earthquakes.

The glacial earthquakes can be registered at teleseismic distances, and the teleseismic signals are sufficiently strong to locate the earthquakes. However, the signals from glacial earthquakes are fundamentally different from the signals generated by tectonic earthquakes. The short-period signal from a 4.9 magnitude glacial earthquake is barely discernable on seismograms *c.* 1000 km away as shown in Fig. 2A. The data record has been filtered from 0.5 to 1.3 sec where *P* (primary) waves normally dominate the seismogram. Close to the epicentre of a glacial earthquake, the *P* wave is clearly visible (at Sødalen and Summit; Fig. 2A), whereas it requires supporting stations to identify the signal at Danmarkshavn approximately 974 km away and the short-period signal is completely lost at Alert 1645 km away. For a tectonic earthquake of similar magnitude, the short-period *P* wave can travel many thousands of kilometres without being dissipated below the noise level. The longer periods in the signal from a glacial earthquake are not dissipated as rapidly as the shorter periods (Fig. 2B) and retain a good quality at teleseismic distances.

The higher-frequency waves generated by a glacial earthquake contain information about processes in and around the glacier during the earthquake. In order to understand the earthquake processes it is necessary to model waveforms recorded at local and regional distances where the full frequency range is retained. This is currently only possible for a small portion of the glacial earthquakes occurring in Green-

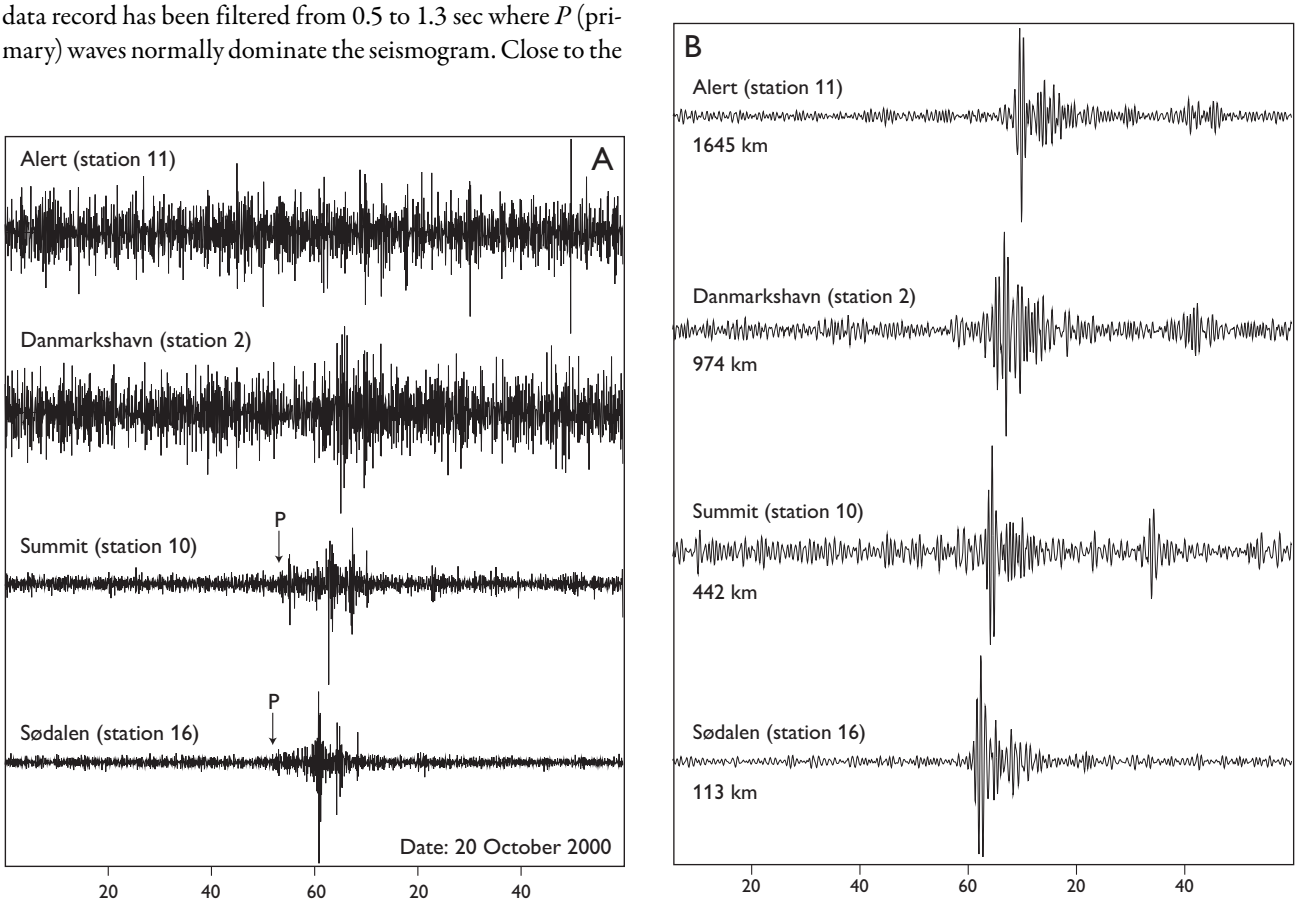

Fig. 2. A large glacial earthquake released by the Kangerlussuaq Gletscher (Fig. 1). The window shows 2 hours of data from four broadband seismographs in Greenland and Canada, located 113–1645 km from the earthquake. Station numbers refer to Fig. 1. The curves show vertical components band-pass filtered from 0.769–2.000 Hz (**A**) and 0.01–0.03 Hz (**B**). The glacial earthquake was registered from *c.* 02:00–02:15 UTC and had a magnitude of 4.9 on the Richter scale according to Ekstrom *et al.* 2003. In **A** the arrival of the *P* wave is marked by arrows on the two closest stations (Summit and Sødalen). The arrival of the *P* wave is commonly only visible at higher frequencies and at stations close by. The data from Sødalen are from a station that was in operation from 2000 to 2002.

land, but with the implementation of the GLISN network the glacial earthquakes can be investigated in greater detail than today.

Glacial rumblings are slow, high-frequency events at the large outlet glaciers, and also appear to be related to calving that can be detected only at local to regional distances (Fig. 3). Rumblings have so far been described in only one publication for the Jakobshavn Isbræ (Rial *et al.* 2009), but can be found in data from other regions of Greenland as well. It has been postulated that up to 30% of the annual iceberg discharge from Jakobshavn Isbræ can be related to rumblings that are registered on seismographs (Rial *et al.* 2009), but it has not yet been possible to make a similar estimate for the glacial earthquakes.

The GLISN project will establish and run a dense network that can capture events both at currently seismologically active glaciers and at glaciers farther to the north should the activity migrate northwards. The seismological signals may provide an early warning of changes in glacier activity.

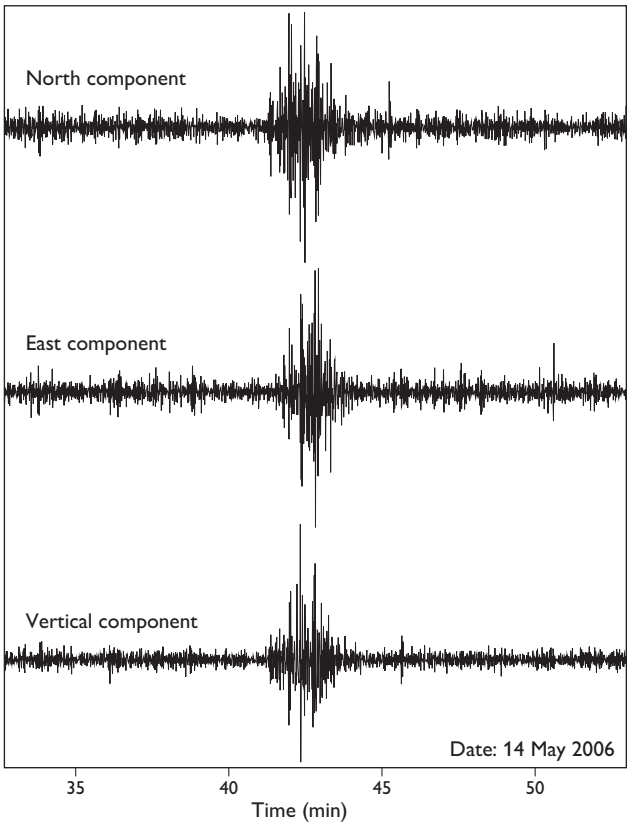

Fig. 3. Rumbling from Jakobshavn Isbræ observed on the broadband seismograph at station 1 (Fig. 1). The window shows 20 minutes of seismic data that have been band-pass filtered from 5 to 9.9 Hz. The glacier rumbling was observed from *c.* 12:41 to 12:44 UTC and is described by Rial *et al.* 2009. On our local scale the event was of magnitude 2.1.

Establishing the network

The aim of the GLISN project is to cover all of Greenland and surrounding areas with as regular a seismological network as feasible (Fig. 1). The stations will be upgraded to a common standard and will provide real-time data online. Stations situated in Greenland communities will transmit data by ADSL broadband, while data from the remote stations will be transmitted by satellite, using the Iridium system. New sites are chosen to cover areas close to sites where glacial seismological events are known to occur, and to ensure monitoring of the whole of Greenland, so that changes in occurrence patterns such as a northwards shift can be detected. The main challenge is the operation of stations in remote areas, not least those on the Greenland ice sheet. Two sites on the ice sheet (sites 12 and 14; Fig. 1) will be equipped with surface seismographs dug into the snow. Since these are quite sensitive to settling snow and loss of levelling, these sites will also be equipped with seismographs in 300 m deep boreholes, in which the seismograph is fixed to ice instead of snow making it more stable. The network upgrade and installation were initiated in 2009, and are planned to be completed in 2011.

International cooperation

GLISN is an international cooperation between Incorporated Research Institutions for Seismology (IRIS) in the USA, Geological Survey of Denmark and Greenland (GEUS), GeoForschungsZentrum Network (GEOFON) in Germany, ETH Zürich in Switzerland, Istituto Nazionale di Geofisica e Vulcanologia (INGV) in Italy, National Institute of Polar Research (NIPR) and Japan Agency for Marine-Earth Science and Technology (JAMSTEC) both in Japan, NORSAR in Norway and Geological Survey of Canada (GSC). The group is open and other participants are welcome.

The operation of broadband stations in Greenland builds on work by GEUS (Dahl-Jensen *et al.* 2003). The contribution from GEUS to establish GLISN is the existing network, consisting of four permanent and four temporary stations, which has been in operation for up to a decade. Since 2002, our German colleagues have operated the only long-term station on the ice sheet at Summit Camp (station 10, Fig. 1), which is now also part of GLISN. Our Swiss colleagues installed two new GLISN stations in north-western Greenland in 2009 and will add one more in 2010. Furthermore, our colleagues from the USA have obtained a three-year grant from the National Science Foundation, providing the bulk of the funding for the project. This grant allows installation of five new stations and upgrading of the existing stations to

meet the technical standards for equipment and installation agreed for GLISN – including provision of real-time data.

Expected outcome

With GLISN we seek to increase our understanding of the processes governing the ice sheet and the dynamics of the outlet glaciers. The complex processes and dynamics must be studied from different angles, such as satellite data acquisition and geodetic and glaciological observations. Seismology, and thus the ability to detect events deep within and below the ice, is a new player in this field, raising many new questions.

Local seismicity in Greenland has not been addressed in detail for many years (Gregersen 1989; Dahl-Jensen 1984). However, increasingly detailed data have been gathered since 2000 (Dahl-Jensen *et al.* 2003) and data acquisition is rapidly increasing after the inauguration of GLISN. The pressure from ice sheets usually dampens earthquakes beneath the ice (Johnston 1987; Stewart *et al.* 2000; Lund & Näslund 2009). If the ice sheet thins and retreats in the future, the frequency of earthquakes related to glacial rebound will probably increase. Seismology is thus a tool to detect changes in the pressure on the subsurface due to climate changes.

GLISN also allows the continuation and expansion of the use of tectonic earthquakes to investigate the structure of the Greenland crust, lithosphere and upper mantle in increasing detail (Dahl-Jensen *et al.* 2003; Darbyshire *et al.* 2004; Kumar *et al.* 2005, 2007; Larsen *et al.* 2006; Ucisik *et al.* 2008).

Acknowledgements

The entire GLISN group forms the backbone of GLISN. The website www.glisn.info provides additional information on contributions and funding.

References

Ahlstrøm, A.P. & the Promice project team 2008: A new programme for monitoring the mass loss of the Greenland ice sheet. Geological Survey of Denmark and Greenland Bulletin **15**, 61–64.

Amundson, J.M., Truffer, M., Lüthi, M.P., Fahnestock, M., West, M. & Motyka, R.J. 2008: Glacier, fjord, and seismic response to recent large calving events, Jakobshavn Isbræ, Greenland. Geophysical Research Letters **35**, L22501, doi:10.1029/2008GL035281.

Anandakrishnan, S. & Bentley, C.R. 1993: Micro-earthquakes beneath Ice Streams B and C, West Antarctica: observations and implications. Journal of Glaciology **39**, 455–462.

Dahl-Jensen, T. 1984: Jordskælv og skorpestruktur i Grønland, 73 pp. Unpublished M.Sc. thesis, Københavns Universitet, Danmark.

Dahl-Jensen, T., Larsen, T., Wölbern, I., Bach, T., Hanka, W., Kind, R., Gregersen, S., Mosegaard, K., Voss, P. & Gudmundsson, O. 2003: Depth to Moho in Greenland: receiver function analysis suggests two Proterozoic blocks in Greenland. Earth and Planetary Science Letters **205**, 379–393.

Darbyshire, F.A., Larsen, T.B., Mosegaard, K., Dahl-Jensen, T., Gudmundsson, O., Bach, T., Gregersen, S., Pedersen, H. & Hanka, W. 2004: A first detailed look at the Greenland lithosphere and upper mantle using Rayleigh wave tomography. Geophysical Journal International **158**, 267–286.

Ekstrom, G., Nettles, M. & Abers, G.A. 2003: Glacial earthquakes. Science **302**, 622–624.

Ekstrom, G., Nettles, M. & Tsai, V.C. 2006: Seasonality and increasing frequency of Greenland glacial earthquakes. Science **311**, 1756–1758.

Gregersen, S. 1989: The seismicity of Greenland. In: Gregersen, S. & Basham, P.W. (eds): Earthquakes at North-Atlantic passive margins: Neotectonics and postglacial rebound, 345–353. Berlin: Springer.

Harrison, W., Echelmeyer, K. A. & Engelhardt, H. 1993: Short-period observations of speed, strain and seismicity on Ice Stream B, Antarctica. Journal of Glaciology **39**, 463–470.

Johnston, A.C. 1987: Suppression of earthquakes by large continental ice sheets. Nature **330**, 467–469.

Kumar, P. *et al.* 2005: The lithosphere–asthenosphere boundary in the North-West Atlantic region. Earth and Planetary Science Letters **236**, 249–257.

Kumar, P., Kind, R., Priestley, K. & Dahl-Jensen, T. 2007: Crustal structure of Iceland and Greenland from receiver function studies. Journal of Geophysical Research **112**, B03301.1–B03301.19.

Larsen, T.B., Dahl-Jensen, T., Voss, P., Jørgensen, T.M., Gregersen, S. & Rasmussen, H.P. 2006: Earthquake seismology in Greenland – improved data with multiple applications. Geological Survey of Denmark and Greenland Bulletin **10**, 57–60.

Lund, B. & Näslund, J.-O. 2009: Glacial isostatic adjustment: implications for glacially induced faulting and nuclear waste repositories. In: Connor, C.B., Chapman, N.A. & Connor, L.J. (eds): Volcanic and tectonic hazard assessment for nuclear facilities, 142–155. Cambridge: Cambridge University Press.

Nettles, M. *et al.* 2008: Step-wise changes in glacier flow speed coincide with calving and glacial earthquakes at Helheim Glacier, Greenland. Geophysical Research Letters **35**, L24503, doi:10.1029/2008GL036127.

O'Neel, S., Mcnamara, D., Marshall, H. & Pfeffer, T. 2006: Seismic evidence for time variation of mechanical failure associated with iceberg calving at Columbia Glacier, AK. EOS Transactions, American Geophysical Union, **87**(52), 1719 only.

Rial, J.A., Tang, C. & Steffen, K. 2009: Glacial rumblings from Jakobshavn ice stream, Greenland. Journal of Glaciology **55**, 389–399.

Stewart, I.S., Sauber, J. & Rose, J. 2000: Glacio-seismotectonics: ice sheets, crustal deformation and seismicity. Quaternary Science Reviews **19**, 1367–1389.

Ucisik, N., Gudmundsson, O., Hanka, W., Dahl-Jensen, T., Mosegaard, K. & Priestley, K. 2008: Variations of shear-wave splitting in Greenland: mantle anisotropy and possible impact of the Iceland plume. Tectonophysics **462**, 137–148.

Authors' address

Geological Survey of Denmark and Greenland, Øster Voldgade 10, DK-1350 Copenhagen K, Denmark. E-mail: *tdj@geus.dk*

The mineral resource assessment project, South-East Greenland: year one

Bo Møller Stensgaard, Jochen Kolb, Troels F.D. Nielsen, Símun D. Olsen, Llewellyn Pilbeam, Diana Lieber and Anette Clausen

South-East Greenland between 62°N and 67°N is one of the lesser known regions in Greenland, having seen only limited geological investigations and only few detailed ones, with the Skjoldungen alkaline igneous province as a notable exception (Nielsen & Rosing 1990). Systematically collected geoscientific data are scarce; however, such data are essential as a basis for geological models and for evaluation of the mineral potential. In order to open up the region for exploration, the Greenland Bureau of Minerals and Petroleum financed a two-year, mainly geochemical programme for 2009 and 2010, which is an initial part of a five to six year project that involves subsequent geophysical surveys, a geological programme and a full-scale resource assessment of the region. The primary objective of the initial geochemical programme is to collect sediment samples for analysis of chemistry and indicator minerals. Supplementary to this, surface water for chemistry is collected and radiometric spectra of representative lithologies are measured. Geological reconnaissance field work focussing on selected key areas is also carried out.

During the past 10–15 years, the Geological Survey of Denmark and Greenland (GEUS) has carried out resource assessments of the Palaeoproterozoic orogens and mobile belts in South and central West Greenland, and most recently, assessments of the North Atlantic craton in West and southern West Greenland were conducted. The current assessment of South-East Greenland will provide the last major contribution needed for a detailed understanding of the Palaeoproterozoic and Archaean geological evolution of the entire southern Greenland, enabling us to develop new geological models for the region. The 2009 field work focused on the area between Timmiarmiit Kangertivat and Bernstorff Isfjord (Fig. 1).

Regional geology

The Archaean North Atlantic craton in South-East Greenland is bounded to the south and north, respectively, by the Palaeoproterozoic Ketilidian and Nagssugtoqidian mobile belts. The eastern part of the latter was formerly denoted the Ammassalik mobile belt (Andrews *et al.* 1973; Escher & Nielsen 1983). An overview of the region was provided by Chadwick *et al.* (1989).

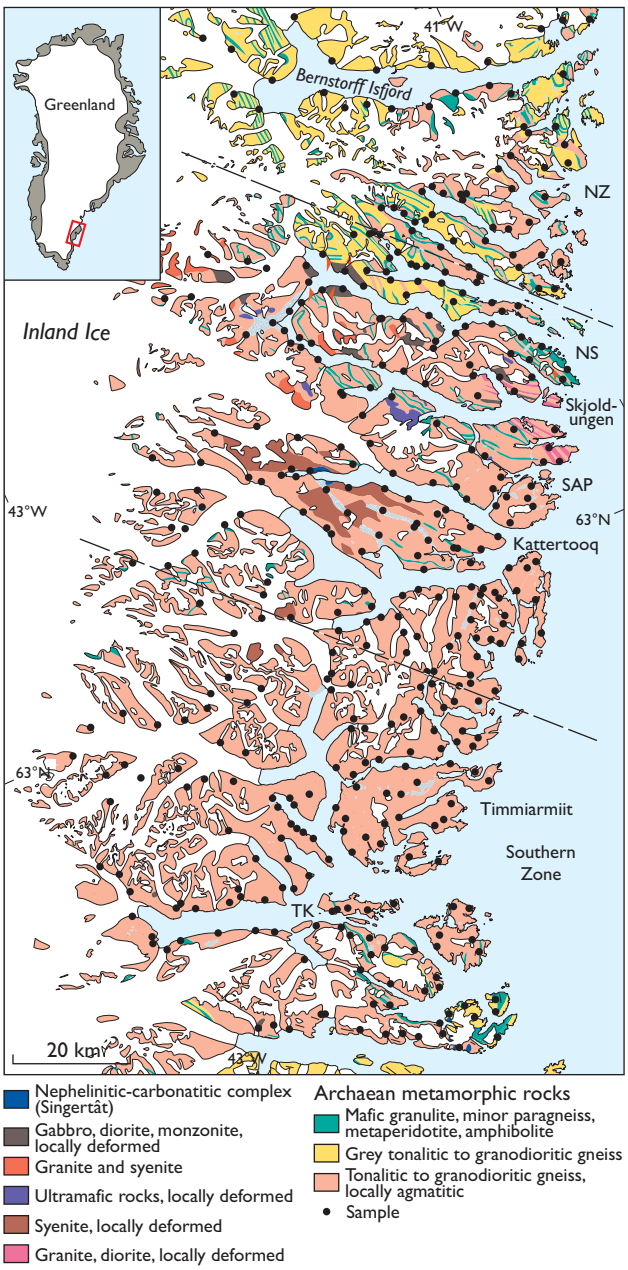

Fig. 1. Geological map of part of South-East Greenland showing the distribution of sediment samples, surface-water samples, indicator mineral samples and radionetric measurements (black dots). The map is based on Escher (1990). **NZ**: northern zone. **NS**: Nordre Skjoldungesund. **SAP**: Skjoldungen alkaline province. **TK**: Timmiarmiit Kangertivat.

Table 1. Differences between three main zones of the Archaean craton in South-East Greenland and encountered mineralisation

Subdivision of the craton	Main lithologies	Regional structural grain	Encountered mineralisations and preliminary mineral potential
Northern zone (NZ)	Numerous layers of supracrustal rocks dominated by mafic granulites. Grey tonalitic to granodioritic gneiss	N–S- to E–W-trending foliation and folds with W-plunging fold axes	Orthomagmatic Ni, Cu, PGE and Au Hydrothermal alteration zones with Au
Skjoldungen alkaline province (SAP)	Tonalitic to granodioritic gneiss, locally agmatitic, supracrustal sequences, alkaline intrusive rocks (granitic to syenitic-monzonitic gabbro, carbonatite-nephelinite rocks)	Strong NW–SE-trending foliation Late conjugate sets of NW–SE- and SW–NE-trending foliation	Alkaline and carbonatite intrusion-related Nb, REE, U and Th. Hydrothermal alteration zone with sulphides and quartz veins. Porphyry Cu, Sn and Mo deposits Iron-oxide copper-gold deposits
Southern zone (SZ)	Agmatitic, tonalitic to granodioritic gneiss Few restricted supracrustal sequences	N–S- to NE–SW-trending foliation and folds with SE-plunging fold axes	Hydrothermal alteration zone with sulphides and quartz veins. Alkaline intrusion-related Nb, REE, U, Th

The craton is dominated by orthogneisses with subordinate belts and slivers of supracrustal rocks (up to 1 km in width and several tens of kilometres along strike), and with late- to post-tectonic alkaline intrusions in the Skjoldungen area. The peak metamorphic facies is granulite grade. Retrogression from granulite facies to amphibolite facies assemblages is common. Based on lithological variation and regional structural grain the craton is subdivided into a northern zone (NZ), a Skjoldungen alkaline province (SAP) and a southern zone (SZ; Table 1; Fig. 1).

The orthogneiss is dominated by an early tonalitic generation intruded by syn- to late-tectonic tonalite and granodiorite, which have subsequently been intruded by post-tectonic granitic to granodioritic sheets (Andrews *et al.* 1973; Escher & Nielsen 1983). The early tonalitic gneiss is characterised by an agmatitic fabric with centimetre to metre scale, rounded to angular fragments of amphibolite, meta-diorite and meta-ultramafic rocks. Radiometric age determinations of four gneiss samples (K/Ar dating on either biotite or hornblende) yielded cooling ages of 2688–2335 Ma (Bridgwater 1971). A granulite facies migmatitic gneiss gave a protolith age of 2781 ± 6 Ma (zircon U/Pb SHRIMP dating; Friend *et al.* 1996).

The supracrustal units comprise amphibolite, metapelite (biotite schist, garnet-quartz gneiss and biotite-garnet-sillimanite-corderite schist), calc-silicate rock and meta-ultramafic rocks including meta-dunite. A 2.8 Ga zircon diffusion age is believed to represent the age of metamorphism and hence a minimum age for the formation of the supracrustal rocks (Andrews *et al.* 1973). A sample of an ordinary amphibolite unit yielded a cooling age of 2445 ± 45 Ma (biotite K-Ar dating, Bridgwater 1971).

Preparation for field work

Prior to the field work, in 2008 and the first half of 2009, existing data and literature from the region were compiled in digital format and the existing 1:500 000 scale geological map of the region (Escher 1990) was modified, updated, and digitised (Fig. 1). Evenly distributed sampling stations were selected from (1) processed remote sensing data from which drainage systems and catchment basins were defined, (2) satellite images, (3) aerial photographs and (4) topographical data. All information and data are stored in a GIS database that will evolve in the coming years and finally comprise all data and observations from the region.

Regional sampling procedure

The regional sampling was carried out by two or three man teams using a helicopter or zodiacs. The chartered vessel M/V *Fox* served as a base. The preferred material for sediment sampling was fine-grained stream sediment from first- or second-order streams. In areas without drainage systems, sediment was collected from drift or scree slopes. The rationale behind sampling sediments is that their composition reflects the bedrock as well as results of possible mineralisation processes in the catchment area. The sediment samples were sieved and split in GEUS laboratories and the fine fraction (<0.1 mm) was analysed for 62 different elements at Activation Laboratories Ltd., Canada. Sediment samples were collected at 506 locations (Fig. 1).

In places with suitable drainage systems, the sediment samples were supplemented by surface water samples, with two samples collected at each locality. Measurements of pH

and conductivity were carried out on one of the samples in the base camp. The other sample, which is used for geochemical analysis of 64 elements at the Activation Laboratories Ltd. in Canada, was acidified before storage. Water samples were collected at 379 localities.

A total of 138 coarse-grained sediment samples was collected for indicator mineral analysis from local drift. The rationale behind this type of sampling is that erosion products of a distinct or mineralised rock type can be traced in the drift, and that specific indicator minerals are diagnostic for the specific rock or process. For example, some minerals can be specific for kimberlite that may carry diamonds. Material was collected with a spade from below the vegetation, if present. Most commonly the drift was till, but locally glaciofluvial sediment was sampled. The material was sieved on a 6.35 mm screen fitted on top of a 20 litres bucket until a sample of *c.* 5 l was reached. The sieved material was then mixed and transferred to a 5 l container for storage and shipment to the laboratory. The mineral grains will be evaluated by Overburden Drilling Management Ltd., Canada, for occurrence of kimberlite, Au-Ni-Cu and platinum-group element (PGE) indicator minerals.

Gamma-ray measurements were undertaken at the sample sites, using a portable multichannel gamma-ray spectrometer in order to determine total gamma radiation and concentration variations of K, U and Th. Finally, representative rock types for geochemistry, petrological investigations and age determinations were collected.

Preliminary results

Based on the reconnaissance work, several types of mineralised rock were identified. All encountered mineral occurrences need more work to establish their settings and to assess their potential.

Small, metre-scale lenses of sulphide-bearing, metamorphosed ultramafic rocks, often hosted within mafic rock sequences ('supracrustal units') were found in the northern zone (Fig. 1; NZ). Several rusty horizons, up to tens of metres wide and continuous along strike for tens of kilometres, were seen within mafic to ultramafic rock sequences in both the northern zone and the central Skjoldungen alkaline province (Fig. 1; NZ and SAP). The horizons were found to contain disseminated or semi-massive to massive sulphide mineralisation with pyrrhotite, chalcopyrite and pentlandite and were encountered at several places along strike. Rock samples from this mineralisation show elevated concentrations of Ni, Cu and Cr (grab samples have yielded up to 0.3% Ni, 0.2% Cu, 0.5% Cr, 24 ppb Pt and 162 ppb Pd). These rock types may contain occurrences of orthomagmatic Ni, Cu and PGE.

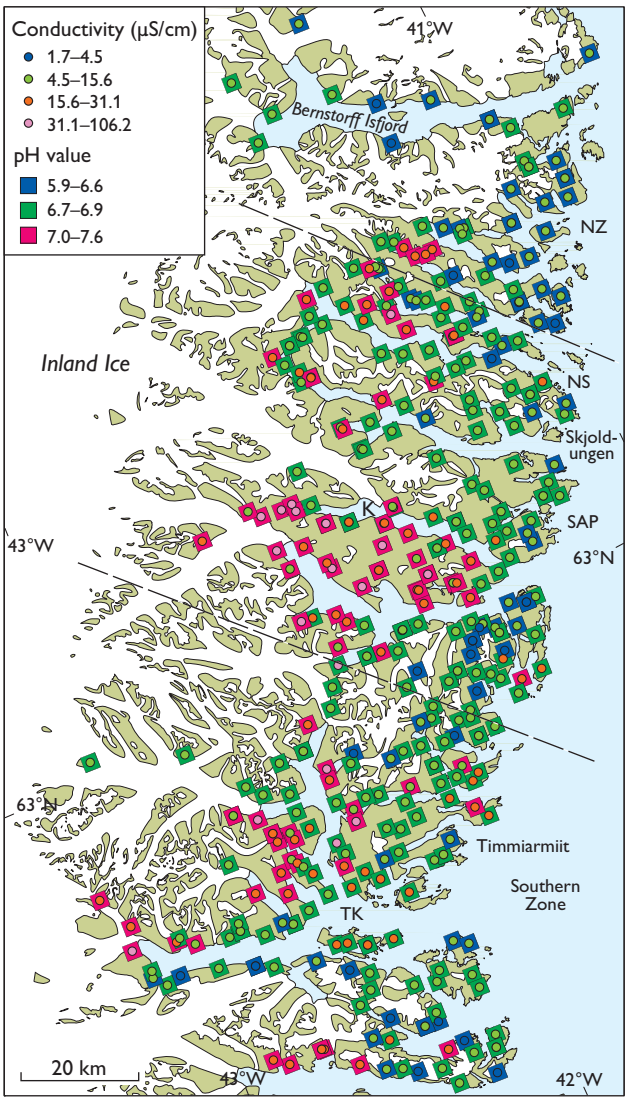

Fig. 2. Conductivity and pH from surface-water samples. The Skjoldungen alkaline province in the central part of the region shows high values of both conductivity and pH. For abbreviations see text to Fig. 1.

Quartz veins within hydrothermal alteration zones (pyrrhotite-chalcopyrite-quartz-biotite-garnet) that are 10–20 m wide and traceable for 100 m to several kilometres along strike were found in the Skjoldungen alkaline province and in the southern zone. Even though samples have only yielded small gold concentrations (maximum 117 ppb Au) it is notable that As, a pathfinder element for gold, shows elevated values (up to 1640 ppm As). The alteration zones and the hydrothermal vein systems are potential gold targets.

The Skjoldungen alkaline province comprises the Singertât carbonatite complex (Nielsen & Rosing 1990; Blichert-Toft *et al.* 1995). Rock samples from the carbonatite yielded a total rare-earth element (REE) concentration of *c.* 2500 ppm to-

gether with elevated values of Sr, Y and Ce (up to 2000 ppm Sr, 120 ppm Y and 1100 ppm Ce). The surrounding orthogneisses also show elevated REE concentrations, which may be a result of a hydrothermal halo related to the complex.

The syntectonic gabbros, granites and syenites in the Skjoldungen alkaline province are rich in magnetite, and the general geological setting may indicate a potential for porphyry copper, tin or molybdenum deposits and iron-oxide–copper–gold deposits.

Results from regional sampling

The field-based gamma-ray measurements of the dominant rock types and the pH and conductivity measurements of surface water provide evidence for significant regional variations. Even though the range of both pH and conductivity values is limited, the measurements clearly reflect the intrusive suites of the Skjoldungen alkaline province, especially the syenites at Kattertooq and western Skjoldungen (Fig. 2), probably due to outwash of alkaline elements into surface waters from the syenites. This is supported by the gamma-ray measured K content, which is elevated within the Skjoldungen alkaline province. Elevated pH, conductivity and K content are also seen in the eastern parts of the Kattertooq and Skjoldungen area, at Nordre Skjoldungesund and at Timmiarmiit in the south. From these data we suggest that alkaline magmatic rocks in the Archaean of South-East Greenland could be much more widespread than previously recognised.

Further work

The results of the analyses of sediment and surface-water samples and the results from the regional indicator-mineral analysis of material collected in 2009 were released in the spring 2010 (Minex 2010). Based on these results, the mining industry can evaluate the mineral potential of one of the least explored regions in Greenland. The data will also be used by GEUS and international research partners to improve our understanding of the geology of the region. The programme will continue in 2010 with similar work in the Tasiilaq region farther north. Many parts of this region are also poorly known and without basal regional data. In addition, aeromagnetic surveys are being considered. The work in 2009 and 2010 provides a basis for more detailed geological work in 2011–2014. The aim of this work is to develop a well-constrained geological model for the entire region which can justify exploration for ore deposits.

Acknowledgements

We gratefully acknowledge help and support from the skipper Niels Peter Trolle and his excellent crew on M/V *Fox*, from Air Greenland pilot Bertil Björk and mechanic Benny M. Sørensen, and friends in Tasiilaq and Kulusuk. The Greenland Bureau of Minerals and Petroleum supported the project financially.

References

Andrews, J.R., Bridgwater, D., Gormsen, K., Gulson, K., Keto, L. & Watterson, J. 1973: The Precambrian of South-East Greenland. In: Park, R.G. & Tarney, J. (eds): The early Precambrian of Scotland and related rocks of Greenland, 143–156. Birmingham University Press.

Blichert-Toft, J., Rosing, M.T., Lesher, C.E. & Chauvel, C. 1995: Geochemical constraints on the origin of the Late Archean Skjoldungen alkaline igneous province, SE Greenland. Journal of Petrology **36**, 515–561.

Bridgwater, D. 1971: Routine K/Ar age determinations on rocks from Greenland carried out for GGU in 1970. Rapport Grønlands Geologiske Undersøgelse **35**, 52–60.

Chadwick, B., Dawes, P.R., Escher, J.C., Friend, C.R.L., Hall, R.P., Kalsbeek, F., Neilsen, T.F.D., Nutman, A.P., Soper, N.J. & Vasudev, V.N. 1989: The Proterozoic mobile belt in the Ammassalik region, South-East Greenland, (Ammassalik mobile belt): an introduction and re-appraisal. Rapport Grønlands Geologiske Undersøgelse **146**, 5–12.

Escher, J.C. 1990: Geological map of Greenland, 1:500 000, Sheet 14, Skjoldungen. Copenhagen: Geological Survey of Greenland.

Escher, J.C. & Nielsen T.F.D. 1983: Archaean gneisses and supracrustal rocks of the Tingmiarmiut region, South-East Greenland. Rapport Grønlands Geologiske Undersøgelse **115,** 79–82.

Friend, C.R.L., Nutman, A.P., Baadsgaard, H., Kinny, P.D. & McGregor, V.R. 1996: Timing of late Archaean terrane assembly, crustal thickening and granite emplacement in the Nuuk region, southern West Greenland. Earth and Planetary Science Letters **142**, 353–365.

Minex 2010: New data from South-East Greenland. Greenland Mineral Exploration newsletter **36**, 2–3. Copenhagen: Geological Survey of Denmark and Greenland and Nuuk: Bureau of Minerals and Petroleum (available at www.geus.dk/minex).

Nielsen, T.F.D. & Rosing, M.T. 1990: The Archaean Skjoldungen alkaline province, South-East Greenland. Rapport Grønlands Geologiske Undersøgelse **148**, 93–100.

Authors' addresses

B.M.S., J.K., T.F.D.N., S.O.L. & L.P., *Geological Survey of Denmark and Greenland, Øster Voldgade 10, DK-1350 Copenhagen K, Denmark.* E-mail: *bmst@geus.dk*

D.L., *Weidekampsgade 27, 2. t.v., DK-2300 Copenhagen S, Denmark.*

A.C., *Bureau of Minerals and Petroleum, P.O. Box 930, DK-3900 Nuuk, Greenland.*

Characterisation of host rocks and hydrothermal alteration of the Qussuk gold occurrence, southern West Greenland

Denis Martin Schlatter and Rasmus Christensen

Gold exploration in the Godthåbsfjord region has been carried out since the early 1990s, and the region is now recognised as a gold province. Several prospects have been drilled and Storø is the most advanced project in the Færingehavn terrane. The gold occurrence at Storø is 2635 Ma old according to $^{207}Pb/^{206}Pb$ age determinations of metamorphic zircons associated with auriferous arsenopyrite (Nutman *et al.* 2007). Qussuk is located in the Akia terrane (Fig. 1), separated from the Færingehavn terrane in the south by the SW–NE-trending Ivinnguit fault. The Ivinnguit and Ataneq faults are spatially associated with several hydrothermal gold occurrences. From north to south these are: Isua, Storø, Bjørneøen, Sadelø, Store Malene and Qilanngaarsuit (Fig. 1; Appel *et al.* 2005; Kolb *et al.* 2009). The Qussuk prospect 20–25 km north of the Ataneq fault is 20 km long, 2–3 km wide, and divided from north to south into the 'Swan N', 'Swan' and 'Plateau' areas (Fig. 1).

In this study, geology, petrography and immobile element geochemistry are used to define a vector to the ore, and we will demonstrate that the Qussuk gold mineralisation shows many characteristics of orogenic gold deposits. This paper is directed towards helping gold exploration to be more efficient in the Qussuk area, in the larger Godthåbsfjord region and elsewhere in the Achaean greenstone belts of southern West Greenland.

Geology of the Qussuk area

The supracrustal rocks are deformed and metamorphosed to amphibolite grade and comprise amphibolite, ultramafic rocks, aluminous gneiss and tonalite (Garde 1997). Deformation is characterised by upright to overturned isoclinal folds; the rocks trend NNE–SSW and are steeply dipping (Garde 2008). The tonalitic orthogneiss precursor intruded into the volcanic rocks dated at 3071 ± 1 Ma in the Qussuk area (U-Pb zircon age) whereas tonalitic orthogneiss is 3060–3000 Ma old (Garde *et al.* 2000). Plagioclase-rich amphibolite units containing both biotite and hornblende are possibly of pyroclastic or volcaniclastic origin as suggested by primary textures such as graded bedding, fragmental textures and fiamme structures (Garde 2007; Garde *et al.* 2007). These primary volcanic textures and the presence of calc-alkaline and tholeiitic andesites at Qussuk led Garde (2007) to the conclusion that these rocks represent an Archaean island arc complex.

A 120 m thick sequence of leuco-amphibolite, amphibolite, aluminous gneiss, biotite schist and pegmatite dykes is found in the 'Swan N' area (Fig. 2). At the contact between the aluminous gneiss and the leuco-amphibolite a 23 m thick zone consists mainly of biotite schist with 5–30 cm thick quartz veins and quartz rods. This zone is interpreted as a hydrothermal alteration zone (Schlatter & Christensen 2010). Continuous sampling of 1–2 m long sections reveals that the gold content averages 1.24 ppm over 23 m including several 1–2 m thick layers of biotite schist with gold contents between 3.3 and 8.4 ppm (Schlatter & Christensen 2010).

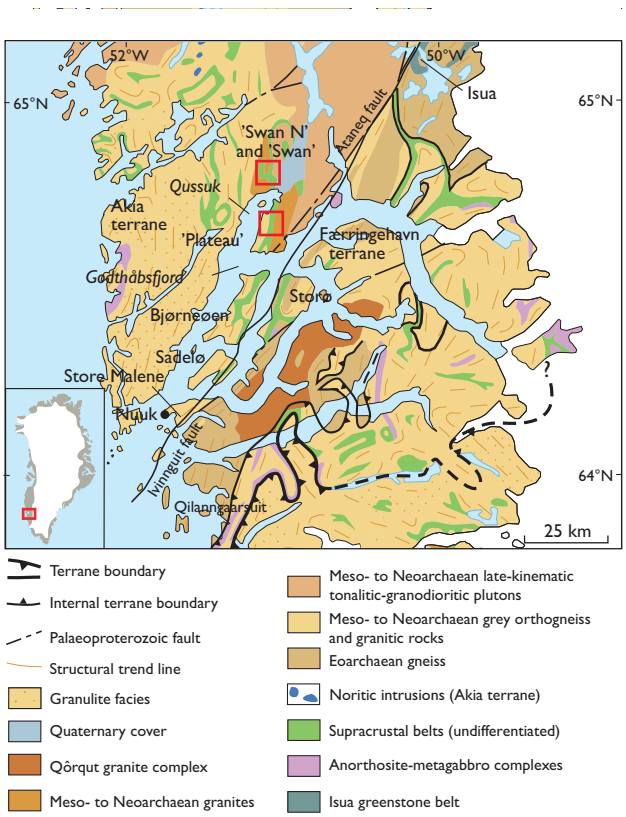

Fig. 1. Geological map of the Godthåbsfjord region showing gold occurrences. The Qussuk prospect is divided into the 'Swan N', 'Swan' and 'Plateau' areas. The red boxes show the Qussuk prospect.

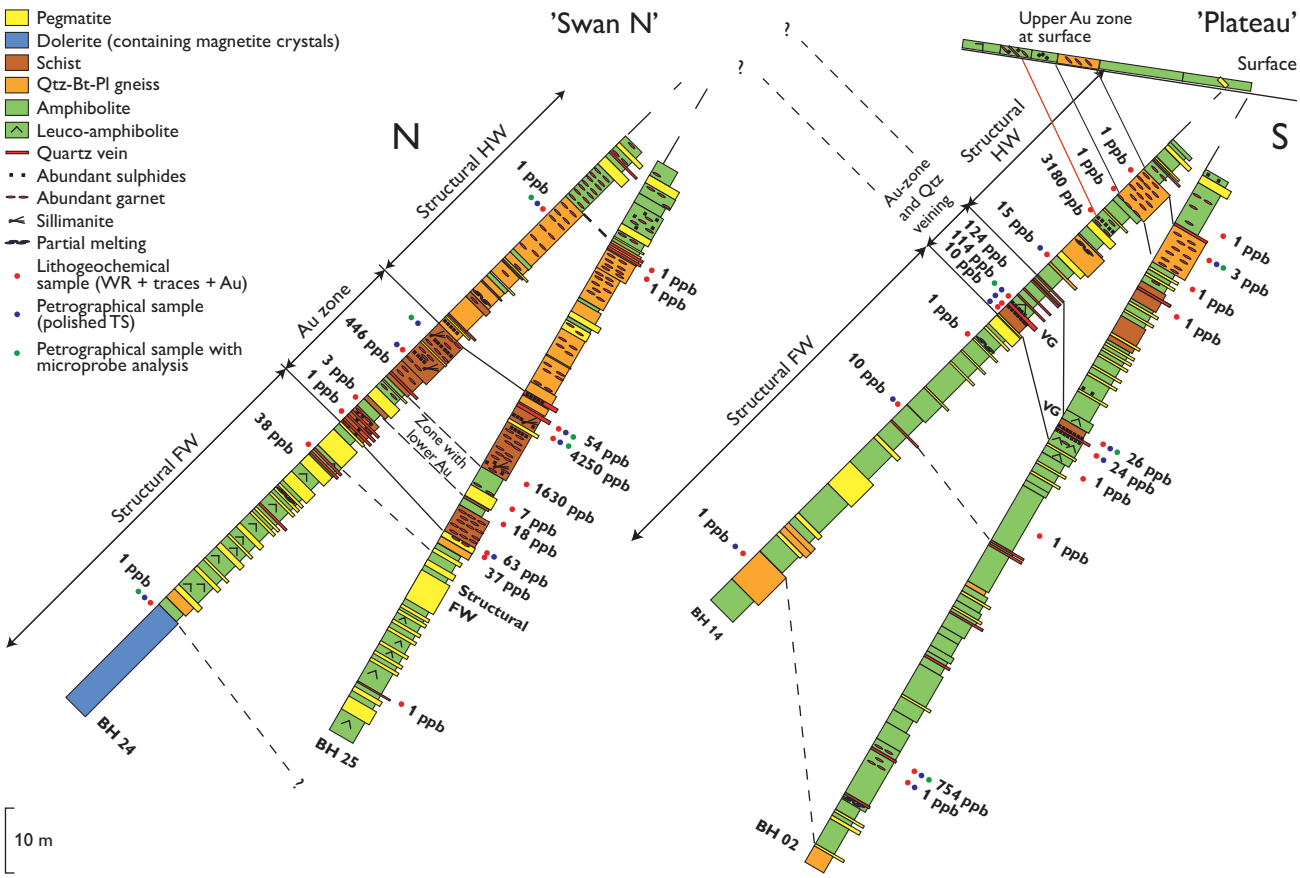

Fig. 2. Borehole logs of BH 24 and BH 25 from 'Swan N' and of BH 02 and 14 from 'Plateau'. The geology is defined from the two bore holes and from outcrops. The alteration zones are narrower in the Plateau area (a few metres) and wider in the 'Swan N' area (tens of metres), possibly because the areas represent wider and narrower shear zones and in turn focus alteration fluids differently. Only the gold contents in the lithogeochemical samples are shown.

A 100 m thick sequence with amphibolite, aluminous gneiss, biotite schist, leuco-amphibolite and pegmatite dykes occurs in the 'Plateau' area (Fig. 2). Several up to 0.5 m thick quartz veins occur at or close to the contact of amphibolite and leuco-amphibolite. One of these contains visible gold and is flanked by a 0.5 m thick inner zone of semi-massive to massive pyrrhotite and an outer zone of biotite-quartz alteration products. Analyses of the quartz veins and the inner alteration zone yielded up to 19 ppm gold over 0.6 m (Schlatter & Christensen 2010). The local rock sequences at 'Plateau' and 'Swan N' are different from each other and no straightforward detailed correlation can be made between the two areas, although they both belong to the same Qussuk-Bjørneøen metavolcanic belt (Garde 2007; Garde *et al.* 2007). The gold-enriched zones in both areas occur close to lithological contacts (Fig. 2) and are structurally controlled by local shear zones and quartz veins. In the 'Swan' area no intersection with gold concentrations above 1 ppm was encountered.

Methods

Analysed drill core sections were 20–25 cm long and a quarter of the core was used. All samples were crushed in Nuuk and analysed at the Actlabs laboratory in Ontario, Canada. Gold was analysed by instrumental neutron activation. A total of 46 drill core samples and eight surface samples were used for geochemical and petrographical investigations. Ten thin sections (242 spots) were analysed by a JEOL JXA-8200 superprobe at the Department of Geography and Geology, University of Copenhagen to determine the chemistry of the main rock phases.

Hydrothermal alteration and lithogeochemical results

The gold mineralisation comprises quartz veins with visible gold and massive or disseminated pyrrhotite. Hydrothermal alteration zones at 'Swan N' and 'Plateau' comprise an inner zone of pyrrhotite, chalcopyrite and gold-quartz veins and

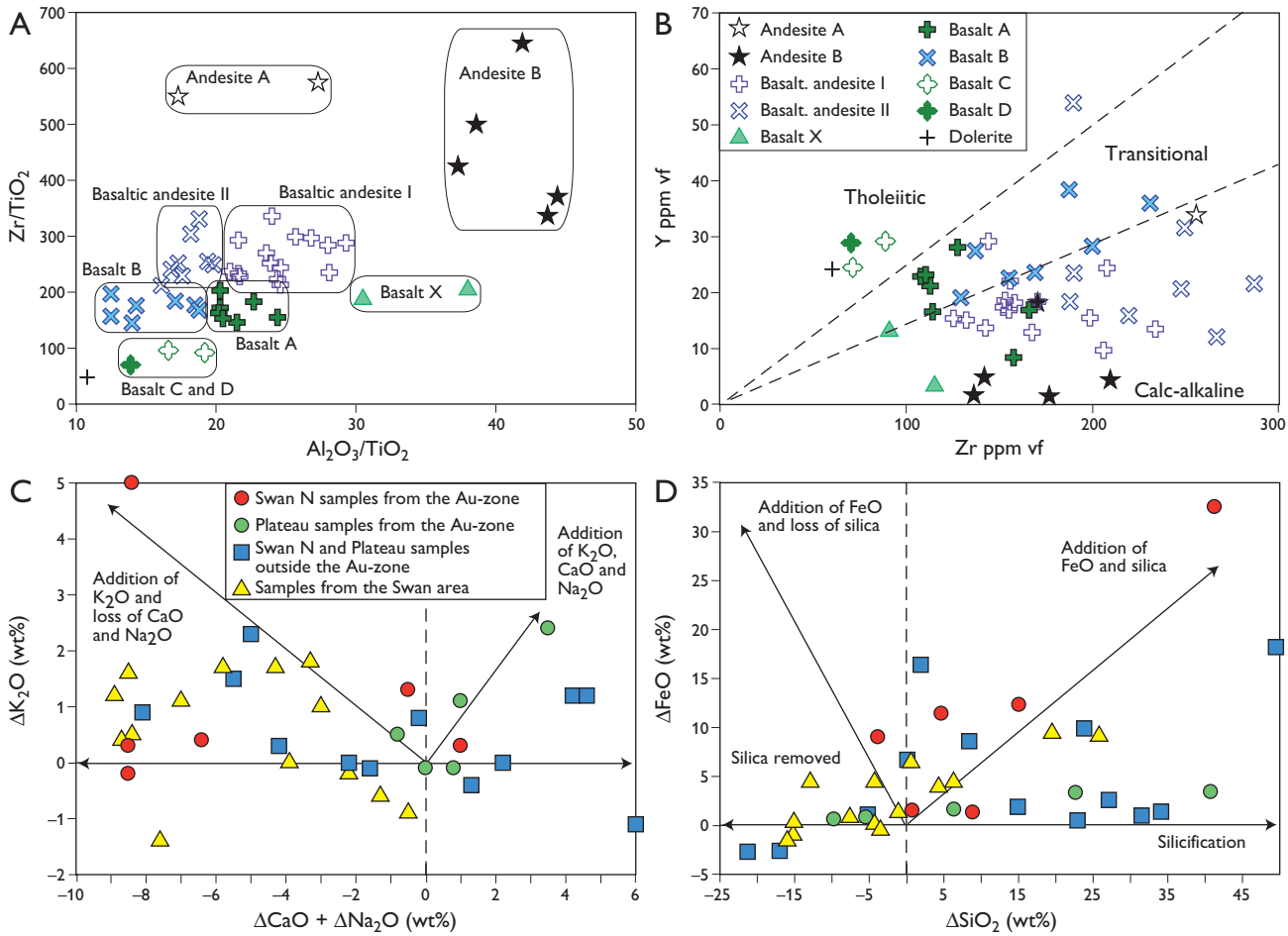

Fig. 3. **A**: Ti, Al, and Zr are commonly considered to be immobile during hydrothermal processes and so their ratios show as primary lithological variations that have not been affected by hydrothermal alteration. The chemical groups form fairly tight clusters in a diagram based on Al_2O_3/TiO_2 versus Zr/TiO_2 and show eight main chemical groups ranging from andesite to basalt (division from Barrett & MacLean 1994). **B**: A diagram based on Zr and Y shows that most of the Qussuk samples have calc-alkaline and transitional magmatic affinity; only a few samples plot in the tholeiitic field (division from Barrett & MacLean 1994). **C**: ΔK_2O versus $\Delta CaO+\Delta Na_2O$ for rocks of the 'Swan N', 'Swan' and 'Plateau' areas. **D:** ΔFeO versus ΔSiO_2 for rocks of the Swan N, Swan and Plateau areas. (**vf** = volatile-free basis, data were normalised after loss on ignition (LOI); results of mass change calculations are reported in wt% change (Δ) relative to the precursor rock).

an outer zone of biotite, muscovite, quartz, and sulphides (Fig. 2). Garnet and sillimanite also occur in the outer zone (Fig. 2), but it is unclear if these are primary metamorphic or hydrothermal alteration minerals. Chlorite replacing biotite and actinolite replacing pyroxene are regarded as retrograde metamorphic minerals.

Application of immobile element methods (Barrett & MacLean 1994) on 50 whole-rock analyses shows that the rocks from 'Plateau', 'Swan N' and 'Swan' can be classified into ten different chemical groups ranging from andesite to basalt (Fig. 3A). The rocks are mainly metabasalts with transitional to calc-alkaline affinity (Fig. 3A, B). A few are tholeiitic (Fig. 3B). The rocks from the gold zones in the 'Swan N' and 'Plateau' areas are mainly basaltic andesite I of calc-alkaline affinity.

Hydrothermal alteration can cause mass gain or loss, which in turn results in dilution or residual concentration of the immobile elements. However, these effects do not change the initial ratio between two immobile elements for a given chemical rock type. Mass changes were calculated using the single precursor approach (MacLean & Barrett 1993). The rocks from the 'Swan N' and 'Plateau' areas show gains or losses in Na_2O and CaO and gains and small losses in K_2O (Fig. 3C). The rocks from the 'Swan' area show losses in CaO and Na_2O and gains and small losses of K_2O (Fig 3C). Most of the samples from the 'Swan N' and 'Plateau' areas have gained FeO and SiO_2, and a few samples have lost SiO_2 and show minor losses in FeO (Fig. 3D) Samples from the 'Swan' area show losses and gains of SiO_2 and gains or small losses of FeO (Fig. 3D).

Discussion and conclusions

Garde (2007) showed that the rocks of the Qussuk area were formed in a volcanic-arc setting and that they were altered during a synvolcanic and epithermal hydrothermal alteration stage, and suggested that gold was introduced during this epithermal event. The presence of plagioclase in rocks from the gold zone, however, suggests that these rocks are neither strongly altered nor extremely affected by acid leaching, because such alteration would cause breakdown of plagioclase due to leaching of Na_2O and CaO. Results from mass change calculations show that several samples from the gold zones have gained Na_2O and CaO or lost only a small part of these mobile elements (Fig. 3C).

The gold occurrences from the 'Swan N' and the 'Plateau' areas are enveloped by biotite schist, which represents enveloping and symmetric hydrothermal alteration halos around the gold mineralisation. Gains of K_2O (Fig. 3C) suggest that biotite formed as a result of hydrothermal alteration which is well known in orogenic gold systems (Eilu & Groves 2001; Groves *et al*. 2003). The occurrence of gold-rich quartz veins and biotite-quartz-sulphide-rich hydrothermal alteration together with mass change calculations (Fig. 3C, D) suggest that the hydrothermal fluids were enriched in K_2O, SiO_2, FeO and Au. The quartz veins with visible gold and the inner pyrrhotite alteration zone cross-cut the main foliation, indicating that the veining occurred later than the formation of the foliation and shows that the gold mineralisation took place during later stages of deformation and metamorphism. Metamorphic minerals of slightly lower metamorphic grade replacing minerals of higher metamorphic grade indicate that hydrothermal gold mineralisation occurred during retrograde upper greenschist to lower amphibolite facies metamorphism.

The present study shows that gold in the Qussuk area is controlled by post-peak, metamorphic, hydrothermal quartz veins and alteration zones akin to orogenic gold systems. However, it remains unclear whether the gold was remobilised from an earlier, possibly syngenetic enrichment or introduced from an external source.

In order to find more gold-mineralised systems in the Qussuk area, rocks of basaltic andesite I should be identified. This rock type is a potential target if the layer is enveloped by proximal alteration (quartz veins, pyrrhotite, elevated gold) and distal alteration (biotite, muscovite, quartz, sulphides, elevated gold concentration).

Acknowledgements

NunaMinerals A/S is thanked for financial contribution to the project.

References

Appel, P.W.U., Coller, D., Vincent, C., Heijlen, W., Moberg, E.D., Polat, A., Raith, J., Schjøth, F., Stendal, H. & Thomassen, B. 2005: Is there a gold province in the Nuuk region? Report from field work carried out in 2004. Danmarks og Grønlands Geologiske Undersøgelse Rapport **2005/27**, 79 pp. + 1 CD-Rom.

Barrett, T.J. & MacLean, W.H. 1994: Chemostratigraphy and hydrothermal alteration in exploration for VHMS deposits in greenstones and younger volcanic rocks. In: Lentz, D.R. (ed.): Alteration and alteration processes associated with ore-forming systems. St. John's: Geological Association of Canada. Short Course Notes **11**, 433–467.

Eilu, P. & Groves, D.I. 2001: Primary alteration and geochemical dispersion haloes of Archaean orogenic gold deposits in the Yilgarn Craton: the pre-weathering scenario. Geochemistry: Exploration, Environment, Analysis **1**, 183–200.

Garde, A.A. 1997: Accretion and evolution of an Archaean high-grade grey gneiss–amphibolite complex: the Fiskefjord area, southern West Greenland. Geology of Greenland Survey Bulletin **177**, 115 pp.

Garde, A.A. 2007: A mid-Archaean island arc complex in the eastern Akia terrane, Godthåbsfjord, southern West Greenland. Journal of the Geological Society (London) **164**, 565–579.

Garde, A.A. 2008: Geochemistry of Mesoarchaean andesite rocks with epithermal gold mineralisation at Qussuk and Bjørneøen, southern West Greenland. Mineral resource assessment of the Archaean Craton 66° to 63°30′N) SW Greenland, contribution no. 8. Danmarks og Grønlands Geologiske Undersøgelse Rapport **2008/4**, 52 pp.

Garde, A.A., Friend, C.R.L., Nutman, A.P. & Marker, M. 2000: Rapid maturation and stabilisation of middle Archaean continental crust: the Akia terrane, southern West Greenland. Bulletin of the Geological Society of Denmark **47**, 1–27.

Garde, A.A., Stendal, H. & Stensgaard, B.M. 2007: Pre-metamorphic hydrothermal alteration with gold in a mid-Archaean island arc, Godthåbsfjord, West Greenland. Geological Survey of Denmark and Greenland Bulletin **13**, 37–40.

Groves, D.I., Goldfarb, R.J., Robert, F. & Hart, C.J.R. 2003: Gold deposits in metamorphic belts: overview of current understanding, outstanding problems, future research, and exploration significance. Economic Geology **98**, 1–29.

Kolb, J., Stensgaard, B.M., Schlatter, D.M. & Dziggel, A. 2009: Controls of hydrothermal quartz vein mineralisation and wall rock alteration between Ameralik and Sermilik, southern West Greenland. Danmarks og Grønlands Geologiske Undersøgelse Rapport **2009/25**, 76 pp. + 1 DVD.

MacLean, W.H. & Barrett T.J. 1993: Lithogeochemical techniques using immobile elements. Journal of Geochemical Exploration **48**, 109-133.

Nutman, A.P., Christiansen, O. & Friend, C.R.L. 2007: 2635 Ma amphibolite facies gold mineralisation near a terrane boundary (suture?) on Storø, Nuuk region, southern West Greenland. Precambrian Research **159**, 19–32.

Schlatter, D.M. & Christensen R. 2010: Geological, petrographical and lithogeochemical investigations on the Qussuk gold mineralisation, southern West Greenland. Danmarks og Grønlands Geologiske Undersøgelse Rapport **2010/10**, 53 pp.

Authors' addresses

D.M.S., *Geological Survey of Denmark and Greenland, Øster Voldgade 10, DK-1350 Copenhagen K, Denmark*. E-mail: *dms@geus.dk*

R.C., *NunaMinerals A/S, Postboks 790, DK-3900 Nuuk, Greenland.*

Zircon record of the igneous and metamorphic history of the Fiskenæsset anorthosite complex in southern West Greenland

Nynke Keulen, Tomas Næraa, Thomas F. Kokfelt, John C. Schumacher and Anders Scherstén

The Fiskenæsset complex in southern West Greenland is part of the North Atlantic craton and is a layered intrusion consisting of gabbro, ultramafic and anorthositic rocks that was deformed during multiple episodes of folding and metamorphism (Myers 1985). We collected late-stage magmatic hornblenditic dykes and adjacent anorthosites and studied these samples integratively with several *in situ* techniques to determine the igneous and metamorphic history of the Fiskenæsset complex. The work presented here is part of an ongoing joint project between the Greenland Bureau of Minerals and Petroleum and the Geological Survey of Denmark and Greenland (GEUS). Here we report on new radiometric ages and mineral chemistry data from anorthosites from the North Atlantic craton in southern West Greenland (Fig. 1).

Geological setting of Majaqqap Qaava

Despite the intense Archaean deformation of the Fiskenæsset area the original stratigraphy of the Fiskenæsset complex was established from detailed field work at Majaqqap Qaava (Myers 1985). Towards the top part of the Fiskenæsset complex hornblenditic pegmatite pipes cut the generally anorthositic and leucogabbroic layering. At Majaqqap Qaava, subvertical hornblenditic dykes are interpreted as representing a late magmatic stage of activity within the Fiskenæsset complex (Myers 1985). The Fiskenæsset complex is surrounded and intruded by younger, mainly tonalitic gneisses (2.87–2.85 Ga; Næraa & Scherstén 2008) that typically occur as felsic sheets intruded parallel to the magmatic layering. Regional amphibolite-facies metamorphism affected the rocks at Majaqqap Qaava, but no granulite-facies metamorphism was recorded for this part of the Fiskenæsset complex (Myers 1985).

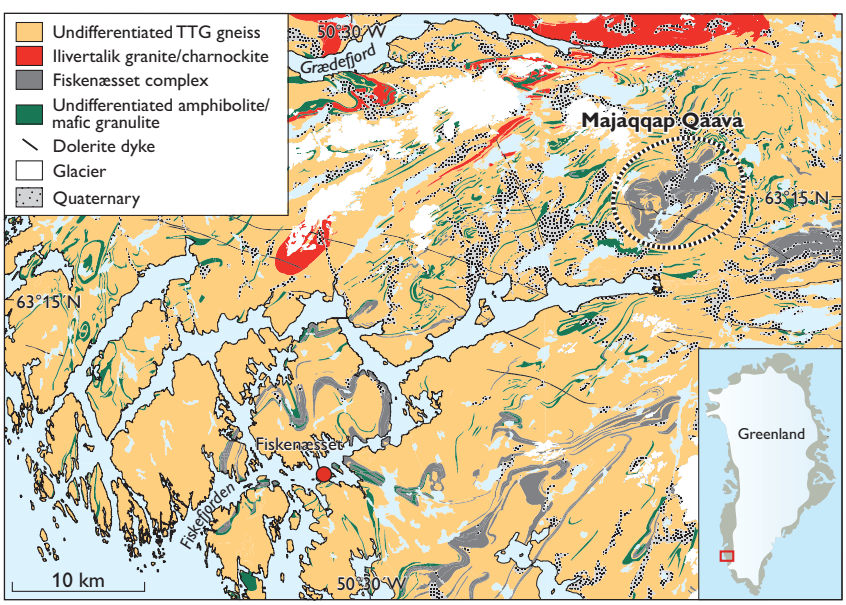

Fig. 1. Simplified geological map of the central part of the North Atlantic craton in southern West Greenland showing Majaqqap Qaava in the Fiskenæsset complex. Based on maps published by the Geological Survey of Denmark and Greenland.

Zircon dating

For U/Pb zircon age determination we selected sample GGU 508216, which consists of hornblenditic dyke material and the surrounding anorthosite rock. The sample was crushed, sieved, and washed on a Wilfley table. The zircons were hand-picked from the heavy mineral fraction, mounted in epoxy resin and polished. Age determination was carried out by laser ablation inductively coupled mass spectrometry using an Element2 and NewWave 213 nm UV-laser system at GEUS following the procedures described in Frei & Gerdes (2009). The results are shown in Fig. 2.

The zircon spot analyses yielded a wide age span, with $^{207}Pb/^{206}Pb$ ages ranging from 2.70 ± 0.03 to 2.95 ± 0.03 Ga (Fig. 2A; 50 concordant grains out of 54). The oldest zircon grains in our sample are *c.* 2.95 Ga (Fig. 2A), which probably represents the intrusion age of the anorthosite complex. New data by A. Polat and co-workers are consistent with this interpretation, as they obtained a Sm-Nd isochron age of *c.* 2.97 Ga and a $^{207}Pb/^{206}Pb$ age of 2.95 Ga for the intrusion of

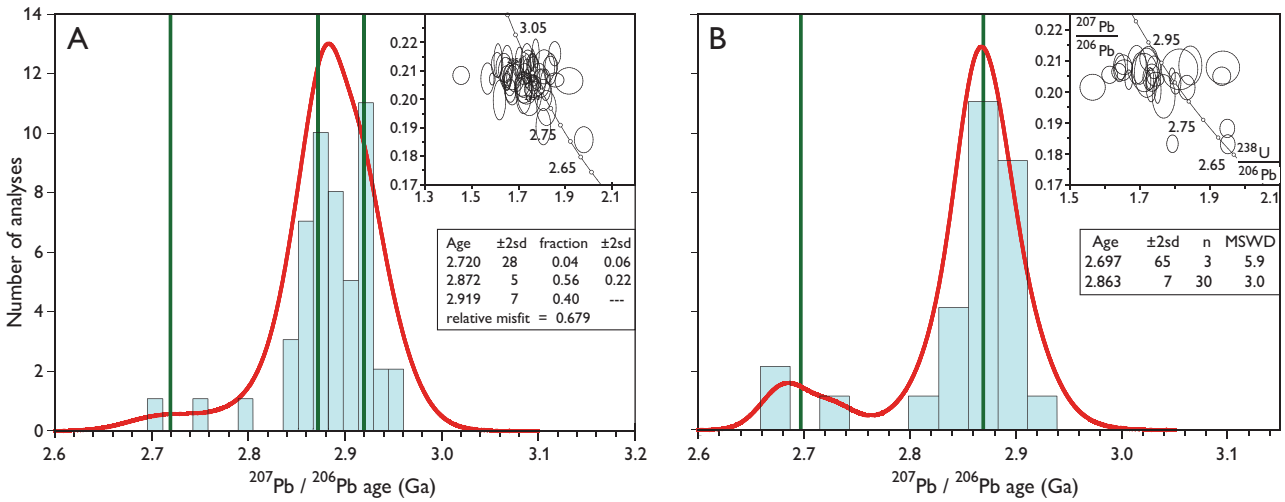

Fig. 2. Zircon U/Pb – Pb/Pb age distributions from hornblenditic dyke material and anorthosite from sample GGU 508216. **A**: Zircon grains hand-picked from crushed material with 90–110% concordant grains. Unmixing of all grains following Ludwig (2003). **B**: *In situ* dating of zircon grains with 90–110% concordant grains. **MSWD**: mean square weighted deviation. n: number of analyses. The green lines show ages discussed in the text.

the Fiskenæsset complex (A. Polat, personal communication 2010). Among the dated, hand-picked grains there appear to be two populations, one at 2.92 Ga and another at 2.87 Ga (Fig. 2A). A third possible component at *c.* 2.70 Ga might represent a minor population of metamorphic grains. A known thermal event at 2.80 Ga involving granulite-facies metamorphism that affected the western part of the Fiskenæsset complex and the intrusion of the Ilivertalik granite (T. Næraa & A. Scherstén, unpublished data) is not recorded among the dated zircon grains from Majaqqap Qaava.

In situ observations

To better understand the three zircon-forming events (*c.* 2.92, *c.* 2.87 and *c.* 2.7 Ga), we observed the zircon grains *in situ* in polished slabs of the anorthosite samples using the scanning electron microscope at GEUS and the electron microprobe at the University of Copenhagen. Zircon grains occur in four different textural settings: (1) associated with ilmenite within the hornblenditic dyke (Fig. 3A), (2) within the hornblenditic dyke, (3) in melt pockets associated with the hornblenditic dyke (Fig. 3B) and (4) in cracks associated with chlorite (Fig. 3C). A further feature in the hornblenditic dyke in the anorthosite is the break-down reaction of the ilmenite in the hornblende to form rutile, titanite and chlorite (Fig. 3D). We dated zircon grains from these four different settings *in situ* using the same ICP-MS instrument as described above.

Interpretation

Based on the *in situ* observations and measurements, our current understanding of the igneous and metamorphic history of the anorthosite at Majaqqap Qaava is as follows: After intrusion of the anorthosite at *c.* 2.97–2.95 Ga, zircon formed at high-temperature conditions, e.g. from a reaction between baddeleyite and ilmenite. Some of these zircon grains can be observed next to ilmenite grains (Fig. 3A); however, no concordant ages were obtained from the *in situ* measurements.

A later thermal event occurred at *c.* 2.92 Ga, which forms the major age component in the zircon population extracted from the crushed sample (Fig. 2A). Since only one *in situ* zircon measurement yields 2.92 Ga, the true nature of this event is unclear. This age might be related to an igneous event that formed the precursors to the amphibolite units in the area (see e.g. Nutman *et al.* 2004), or the earliest onset of tonalitic gneiss formation in the region (Næraa & Scherstén, unpublished data).

Zircon grains from the contact region between the hornblenditic dyke and the anorthosite were observed both in relation to melt pockets (Fig. 3B) and as occurring in the amphibole-anorthite assemblages. These different textural settings yield indistinguishable zircon $^{207}Pb/^{206}Pb$ ages of 2.878 ± 0.011 Ga (mean square weighted deviation = 0.33) and 2.856 ± 0.016 Ga (mean square weighted deviation = 1.3), respectively. There is, however, a large range in ages between the individual analyses. We suggest that this wide age range originates from inheritance or metamorphic overprinting, but the mean age reflects the crystallisation or resetting related to the intrusion of the hornblenditic dykes. The melt pockets in the hornblenditic dykes are likely to represent their final solidification. If correct, and if this age is representative, it implies that the dykes represent a late magmatic event, much later than previously assumed. This interpretation is at odds with field observations, which are best ex-

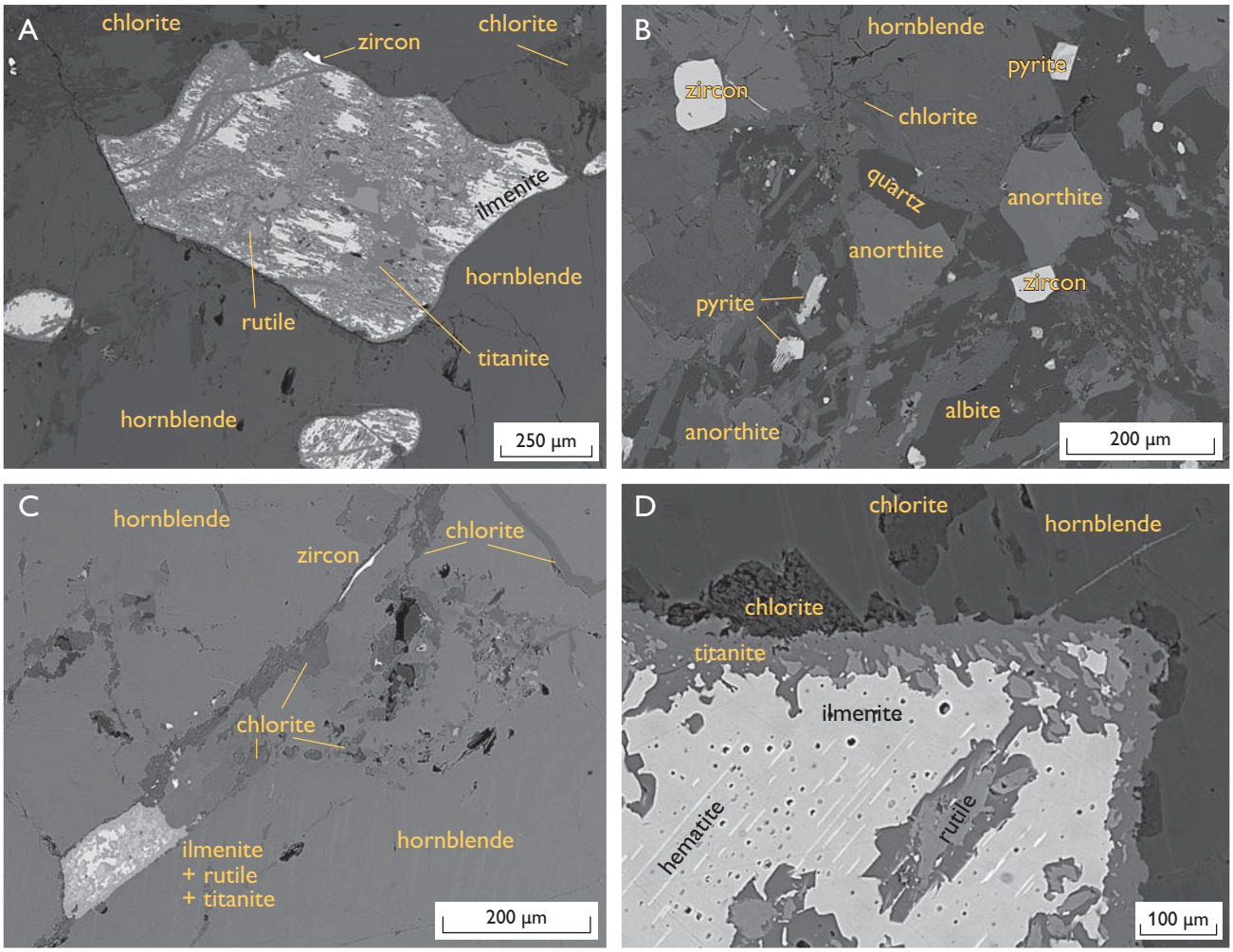

Fig. 3. Backscatter electron contrast mode scanning electron microscope images showing the textural association of zircon grains in the sample GGU 508216 and the observed break down reaction of ilmenite. **A:** Zircon associated with ilmenite. **B**: Zircon grains in melt pockets associated with the hornblenditic dyke that intruded into the anorthosite. **C**: Zircon in chlorite-filled cracks. **D**: Ilmenite in hornblende has reacted with water to form chlorite, titanite and rutile. Detail of the central grain shown in A.

plained by their intrusion into a partly solidified anorthosite crystal mush rather than a brittle solid. Alternatively, part of the hornblenditic dykes could have remelted during the intrusion of tonalitic gneisses in the area at this time (Nutman *et al*. 2004; Næraa & Scherstén 2008). After further cooling hematite lamellae exsolved in the ilmenite, and these lamellae are seen as thin needles in the ilmenite grains (Fig. 3D).

The observed reaction microstructures (Fig. 3D) suggest partial hydration of the assemblage hornblende + ilmenite, which yields the reaction products chlorite + rutile + titanite. This assemblage does not contain quartz. The reaction products are concentrated at the grain boundaries between hornblende and ilmenite, which suggests that the reactions are driven by small amounts of fluid present at the grain boundaries. Since the anorthosites are dry, the extent to which retrograde metamorphic changes can be recorded is a function of the amount of water brought into the system by the hornblenditic dykes. The reactions are likely to have ceased after all the local fluid was consumed. Assuming the reactions took place in an essentially closed system, as water-rich chlorite grew, the composition of the fluid could show considerable variation.

Within the chlorite-filled cracks in the hornblende-rich parts of the sample, newly grown zircon grains up to 100 µm in length are found (Fig. 3C). These zircon grains appear to fill the interstitial space between the chlorite-rimmed hornblende grains. The source of zirconium to form these zircons is most probably the ilmenite grains that broke down in the reaction discussed above. The age of the zircon grains in these chlorite-filled cracks is poorly constrained at 2.70 Ga (Fig. 2B), but this age is in good accordance with the interpretation that the ilmenite break-down reaction occurred

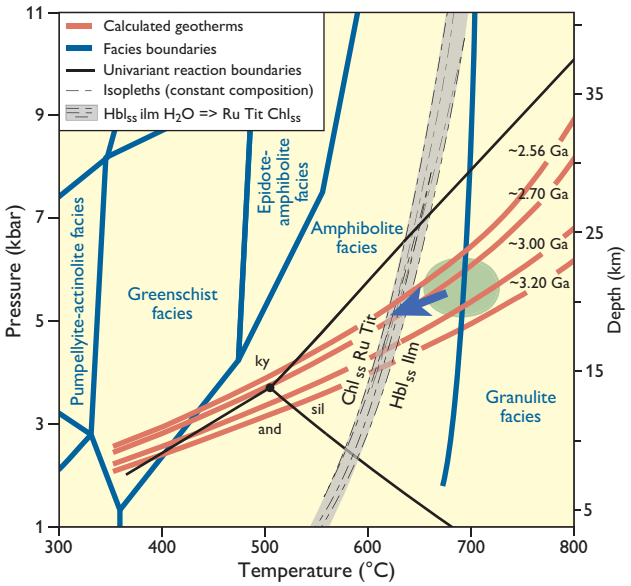

Fig. 4. Pressure–temperature (*P–T*) diagram that shows ranges of *P–T* estimates for modelled compositions of chlorite. The geotherms are based on measured and estimated content as a function of time of radiogenic elements in basaltic and felsic Greenland rocks (see Keulen *et al.* 2009 for further explanation). The pale-green area is the peak *P–T* conditions for regional metamorphism as suggested by Keulen *et al.* (2009). The blue arrow is part of a possible cooling path. **Ru**: rutile. **Tit**: titanite. **Chl$_{ss}$**: chlorite solid solution. **Hbl$_{ss}$**: hornblende solid solution. **Ilm**: ilmenite. **ky**: kyanite. **sil**: sillimanite. **and**: andalusite.

shortly after peak metamorphism (see below). Regional metamorphism was previously dated at 2.72 Ga, based on material from the Nuuk region (e.g. Friend *et al.* 1996) and the same age was reported north of Ilivertalik by Næraa & Scherstén (2008).

Modelling of the metamorphic reaction

Modelling of reactions to determine the approximate conditions of formation is complicated by extensive compositional variation of the amphibole and by potential variation in the fluid composition. Nevertheless, when using *PerPlex* (Connolly 2005) it is possible to locate mineral composition isopleths that approximate microprobe data for the amphibole and chlorite. Modelled compositions are: chlorite: X_{Mg} = 0.81–0.84; hornblende: X_{Mg} = 0.70–79; Al per formula unit = 1.490–1.626, and measured compositions are: chlorite: X_{Mg} = 0.65–0.75; hornblende: X_{Mg} = 0.76–0.80; Al per formula unit = 1.50–1.75.

The *PerPlex* modelling results are shown in Fig. 4. These results fit well with peak metamorphic conditions suggested by Keulen *et al.* (2009). Figure 4 shows the pressure–temperature region relevant to the mineralogy of the studied sample. The reaction seems to have occurred just after peak metamorphic conditions at about 600°C and after peak metamorphism in the area.

As a result of this pilot study on zircon grains and their surrounding minerals in samples from Majaqqap Qaava within the Fiskenæsset complex, southern West Greenland, we are able to show that the anorthosite records a metamorphic history that is more complex than previously recognised. Careful *in situ* observations prove helpful in unravelling the history of these rocks.

Acknowledgements

Alfons Berger is thanked for help at the microprobe, and Fiorella Fabra Aguilera and Mojagan Alaei are thanked for help with sample preparation.

References

Connolly, J.A.D. 2005: Computation of phase equilibria by linear programming: A tool for geodynamic modeling and its application to subduction zone decarbonation. Earth and Planetary Science Letters **236**, 524–541.

Frei, D. & Gerdes, A. 2009: Precise and accurate *in situ* U–Pb dating of zircon with high sample throughput by automated LA-SF-ICP-MS. Chemical Geology **261**, 261–270.

Friend, C.R.L., Nutman, A.P., Baadsgaard, H., Kinny, P.D. & McGregor, V.R. 1996: Timing of late Archaean terrane assembly, crustal thickening and granite emplacement in the Nuuk region, southern West Greenland. Earth and Planetary Science Letters **142**, 353–365.

Keulen, N., Scherstén, A., Schumacher, J.C., Næraa, T. & Windley, B.F. 2009: Geological observations in the southern West Greenland basement from Ameralik to Frederikshåb Isblink in 2008. Geological Survey of Denmark and Greenland Bulletin **17**, 49–52.

Ludwig, K.R. 2003: Mathematical-statistical treatment of data and errors for ^{230}Th/U geochronology. Uranium-Series Geochemistry, Reviews in Mineralogy and Geochemistry **52**, 631–656.

Myers, J.S. 1985: Stratigraphy and structure of the Fiskenæsset complex, southern West Greenland. Bulletin Grønlands Geologiske Undersøgelse **150**, 72 pp.

Næraa, T. & Scherstén, A. 2008: New zircon ages from the Tasiusarsuaq terrane, southern West Greenland. Geological Survey of Denmark and Greenland Bulletin **15**, 73–76.

Nutman, A.P., Friend, C.R.L., Barker, S.L.L. & McGregor, V.R. 2004: Inventory and assessment of Palaeoarchaean gneiss terrains and detrital zircons in southern West Greenland. Precambrian Research **135**, 281–314.

Authors' addresses

N.K., T.N. & T.F.K., *Geological Survey of Denmark and Greenland, Øster Voldgade 10, DK-1350 Copenhagen K, Denmark*. E-mail: *ntk@geus.dk*

J.C.S., *Department of Earth Sciences, University of Bristol, Bristol BS8 1RJ, UK.*

A.S., *Department of Earth & Ecosystem Sciences, Lund University, Sölvegatan 12, S-223 62 Lund, Sweden.*

Application of airborne hyperspectral data to mineral exploration in North-East Greenland

Tapani Tukiainen and Bjørn Thomassen

An airborne hyperspectral survey was organised by the Geological Survey of Denmark and Greenland (GEUS) and carried out in 2000 to test the use of spectral analysis in mineral exploration under Arctic conditions. The hyperspectral data were acquired by using the HyMap imaging system consisting of sensors that collect reflected solar radiation in 126 bands covering the 440–2500 nm wavelength range (Bedini & Tukiainen 2008). The spatial resolution was 4 × 4 m (Tukiainen 2001). Eight sites underlain by Caledonian or post-Caledonian rocks with known mineral occurrences (Fig. 1) were tested. The project was financially supported by the Greenland Bureau of Minerals and Petroleum and the data were analysed by GEUS. Here we provide a summary of the results.

Field work 2005–2009

Ground checks were undertaken in 2005, 2008 and 2009 by GEUS (Thomassen & Tukiainen 2008). The field work by the authors was carried out from light-weight camps in co-operation with International Molybdenum Ltd. that explored the Malmbjerg molybdenum deposit, and with other GEUS activities. The aim was to investigate hyperspectral anomalies and known mineral occurrences. The field work comprised ground measurements of rocks, minerals and their weathering products with a portable spectro-radiometer in order to determine their spectral character and to compare this information with the airborne data. In 2005 and 2008, a PIMA II portable instrument was borrowed from other institutions, but for the 2009 season GEUS purchased an advanced spectro-radiometer, model FieldSpec 3 HiRes. Our investigations showed that there is good correlation between the airborne spectra and the field spectra, thus confirming the quality and stability of the airborne hyperspectral data.

In general, sulphide minerals have poor to weak spectral response in the visible and near-infrared (VNIR) and shortwave infrared (SWIR) spectral regions whereas their alteration products, such as malachite, cerussite, smithsonite and jarosite, are distinctly SWIR-active. However, apart from jarosite, these minerals are virtually non-existent in the region. In contrast, it appears from our study that the hyperspectral detection of typical host- and wall-rock alteration minerals (jarosite, white micas, phengite, kaolinite, dolomite etc.) provides an effective method to outline potential exploration targets.

Main results

Below we present some results that are of relevance for mineral exploration in the region. The reader is referred to Harpøth *et al*. (1986) for a description of the mineral occurrences of the region and to Henriksen *et al*. (2009) for a description of the regional geology. The locations of the described areas are shown in Fig. 1.

Area 1 – Wegener Halvø. This horst-like peninsula exposes a complex pattern of fault blocks involving Neoproterozoic to Triassic sedimentary rocks, with stratabound base-metal mineralisation occurring in the Permo-Triassic section. Disseminated mineralisation hosted by Triassic sandstone and shale could not be detected by the airborne hyperspectral survey due to lack of alteration minerals. However, a close association of dolomitisation with Upper Permian, carbonate-hosted base-metal mineralisation is confirmed by our investigations, making the dolomite map a valuable exploration tool (Fig. 2).

Area 2 – Werner Bjerge. A well-known porphyry molybdenum deposit is hosted in the Malmbjerg granite stock, which is a unit of the Palaeogene Werner Bjerge alkaline intrusive complex. The alteration zones surrounding the deposit constitute an important target for our investigation. Conspicuous high-temperature, potassic and siliceous hydrothermal alteration outlined by muscovite and phengite is well displayed in the hyperspectral data. The high-temperature alteration apparently culminated in greisenisation of the Malmbjerg granite stock, as exemplified by topaz-muscovite-enriched rocks in the stock roof and in the roofing Permo-Carboniferous sandstone (Fig. 3). In addition, the hyperspectral mapping of typical alteration minerals outlines a large number of potential exploration targets with low-temperature argillitic and propylitic alteration elsewhere in the alkaline intrusive complex.

The hyperspectral mapping also defined a locality *c*. 1 × 1.5 km in size immediately south of Werner Bjerge, which displays many spectral similarities to Malmbjerg. The accessible part of this anomaly at 1300 m was found to host a significant number of pyrite- and fluorite-bearing trachytic

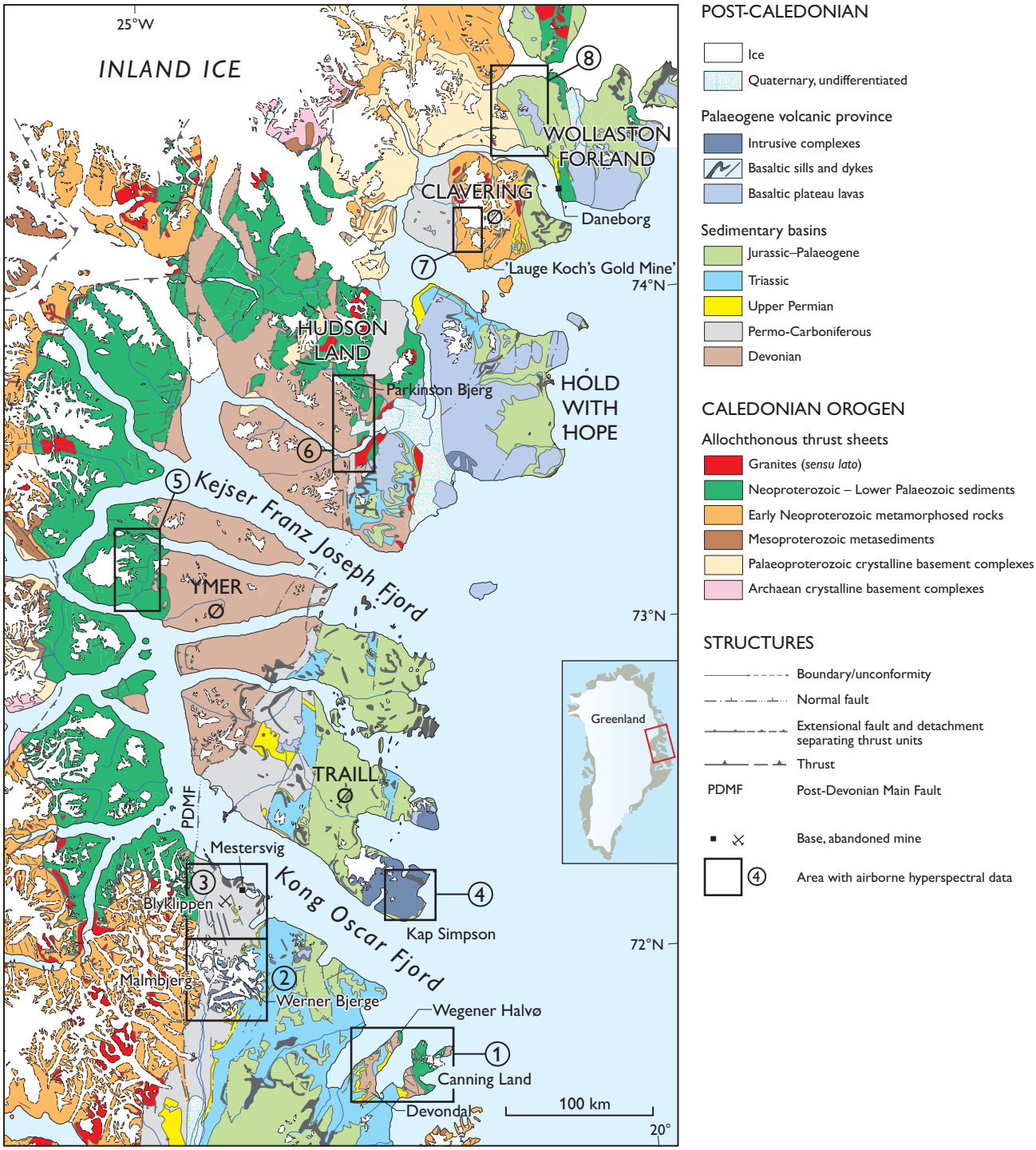

Fig. 1. Geological map of North-East Greenland showing areas covered by airborne hyperspectral data. The numbers refer to the areas discussed in the text. Modified from Henriksen & Higgins (2008).

dykes and sheets a few metres thick in Permo-Carboniferous sandstone. The intrusive trachytic rocks host abundant wall-rock fragments and are highly enriched in potassium and show elevated concentrations of tungsten (max. 35 ppm), molybdenum (max. 21 ppm) and thorium (max. 226 ppm). These rocks may represent the top of a porphyry system with an unexposed granite at a lower level.

Area 3 – Mestersvig. The Permo-Carboniferous sandstones of this area host epithermal lead–zinc-bearing quartz veins, including the mined-out Blyklippen deposit. The min-

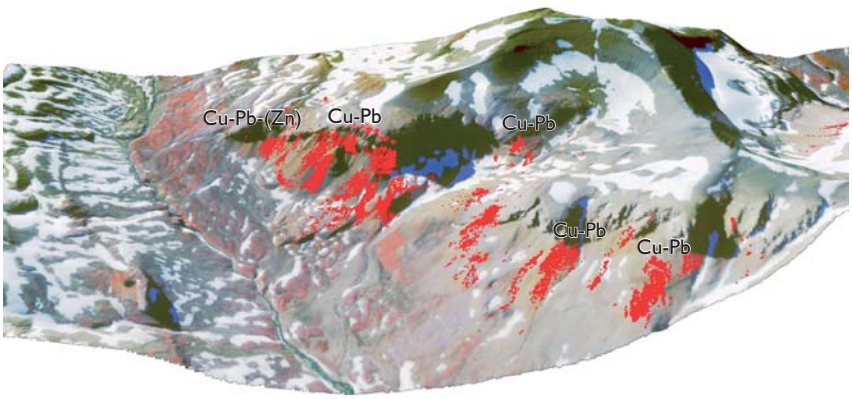

Fig. 2. Perspective view from the south-east of the north slope of Devondal showing dolomitic alteration (red) of Upper Permian limestone. The scree aprons enhance the surface impression of dolomite. Known occurrences of Cu-Pb-(Zn) mineralisation are indicated. Background image is a colour composite of HyMap bands 27(R), 18(G) and 4(B). No vertical exaggeration, relief is 600 m.

eralisation is accompanied by silicification and kaolinisation of the wall rocks, but this association did not clearly define the veins in the airborne survey. However, the airborne data reveal a distinct, *c.* 500 m wide zone of pervasive kaolinisation of the arkosic sandstone some 3 km north-east of the old mine. This could be related to unknown base-metal mineralisation of the Blyklippen type.

Area 4 – Kap Simpson. The Palaeogene Kap Simpson alkaline intrusive complex hosts a caldera structure displaying widespread and intensive hydrothermal alteration. Pyrite is common and traces of molybdenite are known, with base-metal and niobium-bearing quartz and calcite veins in the host Mesozoic sediments. The hyperspectral survey distinguished between low-temperature, fumarole-related alteration (montmorillonite-illite-jarosite and iron oxides) and high-temperature alteration (muscovite-phengite) associated with subvolcanic intrusions. High-temperature potassic alteration and greisen-like spectral signatures on a granite in the north-western part of the intrusive complex define a new exploration target with potential for porphyry-type mineralisation.

Area 5 – Ymer Ø. Ymer Ø hosts a number of E–W-striking, epithermal tungsten, antimony, gold, base-metal-bearing quartz veins in Neoproterozoic sediments. Samples from the antimonite-bearing veins returned up to 23.4% Sb and 4.7 ppm Au. These veins give a weak hyperspectral response, due to the presence of low-temperature argillitic minerals (kaolinite, illite and alunite) in the quartzitic wall rock. However, known scheelite-antimonite-bearing veins are not detected by the hyperspectral survey. This is due to lack of distinct alteration minerals other than quartz in the carbonate wall rock. Distinct linear anomalies detected in the airborne data turned out to originate from 3–5 m thick, E–W-striking, unmineralised rhyolitic veins with kaolinite alteration or weathering products, probably related to the mineralising system.

Area 6 – Hudson Land. Central Hudson Land exhibits various types of mineralisation in a complex pattern of Proterozoic to Palaeogene rocks transsected by a regional, N–S-trending structure, called the Post-Devonian Main Fault. Quartz veins 0.1–1.0 m thick with greisen mineralisation returned up to 1.4% Sn and 0.5% Cu but were not depicted in the airborne data due to their modest size. In contrast, extensive, low-temperature, hydrothermal alteration with associated epithermal base- and noble-metal-bearing veins along the Post-Devonian Main Fault is clearly seen in the hyperspectral data.

Special attention was paid to a Devonian granite stock at Parkinson Bjerg, which is surrounded by geochemical Sn-W-Mo-Nb anomalies. The granite was found to have a pegmatitic core rich in quartz, fluorite and tourmaline, corresponding to a distinct tourmaline and phengite response in the airborne data. This granite is a potential source for the geochemical anomalies. Rock samples returned up to 0.4% Sn, 0.17% Be and 0.1% Y.

Area 7 – Clavering Ø. Extensive rust zones caused by hydrothermal alteration and epithermal base-metal mineralisation along faults occur in Proterozoic metasediments on Clavering Ø. The mineralisation was investigated in the 1930s when a test adit was excavated at the so-called 'Lauge Koch's Gold Mine', which transpired to host a pyrite vein without anomalous gold. The mineralised structures are distinct in the hyperspectral mapping as lineaments with low-temperature alteration minerals such as illite and jarosite. Samples of massive, brecciated pyrite 'ore' with minor fluorite and galena returned <2 ppb Au.

Area 8 – Wollaston Forland. Prior to 2000, no mineralisation had been reported from Wollaston Forland, and the area was included in the airborne survey for biological reasons. The survey showed hyperspectral anomalies caused by jarosite- and muscovite/sericite-rich zones or lithologies in the north-western part of the area, which is underlain by Proterozoic metasedimentary rocks. A scree sample of pyritiferous paragneiss below an anomaly returned 4.1 ppm Ir while another loose block returned 0.38 ppm Au. Surrounding blocks of ultramafic rocks indicate a magmatic component in the area with potential for platinum group mineralisation.

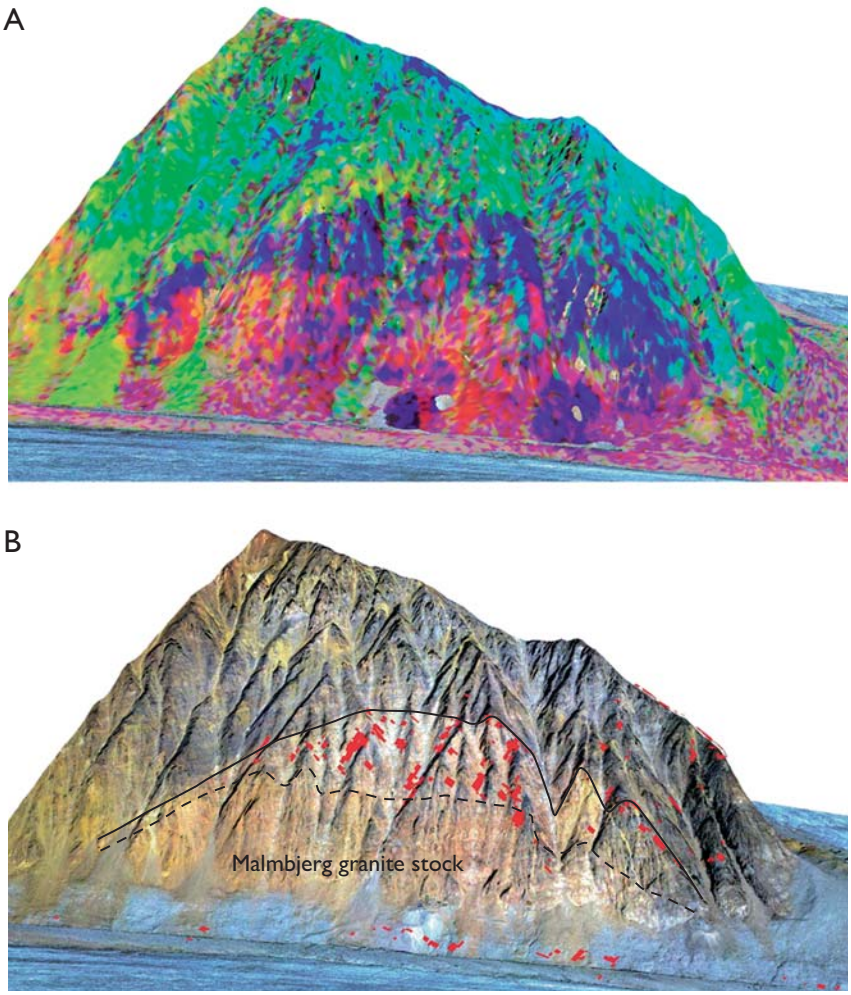

Fig. 3. Perspective view from the south-west of the Malmbjerg granite stock, no vertical exaggeration, relief is 500 m. The digital terrain model is based on Lidar data from International Molybdenum Ltd. (re-sampled at 1 × 1 m resolution). **A**: Minimum noise fraction transformed shortwave infrared data draped on the detailed Digital Terrain Model. Note the compositional zoning of the granite stock and intensive high-temperature alteration of the roofing rocks (hues of yellow and orange). **B**: Orthoscopic Lidar image draped on the detailed Digital Terrain Model. The pixels mapped as topaz/tourmaline-bearing greisen are shown in red. The boundaries of the granite stock are indicated.

Concluding remarks

The present study demonstrates that the hyperspectral method is well suited for mineral exploration in remote and mountainous Arctic regions. The most obvious target for future use of this method in Greenland seems to be the Palaeogene igneous province that stretches for 1100 km along the east coast. This province should be investigated for host- and wall-rock alteration indicative of subvolcanic porphyry-type molybdenum mineralisation.

References

Bedini, E. & Tukiainen, T. 2008: Using spectral mixture analysis of hyperspectral remote sensing data to map lithology of the Sarfartoq carbonatite complex, southern West Greenland. Geological Survey of Denmark and Greenland Bulletin **17**, 69–72.

Harpøth, O., Pedersen, J.L., Schønwandt, H.K. & Thomassen, B. 1986: The mineral occurrences of central East Greenland. Meddelelser om Grønland, Geoscience **17**, 139 pp.

Henriksen, N. & Higgins, A.K. 2008: Caledonian orogen of East Greenland 70°N–82°N: Geological map at 1:1 000 000 – concepts and principles of compilation. In: Higgins, A.K., Gilotti, J.A. & Smith, M.P. (eds): The Greenland Caledonides: evolution of the northeast margin of Laurentia. Geological Society of America Memoir **202**, 345–368.

Henriksen, N., Higgins, A.K., Kalsbeek, F. & Pulvertaft, T.C.R. 2009: Greenland from Archaean to Quaternary. Geological Survey of Denmark and Greenland Bulletin **18**, 126 pp.

Thomassen, B. & Tukiainen, T. 2008: Ground check of airborne hyperspectral anomalies in the greater Mesters Vig area, central East Greenland. Danmarks og Grønlands Geologiske Undersøgelse Rapport **2008/14**, 85 pp.

Tukiainen, T. 2001: Projects MINEO and HyperGreen: airborne hyperspectral data acquisition in East Greenland for environmental monitoring and mineral exploration. Geology of Greenland Survey Bulletin **189**, 122–126.

Authors' addresses

T.T., *Geological Survey of Denmark and Greenland, Øster Voldgade 10, DK-1350 Copenhagen K, Denmark*. E-mail: *tt@geus.dk*

B.T., Present address: *Avannaa Resources Ltd., Dronningens Tværgade 48, DK-1302 Copenhagen K, Denmark*.

Study of a Palaeogene intrabasaltic sedimentary unit in southern East Greenland: from 3-D photogeology to micropetrography

Henrik Vosgerau, Pierpaolo Guarnieri, Rikke Weibel, Michael Larsen, Cliona Dennehy, Erik V. Sørensen and Christian Knudsen

Establishment of robust reservoir models and estimates of subsurface hydrocarbon volumes in relatively unknown subsurface settings can be improved by using data from field analogues. The discovery of the Rosebank oilfield in the Faroe–Shetland Basin showed that intrabasaltic sandstones can form important hydrocarbon reservoirs in volcanic basins (Helland-Hansen 2009). The Sødalen region in southern East Greenland (Fig. 1) forms an excellent field analogue to the Rosebank oilfield where contemporaneous Palaeogene sediments interbedded with lava units can be studied and sampled (Larsen *et al.* 1999). In this area many of the exposures are located along steep, inaccessible cliffs with excellent exposures that are ideal for 3-D photogeological studies based on digital high-resolution photographs taken from a helicopter.

The analogue study reported on here has integrated results from a wide range of spatial scales. On a large scale (kilometre to metre), 3-D photogeology was used to study the extent, geometry and interfingering of volcanic and intrabasaltic sedimentary units. Photogeology was also used to map faults, dykes and sills, which may lead to compartmentalisation (division) of reservoirs. On an intermediate scale (metre to millimetre), sections are logged in the field, sedimentary and volcanic facies are mapped and depositional environments are interpreted. Three-dimensional photogeology is also applied on an intermediate scale to map lateral variations of sedimentary units between logged sections. On a small scale (millimetre to micrometre), mineral-chemical, petrographical and zircon age determinations provide information on sediment source, provenance area and diagenetic influences on reservoir properties.

The analogue study has resulted in a large database, which can form an important source of estimates of reservoir size, geometry and connectivity, and of vertical and lateral variations in the sandstone content of reservoirs. Ultimately this may improve estimates of the actual volumes and recoverable volumes of hydrocarbons in intrabasaltic subsurface sediments.

The 3-D photogeological method

The 3-D photogeological method used in this study was developed at the Geological Survey of Denmark and Greenland (GEUS) and builds on earlier work by Dueholm *et al.* (1993) and Dueholm & Olsen (1993). The method allows the acquisition of geological data from vertical and oblique aerial photographs, with a three-dimensional overview of the outcrops. The oblique photographs (1:15 000–1:17 000 scale) are triangulated with coloured, vertical, aerial photographs (1:27 000 scale) using a 3-D stereo-plotter coupled with stereo-mirror technology. The mapping of geological features includes determination of strata thickness, strike direction and dip values working on a 3-D high resolution vision of the cliffs. The resolution of volcanic and sedimentary beds and geological features is *c.* 10 cm. All the mapped features are stored in a GIS database and 3-D polylines can be exported

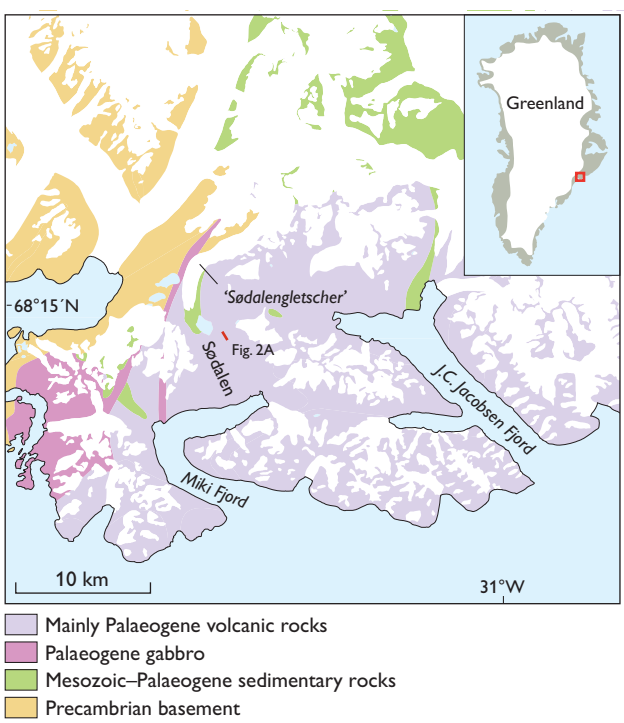

Fig. 1. Map of the Sødalen area in southern East Greenland. The red line shows the location of the profile in Fig. 2A.

A. Large scale

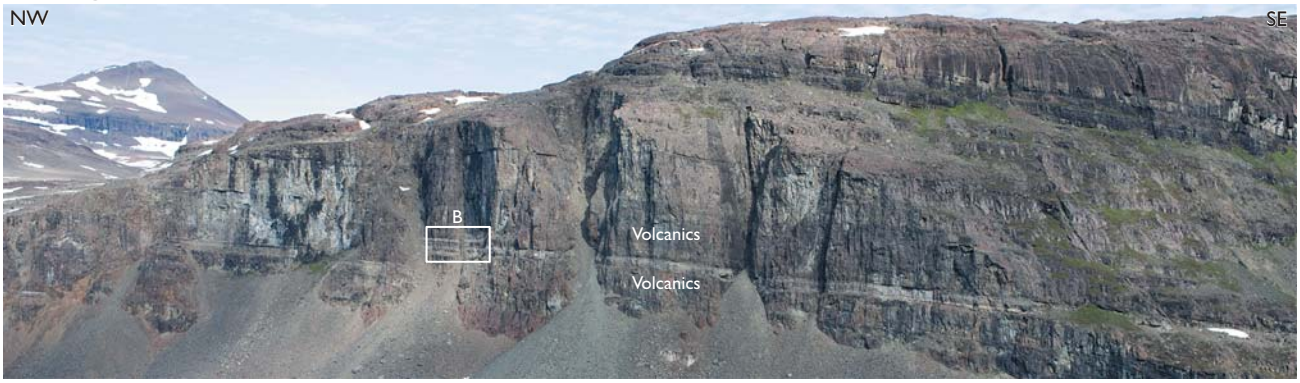

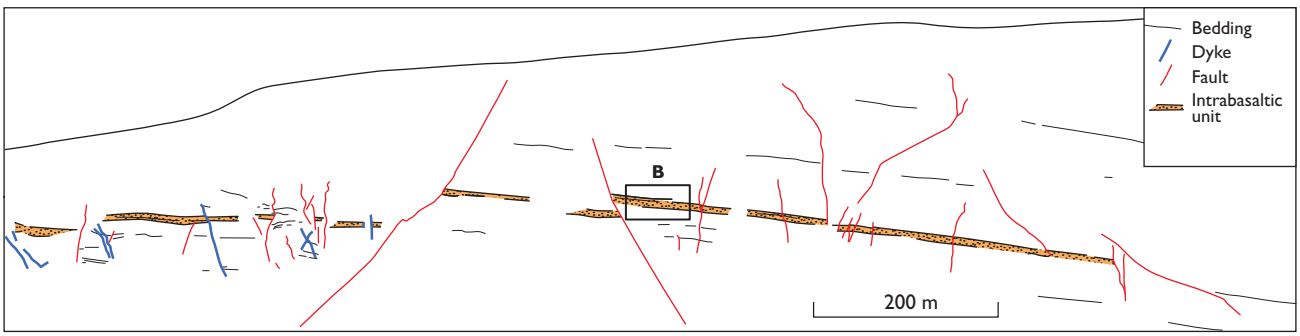

B. Intermediate scale

C. Small scale

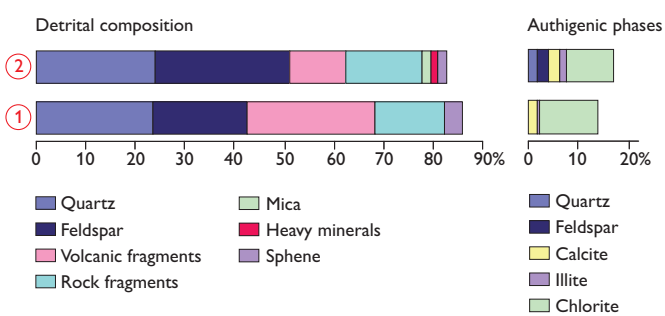

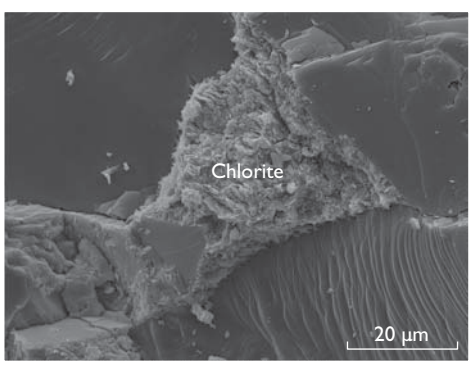

as shape files suitable for 3-D modelling using, for example, Petrel reservoir engineering software. Moreover, using 3-D feature databases in ArcGIS, geological cross-sections can be generated automatically to obtain real representations of outcrops, and then projected onto a topographic profile, where the accuracy is as high as the resolution in the photographs. The oblique photographs used here were small-frame colour photographs taken from a helicopter flying close to the cliff faces (<800 m) and at a constant altitude along straight lines approximately parallel to the cliffs. The photographs were taken with a 60 to 80% overlap using a 22 megapixel digital camera.

On a large scale (kilometre to metre)

On a large scale, 3-D photogeology is used to study the lateral extent and geometry of the intrabasaltic sediments and volcanic rocks and boundary relationships. Evidence of compartmentalisation of the intrabasaltic reservoir analogues, caused for example by dykes, sills or faults, are mapped. Figure 2A shows an oblique view of a 1.2 km section on the eastern side of Sødalen, which is an 8 km long U-shaped valley, orientated SE–NW from Miki Fjord to 'Sødalengletscher' (Fig. 1). The photograph focuses on the stratigraphically lowest intrabasaltic, whitish sedimentary unit, which dips gently to the south-east. The geological cross-section in Fig. 2A is projected on the cliff view, and is obtained from 3-D polylines created during the 3-D photogeological work. Figure 2A illustrates several large-scale features relevant to the analogue study such as: (1) top and bottom geometry of the sandstone unit, (2) density of dykes and faults, which has a large impact on the lateral extension of the layers due to offsetting and (3) an evaluation of reservoir compartmentalisation.

On an intermediate scale (metre to millimetre)

On an intermediate scale, sedimentary and volcanic sections are logged in the field. Facies types are identified, their lateral distribution and vertical stacking patterns are mapped and the boundaries between sedimentary and volcanic units are studied in detail. The 3-D photogeology is also useful on this intermediate scale because the high resolution of the digital photographs allows enlargement to study decimetre-sized features. Photogeology can therefore be very helpful in mapping sedimentary facies assemblages between logged sections as well as key surfaces separating the different facies, such as sequence boundaries and marine-flooding surfaces. The overall depositional environments and the governing mechanisms for facies distribution, such as sediment transport directions, relative sea-level variations and palaeotopography can be interpreted from these studies.

An example of a study on an intermediate scale is illustrated in Fig. 2B where the photograph is an enlargement of a small area on the digital photograph (Fig. 2A). The log of the sedimentary unit of shallow marine sandstone is shown on the left side of the figure. The lower, exposed part of the unit consists of crudely and irregularly bedded sandstones, locally with vertical burrows, interpreted as deposited in the upper shoreface zone. The lower part is overlain by well-sorted, fine to medium-grained, laterally extensive sandstone sheets and wedge-shaped sandstone beds with a large variety of sedimentary structures including local vertical burrows, cross-stratification and parallel bedding. These sandstones are interpreted as deposited in the lower to middle shoreface zone, which implies that the boundary to the underlying upper shoreface sandstones represents a minor flooding surface. On the photograph (Fig. 2B) it is seen that the upper and lower to middle shoreface facies assemblages can be followed laterally for tens of metres. It is also seen that the boundary between the lava units and the sedimentary unit is slightly undulating, and that the invasive lava bed can be followed into the overlying lava to the right. The dyke that cuts through both the sedimentary unit and the lava units may have led to a possible compartmentalisation of the sandstone reservoir.

Fig. 2. *(facing page)* **A**: Oblique photograph (upper) and derived geological cross-section (lower) of the eastern side of Sødalen, an 8 km long U-shaped glacial valley, extending SE–NW from 'Sødalengletscher' to Miki Fjord. For location see Fig.1. The photograph focuses on the lowest intrabasaltic sediments (whitish colour) that dip gently to the south-east. Faults and dykes are also seen. The geological cross-section below is a projection of 3-D polylines along a N–S-oriented profile, slightly different from the NW–SE orientation of the photograph. **B:** Close-up view of the white square in Fig. 2A. A field log of the section (left) labels the sedimentary facies assemblages which can be followed laterally on the photograph. Other important observations include an invasive lava bed and a dyke cutting through both lavas and intrabasaltic sediments. **C:** Detrital and authigenic mineralogical composition of the facies in the sedimentary unit. The larger amount of authigenic phases in the lower-middle shoreface sandstones compared to the upper shoreface sandstones, reflect that these sandstones originally had a larger content of unstable, glass-rich volcanic fragments. The positions of the two samples are shown on Fig. 2B.

On a small scale (millimetre to micrometre)

On a small scale, petrography is used to understand diagenetically induced reductions in porosity and permeability to understand the influence of provenance, sedimentary facies and surrounding 'hot' units on diagenetic processes. Based on intensive sampling in a well-described geological framework controlled by 3-D photogeology and logged sedimentary sections, diagenetic changes are compared with detrital composition, depositional environment and effects from overlying and underlying lava units as well as dykes and sills. Provenance variations are revealed from heavy mineral analysis using computer-controlled scanning electron microscopy, zircon age distributions and petrography. Geochemistry is applied to distinguish different intrabasaltic units.

The intrabasaltic sedimentary rocks consist of a mixture of detrital siliciclastic (quartz, feldspar, mica etc.) and volcaniclastic input (Fig. 2C). The upper shoreface facies is richer in volcanic fragments than the lower-middle shoreface facies, yet it has a lower content of authigenic phases (Fig. 2C). This is unexpected as volcanic fragments traditionally have been associated with intensive alteration thereby liberating elements for extensive authigenic phases. However, the type of volcanic fragments is also crucial for the degree of diagenetic alteration. Glass-rich volcanic fragments are common in the lower-middle shoreface facies, whereas relatively stable volcanic fragments (lath-shaped plagioclase with little interstitial glass matrix) are more abundant in the upper shoreface. Glass-rich volcanic fragments, which are easily altered, result in extensive authigenic formation, including chlorite as shown in Fig. 2C. The stable volcanic fragments behave as plagioclase grains during diagenesis and have less influence on the authigenic phases than the glass-rich volcanic fragments. Consequently, the upper shoreface sandstones show better reservoir properties than the lower-middle shoreface facies.

Conclusions

The field analogue project at Sødalen integrated the three disciplines of 3-D photogeology, sedimentology and petrography, and gave detailed information from kilometre to micrometre scale. Petrographical investigations revealed the diagenetic influence on the reservoir properties. When the diagenetic changes were related to the sedimentary facies, the information on the reservoir properties could be scaled up to sedimentary bodies. The geometry of the sedimentary bodies and the probability of compartmentalisation are defined from 3-D photogeology and logged sedimentary sections. Integration and up-scaling of several types of geological data resulted in a more complete understanding of the geology of the area and can form the basic input for reservoir modelling and as field analogue for hydrocarbon discoveries in a similar, inaccessible geological setting in offshore areas.

Acknowledgements

Chevron and Sindri Group are thanked for their financial contribution to the field work in Greenland.

References

Dueholm, K.S. & Olsen, T. 1993: Reservoir analog studies using multimodel photogrammetry; a new tool for the petroleum industry. AAPG Bulletin 77, 2023-2031. Tulsa, Oklahoma: American Association of Petroleum Geologists.

Dueholm, K.S., Garde, A.A. & Pedersen, A.K. 1993: Preparation of accurate geological and structural maps, cross-sections and block diagrams from colour slides, using multi-model photogrammetry. Journal of Structural Geology **15**, 933–937.

Helland-Hansen, D. 2009: Rosebank – challenges to development from a subsurface perspective. In: Varming, T. & Ziska, H. (eds): Faroe Islands Exploration Conference: Proceedings of the 2nd Conference. Annales Societatis Scientarium Faeroensis, Supplementum **50**, 241–245.

Larsen, M., Hamberg, L., Olaussen, S., Nørgaard-Pedersen, N. & Stemmerik, L. 1999: Basin evolution in southern East Greenland; an outcrop analog for the Cretaceous–Paleogene basins on the North Atlantic volcanic margin. AAPG Bulletin **83**, 1236–1261. Tulsa, Oklahoma: American Association of Petroleum Geologists.

Authors' addresses

H.V., P.G., R.W., E.V.S. & C.K., *Geological Survey of Denmark and Greenland, Øster Voldgade 10, DK-1350 Copenhagen K, Denmark.*

E-mail: *hv@geus.dk*

M.L., *DONG Energy A/S, Agern Alle 24–26, DK-2970 Hørsholm, Denmark.*

C.D., *Chevron Upsteams Europe, Chevron North Sea Ltd., Chevron House, Hill of Rubislaw, Aberdeen AB15 6XL, UK.*

An advancing glacier in a recessive ice regime: Berlingske Bræ, North-West Greenland

Peter R. Dawes and Dirk van As

Greenland is receiving unprecedented international attention, both in scientific and political circles. Characterised by a central ice sheet up to 3.4 km thick (Inland Ice), numerous ice caps and hundreds of outlet glaciers debouching into the surrounding oceans, Greenland supports the second largest ice mass in the world. Analysis of glacier movements, melt rates and ice loss to the sea, provide data with which to assess mass balance changes and thereby predict global sea-level rise. Thus Greenland plays a central role in the current worldwide debate on climate change.

Present-day dynamic ice loss is invariably advertised by the fast moving glaciers of western Greenland with their spectacular calf ice production, such as the ice streams around Disko Bugt reviewed by Weidick & Bennike (2007). This tends to overshadow ice stability and expansion seen in the form of stationary and advancing glaciers elsewhere in Greenland (MODIS 2009). While the seawards acceleration of glacier flow and retreat in frontal positions can be readily attributed to a shift in atmospheric and oceanic conditions (global warming), the same explanation can hardly be used for glaciers with contrasting movement histories.

Aim of this paper

We focus on three west coast, marine-terminating glaciers between 75° and 78°N (Fig. 1) to elucidate the retreat–advance paradox referred to above. Steenstrup Gletscher and Tracy Gletscher are chosen to illustrate the regional pattern of ice recession, including massive ice wasting on a broad front in Melville Bugt, whereas Berlingske Bræ defies this trend by long-lasting advance. The receding glaciers Steenstrup and Tracy are known from regional surveys (e.g. Kollmeyer 1980; Rignot & Kanagaratnam 2006), but the advancing glacier Berlingske Bræ has only been cursorily mentioned in map descriptions (Dawes 1992, 2006).

We present maps showing the terminus fluctuations of the three glaciers based on historical records (Figs 2–4) but the paper's four-page limit prohibits discussion of the early sources. This aspect, climatic records and their relation to ice fluctuations, and comparisons with other Greenland glaciers, will be dealt with in a forthcoming paper.

Historical sources and the 2009 database

T.C. Chamberlin and R.D. Salisbury were the first to investigate glaciers in the region in 1894–95 when they reached as far north as Inglefield Bredning, the location of our northern glacier (Tracy Gletscher). The next milestone was the regional mapping by geologist and cartographer Lauge Koch between 1916 and 1923 who surveyed and described glaciers throughout the region. The 1940s heralded a new era of research with the incoming of aerial photographs and such images are available from the period 1948–1985. Finally in the last decades, satellite images have assured a continual record of the areas covered and uncovered by Greenland glaciers (Weidick 1994). In this paper we make use of such imagery from the period 1963–2009. Table 1 summarises our data sources.

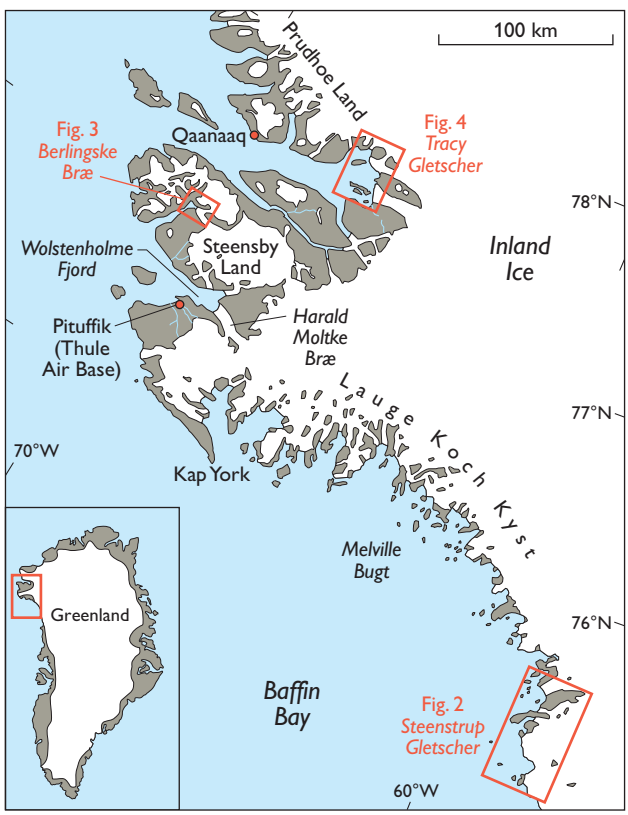

Fig. 1. Map of North-West Greenland showing the locations of the three studied glaciers featured in Figs 2–4.

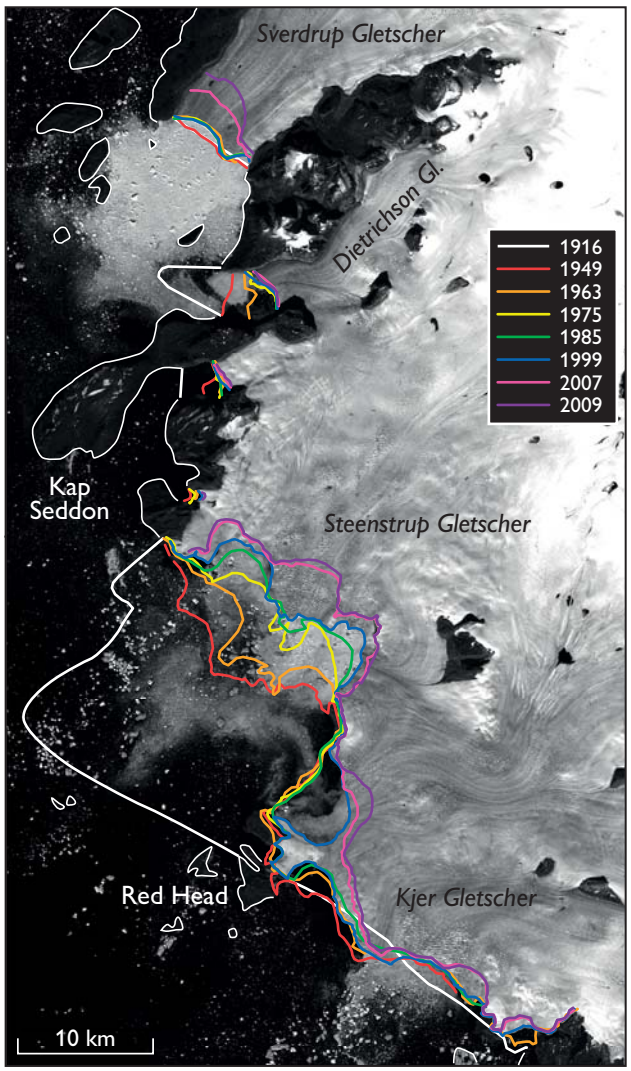

Fig. 2. Satellite image of Steenstrup Gletscher and neighbouring glaciers, southern Melville Bugt, showing eight frontal positions from 1916 to 2009. Thin, white line: coastline. For sources, see Table 1.

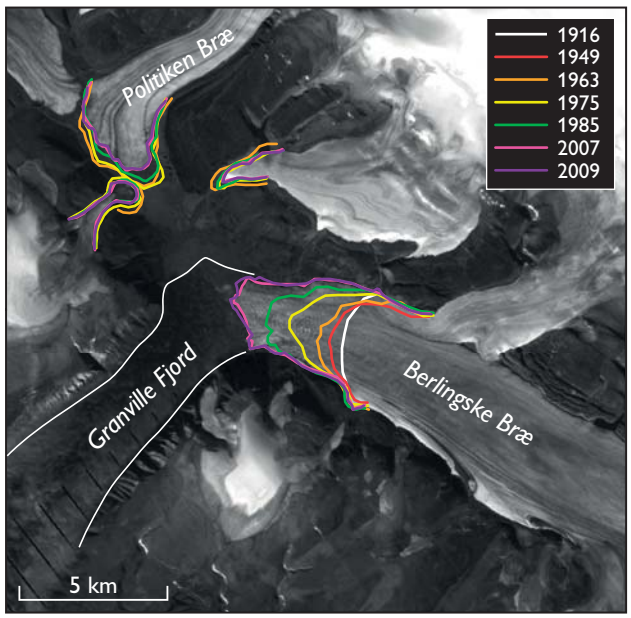

Fig. 3. Satellite image of Berlingske Bræ, Granville Fjord showing seven frontal positions from 1922 to 2009. Thin, white line: coastline. For sources, see Table 1.

Steenstrup Gletscher, Melville Bugt

Steenstrup Gletscher is the widest glacier of the impressive ice front that characterises Lauge Koch Kyst and that calves into Melville Bugt (Figs 1, 2). Stretching from the Kap Seddon peninsula to Red Head, where Steenstrup Gletscher borders the fairly stable Kjer Gletscher, the glacier has an irregular and crevassed floating tongue more than 30 km wide. Ice production from the central part is spectacular, both as regards the number of calved bergs and their size. Koch (1928) noted that large portions of the 25 m high floating tongue become detached and move seawards before being broken up, while Kollmeyer (1980) described the calving of 'jigsaw puzzle type' icebergs in excess of 1 km in length.

As illustrated by Fig. 2, the main fluctuations affected the central part of the floating tongue where drawback since 1916 is almost 25 km. Melville Bugt is noted for its ice-infested waters during summer months and the records show that the nature and position of the ice front can change seasonally depending on the degree of ice congestion. In five months, from spring to autumn 1916, the central part of the front had moved westwards by *c.* 1 km while in 1920, after a summer when Melville Bugt was free of ice, there was recession of more than 6 km (Koch 1928). In contrast, the northern segment of the terminus was stationary between 1916 and 1923.

Table 1. Data for North-West Greenland glacier fluctuations

Year	Type/Medium	Source
1892	Field/Map	Peary (1892)
1916	Field/Map	Koch (1922)
1922	Field/Map	Koch (1932)
1949*	OAP†/Map	Geodetic Institute§
1953	VAP‡	U.S. military
1963	Satellite	Zhou & Jezek (2003)
1971	VAP‡	Greenarctic Consortium
1985	VAP‡	Geodetic Institute
1975	Landsat satellite	NASA and U.S. Geological Survey
1999		
2007		
2009		

*Photography 1948–1950; §1st edition map 1954
†Oblique aerial photography; ‡ Vertical aerial photography

The shrinkage shown in Fig. 2 has produced new bedrock exposures, and Red Head, which was a semi-nunatak in 1916, became an island in 2005.

Berlingske Bræ, Granville Fjord

Berlingske Bræ flows westwards into the head of Granville Fjord from the major ice cap of Steensby Land that has a bridge connection with the Inland Ice (Figs 1, 3). It is the only glacier of several draining into Granville Fjord that currently reaches the sea. The glacier has a rather low gradient and its flow pattern can be traced for about 25 km before being lost to the ice cap. The glacier trunk is 3–4 km wide, and today the terminus is irregular, rather slender and crevassed, and over 2 km across. It is unknown whether the snout is afloat, but the apparent lack of iceberg production suggests it is grounded. An unnamed tributary originating from a more westerly ice cap joins the northern flank of Berlingske Bræ contributing to its westerly flow into Granville Fjord.

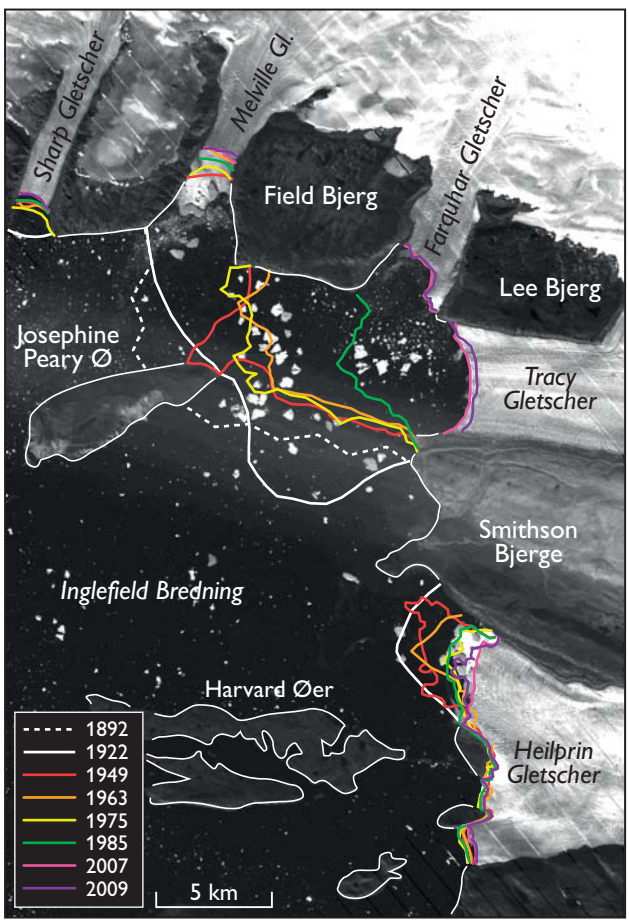

Fig. 4. Satellite image of Tracy Gletscher and neighbouring glaciers, Inglefield Bredning, showing eight frontal positions from 1892 to 2009. Thin, white line: coastline. For sources, see Table 1.

The terminus positions shown in Fig. 3 illustrate a continuous ice advance in excess of 4 km in the last 85 years that has changed the glacier front from being terrestrial to marine. As opposed to when the glacier terminated on land, its tongue now is strongly tapering. The glacier has overrun the entire alluvial gravel plain that in the early 20th century extended beyond its snout and separated it from the fjord, and it has also engulfed bedrock exposures on its southern flank that were mapped by the first author in 1974.

Tracy Gletscher, Inglefield Bredning

Tracy Gletscher is the second largest of six outlet glaciers that debouch into the headwaters of Inglefield Bredning (Figs 1, 4). It is about 5 km wide with a steep front that has a regular concave trace which is probably afloat. The flow pattern of the glacier is recognisable over 30 km before being lost to the east to the Inland Ice proper.

The 115-year record (Fig. 4) shows substantial ice wasting amounting to frontal recession of *c.* 15 km. The terminus positions show that for a century (1892–1985) Tracy Gletscher was coalesced with Farquhar Gletscher. In 1923 the seaward front of the floating confluent ice embracing Melville Gletscher was a cliff 20 m high and 19 km long (Koch 1928). Over the past century the glacier tongue has lost about 100 km^2 of ice, which represents at least 20 km^3 based on Koch's observation.

Recession with the impressive break-up of the confluent ice mass has led to striking landscape changes. For example, longtime nunataks Lee Bjerg and Field Bjerg are now lapped by the sea, while Josephine Peary Ø finally lives up to its name as an island being eventually released from the ice around 1960 (Inûterssuaq Uvdloriaq, personal communication 1971).

Recent glacial history: retreat versus advance

The glaciers of North-West Greenland and their marginal deposits are shown on the Thule 1:500 000 scale geological sheet, and a summary of glacial history is given in the map description (Dawes 2006). The regional pattern of spatial change seen in terms of terminal positions between 1948–50 and 1985 is shown on the maps of Dawes (1988). This information, plus the early records summarised by Koch (1928), the regional analysis of Davies & Krinsley (1962) and satellite data of the last decades, demonstrate that the general recession of the Inland Ice and its outlet glaciers is regional in character and persistent for more than a century. The drastic deglaciation of Melville Bugt has brought the ice limit there close to the early Holocene position (Bennike 2008).

The overall pattern is that glaciers with floating tongues, like Steenstrup and Tracy, have shown by far the largest retreat and ice wastage. The most extensive ice withdrawal has been along the heavily glaciated Lauge Koch Kyst, where the lowering ice surface is being pierced by its rock substratum and where nunataks have become shoreline, and ice-rooted peninsulas insular. However, some glaciers show current fast retreat after decades of stability (e.g. Sverdrup Gletscher; Fig. 2). In general, land-based glaciers show relatively sluggish movement, and some have been almost stationary or only show minor retreat (e.g. Prudhoe Land glaciers; Dawes 2006). It is clear that given the existence of a detailed database, the general recession can be seen to have been interrupted by short periods of comparative stability and even advance (e.g. Harald Moltke Bræ; Mock 1966).

In contrast to this regional recessive regime, Berlingske Bræ shows continual advance for at least 85 years. An explanation of this deviant behaviour must be sought in the fact that the glacier originates from an independent ice cap that responds to changes in temperature and precipitation differently than the Inland Ice. The glacier advance can be a response to increased precipitation on the ice cap or increased basal sliding, both of which could be related to the observed increase in atmospheric temperatures. No matter which, the advance of Berlingske Bræ over such a long period is unexpected in a warming climate.

Conclusions, relevance to global climate research and future work

Berlingske Bræ is located between Steenstrup Gletscher and Tracy Gletscher that are 340 km apart. The two receding glaciers compare with others in Melville Bugt (and in other areas of Greenland) indicating changed mass balance of their source: the Inland Ice. The main causes of this long-lasting change – documented in our data back to 1892 – must be regional, and thus the present warming climate must affect the process. However, whatever the fundamental cause (or causes) controlling regional meltdown, it has been a subordinate factor at Berlingske Bræ where there is long-standing advance.

Seen in terms of the regional, recessive ice regime in which it is located, Berlingske Bræ is anomalous and thus outside mainstream research concerning analysis of dwindling ice masses and their response to global warming. However, if we are to understand the underlying complex processes, and ultimately the effect of climate change on the regional recessive regime, attention should also be paid to such glaciers. Among other things, this research should be directed to discovering why receding and expanding glaciers with century-long contrasting histories occur side by side.

This paper is a contribution to international promotion of this aspect of glacioclimatic research in progress at the Survey, both in our study region and elsewhere in Greenland (e.g. Weidick 2009).

References

Bennike, O. 2008: An early Holocene Greenland whale from Melville Bugt, Greenland. Quaternary Research **69**, 72–76.

Davies, W.E. & Krinsley, D.B. 1962: The recent regimen of the ice cap margin in North Greenland. International Association of Scientific Hydrology **58**, 119–130.

Dawes, P.R. 1988: Geological map of the Thule district, North-West Greenland. 1:100 000 sheets 1–6 and 1:200 000 sheets 7–11. Unpublished maps, Geological Survey of Denmark and Greenland, Copenhagen.

Dawes, P.R. 1992: New geological map of the Thule region, North-West Greenland. Rapport Grønlands Geologiske Undersøgelse **155**, 42–47.

Dawes, P.R. 2006: Explanatory notes to the Geological map of Greenland, 1:500 000, Thule, Sheet 5. Geological Survey of Denmark and Greenland Map Series **2**, 97 pp.

Koch, L. 1922: Note to maps of Melville Bay from Wilcox Point to Cape York and of North Greenland from 81°–83°35´N, 38°–56°W. Meddelelser om Grønland **64**(2), 77–88.

Koch, L. 1928: Contributions to the glaciology of North Greenland. Meddelelser om Grønland **65**(2), 183–464.

Koch, L. 1932: Map of North Greenland, scale 1:300,000. Copenhagen: Geodetic Institute, 19 sheets.

Kollmeyer, R.C. 1980: West Greenland outlet glaciers: an inventory of the major iceberg producers. Cold Regions Science and Technology **1**, 175–181.

Mock, S.J. 1966: Fluctuations of the terminus of the Harald Moltke Bræ, Greenland. Journal of Glaciology **6**(45), 369–373.

MODIS 2009: MODIS studies of Greenland. Moderate Resolution Imagery Spectroradiometer, NASA and Byrd Polar Research Center, http//bprc.osu.edu/MODIS/?p=61.

Peary, R.E. 1892: The North Greenland Expedition of 1891–92. Journal of American Geographical Society **24**, 536–558.

Rignot, E. & Kanagaratnam, P. 2006: Changes in the velocity structure of the Greenland ice sheet. Science **311**, 986–990.

Weidick, A. 1994: Satellite image atlas of glaciers of the world. Greenland. United States Geological Survey Professional Paper **1386–C**, 141 pp.

Weidick, A. 2009: Johan Dahl Land, south Greenland: the end of a 20th century glacier expansion. Polar Record **45**(235), 337–350.

Weidick, A. & Bennike, O. 2007: Glaciation history and glaciology of Jakobshavn Isbræ and the Disko Bugt region, West Greenland: a review. Geological Survey of Denmark and Greenland Bulletin **14**, 78 pp.

Zhou, G. & Jezek, K. 2003: DISP yearly satellite photographic mosaics of Greenland 1962–1963. National Snow and Ice Data Center, Boulder, Colorado. Digital media.

Authors' address

Geological Survey of Denmark and Greenland, Øster Voldgade 10, DK-1350 Copenhagen K, Denmark. E-mail: *prd@geus.dk*

Bathymetry, shallow seismic profiling and sediment coring in Sermilik near Helheimgletscher, South-East Greenland

Camilla Snowman Andresen, Niels Nørgaard-Pedersen, Jørn Bo Jensen and Birger Larsen

The Greenland ice sheet is one of the most significant contributors to the rising global sea level with a contribution of 0.5 mm per year (Rignot & Kanagaratnam 2006). Evidence is emerging that rising temperatures of subsurface ocean currents play a vital role in the recent acceleration of large fast flowing glaciers such as Jakobshavn Isbræ in West Greenland (Holland *et al.* 2008) and Helheimgletscher in South-East Greenland (Straneo *et al.* 2010). Important questions are whether these incursions of warmer water are part of a recurrent phenomenon and indeed exactly how they influence the glaciers. The Geocenter Denmark project SEDIMICE (Linking sediments with ice-sheet response and glacier retreat in Greenland) investigates past ice fluctuations in the Helheimgletscher region in South-East Greenland with regard to magnitude, possible causes and effects. One of the main tasks in this project is to analyse sedimentary deposits in the main fjord Sermilik (Fig. 1), which is influenced by the tidally affected Helheimgletscher that has a short floating tongue. By combining sediment studies with modern climate studies we aim to extrapolate meteorological data back in time.

In August 2009 the Geological Survey of Denmark and Greenland collected short sediment cores in Sermilik near Tasiilaq (Fig. 1). To select core sites and to understand the sedimentary processes, we also acquired data on the bathymetry and conducted shallow seismic profiling. This paper presents some results of the seismic survey, preliminary sediment core data and bathymetrical data from the fjord. Apart from a few isolated depth values, the bathymetry of Sermilik was unknown before the 2009 survey.

Setting

Sermilik is about 80 km long and 7–13 km wide. The terrain around the fjord is alpine with elevations of 300–600 m near the coast and up to 1000 m inland. Frequent glacial and geologically controlled fissure valleys dissect the area in a criss-cross pattern. The northern end of Sermilik branches into three fjords with calving glaciers. The westernmost – Helheimgletscher – is a fast flowing glacier and the third most prolific iceberg producer in Greenland (Rignot & Kanagaratnam 2006).

The climate of the region is low arctic and the weather conditions are influenced by lows moving north along the coast. The fjord is covered by sea ice from December to May. The hydrographic conditions in the fjord are influenced by a 10–20 m thick layer of glacial water, underlain by 100–150 m of

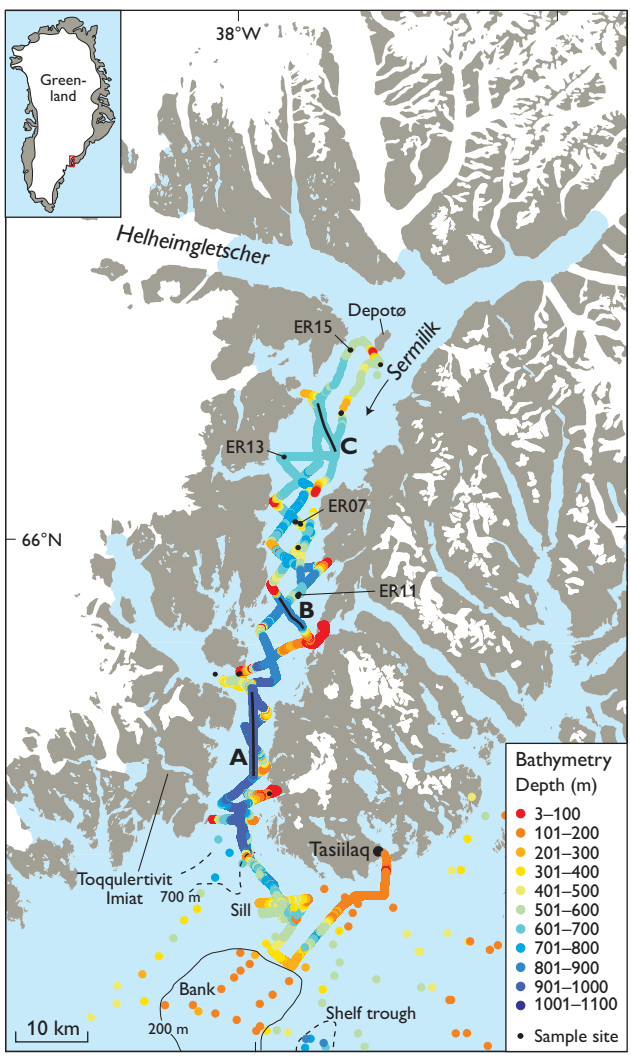

Fig. 1. Study area and bathymetrical data from Sermilik based on data collected in 2009. Depth data on the shelf south of the fjord mouth are from Clausen (1998) and this survey. The positions of the seismic lines A, B and C are indicated by black lines and sediment core sample sites are shown.

polar water. Below the polar water towards the bottom warmer Atlantic water of subtropical origin with temperatures of 3.5–4°C is found (Straneo *et al.* 2010). The inflow of warmer waters into Sermilik takes place via deep troughs in the shelf.

Glacial history of the region

A study from the Toqqulertivit Imiat valley (Fig. 1) shows that a glacier flowed through this valley and most likely coalesced with a glacier flowing south in Sermilik and out over the continental shelf during the Last Glacial Maximum (Roberts *et al.* 2008). Exposure ages of 11.8–9.9 ka (kilo-annum, 10^3 years BP) from bedrock surfaces at high elevations (683–740 m a.s.l.) provide minimum ages for the last deglaciation (Roberts *et al.* 2008). These ages from Toqqulertivit Imiat support the 'maximum' model of a large Last Glacial Maximum ice sheet extending to the shelf break in South-East Greenland (Stein *et al.* 1996; Kuijpers *et al.* 2003). Evidence from the shelf south of Sermilik indicates that the ice margin retreated to the inner shelf around 15.7–14.6 calibrated (cal.) ka (Kuijpers *et al.* 2003). In the Kangerlussuaq region farther north the ice-sheet margin retreated from the outer shelf around 15.5 cal. ka and reached the present outer coast around 13.6–10 cal. ka (Jennings *et al.* 2006). This is in accordance with surface exposure ages from lower Toqqulertivit Imiat indicating that ice retreated to the mouth of Sermilik between 11.1 and 9.7 ka (Roberts *et al.* 2008). These data are further supported by a minimum age of 11 cal. ka for the formation of the local marine limit (at 69 m) and thereby local ice retreat near Tasiilaq (Long *et al.* 2008).

Methods

We used the locally hired motor boats *Erik den Røde* and *Puite* for the work. An Innomar SES-2000 Medium sub-bottom echo sounder from Innomar Tecnologies, Rostock, Germany, was used for bathymetrical and sub-bottom sediment profiling. This parametric device is designed for water depths down to about 2000 m and has the ability to resolve sediment layers a few decimetres thick and penetrate down to about 50 m below the sea floor. The transducer was mounted on a vertical steel tube attached to the side of the boat and a motion sensor was used to compensate for movements of the boat. Additional bathymetrical data were recorded in the inner fjord from the echo sounder of *Erik den Røde* during the sediment coring cruise. Comparisons of depth recordings obtained by the two methods showed that the results are compatible to within a few metres. Sediment coring was performed with a Rumohr lot corer with up to 1.5 m long core liners.

Bathymetrical data from Sermilik

The southern part of Sermilik Fjord is an up to 920 m deep and flat basin (Fig. 1). The bathymetry of the fjord mouth can be described as terminating into a SE-directed trough and a SW-directed trough separated by a broad bank with water depths of less than 200 m. The bathymetry of the SW-directed trough is very uncertain. The shallowest part of the SE-directed trough forms a *c.* 550 m deep sill between the deep fjord and the 800–900 m deep trough that stretches the entire shelf towards the Irmiger Sea.

The deep fjord basin extends up to 40 km northward from the fjord entrance into the middle part of Sermilik where several bathymetrical highs (400–550 m) narrow the connection to the northern part of the fjord. Towards the northern part of Sermilik, the basin floor rises steadily to a depth of about 600–650 m just south of Depotø. The fjord bottom in the inner part is more irregular with channel systems more than 100 m wide and up to 20 m deep. During the survey we could not measure water depths in the inner east–west-trending fjord arm leading up to Helheimgletscher due to semi-permanent sea ice extending tens of kilometres

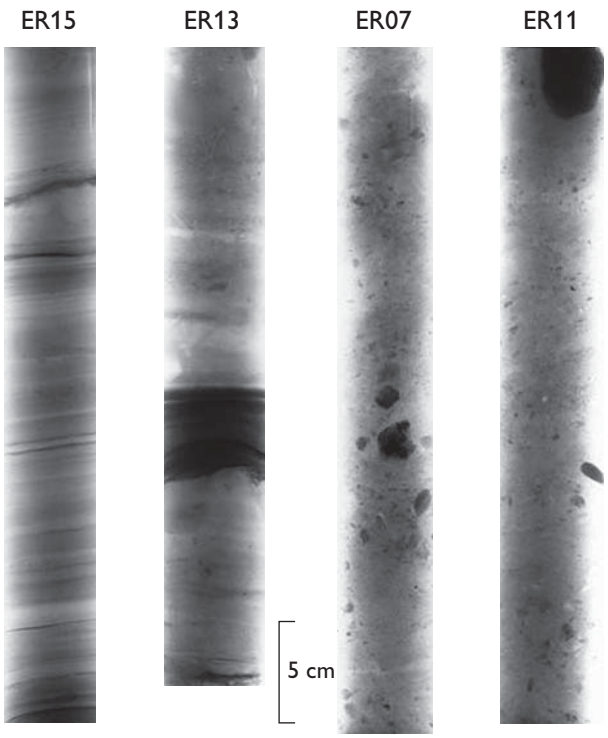

Fig. 2. Selected examples of X-ray radiographs from core ER15 (600 m water depth), ER13 (660 m water depth), ER07 (525 m water depth) and ER11 (600 m water depth) that document different sedimentation regimes. Note the dark sand layer in core ER13 with a lower erosive boundary; this unit is interpreted to be a turbidite. Core sites are shown in Fig.1.

from the Helheimgletscher calving front. However, according to the skipper of *Erik den Røde* (Sigurdur Petursson), water depths up to 800 m are found north-west of Depotø.

Sediment cores

Altogether 19 cores with lengths ranging from 30 to 150 cm were retrieved during the sediment coring cruise. The full sediment core data (sedimentology, geochemistry and chronology) will be presented elsewhere. However, preliminary inspection of cores ER07, ER11, ER13 and ER15 documents the variable sediment regimes that characterise the fjord (Figs 1, 2), and X-ray radiography of the cores show diamicton facies, laminated mud facies and sand layers with erosive lower boundaries. These lithofacies are similar to lithofacies described from sediment cores from Kangerlussuaq (Smith & Andrews 2000) and Scoresby Sund (Dowdeswell *et al.* 1994; Ó Cofaigh & Dowdeswell 2001). For example, core ER15 consists of laminated mud with variable content of pebbles, which is interpreted as ice-proximal glaciomarine sediments mainly deposited by suspension settling from turbid overflow plumes and turbidity currents and occasional iceberg rafting. In contrast, cores ER07 and ER11 are characterised by massive diamicton facies with abundant pebbles, which is interpreted as the result of iceberg rafting. Core ER13 has a unit of diamicton facies above a unit of laminated mud facies. This may reflect an environmental change from a long-lasting sea-ice cover in the fjord prohibiting iceberg passage to a period with increased passage and melting of icebergs. As also suggested by Jennings & Weiner (1996) variable inflow of Atlantic water may influence the melting and traversing of icebergs.

^{210}Pb dating of the upper decimetres of the cores show sedimentation rates >1 cm/yr in ER15, 0.4 cm/yr in ER13 and 0.2 cm/yr in ER11. The decreasing sedimentation rates with increasing distance to the present front of the calving glaciers reflect the decreasing influence from meltwater plume sedimentation.

Seismic profiles

The seismic profile (Fig. 3A) shows an outer flat, deep basin in Sermilik with an upper 4–6 m thick, transparent seismic unit overlying a well-stratified section (>15 m thick) that is characterised by strong, continuous, parallel reflectors. There is no distinct boundary between the two seismic units, as weak, discontinuous, parallel reflectors characterise the uppermost *c.* 2 m of the stratified section. On vertically extremely exaggerated sections, wide lenticular units and stratigraphical onlap structures are visible in some parts of the lower seismic unit. To the north, the transparent upper unit disappears and well-stratified sediments, with some channel features, dominate the seismic profiles (Fig. 3B). The profiles of the bathymetrical highs in the middle part of the fjord are dominated by overlapping diffraction hyperbolae. The inner, shallower part of the fjord is characterised by large channel and levee structures, and broad flank units showing well-stratified sediments in the north-western part of the seismic survey area (Fig. 3C).

Formation of fjord-bottom sediment structures

The sediment unit with a transparent pattern in the outer fjord basin indicates a uniform lithology that possibly origi-

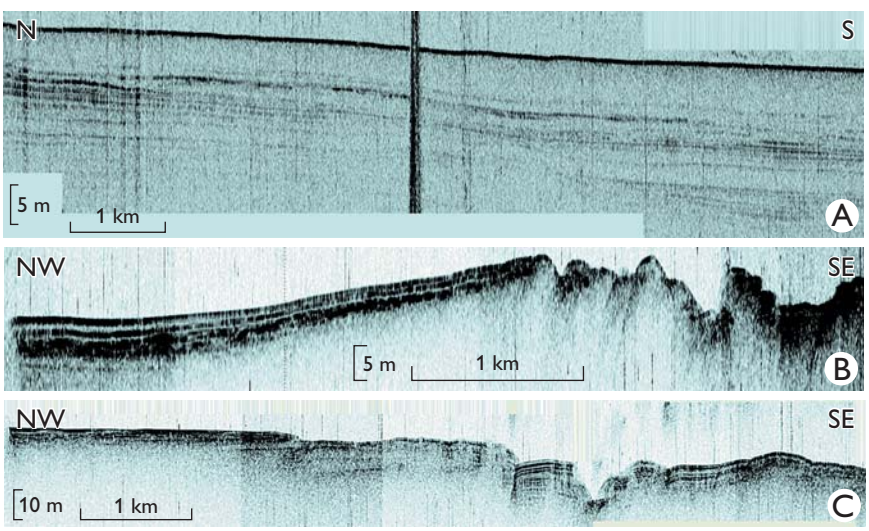

Fig. 3. Representative seismic sections that illustrate different structures in different parts of Sermilik (see text for description and Fig. 1 for location).

nates from suspension sedimentation (meltwater plumes) and ice-rafting during the main part of the Holocene (Fig. 3A). The lower stratified section is interpreted as glaciomarine sediments consisting of turbidites and mass-transport deposits interbedded with suspension-deposited sediments. The lower unit was possibly deposited during the final deglaciation of the main part of Sermilik at about 10 ka (cf. Roberts *et al.* 2008). Turbidite sedimentation typically creates very flat fjord basins with reflectors onlapping basin margins and structural highs. It is possible that the structural highs in the middle part of Sermilik could serve as anchor points for the retreating glacier, causing a stagnation of the fjord glacier front during the last deglaciation.

The inner basin with its apparent active channel and levee sedimentation and over-all fill geometry (Fig. 3C) can be characterised as a progradational–aggradational wedge of sediments with possibly very high sedimentation rates from turbidites and mass flows, as well as plume sedimentation. It is an open question whether the channel systems are directly fed by the Helheimgletscher source, or whether bedrock thresholds in the innermost fjord system prohibit bed transport of glaciogenic sediments. If a deeper sub-basin exists north of Depotø, we can only explain the seismic signature and large channel-levee systems of the inner basin by a very advanced position of Helheimgletscher to near Depotø during the late Holocene. Hopefully, future exposure ages from the land terrain near Depotø by our collaborators can show if the front of Helheimgletscher had a standstill near Depotø during the Little Ice Age.

In conclusion, the seismic survey has revealed a rather complex pattern of sub-bottom sediment structures (down to 50 m) in Sermilik reflecting the early Holocene retreat of Helheimgletscher, probably followed by a Holocene ice advance – perhaps during the Little Ice Age. Preliminary results from analyses of the sediment cores support the interpretation that the glaciomarine sediments in Sermilik is related to settling from meltwater plumes and iceberg rafting. Knowledge of the sediment depositional regime on the fjord bottom from seismic investigations is highly relevant for retrieval of sediment cores suitable for Holocene palaeoclimatic reconstructions. We hope to collect more and longer sediment cores in the fjord in coming years.

Acknowledgements

Geocenter Denmark is thanked for financial support. We would also like to thank our two skippers Bendt Josvassen of M/V *Puite* and Sigurdur Petursson of M/V *Erik den Røde*. Rineke Gieles at the Royal Netherlands Institute for Sea Research is thanked for X-ray radiography of sediment cores.

References

Clausen, L. 1998: The Southeast Greenland glaciated margin: 3D stratal architecture of shelf and deep sea. Geological Society Special Publications (London) **129**, 173–203.

Dowdeswell, J.A., Whittington, R.J. & Marienfeld, P. 1994: The origin of massive diamicton facies by iceberg rafting and scouring, Scoresby Sund, East Greenland. Sedimentology **41**, 21–35.

Holland, D.M., Thomas, R.H., de Young, B., Ribergaard, M. H. & Lyberth, B. 2008: Acceleration of Jakobshavn Isbræ triggered by warm subsurface ocean waters. Nature Geoscience **1**, 659–664.

Jennings, A.E. & Weiner, N.J. 1996: Environmental change in eastern Greenland during the last 1300 years: evidence from foraminifera and lithofacies in Nansen Fjord, 68°N. The Holocene **6**, 179–191.

Jennings, A.E., Hald, M., Smith, M. & Andrews, J.T. 2006: Freshwater forcing from the Greenland Ice Sheet during the Younger Dryas: evidence from southeastern Greenland shelf cores. Quaternary Science Reviews **25**, 282–298.

Kuijpers, A., Troelstra, S.R., Prins, M.A., Linthout, K., Akhmetzhanov, A., Bouryak, S., Bachmann, M.F., Lassen, S., Rasmussen, S. & Jensen, J.B. 2003: Late Quaternary sedimentary processes and ocean circulation changes at the southeast Greenland margin. Marine Geology **195**, 109–129.

Long, A.J., Roberts, D.H., Simpson, M.J.R., Dawson, S., Milne, G.A. & Huybrechts, P. 2008: Late Weichselian relative sea-level changes and ice sheet history in southeast Greenland. Earth and Planetary Science Letters **272**, 8–18.

Ó Cofaigh, C. & Dowdeswell, J.A. 2001: Laminated sediments in glacimarine environments: diagnostic criteria for their interpretation. Quaternary Science reviews **20**, 1411–1436.

Rignot, E. & Kanagaratnam, P. 2006: Changes in the velocity structure of the Greenland Ice Sheet. Science **311**, 986–990.

Roberts, D.H., Long, A.J., Schnabel, C., Freeman, S.P.H.T. & Simpson, M.J.R. 2008: The deglacial history of southeast sector of the Greenland Ice Sheet during the Last Glacial Maximum. Quaternary Science Reviews **27**, 1505–1516.

Smith, L.M. & Andrews, J.T. 2000: Sediment characteristics in iceberg dominated fjords, Kangerlussuaq region, East Greenland. Sedimentary Geology **130**, 11–25.

Stein, R., Nam, S.I., Grobe, H. & Hubberten, H. 1996: Late Quaternary glacial history and short-term ice-rafted debris fluctuations along the East Greenland continental margin. In: Andrews, J.T. *et al.* (eds): Late Quaternary paleoceanography of the North Atlantic margins. Geological Society Special Publications (London) **111**, 135–151.

Straneo, F., Hamilton, G.S., Sutherland, D.A., Stearns, L.A., Davidson, F., Hammill, M.O., Stenson, G.B. & Rosing-Asvid, A. 2010: Rapid circulation of warm subtropical waters in a major glacial fjord in East Greenland. Nature Geoscience **3**, 182–186.

Authors' address

Geological Survey of Denmark and Greenland, Øster Voldgade 10, DK-1350 Copenhagen K, Denmark. E-mail: *csa@geus.dk*

Borax – an alternative to mercury for gold extraction by small-scale miners: introducing the method in Tanzania

Peter W.U. Appel and Jesper Bosse Jønsson

Small-scale mining is extraction of metals, precious stones, industrial minerals and other commodities using simple technologies. At a worldwide scale, an estimated 100 million people depend on income from small-scale mining (Hinton 2006). In Tanzania, there are more than half a million active small-scale miners, most of whom extract gold from placer and hard-rock deposits. Apart from providing a livelihood for thousands of households, small-scale mining reduces migration from rural to urban areas. However, small-scale mining is associated with a number of negative effects, because mining activities have severe impacts on both the local environment and the miners' health. Most significantly the widespread use of mercury for gold extraction results in polluted environments and serious health hazards for the miners themselves and for the population in the vicinity of small-scale gold mining settlements (Bose-O'Reilly *et al.* 2008a, b; 2010; Jønsson *et al*. 2009).

Large amounts of mercury are transferred to the environment from small-scale gold mining activities in Tanzania (Taylor *et al*. 2005). The mercury remains in the environment and constitutes a severe health hazard, also for generations to come. Thus, it is of paramount importance to reduce or, even better, stop the release of mercury from small-scale gold mining. A number of alternative methods have been suggested and tested with limited degrees of success (Hilson & van der Horst 2002). In 2009 Geocenter Denmark financed a project to test the feasibility of using borax as a replacement for mercury in small-scale gold extraction in Tanzania.

Gold extraction

Small-scale gold mining of rock deposits in Tanzania is done by sinking shafts and digging tunnels along gold reefs. The mined ore is crushed to walnut size manually or using a jaw crusher and ground in metal drums with hard steel balls or rods, the so-called ball mills. The pulverised material is flushed down a water channel, the bottom of which is covered by a piece of cloth. The heavy particles are caught in the cloth and the light particles end as tailings. This is called sluicing. The heavy fraction from the cloth is treated with mercury (Fig. 1). The gold particles amalgamate with mercury and can thus be separated from other heavy minerals. The amalgam is placed in a small iron cup over a fire, the mercury evaporates and the gold is left behind. This gold extraction method is not efficient, so the tailings from sluicing and amalgamation are reprocessed up to ten times in order to recover more gold. The amalgamation method is easy to learn and swift. However, as mentioned above, the method causes serious environmental and health problems and is not particularly efficient with respect to gold recovery.

Fig. 1. About 100 g of mercury are added to about 5 kg of concentrate from the sluicing.

Mercury toxicity

During amalgamation the metallic mercury evaporates. Some of the vapour is inhaled by people working in the vicinity and may over time cause irreparable damage to their brains. The rest of the mercury vapour gradually precipitates on the ground and enters the drainage system, where it is transformed to methylated mercury by bacteria. Methylated mercury is water soluble and enters the food chain causing serious damage to humans who are at the top of the food chain. Methylated mercury is extremely harmful to the central nervous system, where it causes tremors, difficulty in walking, tunnel vision, psychological problems and eventually death. There is no cure for permanent mercury poisoning (Clarkson *et al.* 2003).

Unborn babies are especially prone to damage from methylated mercury. If a pregnant mother has mercury in her body, the foetus 'sucks' mercury from her. The nervous system of the foetus is much more sensitive to mercury than that of an adult. A mother with even a low concentration of mercury in her body thus has a high risk of giving birth to mentally or physically disabled children (Davidson *et al.* 1998).

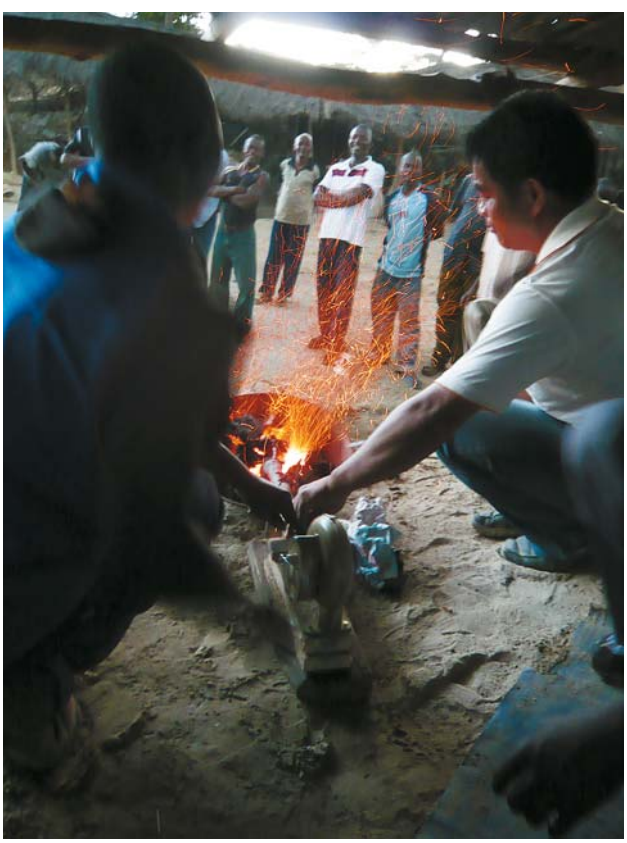

Fig. 2. Vigorous burning of charcoal is achieved with a hand-powered blower.

Gold extraction with borax

The use of chemical borax, also known as sodium borate**,** appears to be one of the more viable ways that have been proposed to reduce or stop the use of mercury by small-scale miners (Spiegel & Veiga 2010). Borax is used for cleaning purposes and is therefore commonly available. The reason for using borax in the smelting process of ore material is that borax reduces the melting point of metals and minerals. Under normal field circumstances small-scale miners cannot smelt gold, as they cannot create the high temperature required to smelt the ore. By adding borax to their concentrate, however, they can extract and smelt their gold.

Gold purchasers already use borax to purify gold with a high content of mercury; however, the method has only recently been applied by small-scale miners. In the Benguet area of the northern Philippines, around 15 000 small-scale gold miners currently mix their gold concentrate with borax, followed by heating and smelting (Leoncio Na-Oy, personal communication 2010). As a consequence, the mercury usage in the area is minimal and the gold recovery rate quite impressive.

The process works as follows: the gold ore is crushed, ground and concentrated as in the case of mercury-based extraction. However, the final product needs to have a very high gold concentration, above 90%, for the borax method to work. This requires skill, practise, and not least time. During testing of the borax method in Tanzania, two ways of smelting gold were applied. The first one involved using charcoal and a blower, the second one the use of acetylene gas.

Charcoal and blower. The gold concentrate is mixed with borax and placed in a plastic bag in a small ceramic bowl filled

Fig. 3. Molten gold in the centre of the glowing clay bowl and charcoal.

Fig. 4. Gold smelting in borax with an acetylene burner.

with charcoal and some borax, with the recommended ratio between gold concentrate and borax being 1 to 3. The charcoal is ignited and vigorous burning is achieved by using a hand-powered blower (Fig. 2). After about 30 minutes the metals and minerals in the concentrate begin to smelt and small drops of gold coalesce at the bottom of the bowl (Fig. 3) and can be picked up with the tip of a knife. The advantage of the blower is that it is inexpensive; the disadvantage is that it takes up to half an hour to smelt the gold.

Acetylene gas. The gold concentrate is mixed with borax and placed in a small plastic bag in a ceramic bowl lined with borax. The gold concentrate–borax mixture is melted with the gas flame and after about 10 minutes the gold melts and coalesces (Fig. 4). The advantage of using acetylene gas is that the miners get their gold fast; the disadvantage is that acetylene is expensive and that the gas bottles are heavy to transport.

What does it take for the miners to accept the borax method?

Changing a well-established habit is difficult and requires very good reasons. The habit of using mercury for gold extraction is clearly such a case, because the mercury method is easy to learn and carry out. Obviously, this makes the introduction of a new and healthier method a challenge, especially because the borax method requires skill and patience. Depending on the skills of the person who prepares the concentrates, the borax method may take between half an hour and an hour longer than the mercury method.

The immediate advantage of using borax is that it does not harm the environment or the people within or close to the mining sites, in the quantities necessary for gold extraction. In addition, borax is cheaper than mercury and produces purer gold than that produced with mercury (Fig. 5). As small-scale miners are often paid according to the gold content in their gold, the gold produced with borax is likely to provide a better price. However, the question still remains whether these advantages are sufficient to make small-scale gold miners swap from mercury to borax. Considering the embedded culture of using mercury, a change from mercury to borax extraction is not likely to come easy. An additional incentive for the miners to convert to the borax method may be needed.

The Geocenter Denmark project that was conducted in two small-scale mining communities in Tanzania in May 2009 demonstrated that abandoned tailings from small-scale gold mining may contain a very high gold content, with up to 100 ppm of gold. The average gold grade in the ore mined by the small-scale miners is in the order of 3 to 50 ppm. It was a puzzle how the miners could loose so much gold in spite of repeated processing. The techniques used by small-scale miners are not sophisticated and in general it is believed that around 50% of the gold is lost. Nevertheless, tailings with up to 100 ppm gold require an explanation.

When small-scale miners treat their concentrate with mercury, they do not recover all the mercury which instead ends up in the tailings. Miners know that they are incapable of recovering all the gold in one go and therefore reprocess the tailings in the ball mills, where the mercury becomes pounded to an extent where it looses its ability to coalesce; it turns into what may be termed mercury flour. This flour cannot easily be recovered, which also goes for the gold amalgamated with it. As a result, all the mercury–gold flour is lost to the tailing dumps. Awareness by the miners that they lose substantial quantities of gold and income as a result of

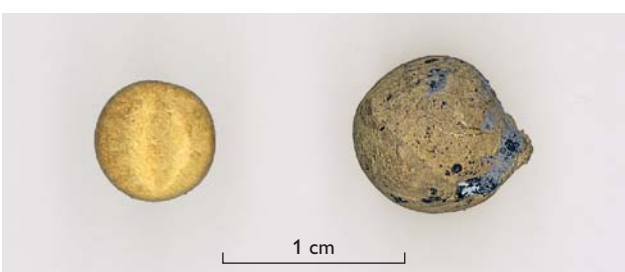

Fig. 5. Gold extracted by borax (left) is pure, whereas gold extracted by mercury (right) contains up to 10% mercury giving it a paler colour.

the mercury technique could be what is needed to facilitate a shift from mercury-based to borax-based gold extraction.

Lessons learned in rural Tanzania

The borax method was tested and demonstrated in the two small-scale gold-mining communities Londoni and Itumbi in Tanzania. The tests were carried out by a small-scale miner from the Philippines, who uses the borax method on a daily basis. In Londoni, a demonstration using charcoal and a blower proved successful and produced a gold tablet of 2.4 grams with a high purity. In Itumbi, the test was carried out by using acetylene gas. The test was successful, a tablet of 3 grams was produced, and the project demonstrated that the method is feasible for small-scale gold miners.

The small-scale miners from Itumbi, a permanent and well-established community, seemed more keen to learn about the mercury-free method than those from Londoni, which is a gold-rush settlement, where most residents come from elsewhere. After the demonstration in Itumbi, the miners expressed their opinion about the method at a small workshop. On the one hand, most miners recognised the potential of using the borax method, as it would significantly reduce mercury usage and improve the purity of their gold. On the other hand, they mentioned the high price of acetylene gas, the fact that borax is not readily available in the region (this is true and ways of making borax available in that part of the country are needed), the longer time required for preparing the concentrate, and the fact that many miners need to process small quantities of gold (e.g. 0.3 gram) on a daily basis to get food on the table, and that the borax method seemed a bit too advanced for such small quantities. Finally, they requested additional instruction and demonstrations in which they could take part before they would be prepared to adopt the new method.

Conclusions

The borax method was received with interest in both small-scale gold-mining communities, but the attitude was more positive in the more permanent settlement of Itumbi where people are more concerned about the environment. The following points must be taken into account before borax has a chance of replacing mercury: (1) Locally produced, inexpensive blowers or acetylene gas must be easily available, as well as access to the necessary expertise, (2) borax must be readily available, (3) a substantial training programme has to be carried out, (4) a link must be established between the small-scale miners and advisers, preferably the local mining authorities, who can guide the miners when technical problems occur and (5) small-scale miners need to understand the link between the borax method and a higher gold recovery rate.

Acknowledgements

The authors would like to thank the small-scale miners who participated in the testing of the borax method. Financial assistance for the research was provided by Geocenter Denmark.

References

Bose-O'Reilly, S., Lettmeier, B., Gothe, R.M., Beinhoff, C., Siebert, U. & Drasch, G. 2008a: Mercury as a serious health hazard for children in gold mining areas. Environmental Research **107**, 89–97.

Bose-O'Reilly, S., Lettmeier, B., Roider, G., Siebert, U. & Drasch, G. 2008b: Mercury in breast milk – a health hazard for infants in gold mining areas? International Journal of Hygiene and Environmental Health **211**, 615–623.

Bose-O'Reilly, S., Drasch, G., Beinhoff, C., Tesha, A., Drasch, K., Roider, G., Taylor, H., Appleton, D. & Siebert, U. 2010: Health assessment of artisanal gold miners in Tanzania. Science of the Total Environment **408**, 796–805.

Clarkson, T.W., Magos, L. & Myers, G.J. 2003: The toxicology of mercury – current exposures and clinical manifestations. New England Journal of Medicine **349**, 1731–1737.

Davidson, P.W. *et al*. 1998: Effects of prenatal and postnatal methylmercury exposure from fish consumption on neurodevelopment: outcomes at 66 months of age in the Seychelles child development study. Journal of American Medical Association **280**, 701–707.

Hilson, G. & van der Horst, R. 2002: Technology, managerial, and policy initiatives for improving environmental performance in small-scale gold mining industry. Environmental Management **30**, 764–777.

Hinton, J.J. 2006: Communities and small scale mining: an integrated review for development planning, 413 pp. Washington: World Bank Group.

Jønsson, J.B., Appel, P.W.U. & Chibunda, R. 2009: A matter of approach: the retort's potential to reduce mercury consumption within small-scale gold mining settlements in Tanzania. Journal of Cleaner Production **17**, 77–86.

Spiegel, S.J. & Veiga, M.M. 2010: International guidelines on mercury management in small-scale gold mining. Journal of Cleaner Production **18**, 375–385.

Taylor, H., Appleton, J.D., Lister, R., Smith, B., Chitamweba, D., Mkumbo, O., Machiwa, J.F., Tesha, A.L. & Beinhoff, C. 2005: Environmental assessment of mercury contamination from the Rwamagasa artisanal gold mining centre, Geita District, Tanzania. The Science of the Total Environment **343**, 111–133.

Authors' addresses

P.W.U.A., *Geological Survey of Denmark and Greenland, Øster Voldgade 10, DK-1350 Copenhagen K, Denmark*. E-mail: *pa@geus.dk*

J.B.J., *Department of Geography and Geology, University of Copenhagen, Øster Voldgade 10, DK-1350 Copenhagen K, Denmark*.

Vietnamese sedimentary basins: geological evolution and petroleum potential

Michael B.W. Fyhn, Henrik I. Petersen, Anders Mathiesen, Lars H. Nielsen, Stig A.S. Pedersen, Sofie Lindström, Jørgen A. Bojesen-Koefoed, Ioannis Abatzis and Lars O. Boldreel

A number of sedimentary basins of various ages are located on- and offshore Vietnam (Fig. 1). Some of them have significant petroleum resources and have thus attracted interest from industry and academia (Rangin *et al.* 1995; Matthews *et al.* 1997; Lee & Watkins 1998; Lee *et al.* 2001). Moreover, Vietnam is located in a position central to the understanding of the geological development of South-East Asia (Hall & Morley 2004). The structural style and the stratigraphy of the Vietnamese basins thus provide a valuable record about the development of South-East Asia throughout the Phanerozoic and the subsequent Eocene as well as younger deformation associated with the collision and indentation of India into Eurasia and the opening of the South China Sea (Fyhn *et al.* 2009a, 2010a).

The Geological Survey of Denmark and Greenland has worked in Vietnam since 1995 to assess the geology and petroleum potential of the Vietnamese basins. Since 2002 the work has been carried out in cooperation with the Department of Geography and Geology, University of Copenhagen, as part of the ENRECA project (Enhancement of Research Capacity in Developing Countries). An integrated part of the project is its training of Vietnamese MSc and PhD students incorporating both training courses at the Department of Geography and Geology and courses held in Vietnam. So far, 10 MSc and 4 PhD students have completed their training under the auspices of the ENRECA project and another 10 are expected to complete their education within the next phase of the project.

The ENRECA project has already completed two phases and a third and final phase has recently started. The initial phase focused on the Phu Khanh and the Song Hong Basins located in the South China Sea offshore north and central Vietnam and the smaller onshore Song Ba Trough (Fig. 1; Bojesen-Koefoed *et al.* 2005; Nielsen *et al.* 2007; Fyhn *et al.* 2009a, b, c). During the second ENRECA phase, completed in 2009, attention shifted towards the Malay – Tho Chu and Phu Quoc basins located in the Gulf of Thailand, SSW of Vietnam (Petersen *et al.* 2009, in press; Fyhn *et al.* 2010a, b). The Phu Quoc Basin continues onshore to the north to form part of the mountainous area between Vietnam and Cambodia. In the recently started third phase of the project, the focus remains on the Phu Quoc Basin in addition to a revisit to the Song Hong Basin on the north Vietnamese margin and onshore beneath the Song Hong (Red River) delta.

The Phu Quoc Basin

The Phu Quoc Basin stretches in a 100–150 km broad belt from the central part of the Gulf of Thailand *c.* 500 km northwards to central Cambodia. The basin is Late Jurassic to Cretaceous in age but is one of the least explored basins in the region and remains to be drilled offshore (Fyhn *et al.* 2010a). In order to assess the geological evolution and the petroleum potential of the basin, regional seismic analyses of the Vietnamese part of the basin were carried out in combination with drilling of the fully cored, 500 m deep ENRECA-2 well on the Phu Quoc island. Data from the ENRECA-2 well were complemented by data from outcrop studies on Phu Quoc and in Cambodia.

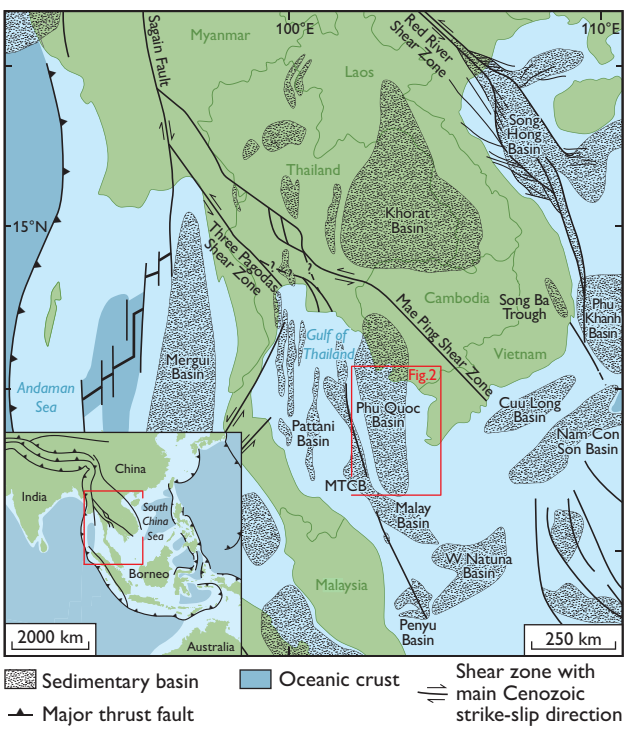

Fig. 1. Map of South-East Asia showing the locations of sedimentary basins and areas underlain by oceanic crust. Strike-slip arrows illustrate the prevailing Eocene–Recent offset directions. **MTCB**: Malay – Tho Chu Basin. The inset map shows a simplified structural outline of the region. Modified from Fyhn *et al.* (2010b).

Alluvial sandstones with an average of *c.* 10% rhyolite-dominated lithic fragments make up the greater part of the up to *c.* 4 km thick sediments filling the Phu Quoc Basin. Only a few, minor, shallow marine sandstone beds have been encountered in the terrestrially dominated succession. The sandstone-dominated succession is intercalated with subordinate alluvial plain and lacustrine silt- and mudstone intervals. Coal fragments are abundant at specific stratigraphic levels but do not contribute to any source potential.

The thicknesses of the deposits are not affected by syn-sedimentary faulting, but gradually increase towards the east, where a coeval, Jurassic–Cretaceous, magmatic arc parallels the eastern basin flank (Fig. 2). This is compatible with a retroarc–foreland basin setting associated with the growth of the magmatic arc located east of the basin that also served as a primary source of sediments for the basin. A distinct basin inversion is indicated by a prominent angular unconformity that caps the Mesozoic basin fill and is associated with spectacular thrust faulting and folding (Fig. 3). The structural complexity increases towards the deeply eroded and hitherto undescribed fold belts that confine the basin to the east and west. The stratigraphic level of erosion increases towards these orogenic belts. Palaeozoic and Lower Mesozoic igneous and sedimentary rocks therefore crop out on small islands and onshore, or subcrop towards the base of the Cenozoic within the Kampot Fold Belt flanking the basin to the east. The inversion unconformity is underlain by Lower Cretaceous deposits and overlain by Middle Eocene and younger deposits, which provide only modest information on the age of the orogenic event. In order to constrain the age of inversion more precisely, apatite fission track analysis (AFTA) was carried out on rock samples from the Kampot Fold Belt collected on islands and in mainland Vietnam. The AFTA samples demonstrate a distinct cooling event that affected the region during the period from Late Paleocene to Early Eocene (Fyhn *et al.* 2010a). The cooling corresponds to uplift and denudation of the area in response to the thrust faulting and basin inversion and thus confines the age of the orogenic event controlling the deformation.

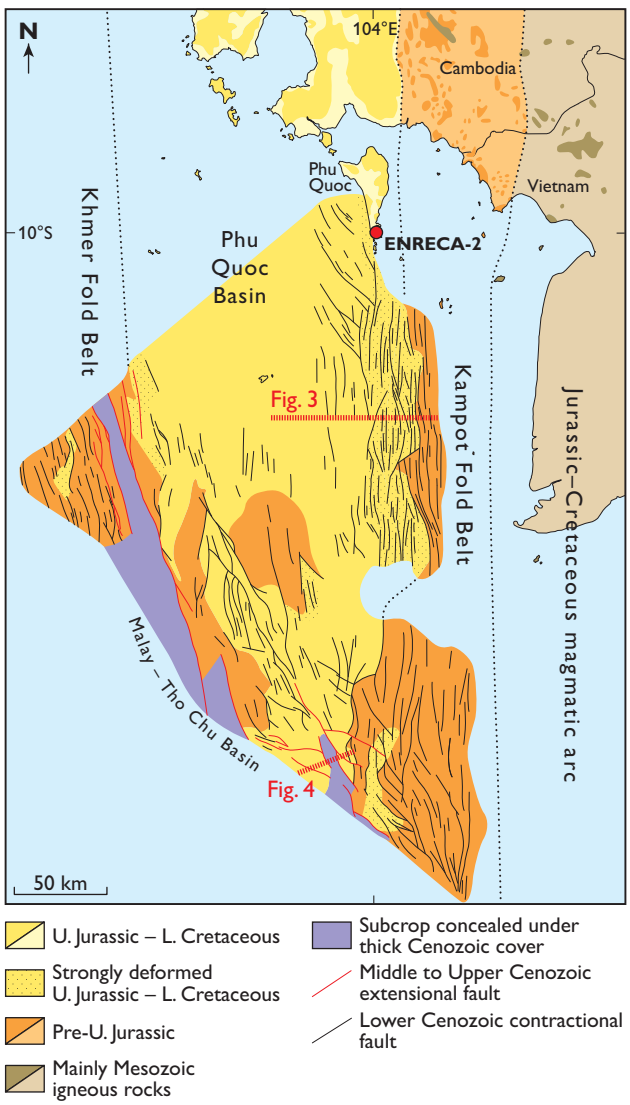

Fig. 2. Subcrop map towards the base Cenozoic top / Mesozoic unconformity outlining the southern part of the Phu Quoc Basin. Fold belts confine the basin to the east and west. Onshore pre-Quaternary outcrops are indicated, outlining the onshore continuation of the Phu Quoc Basin, the Kampot Fold Belt and the SE Indochina Jurassic–Cretaceous magmatic arc. For location see Fig. 1. Modified from Fyhn *et al.* (2010a).

The Malay – Tho Chu Basin

The Malay – Tho Chu Basin constitutes the Vietnamese north-eastern part of the Malay Basin that was initiated somewhere between the Middle and Late Eocene (Fyhn *et al.* 2010b). The Malay – Tho Chu Basin is situated in the central part of the Gulf of Thailand and is therefore superimposed on the southernmost part of the Phu Quoc Basin. Rifting in the area took place between Middle?–Late Eocene and Oligocene time and resulted in the creation of a series of deep grabens filled by continental to shallow marine deposits (Fig. 4; Fyhn *et al.* 2010b). A set of NNW-trending rifts are the dominating structures in the area; they are often distinguished from other, WNW-trending rifts by their downwards steepening, their great depth and their linearity. The NNW-trending rifts seem to have accommodated left-lateral transtension. Large-scale Eocene–Oligocene rifting associated with strike-slip faulting in the region is viewed as a response to the Indian–Eurasian collision that forced the neighbouring parts of South-East Asia away from the collision zone through a series of lateral shear zones (e.g. Tapponnier *et al.* 1986; Fyhn *et al.* 2009a, 2010b), although

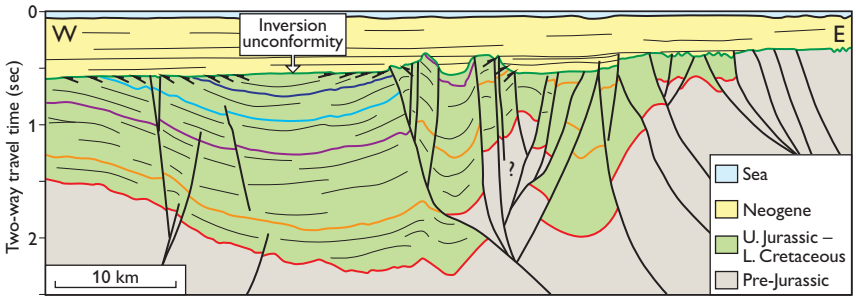

Fig. 3. Offshore stratigraphic profile across the Phu Quoc Basin. Jurassic–Cretaceous subsidence was most intense simultaneous with the magmatic arc developing to the east. A prominent inversion unconformity separates the Mesozoic thrust-faulted strata from the truncating unconformity of the base of the Neogene deposits. Modified from Fyhn *et al.* (2010a).

other theories exist (Morley 2002; Hall & Morley 2004; Watkinson *et al.* 2008; Hall 2009). Around the onset of the Miocene, rifting declined and thermal sagging came to dominate throughout the Neogene. This resulted in broadening of the subsiding area and increasing marine influence. Deltaic and shallow marine siliciclastics therefore prevail in the Neogene succession of the basin.

Petroleum exploration in the Malay – Tho Chu Basin began during the early 1970s, encouraged by successful exploration immediately south of Vietnamese territory. The first well was drilled in 1994. Since then, significant gas, condensate and oil discoveries have been made in several wells drilled in this basin, but only a few discoveries are as yet considered commercial. A re-evaluation of the existing exploration strategies is therefore desirable in order to optimise and focus future exploration. Exploration has mainly aimed at Early to Middle Miocene fluviodeltaic sand reservoirs with Late Neogene structural trapping mechanisms. Potential source rocks have been interpreted as alginite-bearing lacustrine shales and humic coals situated in the Palaeogene synrift and in the lowermost post-rift sections.

The few potential source-rock levels penetrated by wells have shown remarkably low vitrinite reflectance (VR) values compared to VR values obtained from overlying Neogene coals (data presented in Petersen *et al.* 2009). The maturity trends of such VR data sets are not well constrained as they produce suspiciously low thermal maturity gradients. However, suppressed VR values may occur in algenite-rich rocks. VR suppression is therefore particularly common in lacustrine shales with high HI (hydrogen index) values. The fluorescence alteration of multiple macerals (FAMM) technique is an accurate method to determine thermal maturity in rocks including those containing vitrinite with suppressed and enhanced VR values (Willkins *et al.* 1992). By combining conventional VR measurements and the FAMM technique a revised, higher and more reliable thermal maturity gradient has been established (Petersen *et al.* 2009). 2-D modelling of the maturation history of the basin was carried out based on the revised thermal maturity gradient, detailed seismic mapping, borehole information and new custom kinetics for petroleum generation; the latter was determined from lacustrine source rock samples and a terrestrially influenced mudstone collected from wells (Petersen *et al.* in press).

Maturation modelling indicates that most of the syn-rift succession in the Vietnamese Malay Basin is located in, or has passed through, the main oil and gas windows. Carbonaceous

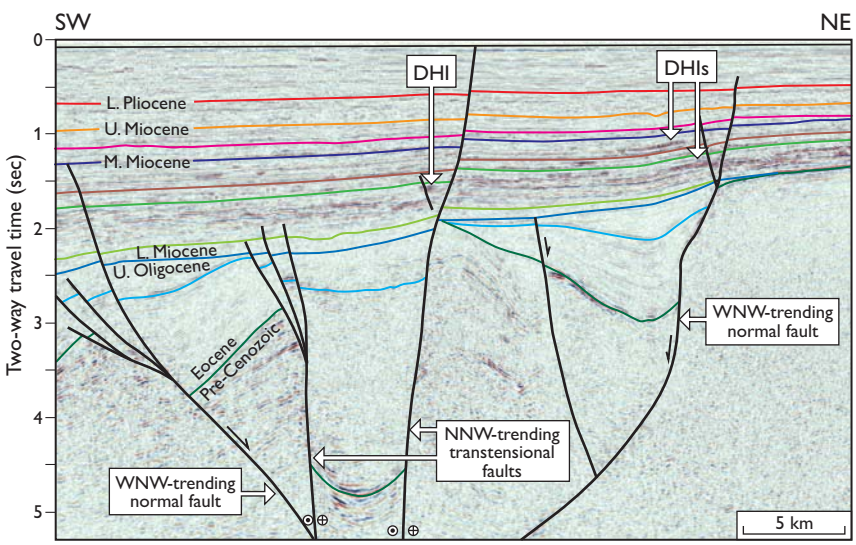

Fig. 4. Seismic transect across a NNW-trending Palaeogene graben bounded by steep transtensional faults and half grabens confined by more gently dipping WNW-trending normal faults that link up with the steep faults at depth. Deposition broadened across basement highs following the Palaeogene synrift period due to regional thermal sagging. DHIs (direct hydrocarbon indicators) within the Miocene succession are frequently associated with structural traps formed during the Late Neogene. Modified from Fyhn *et al.* (2010b).

syn-rift deposits have therefore undergone adequate maturation and may have produced and expelled significant quantities of hydrocarbons. The oldest deposits in the deepest part of syn-rift depressions entered the oil window during the Palaeogene syn-rift period but the main oil generation generally took place during Early and Middle Miocene times. 2-D modelling of the hydrocarbon generation therefore indicates that the main risks in the tested play types are (1) the timing of petroleum generation relative to trap formation completed in the Late Neogene, (2) the pervasive faulting, which may have complicated petroleum migration to the structures and breached charged traps and (3) the distribution and amount of matured source rocks in smaller grabens. Based on the above-mentioned criteria and the presence of direct hydrocarbon indicators (DHI), an untested alternative play type is proposed relying on syn-rift sandstones located up-dip from and near source-rock intervals with Palaeogene structural and stratigraphic trapping mechanisms that did not experience subsequent Neogene deformation.

Acknowledgements

The ENRECA project is funded by the Danish Ministry of Foreign Affairs through DANIDA. Geocenter Denmark provided additional financial support. Vietnam Petroleum Institute (PetroVietnam) is thanked for providing data and permission to publish this paper.

References

Bojesen-Koefoed, J.A., Nielsen, L.H., Nytoft, H.P., Petersen, H.I., Dau, N.T., Hien, L.V., Duc, N.A. & Quy, N.H. 2005: Geochemical characteristics of oil seepages from Dam Thi Nai, central Vietnam: implications for hydrocarbon exploration in the offshore Phu Khanh Basin. Journal of Petroleum Geology **28**, 3–18.

Fyhn, M.B.W., Boldreel, L.O. & Nielsen, L.H. 2009a: Geological development of the central and south Vietnamese margin: implications for the establishment of the South China Sea, Indochinese escape tectonics and Cenozoic volcanism. Tectonophysics **478**, 184–204.

Fyhn, M.B.W., Boldreel, L.O. & Nielsen, L.H. 2009b: Tectonic and climatic control on growth and demise of the Phanh Rang Carbonate Platform offshore south Vietnam. Basin Research **21**, 225–251.

Fyhn, M.B.W. *et al.* 2009c: Geological evolution, regional perspectives and hydrocarbon potential of the northwest Phu Khanh Basin, offshore Central Vietnam. Marine and Petroleum Geology **26**, 1–24.

Fyhn, M.B.W., Pedersen, S.A.S., Boldreel, L.O., Nielsen, L.H., Green, P.F., Dien, P.T., Huyen, L.T. & Frei, D. 2010a: Palaeocene – early Eocene inversion of the Phuquoc – Kampot Som Basin: SE Asian deformation associated with the suturing of Luconia. Journal of the Geological Society of London **167**, 281–295.

Fyhn, M.B.W., Boldreel, L.O. & Nielsen, L.H. 2010b: Escape tectonism in the Gulf of Thailand: Paleogene left-lateral pull-apart rifting in the Vietnamese part of the Malay Basin. Tectonophysics **483**, 365–376.

Hall, R. 2009: Hydrocarbon basins in SE Asia: understanding why they are there. Petroleum Geoscience **15**, 131–146.

Hall, R. & Morley, C.K. 2004: Sundaland Basins. In: Clift, P. *et al.* (eds): Continent–ocean interactions within East Asian marginal seas. Geophysical Monograph **149**, 55–85.

Lee, G.H. & Watkins, J.S. 1998: Seismic sequence stratigraphy and hydrocarbon potential of the Phu Khan Basin, offshore central Vietnam, South China Sea. AAPG Bulletin **82**, 1711–1735. Tulsa, Oklahoma: American Association of Petroleum Geologists.

Lee, G.H., Lee, K. & Watkins, J.S. 2001: Geological evolution of the Cuu Long and Nam Con Son Basins, offshore southern Vietnam, South China Sea. AAPG Bulletin **85**, 1055–1082. Tulsa, Oklahoma: American Association of Petroleum Geologists.

Matthews, S.J., Fraser, A.J., Lowe, S., Todd, S.P. & Peel, F.J. 1997: Structure, stratigraphy and petroleum geology of the SE Nam Con Son Basin, offshore Vietnam. In: Fraser, A.J., Matthews, S.J. & Murphy, R.W. (eds): Petroleum geology of Southeast Asia. Geological Society Special Publications (London) **126**, 89–106.

Morley, C.K. 2002: A tectonic model for the Tertiary evolution of strike-slip faults and rift basins in SE Asia. Tectonophysics **347**, 189–215.

Nielsen, L.H., Petersen, H.I., Thai, N.D., Duc, N.A., Fyhn, M.B.W., Boldreel, L.O., Tuan, H.A., Lindstrøm, S. & Hien, L.V. 2007: A Middle–Upper Miocene fluvial–lacustrine rift sequence in the Song Ba Rift, Vietnam: an analogue to oil-prone, small-scale continental rift basins. Petroleum Geoscience **13**, 145–168.

Petersen, H.I., Sherwood, N., Mathiesen, A., Fyhn, M.B.W., Dau, N.T., Russell, N., Bojesen-Koefoed, J.A. & Nielsen, L.H. 2009: Application of integrated vitrinite reflectance and FAMM analyses for thermal maturity assessment of the northeastern Malay Basin, offshore Vietnam: implications for petroleum prospectivity evaluation. Marine and Petroleum Geology **26**, 319–332.

Petersen, H.I., Mathiesen, A., Fyhn, M.B.W., Dau, N.T., Bojesen-Koefoed, J.A., Nielsen, L.H. & Nytoft, H.P. in press: Modeling of petroleum generation in the Vietnamese part of the Malay Basin using custom kinetics. AAPG Bulletin. Tulsa, Oklahoma: American Association of Petroleum Geologists.

Rangin, C., Klein, M., Roques, D., Le Pichon, X. & Trong, L.V. 1995: The Red River fault system in the Tonkin Gulf, Vietnam. Tectonophysics **243**, 209–222.

Tapponnier, P., Peltzer, G. Armijo, R. 1986: On the mechanics of the collision between India and Asia. In: Coward, M.P. & Ries, A.C. (eds): Collision tectonics. Geological Society Special Publications (London) **19**, 115–157.

Watkinson, I., Elders, C. & Hall, R. 2008: The kinematic history of the Khlong Marui and Ranong Faults, southern Thailand. Journal of Structural Geology **30**, 1554–1571.

Wilkins, R.W.T., Wilmshurst, J.R., Russell, N.J., Hladky, G., Ellacott, M.V. & Buckingham, C.P. 1992: Fluorescence alteration and the suppression of vitrinite reflectance. Organic Geochemistry **18**, 629–640.

Authors' addresses

M.B.W.F., H.I.P., A.M., L.H.N., S.A.S.P., S.L., J.A.B-K. & I.A., *Geological Survey of Denmark and Greenland, Øster Voldgade 10, DK-1350 Copenhagen K, Denmark.* E-mail: *mbwf@geus.dk*

L.O.B., *Department of Geography and Geology, University of Copenhagen, Øster Voldgade 10, DK-1350 Copenhagen K, Denmark.*

Potential for permanent geological storage of CO_2 in China: the COACH project

Niels E. Poulsen

The challenge of climate change demands reduction in global CO_2 mission. Carbon dioxide capture and storage (CCS) technology can be used to trap and store carbon dioxide gas emitted by coal-burning plants and this can reduce the world's total CO_2 emission by about one quarter by 2050 (IEA 2008, 2009; IPCC 2005). Experience from the storage sites of Sleipner in the Norwegian North Sea, Salah in Algeria, Nagaoka in Japan, Frio in USA and other sites shows that geological structures can safely accommodate CO_2 produced and captured from large CO_2 point sources. CCS is regarded as a technology that will make power generation from coal sustainable, based on cost-effective CO_2 capture, transport and safe geological storage of the released CO_2.

China has large coal reserves (DeLaquil *et al.* 2003), and is not about to give up on this reliable source of fossil fuel. Hence a large production of CO_2 can be expected to continue for many years. China also has a large theoretical geological carbon dioxide storage capacity in onshore areas with deep saline formations (Dahowski *et al.* 2009). In an extensive collaborative research effort between Chinese and European scientists, the COACH project (Cooperation Action within CCS China-EU) was successful in building the expertise, developing the capture technologies and mapping transportation routes for CO_2, and it produced two scenarios for geological storage of CO_2 in China.

The aim of the COACH project was to initiate a durable cooperation between Europe and China in response to China's rapidly growing energy demand. The project ran from November 2006 to October 2009 and was set up and funded by the European Commission under the memorandum of understanding on Near Zero Emissions Coal, to build demonstration plants in China. Twenty partners consisting of eight Chinese and twelve European partners evaluated the feasibility of establishing CCS in China (COACH 2009). COACH had four work packages dealing with (1) knowledge sharing and capacity building, (2) capture technologies, (3) permanent geological storage of CO_2 and (4) recommendations and guidelines for implementation. Three tasks were carried out under the

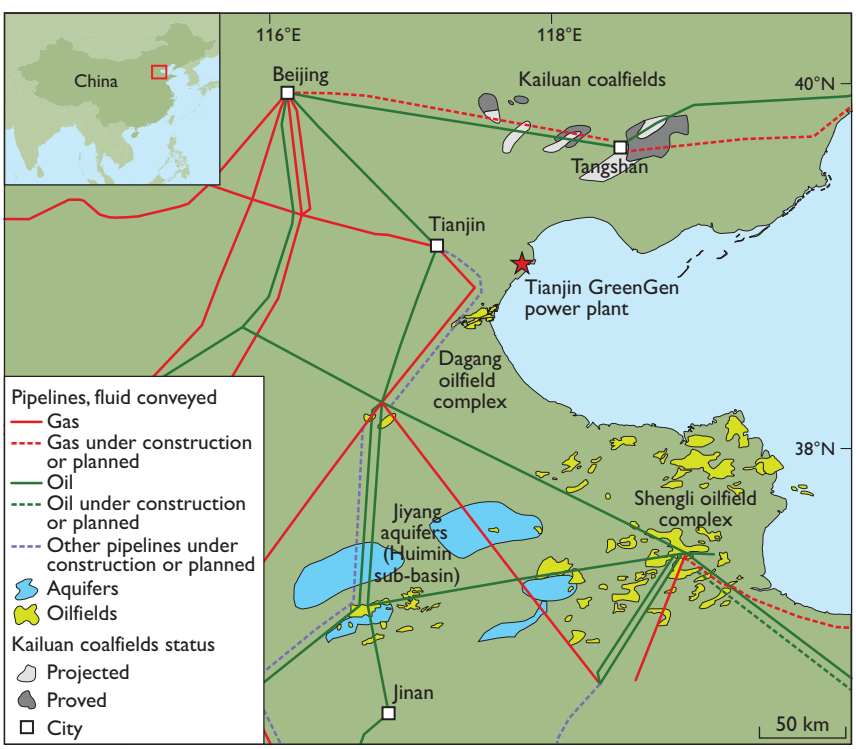

Fig. 1. Map of the study area in eastern China showing CO_2 sources, proposed pipeline network and potential storage sites. Based on data from the Energy, Environment and Economy Research Institute, Tsinghua University; Institute of Geology and Geophysics, Chinese Academy of Sciences; China University of Mining and Technology; Research Institute of Petroleum Exploration and Development, PetroChina and the China University of Petroleum (CUP). The outline of the Shengli oilfield complex and the pipeline data are from 'Energy Map of China 2008', © The Petroleum Economist Ltd, London. © British Geological Survey. British Geological Survey produced the GIS map.

third work package: (a) capacity estimates at regional level, (b) mapping of the geology and emission point sources and (c) improving methods for storage capacity assessment and site selection criteria. The Geological Survey of Denmark and Greenland and Tsinghua University in Beijing shared the leadership of the third work package. This short article presents the results of the work conducted on the potential for geological storage of CO_2 in China.

Background and methods

Aims of the Carbon Sequestration Leadership Forum

The aim of CO_2 storage is the permanent removal of CO_2 from the atmosphere. The European Union has supported current research on CO_2 capture and storage methods for more than a decade, with emphasis on capture techniques, transport and geological storage. The results of the research on geological storage are summarised in a comprehensive manual by Chadwick *et al.* (2008). Internationally recognised standards for capacity assessments were established by the Carbon Sequestration Leadership Forum (CSLF) in 2004–2005 and a task force on capacity estimation standards has been active since presenting comprehensive definitions, concepts and methods (Bachu *et al.* (2007a, b). These capacity standards were reviewed for the COACH project by Poulsen *et al.* (2009) and were used for the work on permanent CO_2 storage estimates in China (Zeng *et al.* 2009).

Fig. 2. An example of a Shengli oilfield production site.

Comparison of methods

Various methods are available for calculation of CO_2 storage capacity in a geological environment (Koide *et al.* 1992, 1995; Tanaka *et al.* 1995; Shafeen *et al.* 2004) . The methods used in the COACH project (Poulsen *et al.* 2009) were based on Bachu *et al.* (2007a, b) and used in the COACH database to estimate the storage capacity of hydrocarbon fields. Estimates made by the China University of Petroleum applied Tanaka *et al.*'s (1995) method for computing the storage capacity in the Shengli oilfield complex (Zeng *et al.* 2009).

The two methods proposed by the CSLF task force and Tanaka *et al.* (1995) are basically identical in their approach. Both methods are based on a volumetric approach and are applicable to site, regional and basin-scale CO_2 storage capacity estimates. Both can be considered as 'simple' equation models, which try to calculate an 'approximation' of a possible storage capacity. The methods gave almost identical results when applied to the Shengli oilfield complex (Table 1). There are, however, some differences in the approach to CO_2 behaviour in the storage site. The CSLF method works with replacement of oil, gas or formation water but does not incorporate dissolution of CO_2 in formation water. The method of Tanaka *et al.* (1995), on the other hand, operates with a free phase of CO_2 and takes into account dissolution of CO_2 in the formation water, but it does not considerer the time period needed for the dissolution (Poulsen *et al.* 2009).

Long term behaviour of CO_2 in a storage site

The long term behaviour of CO_2 in a storage site depends on (1) a number of reservoir parameters (temperature, pressure, capillary pressure, porosity, permeability, and the cap rock permeability and capillary entry pressure), (2) the CO_2 composition, (3) the formation water and (4) time (Chadwick *et al.* 2008). The solubility of CO_2 in formation water varies with salinity, temperature and pressure of the formation water (the brine). The dissolution of CO_2 in pure water increases with increasing pressure (and thus increasing depth) up to approximately 7 Mpa. On the other hand, the CO_2 solubility in a brine decreases with increasing temperature and salinity and thus in most cases decreases with depth (Bachu & Adams 2003). The

Table 1. Summary of geological sites assessed for geological storage of CO_2 after Zeng *et al.* (2009)

Storage site	Capacity	Injectivity	Seal
Dagang oilfield complex	Selected 7 fields 22 Mt Largest Gangdong field 10 Mt	1000 mD Some compartmentalisation by faulting and stratigraphy	Mudstones
Shengli oilfield complex	472 Mt using CSLF methodology and 463 Mt using CUP method	1000–2500 mD Some compartmentalisation by faulting and stratigraphy	Lower Jurassic mudstones
Huimin Sag aquifers (Jiyang)	For Huimin sub-basin 50 Gt For selected troughs in sub-basin 0.7 Gt	Permeability around 1600 mD in neighbouring oilfields	Mudstones of Minghuanzhen Fm
Kailuan coalfield	504 Gt adsorbed onto coal and 38 100 Mt void capacity	Permeability generally low 3.7 mD in Taiyuan Formation and 0.1 mD in Shanxi and Xiashihezi Fm	Mudstones

result is that in general, the solubility of CO_2 in the brine decreases with increasing salinity (Shafeen *et al.* 2004).

The buoyancy of injected supercritical CO_2 leads to an upward gravity-driven flow of CO_2 towards the top of the formation where it forms a plume below the cap rock. CO_2 (liquid or supercritical) and water are immiscible, but CO_2 can dissolve to a certain extent in water. Due to the slow solubility of CO_2 in brine, a large volume of brine is necessary to dissolve a given amount of CO_2. The density of the brine increases with increasing CO_2 dissolution and a downward gravity-driven flow will be induced by the increased density of the CO_2-saturated brine. On the initiation of storage, before the plume of saturated brine has reached the bottom, the overall dissolution rate is essentially constant due to rapid convective overturn (Ennis-King & Paterson 2007). At a later stage during storage the saturated brine forms a gravity current propagating outwards from the CO_2 source.

Activities and results

The main purpose of the COACH project was to prepare the way for CO_2 capture and storage in China. In order to achieve this, the COACH partners developed an integrated gasification combined cycle capture technique. This is a coal-based energy system with hydrogen production using coal gasification, electricity generation from a combined cycle hydrogen turbine and fuel cell system, and capture of the CO_2.

The partners have mapped emission sources and investigated potential CO_2 storage sites in eastern China (Fig. 1, Table 1). The storage potential of the selected sites was evaluated using published data or data provided by the Research Institute of Petroleum (PETROCHINA). Particular oilfields, saline aquifers and un-exploitable coal beds were investigated. Several test sites are available in some of the oilfields. The storage potential in oilfields is 10–500 Mt, (pilot scale level; Fig. 1, Table 1). Following this, a CO_2 transport infrastructure based on connecting CO_2 sources and storage sites by pipeline or ship has been suggested (Fig. 1; Table 1).

The saline Jiyang aquifers in the Huimin sub-basin show storage capture at an industrial scale (around 50 Gt; Fig. 1, Table 1), but further geological investigations are required. The security of energy supply is a key consideration in China, and enhanced oil recovery (EOR) could be an option. Some of the oilfields in the Dagang and Shengli oilfield complexes may be suitable for an enhanced oil recovery pilot project. Injecting CO_2 into oilfields approaching depletion will not only store CO_2, but may also enhance or prolong oil recovery (COACH 2009).

The coals of the Kailuan coalfield have low permeability and probably low injectivity, but a high theoretical ability to adsorb CO_2 (Fig. 1, Table 1). In general, however, the storage capacity in coal seams is uncertain. On the other hand, it has been demonstrated that injection of CO_2 into coal beds can lead to methane production (enhanced coal bed methane recovery; Yu *et al.* 2007). At the same time it is a very attractive option for geological CO_2 storage as CO_2 is strongly absorbed onto the coal.

Two scenarios for possible CO_2 capture and storage demonstration projects have been proposed by work package 4, based on the mapping of emission point sources, geology, and capacity estimates by work package 3 together with economic analyses. The first scenario is for a pilot scale site with 0.1–1 Mt CO_2/year stored in the Dagang or Shengli oilfield complexes. The second scenario is intended for industrial-scale storage at 2–3 Mt CO_2/year, which could be accommodated in the Shengli oilfield complex or potentially in the saline formations in the Huimin sub-basin. The pilot scale scenarios focus initially on enhanced oil recovery for storage where this is feasible. The large-scale option could begin with enhanced oil recovery but would need to switch to saline

aquifer storage once the potential reservoir and sealing formations have been adequately investigated. Both scenarios are based on capture of CO_2 from the Tianjin GreenGen power plant (COACH 2009).

Final remarks

In 2005 construction began of the coal-based Tianjin GreenGen power plant (Fig. 1) and electricity production started in 2009. It will be the first near-zero emission power plant in China. Research over the next decade is expected to develop and demonstrate the efficiency of coal-based power generation, mostly by recycling energy lost in the process. The goal is to achieve sustainability of coal-based power generation.

The project concludes that there is significant potential to develop carbon dioxide capture and storage technologies in China and to make major reductions in CO_2 emissions over the next century.

Experience from the storage sites Sleipner in the Norwegian North Sea, In Salah in Algeria, Nagaoka in Japan, Frio in USA and other sites shows that geological structures can safely accommodate CO_2 produced and captured from large point sources. Thus, geological storage of CO_2 can contribute considerably to the reduction of CO_2 emission in China and other countries.

Acknowledgements

COACH was funded as part of the 6th framework programme for research by the European Commission (project no. 038966). Nikki Smith from the British Geological Survey is thanked for producing the map used in Fig. 1.

References

Bachu, S., & Adams, J. J. 2003: Sequestration of CO_2 in geological media in response to climate change: capacity of deep saline aquifers to sequester CO_2 in solution. Energy Conversion and Management **44**, 3151–3175.

Bachu, S., Bonijoly, D., Bradshaw, J., Burruss, R., Christensen, N.P. Holloway, S., & Mathiassen, O.M. 2007a: Estimation of CO_2 storage capacity in Geological Media – Phase 2. Work under the auspices of the Carbon Sequestration Leadership Forum (www.cslforum.org). Final report from the task force for review and identification of standards for CO_2 storage capacity estimation, 43 pp. Washington: Carbon Sequestration Leadership Forum.

Bachu, S., Bonijoly, D., Bradshaw, J., Burruss, R., Holloway, S., Christensen, N.P. & Mathiassen, O.M. 2007b: CO_2 storage capacity estimation: methodology and gaps. International Journal of Greenhouse Gas Control **1**, 430–443.

Chadwick, A., Arts, R., Bernstone, C., May, F., Thibeau, S. & Zweigel, P. (eds) 2008: Best practice for the storage of CO_2 in saline aquifers – observations and guidelines from the SACS and CO2STORE projects. British Geological Survey Occasional Publication **14**, 267 pp.

COACH 2009: Project N° 038966: COACH, Cooperation Action within CCS China-EU, Executive Report, 38 pp.

Dahowski, R.T., Li, X., Davidson, C.L., Wei, N., Dooley, J.J. & Gentile, R.H. 2009: A preliminary cost curve assessment of carbon dioxide capture and storage potential in China. Energy Procedia **1**, 2849–2856.

DeLaquil, O., Wenying, C., & Larson, E.D. 2003: Modeling China's energy future. Energy for Sustainable Development **7**, 40–56.

Ennis-King, J. & Paterson, L. 2007: Coupling of geochemical reactions and convective mixing in the long-term geological storage of carbon dioxide. International Journal of Greenhouse Gas Control **1**, 86–93.

IEA (International Energy Agency) 2008: Energy technology perspectives: scenarios and strategies to 2050, 650 pp. Paris, France.

IEA (International Energy Agency) 2009: Technology roadmap. Wind energy, 52 pp. Paris: International Energy Agency.

Koide, H., Tazaki, Y., Noguchi, Y., Nakayama, S., Iijima, M., Ito, K., & Shindo, Y. 1992: Subterranean containment and long term storage of carbon dioxide in unused aquifers and in depleted natural gas reservoirs. Energy Conversion Management **33**, 619–626.

Koide, H., Takahashi, M., Tsukamoto. H. & Shindo, Y. 1995: Self-trapping mechanism of carbon dioxide in aquifer disposal. Energy Conversion Management **36**, 505–508.

Metz, B. *et al.* (eds) 2005: Carbon dioxide capture and storage. IPCC 2005, 431 pp. Cambridge University Press.

Poulsen, N.E., Chen, W., Dai, S., Ding, G., Kirk, K., Li, M., Zeng, R., Vangkilde-Pedersen, T., Vincent, C.J. & Vosgerau, H.J. 2009: D3.3. Improving methodologies for storage capacity assessment and site selection criteria. EU project no. 038966. COACH work package 3 report. EU deliverable D3.3, 45 pp. EU COACH project, Brussels.

Shafeen, A., Croiset, E., Douglas, P.L. & Chatzis, I. 2004: CO_2 sequestration in Ontario, Canada. Part I: storage evaluation of potential reservoirs. Energy Conversion and Management **45**, 2645–2659.

Tanaka, S., Koide, H. & Sasagawa, A. 1994: Possibility of underground CO_2 sequestration in Japan. Energy Conversion and Management **36**, 527–530.

Yu, H., Zhou, G., Fan, W. & Ye, J. 2007: Predicted CO_2 enhanced coalbed methane recovery and CO_2 sequestration in China. International Journal of Coal Geology **71**, 345–357.

Zeng, R., Li M., Dai, S., Zhang, B., Ding, G. & Vincent, C. 2009: Assessment of CO_2 storage potential in the Dagang oilfield, Shengli oilfield and Kailuan coalfield. COACH work package 3 report. EU deliverable D3.1, 45 pp. EU COACH project, Brussels.

Author's address

Geological Survey of Denmark and Greenland, Øster Voldgade 10, DK-1350 Copenhagen K, Denmark. E-mail: *nep@geus.dk*

Thin-skinned thrust-fault tectonics offshore south-west Vietnam

Stig A. Schack Pedersen, Lars Ole Boldreel, Emil Bach Madsen, Mette Bjerkvig Filtenborg and Lars Henrik Nielsen

In the *c.* 40 000 km^2 large Phu Quoc basin south-west of Vietnam reflection seismic data suggest a thin-skinned thrust-fault complex concealed by Neogene marine sediments (Fig. 1; Fyhn *et al.* 2010). The deformed sedimentary succession in the complex is of Early Cretaceous age, which is documented by biostratigraphical studies of outcrops and a 500 m deep well on the Phu Quoc island. A model for the thrust-fault deformation suggests that piggy-back basins were formed during displacement along the thrust faults. The translation was 3–8 km from east to west. The model is based on detailed structural analyses of 36 seismic sections that cover the Phu Quoc basin (Fig. 1). The main structural elements in the complex are flats and ramps with hanging-wall anticlines developed above the ramps. The crests of the hanging-wall anticlines occur as remnants of partially eroded structural highs. This paper describes the thin-skinned thrust-fault structures that form the basis for the interpretation of the concealed fold-belt complex in the Phu Quoc basin.

Architectural framework of the fold belt

Along the west coast of Vietnam folded and thrust-deformed Mesozoic and Palaeozoic sedimentary rocks form a N–S-striking fold belt referred to as the Kampot fold belt (Fyhn *et al.* 2010). To the north the fold belt continues into a hilly area at the border between Vietnam and Cambodia, where it forms a mountain range. To the south, offshore the west coast of Vietnam, the fold belt is concealed below Neogene marine sediments.

From west to east the fold belt is divided into a distal, intermediate and proximal part (Fig. 1). The distal part is a frontal wedge that passes into the foreland about 100 km west of the Vietnam coast. The intermediate part is characterised by moderately folded, hanging-wall anticlines with thrust displacements in the order of a few kilometres. The transition from the intermediate to the proximal parts is located close to the Nam Du archipelago (Pedersen *et al.* 2009). Two interpreted, representative seismic sections have been selected to illustrate the architectural style in structural cross-sections perpendicular to the main trend of the thrust-fault belt (Figs 2, 3).

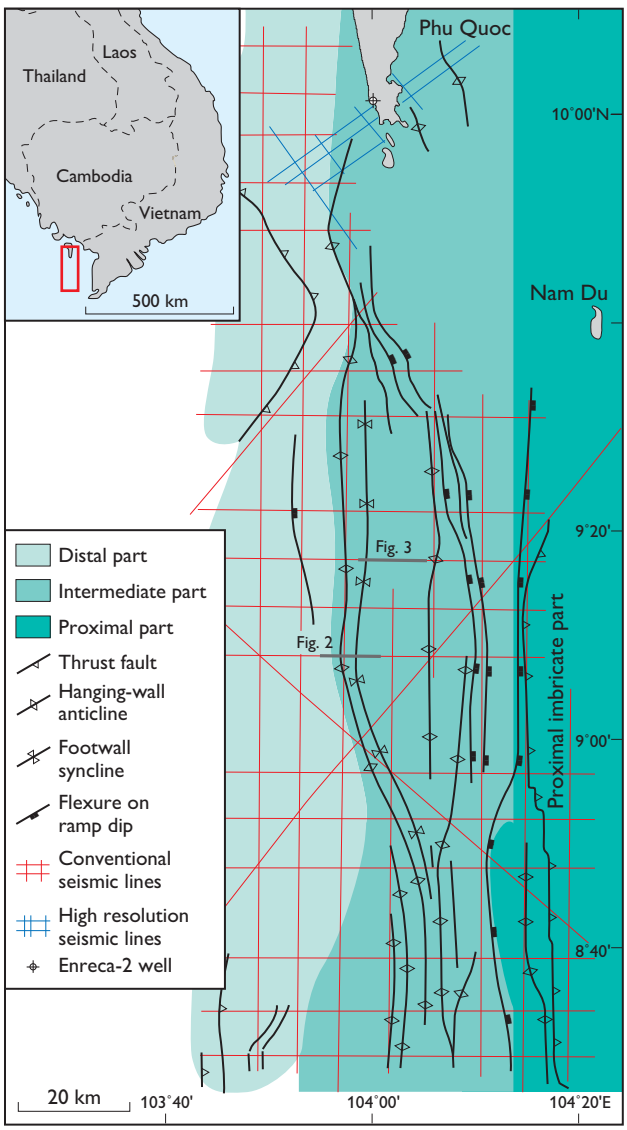

Fig. 1. Map of the study area off SW Vietnam, showing the seismic grid which formed the basis for the study of the Phu Quoc basin. On the map the main structural elements are shown with the trends of anticlines and thrust faults interpreted from the seismic sections. The location of the 500 m deep well ENRECA-2 on the Phu Quoc island and the position of the two cross-sections in Figs 2 and 3 representing the distal and the intermediate parts of the deformation complex are also shown. The inset map shows the location of the investigated area in SE Asia.

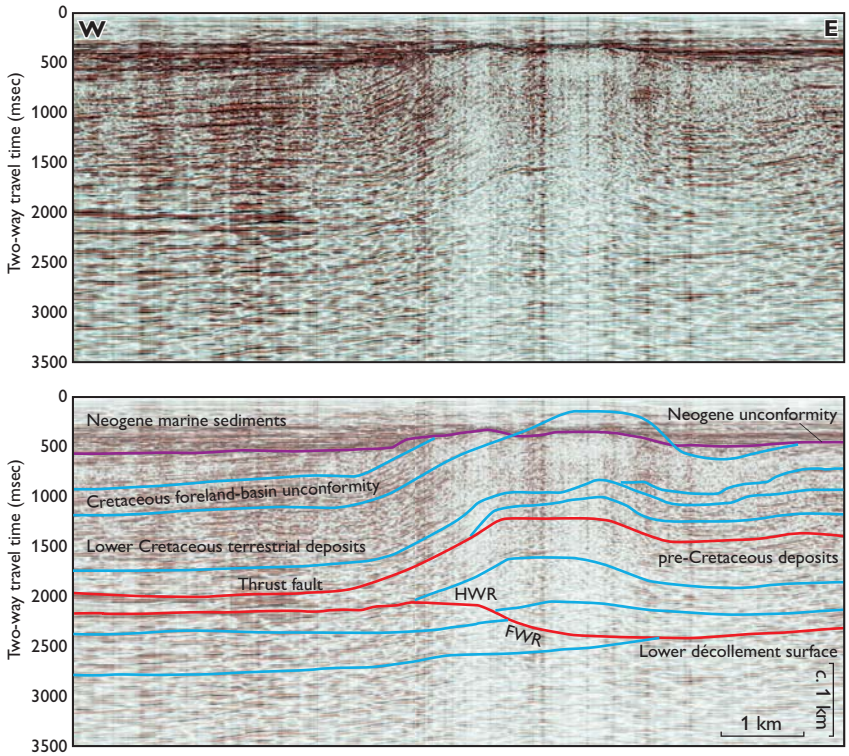

Fig. 2. Seismic section representing the distal part of the tectonic complex. In the western part of the cross-section the most distally appearing hanging-wall anticline is seen, and to the west the almost planar horizontal bedding extends into the foreland basin. Beds in the youngest Phu Quoc unit onlap the moderately dipping beds on the western limb of the hanging-wall anticline, and these beds as well as the top of the hanging-wall anticline are truncated by the Neogene unconformity. **HWR**: hanging-wall ramp, **FWR**: footwall ramp. Blue lines: prominent bedding surfaces. Red lines: thrust faults. Purple line: the main Neogene unconformity that truncates the structures in the tectonic complex. For location see Fig. 1.

The distal part of the tectonic complex

The distal part of the complex passes gradually into the undeformed foreland where almost horizontally bedded Cretaceous sediments occur, which are separated from overlying Neogene marine sediments by a distinct unconformity. Thrust-faults dipping <2° are found from the foreland towards the intermediate part. A number of minor ramps are present until the main décollement zone passes into a deeper level along a moderately dipping ramp, above which the westernmost, major hanging-wall anticline is seen (Fig. 2).

The main décollement zone is located below 2.5 km of sediments in the distal area, west of the foreland-near, hanging-wall anticline. The ramp takes the décollement zone down to 3 km below surface. At this depth the resolution of the seismic data becomes low, so no further interpretations are carried out. The hanging-wall anticline is relatively flat-topped, which corresponds well with a model for hanging-wall anticlines where the displacement is about half the thickness of the thrust-faulted sedimentary rock unit (Pedersen 2006). The western limb of the hanging-wall anticline dips *c.* 25°W, and the uppermost depositional unit below the Neogene unconformity on-laps the dipping limb. The beds in this unit are gently tilted towards the west due to the main, gentle dip of the depositional wedge in the frontal part of the thrust system. Therefore this uppermost depositional unit may be regarded as a piggy-back basin, which was formed during the translation of the frontal part of the thrust-fault complex. Interpretations of the seismic sections north of the presented cross-section show additional examples of piggy-back basins. The most important of these is a basin found south-east of the Phu Quoc island. It formed between two hanging-wall anticlines during their fold and translation development. In addition, we have interpreted the gently deformed Lower Cretaceous deposits that were penetrated by the ENRECA-2 well on the Phu Quoc island to continue into the deformed succession offshore. In our tectonic model the environment surrounding Phu Quoc island is regarded as located at the transition from the distal to the intermediate part of the tectonic complex.

The intermediate part of the tectonic complex

Two or more levels of thrust faults with flats and ramps have developed in the intermediate part of the complex (Figs 1, 3). The number of ramps increases eastwards, which leads to an increasing number of hanging-wall anticlines, some of which are interpreted to have developed into antiformal stacks. The appearance of duplex structures initially lifted the top of the tectonic complex to a higher level. However, this is only recognised as a deeper level of erosion into the tectono-stratigraphic units. The displacement increases to 3–8 km resulting in some variation in the structural style of

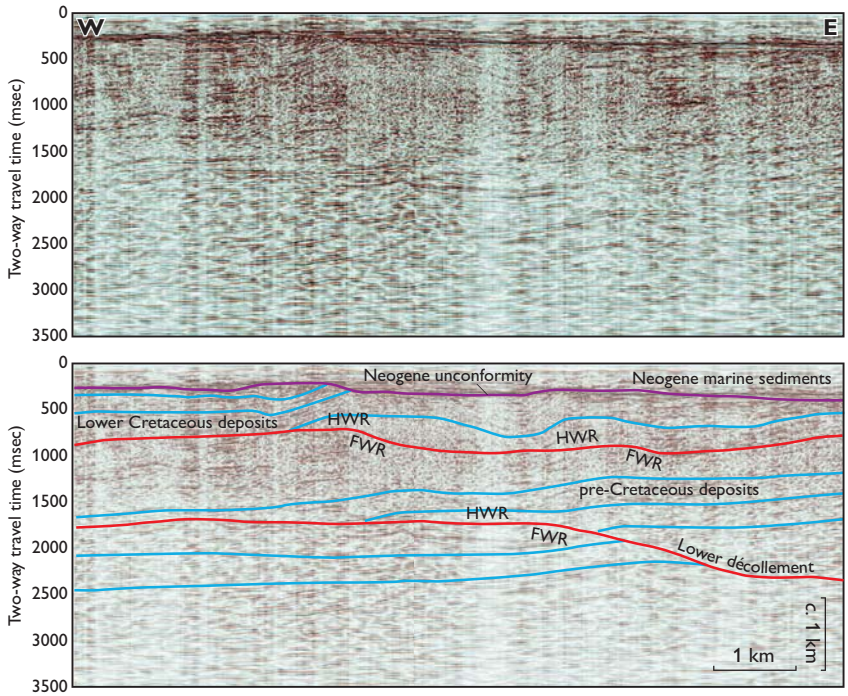

Fig. 3. Seismic section representing the intermediate part of the tectonic complex. This part is characterised by increasing numbers of hanging-wall anticlines and thrust faults. The upper thrust fault constitutes an upper flat to the west, an upper footwall ramp (**FWR**) that connects the upper flat to an intermediate flat, and a lower footwall ramp that continues into the lower flat to the east. Each footwall ramp corresponds to a hanging-wall anticline above a displaced hanging-wall ramp (**HWR**). Due to the presence of two footwall ramps a prominent syncline developed between the two hanging-wall anticlines. Blue lines: prominent bedding surfaces. Red lines: thrust faults. Purple line: the main Neogene unconformity that truncates the structures in the tectonic complex. For location see Fig. 1.

the hanging-wall anticlines. At the transition from the intermediate to the proximal part, erosional remnants of the hanging-wall anticlines are preserved as scattered islands rising a few hundred metres above sea level. The easternmost island in the Nam Du archipelago provides an example of this. On this island the thrust deformation elevated Permian rhyolitic hyaloclastics to a surface-near position (Pedersen *et al*. 2009).

The proximal part of the tectonic complex

The proximal part of the tectonic complex is only covered by seismic data only in the south-eastern part of the study area (Fig. 1). Here steeply dipping imbricate structures with 200–500 m thick thrust sheets occur. The depth to the décollement zone is more than 3 km. Onshore the imbricate structures in the proximal part are exposed in the mountain range at the border between Vietnam and Cambodia. In this area the general dip of the thrust sheets is about 30°, and the deformed sedimentary rocks comprise Upper Palaeozoic sandstones and shales, Permian carbonates and Triassic sandstones, arkoses and conglomerates. In the thrust-fault zones, shearing and low-grade metamorphism have altered the sediments with recrystallisation of albite and formation of chlorite and biotite, corresponding to lower to medium greenschist facies. No minerals indicating higher metamorphic grades have been recognised. One of the small islands *c.* 50 km north-north-east of Nam Du is located in the proximal part. On this island, Permian carbonates are thrust-faulted over Jurassic shales and sandstones. A granitic plug occurs in the middle part of the island and granitic sills have intruded the Jurassic succession. The intrusions are of lower Cretaceous age (Pedersen *et al*. 2009).

Cretaceous granitic intrusions occur on the mainland east of the proximal part of the tectonic complex. They form a Cretaceous magmatic arc in the hinterland zone of the Kampot fold belt (Fyhn *et al*. 2010). The intrusive age of the granites is based on radiometric dating, and the dating of the uplift and erosion is based on fission-track studies that indicate exhumation during the Eocene (Fyhn *et al*. 2010).

Discussion

The timing of the deposition of the basin fill and the deformation of the Phu Quoc basin are addressed by the tectonic model. The structural interpretation of the thrust-fault structures implies that the piggy-back basins formed in the Cretaceous, which in turn suggests that the deformation started in the Cretaceous. However, according to the apatite fission-track analysis the sedimentary rocks in the Phu Quoc basin and the Kampot fold belt were buried to a depth where the temperature exceeded 100°C (Fyhn *et al*. 2010). This indicates burial below 2–3 km of sediments that were entirely eroded away in the early Eocene when the main exhumation

of the region occurred (Fyhn *et al.* 2010). It is suggested that the compressional deformation was caused by subduction of the westernmost part of the Pacific Ocean plate (Metcalfe 1996). Erosion of the up-thrust, pre-Cretaceous rock units in the Kampot fold belt supplied sediments for the Cretaceous deposits in the Phu Quoc basin. The progressing compression led to deformation of the proximal part of the basin. A cross-section of the tectonic complex indicates a 200 km wide zone and the shortening of the complex is roughly estimated to be 50%. Assuming a compressional orogenic translation in the order of 5 cm/y, the deformation lasted *c.* 4 million years. Following the deformation, granites were intruded into the fold belt as the subducted sedimentary rocks below the fold belt began to melt. The age of the intrusions corresponds with the Cretaceous deformation in the distal part of the tectonic complex. The crucial issue is to understand the mechanism that caused uplift in the Eocene and subsidence in the Neogene. We suggest that the subducted slab with a top layer of granitic composition was less dense than the base of the overlying lithosphere, and that this could cause a regional but orogenically passive uplift. The uplift was followed by Eocene–Miocene erosion and denudation before the raised granitic lithosphere cooled, which led to the Neogene subsidence that created new accommodation space in the area above the Phu Quoc basin.

Conclusion

The deposits in the Phu Quoc basin off south-west Vietnam were affected by a Late Mesozoic orogeny. The tectonic complex at Nam Du archipelago is characterised by thin-skinned thrust-fault deformation with a distal part to the west, an intermediate part around the Nam Du archipelago, and a proximal part, which includes a hilly area in the onshore part of the Kampot fold belt. The hinterland of the tectonic complex includes a magmatic arc represented by granitic plutons exposed in the south-western part of Vietnam.

The orogenic deformation of the complex is interpreted to be of early–middle Cretaceous age. The complex was successively buried by a more than two kilometres thick package of sediments that was removed by erosion during uplift in the early Eocene. Finally subsidence in the Neogene resulted in sedimentation that covered the Mid-Tertiary unconformity.

Acknowledgements

We thank Vietnam Petroleum Institute and PetroVietnam for permission to use the commercial seismic data and permission to publish Figs 2 and 3. The company Landmark is thanked for a university grant to the Department of Geography and Geology at Copenhagen University. The ENRECA programme of DANIDA is thanked for financial support.

References

Fyhn, M., Pedersen, S.A.S., Boldreel, L.O., Nielsen, L.H., Green, F.P., Dien, P.T., Huyen, L.T. & Frei, D. 2010: Palaeocene – early Eocene inversion of the Phuquoc-Kampot Som basin: SE Asian deformation associated with the suturing of Luconia. Journal of the Geological Society (London) **167**, 281–295.

Metcalfe, I. 1996. Pre-Cretaceous evolution of SE Asian terranes. In: Hall, R., Blundell, D. (eds.): Tectonic Evolution of Southeast Asia. Geological Society Special Publication (London) **106**, 97–122.

Pedersen, S.A.S.2006: Strukturer og dynamisk udvikling af Rubjerg Knude Glacialtektoniske Kompleks, Vendsyssel, Danmark. Geologisk Tidsskrift **2006**, 1, 46 pp.

Pedersen, S.A.S., Fyhn, M. Dien, P.T., Boldreel, L.O., Nielsen, L.H., Green, F.P., Huyen, L.T. & Mai, L.*C.* 2009: Structural geology of the Nam Du island and neighbouring areas in the Phu Quoc basin, SW Vietnam. Danmarks og Grønlands Geologiske Undersøgelse Rapport **2009/7**, 47 pp.

Authors' addresses

S.A.S.P. & L.H.N., *Geological Survey of Denmark and Greenland, Øster Voldgade 10, DK-1350 Copenhagen K, Denmark*. E-mail: *sasp@geus.dk*

L.O.B., E.B.M. & M.B.F., *Department of Geography and Geology, University of Copenhagen, Øster Voldgade 10, DK-1350 Copenhagen K, Denmark.*

Interactive web analysis and presentation of computer-controlled scanning electron microscopy data

Peter Riisager, Nynke Keulen, Uffe Larsen, Roger K. McLimans, Christian Knudsen and Jørgen Tulstrup

In the following we describe the result of the Titan Project, an interactive web application (Titan) developed at the Geological Survey of Denmark and Greenland (GEUS) together with DuPont Titanium Technologies. The main aim of Titan is to make computer-controlled scanning electron microscopy (CCSEM) data, generated at GEUS, available via the internet. In brief, CCSEM is a method automatically to detect particles with a scanning electron microscope (SEM), and based on computer-controlled imagery to measure the chemistry and grain morphology of each particle in a given sample (Knudsen *et al.* 2005; Bernstein *et al.* 2008); Keulen *et al.* 2008. Titan makes data available on-line so that the user can interact with the data sets and analyse them using a web browser. In addition to CCSEM data, Titan contains a global database of titanium deposits and various reports. The web application is customised, such that the functionality and amount of data available for a given user depend on the privileges of that user.

Data

A prerequisite for making Titan available on the internet is that the data are stored in a relational database allowing for fast querying and retrieval. A detailed description of the data model is not given here, but we will make a short overview of the different data types and how the data are inserted and managed in the database. The data are stored in an Oracle 10g database that is housed and maintained by GEUS (Tulstrup 2004).

CCSEM data

CCSEM data are uploaded to the Jupiter database via a desktop program developed with the Delphi software tool at GEUS (Fig. 1). Typical CCSEM samples consist of roughly one thousand grains. For each grain *c.* 30 analytical parameters are measured including elemental composition, grain size and grain shape. All parameters are stored in the database including the energy dispersive X-ray spectrum for each grain (from which the elemental composition of the grain is determined) as well as backscatter-mode SEM images of the sample. The number of measurements currently stored in the database exceeds 54 million (Fig. 2), and the number continues to grow at a rate of *c.* 15 million per year. Once data are uploaded, each grain is classified according to a mineral classification scheme that is implemented using Oracle database PL/SQL procedures. The mineral classification scheme is based on the measured concentration of elements, and different schemes are available depending on the type of sample. For example, there is a mineral classification scheme for heavy mineral concentrates, while another scheme is applied for soil samples.

Titanium deposits and reports

Data on titanium deposits can be entered directly into the database through Titan, and at present it contains detailed information about more than 600 deposits around the world.

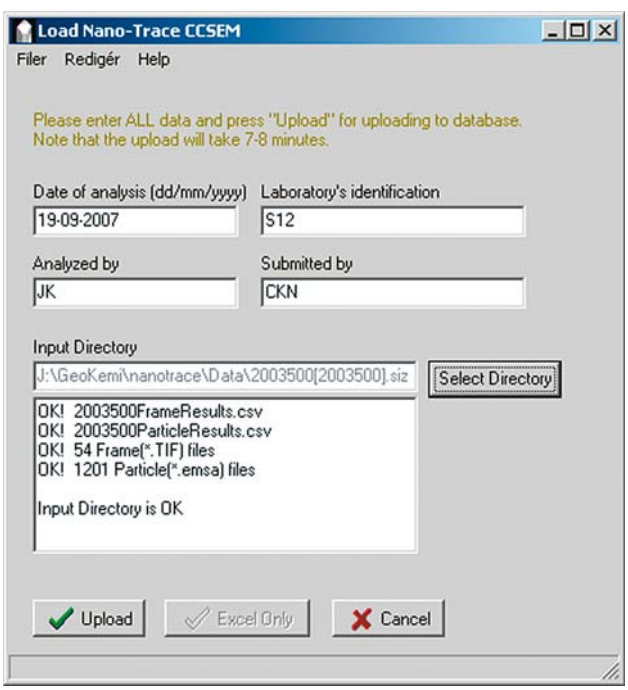

Fig. 1. Entry of sample metadata and uploading of CCSEM data to the database using a desktop programme. The energy dispersive X-ray spectrum for each grain and backscatter-mode SEM images of the sample are also uploaded.

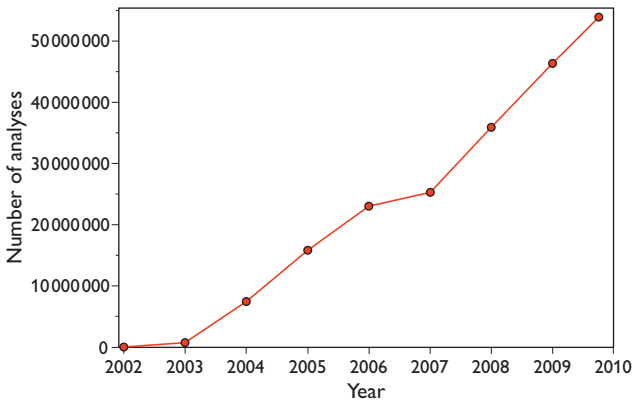

Fig. 2. Number of measurements in the Titan database as a function of time. Currently the database contains *c.* 54 million measurements.

Reports and report metadata are uploaded to the database via the web application. The option to create, read, update, and delete deposits and reports is restricted to certain users and managed by strict user control.

Web interface

The web application is based on open-source software, mainly Java, and is running in an open-source JBoss Application Server housed and maintained by GEUS. Access to Titan requires login with username and password. Once logged in, the system assigns the user a specific role with specific priviliges allowing certain analytical functions. The user control is also extended to the individual CCSEM samples so that each group of users can see and interact with only a restricted subset of CCSEM samples. The CCSEM data can be accessed using an interactive geological map web page (Fig. 3) or by alphanumeric search criteria. When a sample is found, various recalculated data for that sample are available in table formats, and back-scatter mode SEM images or other files, such as outcrop pictures related to the sample, can be viewed or downloaded. If users want to work with the data off-line, data can be exported to Microsoft Excel format or a customised PDF report can be generated. Most importantly, the user has the option to visualise and interact with the data using various plots. For example, the elemental composition of all the mineral grains in a given sample can be presented in a scatter plot (Fig. 4), where the user defines the elements assigned to the x and y axes and which minerals should be plotted. The user can select which minerals to be plotted for analysis and comparison of apparent grain sizes (Fig. 5). This gives the user quick and easy access to make the desired analyses and plots. The on-line access has the added benefit that users around the world always have live access to the database, meaning that as soon as new data are uploaded the users can start interacting with them.

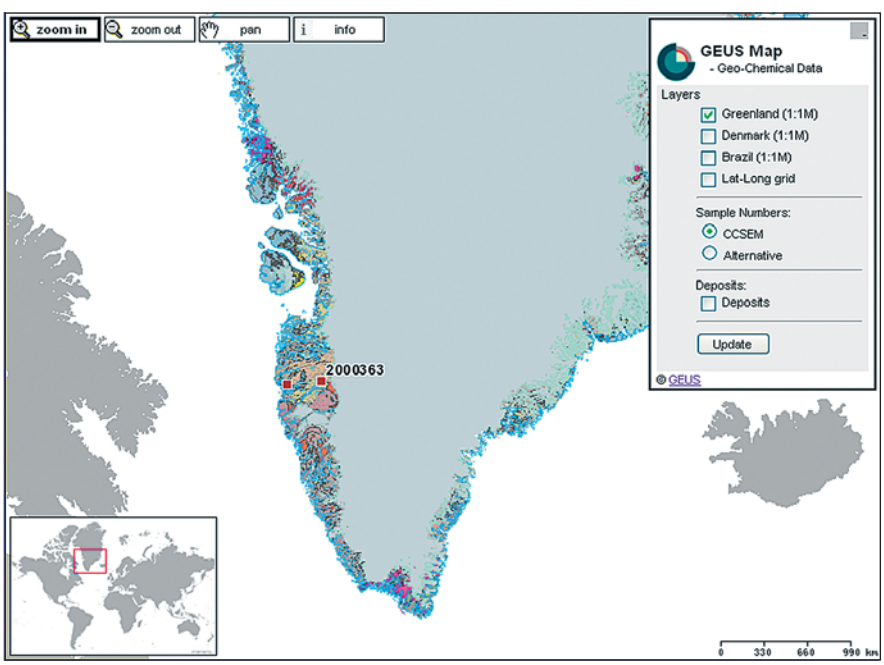

Fig. 3. The Titan web application includes an interactive map that allows the user to search for CCSEM samples based on their geographic sampling coordinates. Clicking on a sample on the map takes the user to other screen images where one can interact with the actual data (Figs 4, 5).

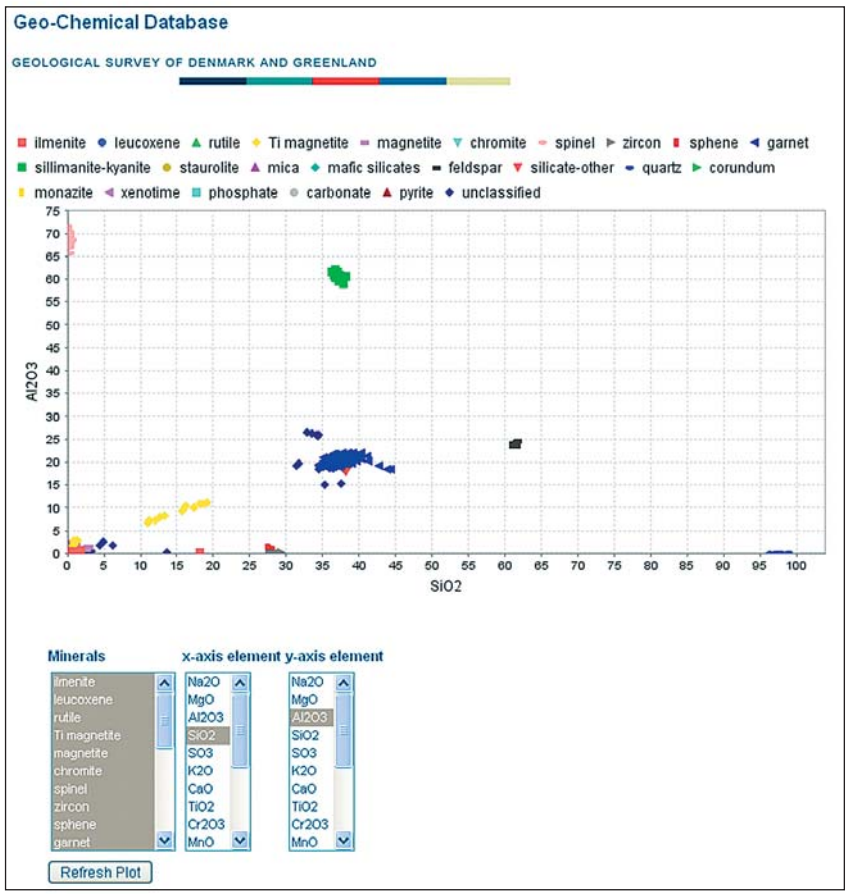

Fig. 4. Analysis of CCSEM data with an interactive scatter plot using Titan. The user defines the elements assigned to the x and y axes, and which minerals are plotted.

Examples of applications

Titan has successfully delivered data to scientists working at GEUS as well as various external end-users. In the following we will give some short examples of the use of Titan.

Tracing kimberlite-indicator minerals for diamond prospection

The elemental compositions of megacrystal and xenocrystal phases within kimberlitic rocks are used as an important diamond exploration tool. Preliminary studies have demonstrated the excellent potential of CCSEM to determine the elemental composition of minor elements in these minerals in a reliable and more cost-efficient manner than conventional electron microprobe analysis (Keulen *et al.* 2009).

Exploration and ore deposit evaluation

Mineralogical characterisation of sediments is a prerequisite for exploration and exploitation of valuable sediment occurrences, such as heavy mineral deposits. With Titan we have characterised individual mineral particles in heavy mineral sands, with the aim of detecting heavy mineral ore deposits (Knudsen *et al.* 2005; Bernstein *et al.* 2008).

Soil sample mineralogy for the cement industry

Cement manufacture causes emission of large quantities of airborne pollutants including greenhouse gases. With Titan we have studied the raw materials used in cement production to optimise the performance of the grinding mill and the sintering process, with the ultimate aim to lower energy consumption at high temperatures (Keulen *et al.* 2008).

Sediment provenance studies for oil exploration and sedimentary basin analysis

Sediment provenance studies are an important aspect in the evaluation of possible sandstone reservoirs. Titan has served as an indispensable tool to determine source, compositional

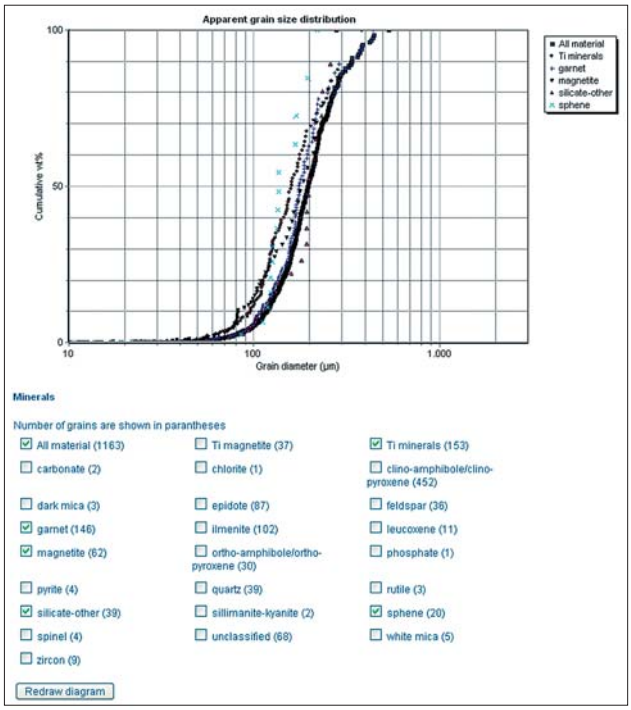

Fig. 5. Analysis and comparison of the apparent grain size distributions of the various mineral fractions in the sample using Titan. The plot is interactive, allowing the user to choose which minerals are plotted.

variation and sedimentary pathways of several sedimentary deposits relevant for oil exploration (Knudsen *et al.* 2005; Bernstein *et al.* 2008).

Concluding remarks

Earth science is becoming an increasingly more quantitative science with new insights, more often than not, derived from detailed measurements. The Titan Project represents an example where advanced geoscientific instrumentation has allowed us to design projects that were not previously feasible, thereby opening new scientific research areas (e.g. Bernstein *et al.* 2008; Keulen *et al.* 2008, 2009). It is, however, important to underline that this progress does not only include the scientific instruments and analyses themselves, it also represents a major challenge to store and analyse the huge quantities of data generated (Fig. 2). In this paper we have demonstrated that information technology plays a central role in facilitating the storage, retrieval and analysis of large geoscientific datasets.

Storing and distributing geological data are important aspects of national geological surveys, and it is important that GEUS follows in the footsteps of other national surveys in order to take full advantage of the new opportunities offered by the revolution of information technology. The Titan Project demonstrates that GEUS has the in-house expertise to develop technologies that address the full life cycle of geoscientific data from the raw instrument output, to store data securely in a database, analyse and reduce data, and finally distribute the data providing on-line and interactive access to the data. The know-how from the Titan Project is currently being applied to other similar projects at GEUS. Finally, we would like to point out that besides the scientific and societal rationale of Titan, it continues to be used by commercial partners. In fact, the application itself has almost exclusively been financed by industrial partners.

References

Bernstein, S., Frei, D., McLimans, R.K., Knudsen, C. & Vasudev, V.N. 2008: Application of CCSEM to heavy mineral deposits: Source of high-Ti ilmenite sand deposits of South Kerala beaches, SW India. Journal of Geochemical Exploration **96**, 25–42.

Keulen, N., Frei, D., Bernstein, S., Hutchison, M.T., Knudsen, C. & Jensen, L. 2008: Fully automated analysis of grain chemistry, size and morphology by CCSEM: examples from cement production and diamond exploration. Geological Survey of Denmark and Greenland Bulletin **15**, 93–96.

Keulen, N., Hutchison, M.T. & Frei, D. 2009: Computer-controlled scanning electron microscopy: A fast and reliable tool for diamond prospecting. Journal of Geochemical Exploration **103**, 1–5.

Knudsen, C., Frei, D., Rasmussen, T., Rasmussen, E.S. & McLimans, R. 2005: New methods in provenance studies based on heavy minerals: an example from Miocene sands in Jylland, Denmark. Geological Survey of Denmark and Greenland Bulletin **7**, 29–32.

Tulstrup, J. 2004: Environmental data and the Internet: openness and digital data management. Geological Survey of Denmark and Greenland Bulletin **4**, 45–48.

Authors' addresses

P.R., N.K., U.L., C.K. & J.T., *Geological Survey of Denmark and Greenland, Øster Voldgade 10, DK-1350 Copenhagen K, Denmark.* E-mail: *pri@geus.dk*

R.K.McL., *DuPont Titanium Technologies, Experimental Station, E352/217, Route 141 and Henry Clay, Wilmington, DE 19808, USA.*

De Nationale Geologiske Undersøgelser for Danmark og Grønland (GEUS)

Geological Survey of Denmark and Greenland
Øster Voldgade 10, DK-1350 Copenhagen K
Denmark

The series *Geological Survey of Denmark and Greenland Bulletin* started in 2003 and replaced the two former bulletin series of the Survey, viz. *Geology of Greenland Survey Bulletin* and *Geology of Denmark Survey Bulletin*. Some of the twenty-one volumes published since 1997 in those two series are listed on the facing page. The present series, together with *Geological Survey of Denmark and Greenland Map Series*, now form the peer-reviewed scientific series of the Survey.

Geological Survey of Denmark and Greenland Bulletin

1	The Jurassic of Denmark and Greenland, 948 pp. (28 articles), 2003. *Edited by* J.R. Ineson & F. Surlyk.	500.00
2	Fish otoliths from the Paleocene of Denmark, 94 pp., 2003. *By* W. Schwarzhans.	100.00
3	Late Quaternary environmental changes recorded in the Danish marine molluscan faunas, 268 pp., 2004. *By* K.S. Petersen.	200.00
4	Review of Survey activities 2003, 100 pp. (24 articles), 2004. *Edited by* M. Sønderholm & A.K. Higgins.	180.00
5	The Jurassic of North-East Greenland, 112 pp. (7 articles), 2004. *Edited by* L. Stemmerik & S. Stouge.	160.00
6	East Greenland Caledonides: stratigraphy, structure and geochronology, 93 pp. (6 articles), 2004. *Edited by* A.K. Higgins & F. Kalsbeek.	160.00
7	Review of Survey activities 2004, 80 pp. (19 articles), 2005. Edited by M. Sønderholm & A.K. Higgins.	180.00
8	Structural analysis of the Rubjerg Knude Glaciotectonic Complex, Vendsyssel, northern Denmark, 192 pp., 2005. *By* S.A.S. Pedersen.	300.00
9	Scientific results from the deepened Lopra-1 borehole, Faroe Islands, 156 pp. (11 articles), 2006. *Edited by* J.A. Chalmers & R. Waagstein.	240.00
10	Review of Survey activities 2005, 68 pp. (15 articles), 2006. *Edited by* M. Sønderholm & A.K. Higgins.	180.00
11	Precambrian crustal evolution and Cretaceous–Palaeogene faulting in West Greenland, 204 pp. (12 articles), 2006. *Edited by* A.A. Garde & F. Kalsbeek..	240.00
12	Lithostratigraphy of the Palaeogene – Lower Neogene succession of the Danish North Sea, 77 pp., 2007. *By* P. Schiøler, J. Andsbjerg, O.R. Clausen, G. Dam, K. Dybkjær, L. Hamberg, C. Heilmann-Clausen, E.P. Johannessen, L.E. Kristensen, I. Prince & J.A. Rasmussen.	240.00
13	Review of Survey activities 2006, 76 pp. (17 articles), 2007. *Edited by* M. Sønderholm & A.K. Higgins.	180.00
14	Quaternary glaciation history and glaciology of Jakobshavn Isbræ and the Disko Bugt region, West Greenland: a review, 78 pp., 2007. *By* A. Weidick & O. Bennike.	200.00
15	Review of Survey activities 2007, 96 pp. (22 articles), 2008. *Edited by* O. Bennike & A.K. Higgins.	200.00
16	Evaluation of the quality, thermal maturity and distribution of potential source rocks in the Danish part of the Norwegian–Danish Basin, 66 pp., 2008. *By* H.I. Petersen, L.H. Nielsen, J.A. Bojesen-Koefoed, A. Mathiesen, L. Kristensen & F. Dalhoff.	200.00
17	Review of Survey activities 2008, 84 pp. (19 articles), 2009. *Edited by* O. Bennike, A.A. Garde & W.S. Watt.	200.00
18	Greenland from Archaean to Quaternary. Descriptive text to the 1995 Geological map of Greenland, 1:2 500 000. 2nd edition, 126 pp., 2009. *By* N. Henriksen, A.K. Higgins, F. Kalsbeek & T.C.R. Pulvertaft.	280.00
19	Lithostratigraphy of the Cretaceous–Paleocene Nuussuaq Group, Nuussuaq Basin, West Greenland, 2009. *By* G. Dam, G.K. Pedersen, M. Sønderholm, H.H. Midtgaard, L.M. Larsen, H. Nøhr-Hansen & A.K. Pedersen.	300.00
20	Review of Survey activities 2009, 106 pp. (23 articles), 2010. *Edited by* O. Bennike, A.A. Garde & W.S. Watt.	

Geological Survey of Denmark and Greenland Map Series

1	Explanatory notes to the Geological map of Greenland, 1:500 000, Humboldt Gletscher, Sheet 6, 48 pp. + map, 2004. *By* P.R. Dawes.	280.00

2	Explanatory notes to the Geological map of Greenland, 1:500 000, Thule, Sheet 5 (1991), 97 pp. + map, 2006. *By* P.R. Dawes.	300.00
3	Explanatory notes to the Geological map of Greenland, 1:100 000, Ussuit 67 V.2 Nord, 40 pp. + map, 2007. *By* J.A.M. van Gool & M. Marker.	280.00
4	Descriptive text to the Geological map of Greenland, 1:500 000, Dove Bugt, Sheet 10, 32 pp. + map, 2009. *By* N. Henriksen & A.K. Higgins.	240.00

Geology of Greenland Survey Bulletin (173–191; discontinued)

175	Stratigraphy of the Neill Klinter Group; a Lower – lower Middle Jurassic tidal embayment succession, Jameson Land, East Greenland, 80 pp., 1998. *By* G. Dam & F. Surlyk.	250.00
176	Review of Greenland activities 1996, 112 pp. (18 articles), 1997. *Edited by* A.K. Higgins & J.R. Ineson.	200.00
177	Accretion and evolution of an Archaean high-grade grey gneiss – amphibolite complex: the Fiskefjord area, southern West Greenland, 115 pp., 1997. *By* A.A. Garde.	200.00
178	Lithostratigraphy, sedimentary evolution and sequence stratigraphy of the Upper Proterozoic Lyell Land Group (Eleonore Bay Supergroup) of East and North-East Greenland, 60 pp., 1997. *By* H. Tirsgaard & M. Sønderholm.	200.00
179	The Citronen Fjord massive sulphide deposit, Peary Land, North Greenland: discovery, stratigraphy, mineralization and structural setting, 40 pp., 1998. *By* F.W. van der Stijl & G.Z. Mosher.	200.00
180	Review of Greenland activities 1997, 176 pp. (26 articles), 1998. *Edited by* A.K. Higgins & W.S. Watt.	200.00
181	Precambrian geology of the Disko Bugt region, West Greenland, 179 pp. (15 articles), 1999. *Edited by* F. Kalsbeek.	240.00
182	Vertebrate remains from Upper Silurian – Lower Devonian beds of Hall Land, North Greenland, 80 pp., 1999. *By* H. Blom.	120.00
183	Review of Greenland activities 1998, 81 pp. (10 articles), 1999. *Edited by* A.K. Higgins & W.S. Watt.	200.00
184	Collected research papers: palaeontology, geochronology, geochemistry, 62 pp. (6 articles), 1999.	150.00
185	Greenland from Archaean to Quaternary. Descriptive text to the Geological map of Greenland, 1:2 500 000, 93 pp., 2000. *By* N. Henriksen, A.K. Higgins, F. Kalsbeek & T.C.R. Pulvertaft.	225.00
186	Review of Greenland activities 1999, 105 pp. (13 articles), 2000. *Edited by* P.R. Dawes & A.K. Higgins.	225.00
187	Palynology and deposition in the Wandel Sea Basin, eastern North Greenland, 101 pp. (6 articles), 2000. *Edited by* L. Stemmerik.	160.00
188	The structure of the Cretaceous–Palaeogene sedimentary-volcanic area of Svartenhuk Halvø, central West Greenland, 40 pp., 2000. *By* J. Gutzon Larsen & T.C.R. Pulvertaft.	130.00
189	Review of Greenland activities 2000, 131 pp. (17 articles), 2001. *Edited by* A.K. Higgins & K. Secher.	160.00
190	The Ilímaussaq alkaline complex, South Greenland: status of mineralogical research with new results, 167 pp. (19 articles), 2001. *Edited by* H. Sørensen.	160.00
191	Review of Greenland activities 2001, 161 pp. (20 articles), 2002. *Edited by* A.K. Higgins, K. Secher & M. Sønderholm.	200.00

Geology of Denmark Survey Bulletin (36–37; discontinued)

36	Petroleum potential and depositional environments of Middle Jurassic coals and non-marine deposits, Danish Central Graben, with special reference to the Søgne Basin, 78 pp., 1998. *By* H.I. Petersen, J. Andsbjerg, J.A. Bojesen-Koefoed, H.P. Nytoft & P. Rosenberg.	250.00
37	The Selandian (Paleocene) mollusc fauna from Copenhagen, Denmark: the Poul Harder 1920 collection, 85 pp., 2001. *By* K.I. Schnetler.	150.00

Prices are in Danish kroner exclusive of local taxes, postage and handling

Note that information on the publications of the former Geological Survey of Denmark and the former Geological Survey of Greenland (amalgamated in 1995 to form the present Geological Survey of Denmark and Greenland) can be found on *www.geus.dk*